Bicaudal C1 promotes pancreatic NEUROG3+ endocrine progenitor differentiation and ductal morphogenesis

THÈSE N^{O} 6575 (2015)

PRÉSENTÉE LE 29 MAI 2015

À LA FACULTÉ DES SCIENCES DE LA VIE
UNITÉ DU PROF. CONSTAM
PROGRAMME DOCTORAL EN APPROCHES MOLÉCULAIRES DU VIVANT

ÉCOLE POLYTECHNIQUE FÉDÉRALE DE LAUSANNE

POUR L'OBTENTION DU GRADE DE DOCTEUR ÈS SCIENCES

PAR

Laurence Anne E LEMAIRE

acceptée sur proposition du jury:

Prof. P. Gönczy, président du jury
Prof. D. Constam, Prof. A. Grapin-Botton, directeurs de thèse
Prof. C. Brisken, rapporteuse
Prof. F. Lemaigre, rapporteur
Prof. T. Petrova, rapporteuse

ÉCOLE POLYTECHNIQUE
FÉDÉRALE DE LAUSANNE

Suisse
2015

« Je suis de ceux qui pensent que la science est d'une grande beauté. Un scientifique dans son laboratoire est non seulement un technicien : il est aussi un enfant placé devant des phénomènes naturels qui l'impressionnent comme des contes de fées. Nous ne devrions pas laisser croire que tout progrès scientifique peut être réduit à des mécanismes, des machines, des rouages, quand bien même de tels mécanismes ont eux aussi leur beauté. Je ne crois pas non plus que l'esprit d'aventure risque de disparaître dans notre monde. Si je vois quelque chose de vital autour de moi, c'est précisément cet esprit d'aventure, qui semble qui me paraît indéracinable et s'apparente à la curiosité. Sans la curiosité de l'esprit, que serions-nous ? Telle est bien la beauté et la noblesse de la science : désir sans fin de repousser les frontières du savoir, de traquer les secrets de la matière et de la vie sans idée préconçue des conséquences éventuelles. »

Marie Skłodowska Curie

Ève Curie, Marie Curie, éd. Da Capo Series in Science, p. 341

1 ABSTRACT

Mutations in Bicaudal C1 (*BICC1*), an RNA binding protein involved in translational regulation, have been associated with cystic kidney disease both in humans and in mice. Since kidney cysts associate with pancreatic defects in several human syndromes, we investigated the function of BICC1 in pancreas development. We found that pancreatic expression of BICC1 was restricted to the bipotent progenitors from E12.5 and later to the ducts. Deletion of *Bicc1* caused pancreatic cysts, starting with duct dilation at E14.5. Around birth, ductal cells were hyperproliferative. However, the mitotic index was not increased at E14.5, arguing that the proliferation is not the cause of cyst formation. The expression of PKD2, which is mutated in 15% of the patients with autosomal polycystic kidney disease, was downregulated already before ducts start to enlarge, consistent with a role downstream of BICC1 that has been reported in kidney and in osteoblasts. Conversely, two other targets of BICC1 in kidneys, ADCY6 and PKIA, were not affected by *Bicc1* deletion in E15.5 pancreata. In addition, after E14.5, but still before birth, *Bicc1* deletion led to a decrease in the number of endocrine cells. Only half of the normal numbers of beta, delta, PP, and epsilon cells were present in *Bicc1* KO pancreata. Alpha cells were reduced by 20%. Neither proliferation nor survival of the endocrine cells was affected in *Bicc1* KO pancreata. Instead, we observed in *Bicc1* KOs a reduction of the production of endocrine progenitor cells expressing NEUROG3^{+}, a major regulator of endocrine cell differentiation. *Bicc1* deletion reduced the activity of *Neurog3* promoter. Therefore, direct translation regulation of *Neurog3* by BICC1 can be ruled out. However, the transcriptional activators of *Neurog3* promoter, HNF1B, ONECUT1, PDX1, FOXA2, SOX9 and its transcriptional repressor, HES1, were unaffected by *Bicc1* deletion, arguing that they unlikely mediate BICC1 regulation of NEUROG3^{+} cell production. Finally, new *BICC1* variants have been uncovered in patients with cystic kidneys, and the two oldest diabetes. Contrary to what has been observed with previously reported mutations, the variants did not affect the ability of BICC1 to inhibit canonical WNT signaling. In conclusion, this study showed that BICC1 is important to maintain duct homeostasis and endocrine progenitor production. BICC1 may thus be a susceptibility factor for diabetes when it is mutated.

Keywords: Bicaudal C1, RNA-binding protein, embryo, pancreas, endocrine progenitors, endocrine cells, MODY, Cysts

2 RESUME

La polykystose rénale chez la souris et la dysplasie rénale multikystique chez l'humain peuvent être associées à la perturbation ou l'inactivation de Bicaudal C (*BICC1*), une protéine liant l'ARN et régulant la traduction des RNA messagers. En raison de l'existence de syndromes associant des kystes rénaux et un dysfonctionnement du pancréas, nous nous sommes intéressés à la fonction de BICC1 durant l'organogenèse pancréatique. Chez la souris, le domaine d'expression de BICC1 est restreint aux progéniteurs à double potentialités à 12 jours et demi après la fertilisation et par la suite aux canaux pancréatiques. Dans le pancréas, l'absence de *Bicc1* provoque la formation de kystes commençant par une dilatation des canaux à 14 jours et demi. Aux alentours de la naissance, les cellules canalaire prolifèrent plus activement. Cependant, l'augmentation de la prolifération n'est pas la cause initiale des kystes car la proportion des cellules qui se divisent n'est pas accrue à 14 jours et demi. Par contre, on a observé, avant même l'élargissement des canaux, une diminution de l'expression de PKD2. Hors, 15% des cas de polykystoses rénales autosomiques dominantes sont causés par une mutation dans le gène de *PKD2*. De plus, chez la souris, il a été découvert que son expression est régulée par BICC1 dans les ostéoblastes et dans les reins. En revanche, dans le pancréas des mutants à 15 jours et demi, je n'ai pas observé de changement de l'expression de deux autres protéines, ADCY6 et PKIA, elle aussi régulée par BICC1 dans les reins. Par ailleurs, à la naissance, le nombre de cellules endocrines bêta, delta, PP et epsilon est réduite de moitié alors qu'il y a que 20% de cellules alpha en moins chez les mutants *Bicc1*. Ces déficits ne sont pas observés à 14 jours et demi et ne sont pas causés par une diminution de leur survie ou de leur capacité à proliférer. Cependant, l'aptitude des progéniteurs à se différentier en progéniteurs endocrines exprimant *Neurog3*, un facteur de transcription nécessaire pour continuer la différentiation en cellule endocrine, est réduite chez les mutants. La régulation par BICC1 de la traduction de *Neurog3* peut être exclue puisque l'absence de BICC1 affecte l'activité du promoteur de *Neurog3*. Néanmoins, l'expression des activateurs transcriptionnels de *Neurog3*, HNF1B, ONECUT1, PDX1, FOXA2, SOX9, et de son répresseur transcriptionnel, HES1, ne change pas chez les mutants *Bicc1*. Ils ne relayent donc pas la régulation par BICC1 de la production de cellules positive pour NEUROG3. Pour finir, de nouveaux allèles de *BICC1* ont été identifiés chez des patients présentant des

kystes rénaux et pour certains d'entre eux, un diabète. Nonobstant ce qui a été observé avec les premières mutations de *BICC1* découvertes, la capacité de BICC1 d'inhiber la voie de signalisation canonique de WNT n'est pas altérée par les nouveaux variants de BICC1. Pour conclure, cette étude montre que BICC1 est essentiel pour l'homéostasie des canaux pancréatiques et promeut la production des progéniteurs endocrines. En raison de cette capacité, des mutations affectant la fonction de BICC1 pourraient être un facteur de susceptibilité au diabète.

Mots-clefs : Bicaudal C1, protéine liant l'ARN, embryon, pancréas, progéniteurs endocrines, cellules endocrines, MODY, kystes

3 ABBREVIATIONS

Table 1: list of the abbreviation used in this work and their meaning

Abbreviation	Meaning
%	percent or g per 100ml
°C	celsius degree
3D	3 dimensions
3'-UTR	3'- untranslated region
Ac Tub	acetyl tubulin
ADCY	adenylate cyclase
ADPKD	autosomal dominant polycystic kidney disease
Al488	alexa488
Al568	alexa568
Al647	alexa647
ANOVA	analysis of variance
ARPKD	autosomal recessive polycystic kidney disease
ATP	Adenosine triphosphate
bHLH	basic helix-loop-helix
Bicc1	Bicaudal C1
BMP	bone morphogenetic protein
bTC	beta cell line
C_2H_2	paired cystine and histidine type
$C_6FeK_3N_6$,	Potassium ferricyanide
$C_6FeK_4N_63H_2O$	Potassium ferrocyanide trihyrate
Ca^{2+}	calcium ion
cAMP	cyclic adenosine monophosphate
cDNA	complementary deoxyribonucleic acid
CCR4-NOT	CCR4 deadenylase complex
COPII	Coat protein II
DAPI	4′,6-Diamidino-2-phenyindole
DBA	Dolichos Biflorus Agglutinin
DBA	dolichos biflorus agglutinin
DESeq	Differential expression analysis for sequence count data
DVL	Dishevelled

Abbreviation	Meaning
E	embryonic day
e. g.	*exempli gratia*
ECL	enhanced chemiluminescence
EGF	epithelium growth factor
EGTA	Ethylene Glycol Tetraacetic Acid
ESRD	end stage renal disease
FDR	false discovery rate
FGF	fibroblast growth factor
FZD	frizzled receptor
g/l	gram per litre
Gcg	Glucagon
Ghr	ghrelin
H_2O	water
HA-tag	Influenza Hemagglutinin peptide-tag
HEK293T cell	human embryonic kidney 293 cell
HES family	hairy and enhancer of split family factors
HNF	hepatic nuclear factor
Hprt1	*Hprt*
HRP	horseradish peroxydase
i. e.	*id est*
Ins	Insulin
K^+	potassium ion
KCl	potassium chloride
KH	K homology RNA-binding domain
KO	knockout
M	Molar
mA	milliAmper
MAPK (signaling) pathway	MAP kinase signaling pathway
$MgCl_2$	Magnesium Chloride
Mir17-92	miR-17~92 miRNA cluster

Abbreviation	Meaning
ml	millilitre
µm	micrometer
mM	milliMolar
mRNA	RNA messenger
n	number of specimens
Na+	sodium ion
Na^+K^+ATPase	sodium potassium pump
NaCl	sodium chloride
Neurog3	Neurogenin3
ng	nanogram
NOTCH	notch family
OCT	*Optimal cutting temperature*
P	postnatal day
PBS	phosphate buffer saline
PCP	planar cell polarity pathway
PDE1	phosphodiesterase 1 (a, b and c)
PFA	paraformaldehyde
pH	potential of hydrogen
PHH3	Phospho-histone H3
phospho-	phosphorylated
PKA	protein kinase A, cAMP dependent
PKC	Protein kinase C
PKD	polycystic kidey disease
Pkd1	polycystic kidney disease 1 homolog
Pkd2	polycystic kidney disease 2
Pkhd1	polycystic kidney and hepatic disease 1
PNDM	permanent neonatal diabetes

Abbreviation	Meaning
polyA	Polyadenylic acid
Ppy	pancreatic polypeptide
Q-PCR	quantitative real time polymerase chain reaction
RFP	red fluorescent protein
RNA	ribonucleic acid
rpkm	read per kilobase per million
SAM	sterile alpha motif
SDS	Sodium dodecyl sulfate
SMART	simple molecular architecture research tool
Sst	somatostatin
SUR	sysematic uniform random sampled
TBST	Tris buffer saline Triton
TBSTw	Tris buffer saline Tween20
TNDM	transient neonatal diabetes
Tris	Tris(hydroxymethyl)aminomethane
TUNEL	terminal deoxynucleotidyl transferase-dUTP nick end labeling assay
VANGL	VANGL1 and VANGL2
vs	*versus*
WNT	WNT family members
WT	wild-type
X-gal	5-bromo-4-chloro-3-indolyl-beta-D-galacto-pyranoside
YFP	yellow fluorescence protein

Some of the most important genes are included in this table. All the other gene symbols present in this work are listed with their full official name in Table 11 in the Appendix.

4 TABLE OF CONTENTS

5 PREAMBLE

There are several syndromes which associate kidney cysts and diabetes. For instance, young adults with *HNF1B* mutations have MODY5, a syndrome characterized by renal cysts and diabetes. Similarly newborns without functional GLIS3 develop neonatal diabetes with hypothyroidism, and some of them harbor cysts in the kidneys (Lindner et al., 1999; Senée et al., 2006). Therefore genes endowed with a role in kidney homeostasis may be important for beta cell generation and function or vice versa. Moreover, the renal-hepatic-pancreatic dysplasia syndrome associating fibrosis and cysts in the kidneys, the liver, and the pancreas (Ivemark et al., 1959). In mice, the inactivation of *Pkd1* or *Pkd2* associate cystic kidney disease and pancreatic cysts, suggesting similar mechanisms of ductal homeostasis in both organs (Wu et al., 2000; Lu et al., 2001; Wu et al., 2002). *BICC1* mutation has been recently associated with human kidney dysplasia (Kraus et al., 2012), and *Bicc1* mutant mice have been used as a model for autosomal recessive polycystic kidney disease (Nauta et al., 1993; Flaherty et al., 1995). Moreover, targeted deletion of *Bicc1* in mice results in cysts in kidneys and in the pancreas (Tran et al., 2010; Piazzon et al., 2012).

Prompted by the idea that genes involved in the formation of kidney cysts could be associated to defects in beta cells, leading to diabetes and/or to cysts in the pancreas, my PhD project has focused on the role of BICC1 during murine pancreas development, principally on its role in ductal homeostasis and endocrine cell differentiation. In addition, I have started to characterize the functionality of new *BICC1* variants identified by the groups of Pr. Bingham, Pr. Ellard, and Pr Hattersley, in patients with renal cysts kidneys and, for the oldest patients, diabetes. The majority of the results have been recently published in (Lemaire et al., *in press*) with the exception of the characterization of E12.5 *Bicc1* KO pancreata, the microRNA sequencing performed on E13.5 *Bicc1* KO and WT pancreatic dorsal buds and, the study of human BICC1 variants.

During my PhD, I have also characterized two mouse lines, a transgenic *Neurog3*-RFP line and a knock-in *Sox17*^{CREGFP} line. The corresponding articles are provided in the Appendix (Choi et al., 2012; Kim et al., 2015).

6 INTRODUCTION

6.1 Pancreas physiology and Diabetes

6.1.1 Pancreas physiology

The pancreas is an abdominal organ with a dual function. It is involved in digestion by secreting pancreatic enzymes from the acini. The exudates are collected by a ductal network and converge in the duodenum with bile fluid.

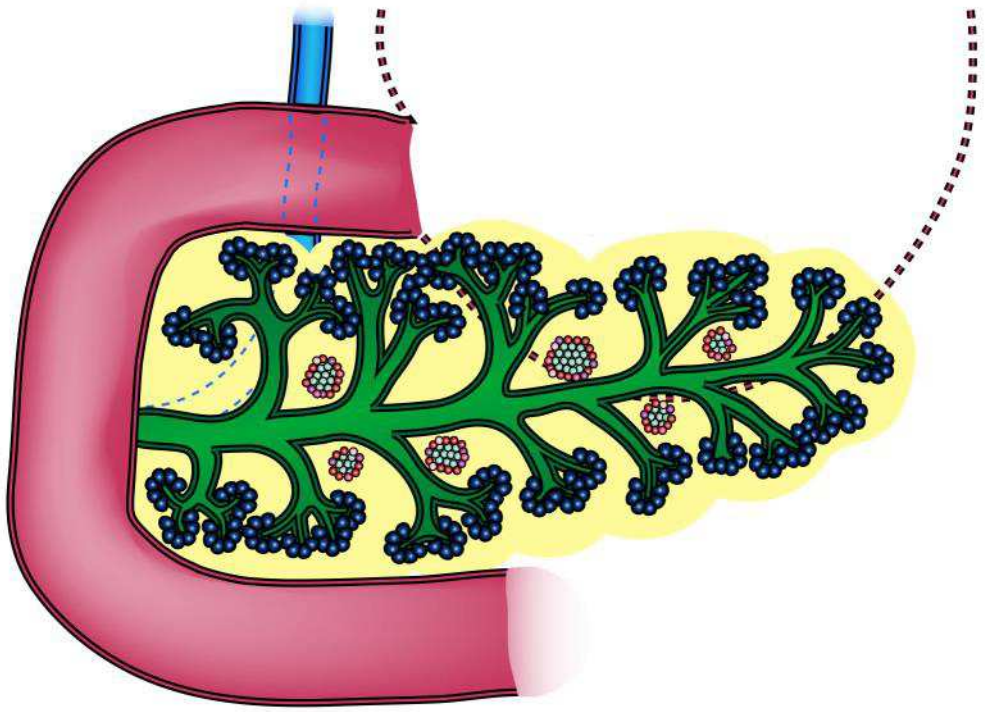

Fig. 1: Scheme representing the adult pancreas

Pancreas is an abdominal organ. It is composed of an acinar compartment (blue) connected by ducts (green) to the duodenum, and the islets of Langerhans (light blue, red, pink and purples) are scattered in the exocrine compartment (color code corresponds to Fig. 2).

The islets of Langerhans provide the other function. They are composed of 5 different cell types. Beta cells, the most numerous, secrete insulin (INS). Alpha cells secrete glucagon (GCG). Delta cells secrete somatostatin (SST). These hormones are involved in blood glucose homeostasis, with insulin lowering glycemia, glucagon having the opposite effect and somatostatin controlling, in a paracrine manner the secretion of INS and GCG. SST also controls the secretion of growth hormones, among other functions. PP cells secrete pancreatic polypeptide (PPY) that is involved in digestion and food intake regulation as well as mood control. Epsilon cells secrete ghrelin (GHR) also to stimulate food intake (Fig. 1) (Norris and Carr, Chemical Regulation of Feeding, Digestion and Metabolism, in Vetebrate Endocrinology, 2013).

6.1.2 Diabetes mellitus

Diabetes is one of the most challenging diseases of the 21st century. 390 million people suffer from diabetes worldwide and 4.9 million died of a consequence of diabetes in 2014 (International Diabetes Federation, 2014 update, in IDF Diabetes Atlas, 2014). It is characterized by hyperglycemia due to a defect in glucose homeostasis. Hyperglycemia causes polydipsia and polyuria associated with glycosuria distinguishes it from diabetes insipidus. The long term complications associated with diabetes mellitus include cardiovascular diseases and kidney failure (Scobie and Samaras, Chapter 3: Type 1 diabetes and Chapter 4: Type 2 diabetes, in Fast facts: Diabetes mellitus, 2014)

The different types of diabetes are classified based on their etiology and time of apparition. Type II diabetes is the most prevalent accounting for nearly 90% of all diabetic cases. It mainly appears in adulthood between 40 and 60 years of age. It is a metabolic disease caused by the inability of peripheral cells to respond to insulin and, thus, reduce blood glucose level. In response to such peripheral resistance, beta cells increase their insulin secretion until they slowly die of exhaustion (Scobie and Samaras, Chapter 4: Type 2 diabetes, in Fast facts: Diabetes mellitus, 2014b). Treatment of type II diabetes is initially by an adapted diet and by drugs that normalize glycemia by inhibiting liver neoglucogenesis or by promoting insulin secretion. But as beta cells become dysfunctional insulin injections are needed to lower the glycemia (Inzucchi et al., 2015). Type I diabetes, the second most common type, is an autoimmune disease characterized by immune attack

against the beta cells leading to their destruction. It is thus directly insulin dependent. Patients developing type I diabetes are also younger, being in their childhood or their early twenties (Scobie and Samaras, Chapter 3: Type 1 diabetes, in Fast facts: Diabetes mellitus, 2014a).

6.1.2.1 Monogenic diabetes

The etiology of type I and type II diabetes is multifactorial as it involves both complex genetic predisposition and environmental cues. By contrast, other more rare forms of diabetes are monogenic, which means that they are caused by a mutation in only one gene. Monogenic forms of diabetes are usually characterized by an absence of autoimmune reaction, and their onset is earlier than type II diabetes. Mature onset diabetes of the young (MODY) syndromes are characterized by an onset before the age of 25, even though some patients may develop it later (reviewed in Ashcroft and Rorsman, 2012). Rare infants (1/400000 birth) develop diabetes in the first months of life. The disease is called neonatal diabetes, and is either transient neonatal diabetes (TNDM), when babies recover, or permanent (PNDM) (reviewed in Polak and Shield, 2004). The monogenic causes of diabetes not only shed important light on pathogenesis and beta cell physiology, but also on beta cell ontogeny, as some of the genes mutated in monogenic diabetes regulate beta cell formation. They also give insight on the similarities and discrepancies between human and mouse models as the mouse model do not always recapitulate the corresponding human disease. Forms of monogenic diabetes are reviewed in Tables 2 and 3.

Table 2: MODY

Name	Muta-tion	Transmission mode	Other defect[1]	Mouse phenotype[2]	References[3]
Altröm disease	*ALMS1*	Recessive	Yes*	Type II diabetes	(Collin et al., 2002; Hearn et al., 2002; Collin et al., 2005)
MODC[4]	*GATA4*	dominant	Yes	Ventral pancreas agenesis (tetraploid complementation)	(Watt et al., 2007; Shaw-Smith et al., 2014)
MODY	*KCNJ11*	Dominant, relapse from TNDM	Yes	Neonatal diabetes (gain of function)	(Koster et al., 2000; Flanagan et al., 2007)
MODY	*ABCC8*	Dominant, relapse from TNDM	Yes	impaired glucose tolerance	(Seghers et al., 2000; Flanagan et al., 2007; Bowman et al., 2011)
MODY	*6q22-23*	Imprinted gene, paternal inheritance relapse from TNDM	Yes	Overexpression: neonatal hyperglycemia, adult glucose intolerance	(Shield et al., 1997; Ma et al., 2004)
MODY1	*HNF4A*	Dominant	No	Embryonic lethal Impaired glucose tolerance (pancreas specific deletion)	(Chen et al., 1994; Yamagata et al., 1996; Gupta et al., 2005)
MODY2	*GCK*	Dominant	No	Glucose intolerance	(Vionnet et al., 1992; Terauchi et al., 1995)
MODY3	*HNF1A*	Dominant	No	Diabetes	(Yamada et al., 1997; Pontoglio et al., 1998)
MODY4	*PDX1*	Dominant	No	Pancreas agenesis	(Offield et al., 1996; Stoffers et al., 1997a)
MODY5	*HNF1B*	Dominant	Yes *	Neonatal diabetes (pancreas specific deletion)	(Horikawa et al., 1997; Lindner et al., 1999; De Vas et al., 2015)
MODY6	*NEURO D1*	Dominant	No	Neonatal diabetes	(Naya et al., 1997; Malecki et al., 1999)
MODY7	*KLF11*	Dominant	No	Impaired INS secretion, no diabetes	(Neve et al., 2005; Bonnefond et al., 2011)
MODY8[5]	*CEL*	Dominant	Yes	No glucose intolerance phenotype	(Ræder et al., 2005; Vesterhus et al., 2010)
MODY9	*PAX4*	Dominant	No	Neonatal diabetes based on observed symptoms	(Sosa-Pineda et al., 1997; Plengvidhya et al., 2007)
MODY10	*INS*	Dominant	No	Diabetes at week 7 (Dominant negative of Ins2)	(Yoshioka et al., 1997; Edghill et al., 2007)
MODY11	*BLK*	Dominant	No	Not reported	(Texido et al., 2000; Maciej et al., 2009)
Wolfram syndrome (MODY before 15 year old)	*WFS1*	Recessive	Yes	Impaired glucose tolerance	(Inoue et al., 1998; Ishihara et al., 2004)

Classification based on OMIM (http://www.ncbi.nlm.nih.gov/omim/).

[1] * kidney defects
[2] If not stated, KO
[3] First mutation described
[4] Onset in childhood
[5] diabetes and exocrine pancreatic dysfunction

Table 3: Transient and permanent neonatal diabetes mellitus

Name	Mutation	Transmission mode	Other defect[6]	Mouse phenotype[7]	References[8]
Fanconi-Bickel syndrome: (PNDM)	*SLC2A2*	Recessive	Yes	Diabetes	(Guillam et al., 1997; Yoo et al., 2002)
IPEX (PNDM – Type I diabetes)	*FOXP3*	X linked	Yes	Earlier diabetes onset in NOD background than NOD mice	(Wildin et al., 2001; Chen et al., 2005)
PNDM	*ABCC8*	Recessive	Yes	impaired glucose tolerance	(Seghers et al., 2000; Ellard et al., 2007)
		Dominant	Yes		(Babenko et al., 2006)
PNDM	*GCK*	Recessive	Yes	Neonatal diabetes	(Terauchi et al., 1995; Njølstad et al., 2001)
PNDM	*GATA4*	Dominant	Yes	Ventral pancreas agenesis (tetraploid complementation)	(Watt et al., 2007; Shaw-Smith et al., 2014)
PNDM-Pancreas agenesis	*GATA6*	Dominant	Yes	Ventral pancreatic agenesis (tetraploid complementation)	(Watt et al., 2007; Lango Allen et al., 2011)
PNDM	*GLIS3*	Recessive	Yes*	Neonatal diabetes	(Senée et al., 2006; Kang et al., 2009b)
PNDM	*INS*	Recessive	No	Neonatal diabetes	(Duvillie et al., 1997; Garin et al., 2010)
		Dominant	No	Diabetes at week 7 (Dominant negative Ins2)	(Yoshioka et al., 1997; Støy et al., 2007)
PNDM	*KCNJ11*	Dominant	Yes	Neonatal diabetes (GOF)	(Koster et al., 2000; Gloyn et al., 2004)
PNDM	*MNX1*	Recessive	Yes	Dorsal lobe agenesis, less insulin cell (relative)	(Harrison et al., 1999; Bonnefond et al., 2013; Flanagan et al., 2014)
PNDM	*NEUROG3*	Recessive	Yes	Neonatal diabetes	(Gradwohl et al., 2000; Rubio-Cabezas et al., 2011)
PNDM	*NEUROD1*	Recessive	Yes	Neonatal diabetes	(Naya et al., 1997; Rubio-Cabezas et al., 2010)
PNDM	*NKX2.2*	Recessive	Yes	Neonatal diabetes	(Sussel et al., 1998; Flanagan et al., 2014)
PNDM	*PAX6*	Recessive	Yes	Glycemia not tested	(St-Onge et al., 1997; Solomon et al., 2009)

[6] * kidney defect
[7] If not stated, KO phenotype
[8] First mutation described

PNDM with or without pancreas agenesis	*PDX1*	Recessive	Yes	Pancreas agenesis	(Offield et al., 1996; Stoffers et al., 1997b; Nicolino et al., 2010)
PNDM	*PTF1A*	Recessive	Yes	Pancreas agenesis	(Krapp et al., 1998; Sellick et al., 2004)
PNDM	*RFX6*	Recessive	Yes	No Insulin cells, glycemia not tested	(Smith et al., 2010)
Thiamine-responsive megaloblastic anemia with diabetes and deafness (PNDM)	*SLC19A2*	Recessive	Yes	Diabetes after 2 weeks on thiamin free diet, no phenotype on normal diet	(Oishi et al., 2002; Olsen et al., 2007)
TNDM1	6q22-23 regions	Imprinted genes, paternal inheritance	Yes	Overexpression: neonatal hyperglycemia, adult glucose intolerance	(Temple et al., 1995; Temple et al., 1996; Ma et al., 2004)
TNDM2	*ABCC8*	dominant	Yes	impaired glucose tolerance	(Seghers et al., 2000; Babenko et al., 2006; Proks et al., 2006)
TNDM3	*KCNJ11*	dominant	Yes	Neonatal diabetes (gain of function)	(Koster et al., 2000; Gloyn et al., 2004)
Wolcott-Rallison syndrome (PNDM)	*EIF2AK3*	Recessive	Yes	Diabetes	(Delépine et al., 2000; Harding et al., 2001)

Classification based on OMIM (http://www.ncbi.nlm.nih.gov/omim/).

6.2 Pancreas organogenesis

6.2.1 Pancreatic epithelium morphogenesis

In mouse, two regions of the foregut become committed to a pancreatic fate at E8. The first sign of pancreas formation is their thickening, which occurs for the dorsal bud at E9 and for the ventral bud at E9.5 The epithelium then evaginates into the surrounding mesenchyme, forming a bud (Wessells and Cohen, 1967; Spooner et al., 1970)[9]. At E10.5, the bud is mainly composed of multipotent progenitors able to give rise to endocrine cells, acinar cells and ductal cells (Fig. 2, 3) (Pan et al., 2013).

[9] Spooner *et al* describe the formation of the ventral bud in rats.

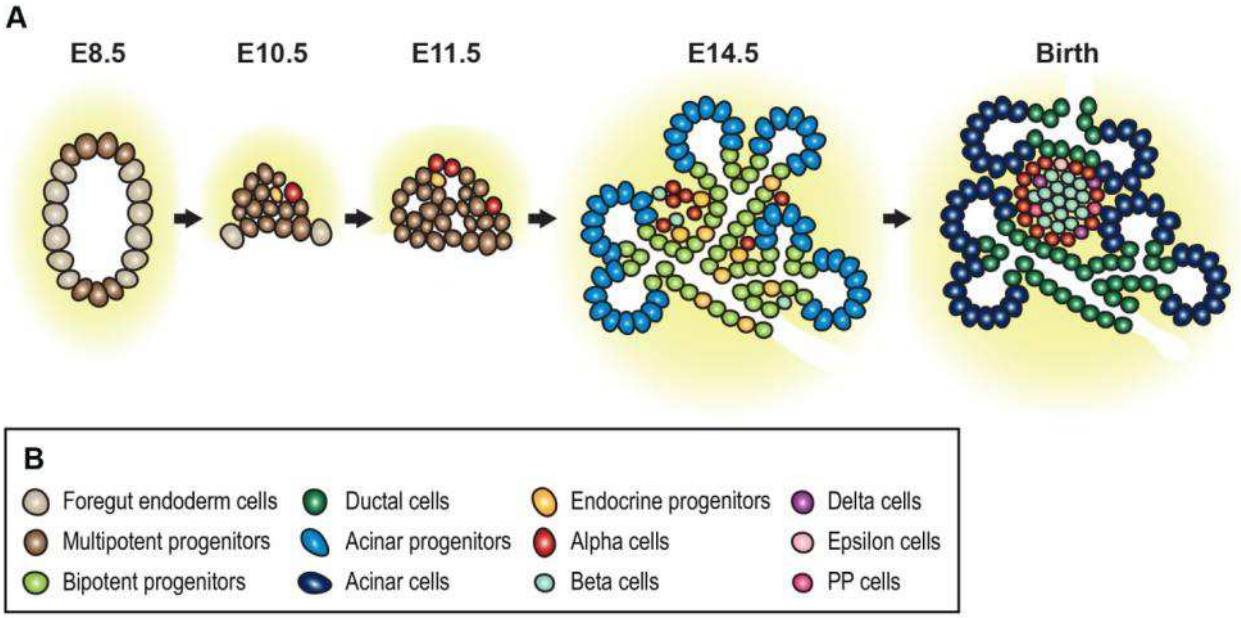

Fig. 2: Pancreas morphogenesis

(A) The pancreas is specified in two regions of the foregut (brown) at E8. They grow and bud into the surrounding mesenchyme (light yellow). A few endocrine progenitors (yellow) and GCG^+ cells (red) are already present. Around E11.5, microlumens form, and fuse. The plexus then rearranges to form the pancreatic tree composed of a trunk of bipotent progenitors (light green) and ended by acinar progenitors (light blue). After the secondary transition has started, bipotent progenitors differentiate more into endocrine progenitors (yellow) that leave the ducts, and differentiate further into endocrine cells (red and turquoise blue). The bipotent progenitors, which did not become endocrine progenitors, differentiate into ductal cells (dark green). The acinar progenitors (light blue) have differentiated into acinar cells (dark blue). Endocrine cell clusters (red, light pink, fuchsia, purple and turquoise blue) present at earlier stages aggregate and reorganize to form the mature islet of Langerhans around birth.

(B) The color code depicting the different cell types.

The cells in the epithelial bud will then rearrange. Apical polarity cues start to be targeted to one side of the cells, in a coordinated manner between cells, resulting in the formation of microlumens. Lumens progressively fuse to form a tubular plexus at E12.5 (Kesavan et al., 2009; Villasenor et al., 2010). The plexus is composed of tubules ending by tips forming a tree-like structure. The pancreas is still mainly composed of multipotent pancreatic progenitors, with few endocrine progenitors and endocrine cells (Fig. 2, 3) (Georgia et al., 2006; Seymour et al., 2007). Dorsal and ventral buds fuse around E13 (Villasenor et al., 2010).

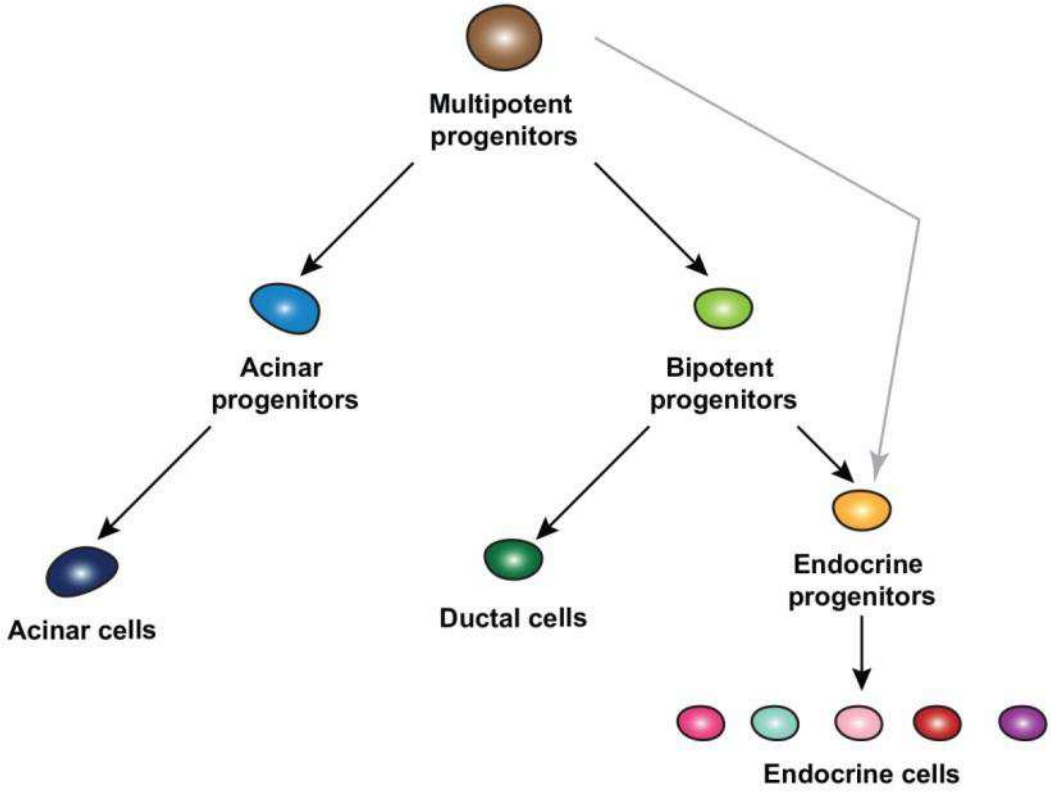

Fig. 3: Pancreatic cell lineage ontogeny

Multipotent progenitors can give rise to all cell lineages in the pancreas. After the specification of the tip *vs* trunk domain, acinar progenitors at the tips give rise to acinar cells, while bipotent progenitors differentiate into endocrine progenitors, or adopt a ductal cell fate. The former leave the trunk domain and differentiate into the five endocrine cell types present in the pancreas. Ontogeny has been inferred from lineage tracing experiments using reporters or a CRE recombinase under the promoter of a gene of interest (Gu et al., 2003; Zhou et al., 2007; Pan et al., 2013) as well as KO data analysis.

The cell color code is the same as used in Fig. 2.

After E13.5, the plexus reorganization starts (Villasenor et al., 2010). Endocrine cells differentiation is greatly enhance; it is the so-called secondary transition (Mori and Haga, 1960; Rutter et al., 1968). The cells present in the distal domain, also called tips, restrict their potency, and by E13.5, become committed to the acinar fate (Zhou et al., 2007; Schaffer et al., 2010; Pan et al., 2013). Progenitors present in the proximal domain, referred to trunk, become bipotent, and give rise to either ductal cells or endocrine progenitor cells expressing NEUROG3, a major transcription factor for the endocrine differentiation program (Gradwohl et al., 2000; Schaffer et al., 2010). The endocrine progenitors born in the epithelial layer lining ducts delaminate, while they differentiate into the different endocrine cell types (Fig. 2, 3) (Gouzi et al., 2011).

There is scant information on how cells choose to differentiate into one or the other endocrine cell type. It has been reported than endocrine progenitors are unipotent. However, they rarely divide (Desgraz and Herrera, 2009; Miyatsuka et al., 2011). It is thus logical that one pancreatic progenitor gives rise to one type of endocrine cells. The different endocrine cell types do not arise at the same time. Indeed, they are produced in different overlapping waves, suggesting that their progenitors are competent to give rise to different cells at different moments (Johansson et al., 2007). The first endocrine cells expressing GCG are already present at E9.5 (Pictet et al., 1972; Rall et al., 1973). The GCG^+ cell production becomes minor by E14.5. INS^+ cells are produced from E10.5 forward. However, the first are immature in the sense that they produce low levels of INS, that they miss many molecular hallmarks of beta cells, and that they co-express GCG. PP cells start to be produced from the same stage while delta cells arise only later, from E14.5 onward (Johansson et al., 2007). The endocrine cells are scattered between the bipotent progenitor cords, or form small clusters during embryonic development. Around birth, endocrine cells reorganize to form the mature islets of Langerhans with beta cells in the center surrounded by the other endocrine cells types in mice (Fig. 2, 3) (Pictet et al., 1972; Herrera et al., 1991). During development, the expansion in size of the islets is mainly due to the convergence of endocrine cells, and, for a small part, to the ability of endocrine cells to proliferate in the late developmental stages (Pictet et al., 1972; Deltour et al., 1991; Finegood et al., 1995; Jensen et al., 2000a). After birth, massive expansion of the islets is due to proliferation (Finegood et al., 1995; Georgia and Bhushan, 2004).

6.2.2 Pancreatic stroma formation

The pancreatic stroma is composed of blood vessels, mesenchymal cells, neurons and immune cells.

6.2.2.1 Mesenchymal cells in pancreatic organogenesis

The mesenchymal cells of the pancreas originate from the splanchnopleura of the lateral plate mesoderm (Wessells and Cohen, 1967). At E8.5-9.5, they are still in lateral position and they are not yet in contact with the dorsal pancreas anlage, which initially abuts the notochord and subsequently the dorsal aorta, as it fuses

medially from the two lateral aortas (Wessells and Cohen, 1967). The splanchnopleural mesodermal cells will migrate along the lateral side of the gut towards the dorsal pancreas primordium and separate it from the dorsal aorta. At E10.5 they surround the pancreatic buds (Wessells and Cohen, 1967). Thereafter, the mesenchyme is intermingled between the ducts and around the epithelium (Villasenor et al., 2010). The proportion of mesenchyme *vs* epithelium is progressively reduced and, at E18.5, represents 5% of the total pancreas (Landsman et al., 2011). In its absence, neither growth nor branching occurs at early stages (Golosow and Grobstein, 1962; Edsbagge et al., 2005). At later stages, the mesenchymal cells also promote growth of progenitors without affecting differentiation (Landsman et al., 2011). This is due to the secretion of signaling factors by mesenchymal cells and their molecular nature is further discussed on p 47. After birth, some pancreatic stellate cells, the fibroblasts mainly present around the acini, originate from these mesenchymal cells, while others come from the bone marrow (Apte et al., 1998; Watanabe et al., 2009). They play important roles in extracellular matrix maintenance and therefore pancreas homeostasis (reviewed in Masamune and Shimosegawa, 2013).

6.2.2.2 Blood vessels in pancreas organogenesis

Blood vessels have a complex role during pancreas organogenesis. After the specification of the dorsal pancreas primordium and initial induction by signals from the notochord, the dorsal aorta is required for the dorsal pancreas development. It induces and maintains the expression of pancreas progenitor markers, such as PDX1 and PTF1A. Furthermore, it has indirect activities by promoting the survival of the pancreatic mesenchyme, which is necessary for pancreas development (Lammert et al., 2001; Yoshitomi and Zaret, 2004; Jacquemin et al., 2006). It is unclear whether there are similar signals acting on the ventral pancreas, but the vitelline veins contacting it do not appear necessary in early organogenesis (Yoshitomi and Zaret, 2004).

At E10.5, blood vessels surround the buds. At E11.5, when the pancreatic epithelium starts to reorganize, blood vessels invade the buds. Initially, they are close to the pancreatic proximal domain, and are excluded from the distal domain (Pierreux et al., 2010). The presence of blood vessels in the proximal domain

promotes pancreatic growth, in part via a decrease in pancreas progenitor proliferation (Magenheim et al., 2011b; Sand et al., 2011) and because of their negative influence on acinar differentiation (Pierreux et al., 2010; Magenheim et al., 2011b).

Their effect on endocrine differentiation is more controversial. Blood vessels may have no effect (Sand et al., 2011), or inhibit it (Magenheim et al., 2011b). On the contrary, Pierreux and co-workers suggest that blood vessels might even promote endocrine differentiation (Pierreux et al., 2010). In line with this observation, Lammert and colleagues observed ectopic INS^+ cells in the presence of an excess of blood vessels (Lammert et al., 2001). These discrepancies may be caused by the fact that endocrine and endothelial cells influence each other, or may be due to the embryonic stage of observation. For example after birth, endothelial cells are tightly associated with beta cells, and promote both their function and their proliferation (Duvillié et al., 2002; Brissova et al., 2006; Nikolova et al., 2006).

6.2.2.3 Glial and Neural cells in pancreas organogenesis

Pancreatic neural and glial cells originate from the neural crest (Nekrep et al., 2008). Neural crest cells arrive in the pancreas at E10.0 (Plank et al., 2011). In the absence of neural crest cells, no neurons or glial cells are observed in the pancreas. Consequently, the beta cell mass expands excessively due to an increase of beta cell proliferation. However, the resulting beta cells are not mature, indicating that glial cells and/or neurons promote beta cell differentiation (Plank et al., 2011). Nevertheless, the signals mediating this potent influence on beta cell proliferation are elusive.

6.2.2.4 Immune cells in pancreas organogenesis

Immune cells marked by PTPRC, also called CD45, are already present in the E12.5 pancreas (Geutskens et al., 2005; Sand et al., 2011). Macrophages positive for EMR1, also called F4/80, are first detected at E14.5 (Banaei-Bouchareb et al., 2004; Geutskens et al., 2005). However, there is a paucity of information about the function of macrophages or more generally immune cells, in this organ. Beta cell proliferation, and therefore beta cell mass, is impaired in mice deficient for CSF1 which have extremely few to no $EMR1^+$ macrophages.

This result is in line with *in vitro* observations. The expansion of macrophage population by CFS1 increases the beta cell mass, in pancreatic explants (Banaei-Bouchareb et al., 2004; Geutskens et al., 2005). However, as these studies relied on the depletion or addition of CSF1 to control the macrophage number, one cannot rule out the possibility that CFS1 may also directly affect the beta cell mass. Dendritic cell numbers were minimal in the developing pancreas (Banaei-Bouchareb et al., 2004), and no other immune cell type has been described during pancreas organogenesis.

6.2.3 Transcriptional control of pancreas development

Transcription factors play an important role in pancreas organogenesis, as they drive the differentiation cascades. Thereafter, the same transcription factors are required for the function of the different cell types. Many of these transcription factors form highly interconnected networks that presumably stabilize specific cellular states. In some instances, a given factor has different functions depending on the stage of development and the cell type. In addition, different factors may regulate targets together. For instance, during proximal distal domain boundary establishment, PTF1A and NKX6.1, initially co-expressed in multipotent progenitors antagonize each other and respectively segregate to distal acini and proximal bipotent progenitors. PTF1A specifies acinar progenitors while NKX6.1 promotes bipotent progenitor fate (Schaffer et al., 2010). Other transcription factor interactions in multipotent or bipotent progenitors are depicted in (Fig. 4). Their interactions aim to principally stabilize pancreatic progenitor identity and are discussed in details in the subsequent sections.

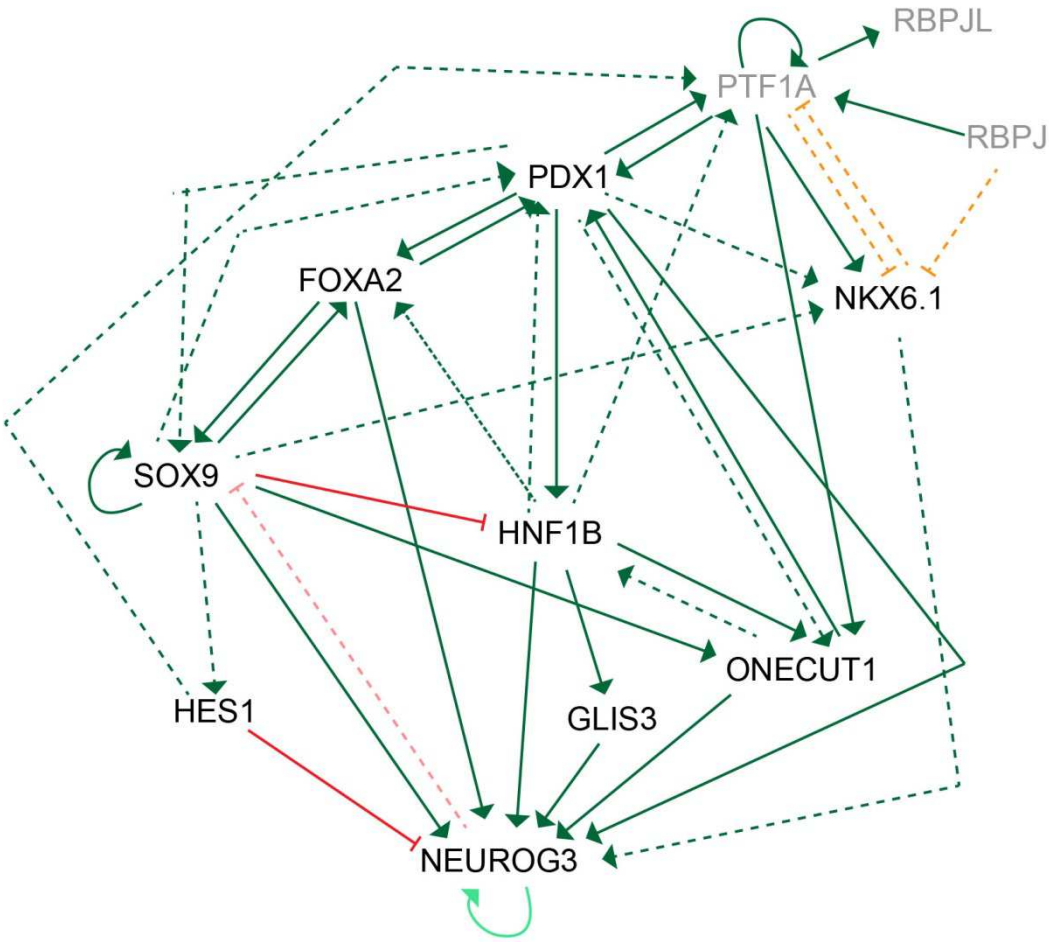

Fig. 4: Gene regulatory network in multipotent progenitors and bipotent progenitors.

Transcription factor relationships in multipotent progenitors are represented by green arrows for the activation of gene expression and red arrows for the repression of the expression. Dashed arrows denote evidence of interaction without direct activation or repression. During the establishment of the proximal distal domain boundaries, PTF1A and NKX6.1 antagonize each other (orange arrows). Gray transcription factors are absent in bipotent progenitors. The inhibition of HNF1B by SOX9 and the promotion of the expression of ONECUT1 have only been found *in vitro* (Dubois et al., 2011).

When NEUROG3 starts to be expressed, it promotes its own expression (light green arrow) and represses at least SOX9 (light red arrow) to enable endocrine cell differentiation.

The scheme is adapted from the review (Arda et al., 2013), and based on the following refrences (Jacquemin et al., 2003a; Pedersen et al., 2005; Wiebe et al., 2007; Oliver-Krasinski et al., 2009; Schaffer et al., 2010; Dubois et al., 2011; Yang et al., 2011; Ahnfelt-Rønne et al., 2012; Kim et al., 2012; Shih et al., 2012; Thompson et al., 2012; Ejarque et al., 2013; De Vas et al., 2015)

The main transcription factors involved in pancreas organogenesis, with emphasis on those used in this study, are reviewed here.

6.2.3.1 PDX1

PDX1 is a homeodomain protein (Ohlsson et al., 1993). Its expression starts at E8.5 in the prospective pancreatic regions. It is expressed in the multipotent progenitors from E9.5. From E16.5, its expression is reduced in the acinar cells, where it remains only at low levels in adults. At E18.5 its expression is largely restricted to beta cells and a subset of delta cells (Ohlsson et al., 1993; Guz et al., 1995; Wu et al., 1997; Wescott et al., 2009). It is noteworthy that the expression level of PDX1 varies depending on its function. Low expression is sufficient for its activity in the stomach and the duodenum, where it is also expressed. Higher expression is required in the bipotent progenitors and the highest level is required in beta cells, as shown in elegant studies controlling *Pdx1* dosage (Guz et al., 1995; Fujitani et al., 2006).

Pancreatic progenitors

PDX1 is necessary for the maintenance of the pancreatic progenitor pool. Indeed, mice homozygote for a *Pdx1* null allele have a highly hypoplastic pancreas and die shortly after birth (Jonsson et al., 1994; Offield et al., 1996). The remnant pancreas comes from the dorsal pancreas and is composed of a poorly branched epithelium lacking acinar cells. In these mutants, GCG^+ cells form normally until E9.5, but are reduced at later stages, while the other endocrine cells are absent. PDX1 is not necessary for the specification of either dorsal or ventral buds, as their size is unchanged at E9.5 in *Pdx1* KOs (Offield et al., 1996). Indeed, the absence of PDX1 from E12.5 causes the same phenotype. PDX1 is later involved in the production of mature ducts (Hale et al., 2005). It is indeed able to bind and activate *Foxa2* and *Hnf1b* promoters, while it indirectly regulates *Onecut1* and *Sox9*. All of them are transcription factors important for the pancreatic progenitor and ductal identity (Oliver-Krasinski et al., 2009). In addition, the inactivation of *Pdx1* from E13.5 highlights a function in acinar differentiation as it results in a more mature and branched epithelium but with few and highly immature acini (Hale et al., 2005).

PDX1 also plays a role in endocrine cell differentiation. Hypomorph *Pdx1* homozygote pancreata have less endocrine progenitors and therefore a global decrease of endocrine cells. It is caused by the ability of PDX1 to activate the *Neurog3* promoter (Oliver-Krasinski et al., 2009).

Beta cells

PDX1 is also required for beta cell function. Beta-cell specific deletion of *Pdx1* causes diabetes in mice (Ahlgren et al., 1998). Moreover INS secretion is already impaired if beta cells only express half of the normal dose of PDX1 or express the hypomorphic *Pdx1* allele. Mice carrying these mutations thereby become glucose intolerant over time (Ahlgren et al., 1998; Oliver-Krasinski et al., 2009).

6.2.3.2 HNF1B

Hnf1b is already detected in the gut at E8.5 (Poll et al., 2006). It is expressed from E9.5 in the multipotent progenitors of the dorsal and ventral pancreas. After E13.5 it is restricted to the bipotent progenitors. At E18.5 and after birth, it remains in a subset of ductal cells (Maestro et al., 2003; Haumaitre et al., 2005). HNF1B plays several roles during development. Its deletion causes peri-implantation lethality due to its importance in visceral endoderm formation (Barbacci et al., 1999; Coffinier et al., 1999b). Specific *Hnf1b* deletion in kidneys causes cyst formation (Gresh et al., 2004). HNF1B is present from E9.5 in the mesonephros. It is subsequently present in the tubule epithelium but not in glomeruli. It is also necessary for liver organogenesis, where it starts to be expressed from E9.5 (Barbacci et al., 1999; Coffinier et al., 1999a; Coffinier et al., 2002).

Specification

Using tetraploid aggregation chimera to circumvent early lethality, it has been shown that HNF1B is important for pancreatic specification. In the mutants, the dorsal bud is smaller and the ventral does not form. In *Hnf1b* absence, *Onecut1*, one of its direct targets, is lost in the prospective regions of the pancreas, causing this specification defect (Haumaitre et al., 2005; Poll et al., 2006).

Pancreatic progenitors

HNF1B is important for maintaining the identity of the multipotent progenitors. The dorsal bud of the tetraploid complementation chimeras mentioned above fails to grow, and regress by E13.5. Before complete regression, pancreatic progenitors do not correctly express factors necessary for their function, *Ptf1a* and

Onecut1, while *Pdx1* is not affected. *Hnf1b* KOs fail to produce endocrine progenitors and subsequently endocrine cells (Haumaitre et al., 2005). Upon inactivation of HNF1B from E12.5 in the pancreatic epithelium, the defects are less severe, even though the pancreas is highly hypoplastic at birth, revealing later functions of HNF1B. The acinar cells fail to differentiate properly. *Hnf1b* mutant pancreata have a near complete loss of endocrine cells due to the failure to produce endocrine progenitors. Indeed HNF1B is able to activate the *Neurog3* promoter (De Vas et al., 2015).

Ductal cells

HNF1B also has a role in ductal homeostasis. If it is absent from E12.5, cysts start to form from E14.5. They are characterized by a reduction of ductal markers such as HNF6 and MUC1 but also the loss of primary cilia. Major genes involved in cystic diseases such as *Cys1*, *Pkhd1*, *Glis3*, *Bicc1*, *Pkd2* and *Pkd1* are dysregulated. Some of them are directly activated by HNF1B (De Vas et al., 2015). The pancreatic ductal cystic phenotype reminds of the kidney phenotype observed when *Hnf1b* is specifically deleted in kidneys. Cysts in different organs are discussed in depth from p 53. In *Hnf1b* kidney mutants, cysts appear from P0 and, cystic associated gene expression is also altered. However, contrary to the pancreatic deletion, *Pkd2* is downregulated and *Pkd1* is unchanged, suggesting that although HNF1B controls the kidney and pancreatic ductal homeostasis, its downstream effectors may vary between both organs (Gresh et al., 2004)

6.2.3.3 PTF1A

PTF1A is a bHLH transcription factor forming a heterooligomer. Its transcriptional activity depends on its different binding partners (Roux et al., 1989; Krapp et al., 1996; Beres et al., 2006; Masui et al., 2007). It is expressed from E8.5 in the prospective ventral pancreas and 0.25 days later in the prospective dorsal pancreas. PTF1A is expressed in the multipotent progenitors. From E12.5-E13.5, its expression is restricted to the distal tips. At the end of gestation PTF1A is expressed in the acinar cells (Hald et al., 2008).

Multipotent progenitors

PTF1A is important for the multipotent progenitor identity. Its deletion causes drastic dorsal pancreas hypoplasia while the ventral bud fails to grow. Fewer endocrine progenitors and subsequently endocrine cells are present in *Ptf1a* KO pancreata (Krapp et al., 1998; Kawaguchi et al., 2002; Burlison et al., 2008). PTF1A appears to strengthen a pancreas identity initially specified by PDX1 and possibly other genes. In the absence of PTF1A, the cells of the ventral bud, which forms, are incorporated into the duodenum (Kawaguchi et al., 2002; Burlison et al., 2008). In multipotent progenitors, PTF1A interacts with RBPJ, a transcription activator of the NOTCH signaling pathway, to induce gene expression (Masui et al., 2007). Together, they activate *Pdx1*, *Onecut1* and *Nkx6.1* (Thompson et al., 2012). Inhibition of PTF1A binding to RBPJ by point mutations causes the same phenotype as *Ptf1a* deletion, arguing that the early role of PTF1A involves RBPJ (Masui et al., 2007).

Pdx1 and Ptf1a epistasis

Pdx1 KO and *Ptf1a* KO have a similar phenotype *i. e.* hypoplasia. However, the *Pdx1* KO phenotype is more severe and double KOs for *Pdx1* and *Ptf1a* have the same phenotype than the single *Pdx1* KO (Burlison et al., 2008). Moreover, pancreas morphogenesis is rescued in animals expressing PDX1 under the promoter of *Ptf1a* (Kawaguchi et al., 2002). It argues that PDX1 acts upstream of PTF1A. However, a feedback loop does exist, since PTF1A is able to activate the *Pdx1* promoter. Moreover, PDX1 is not the only input promoting PTF1A expression, since *Ptf1a* is still expressed, albeit at lower levels in *Pdx1* KOs (Burlison et al., 2008; Thompson et al., 2012).

Acinar cells

Ptf1a KO pancreata do not develop any acinar compartment (Krapp et al., 1998). The switch between a multipotent pancreatic progenitor program to an acinar differentiation/function program is operated by swapping RBPJ for RBPJL (Beres et al., 2006). *Rbpj* is progressively down-regulated while *Rbpjl* is upregulated at the same time as PTF1A is restricted to the distal domain of the pancreatic epithelium. A

heterooligomer with RBPJL and PTF1a is able to activate acinar genes and RBPJL thus maintaining the acinar identity (Masui et al., 2007).

6.2.3.4 SOX9

SOX9 is expressed from E9.5 in the pancreatic buds. It is expressed in the multipotent progenitors, and thereafter, its expression is restricted to the bipotent progenitors by E15.5, as it becomes progressively excluded from the distal domain. While a subset of endocrine progenitors expresses SOX9, it is turned down as they differentiate into endocrine cells (Lynn et al., 2007; Seymour et al., 2007; Dubois et al., 2011).

Multipotent and bipotent progenitors

The absence of SOX9 during early pancreas development causes pancreatic hypoplasia. The remnant pancreas is cystic and fewer acini are present. Multipotent progenitor proliferation and survival are impaired, resulting in smaller buds at E11.5 (Seymour et al., 2007). Progenitors also lose their identity, and start to express liver markers (Seymour et al., 2012). *Sox9* KOs progenitors lose the expression of PDX1 while ONECUT1 and HNF1B remain unaffected, even though there is some *in vitro* evidence that they are SOX9 direct targets (Lynn et al., 2007; Dubois et al., 2011). In *Sox9* KOs, endocrine cells are nearly absent due to the lack of endocrine progenitor differentiation (Seymour et al., 2007; Shih et al., 2012). Indeed, SOX9 is able to activate *Neurog3* promoter, promoting, thus, endocrine progenitor production (Lee et al., 2001; Seymour et al., 2008). In support of this idea, all endocrine progenitors come from $SOX9^{+}$ cells in mosaic pancreata formed of WT and *Sox9* KO cells (Shih et al., 2012). In *Sox9* heterozygotes, endocrine progenitors and their endocrine cell progeny are reduced by half, leading to glucose intolerance in the adult (Lynn et al., 2007; Seymour et al., 2008; Dubois et al., 2011).

Ductal cells

Like HNF1B, SOX9 is important for ductal cell identity. Ducts are enlarged and later become cystic in pancreata in which *Sox9* is deleted from E12.5 (Dubois et al., 2011; Shih et al., 2012). The ductal cells fail to express key ductal markers such as PKD2. They also have less primary cilia (Shih et al., 2012). HNF1B

expression is not affected in *Sox9* KO pancreata and *vice versa*. Therefore, they likely function in parallel pathways (Shih et al., 2012; De Vas et al., 2015).

6.2.3.5 ONECUT1

ONECUT1 is a transcription factor containing a single cut domain and a homeodomain. It was first identified in the liver, where it is expressed from E8.5 (Lemaigre et al., 1996; Jacquemin et al., 2003a). During pancreas organogenesis, it is expressed from E8.5 in the prospective dorsal and ventral pancreas, before PDX1 starts to be expressed. While before E13.5 it is expressed in the multipotent progenitors, it is then restricted to the bipotent progenitors and later to the ducts. While endocrine progenitors express ONECUT1, like HNF1B, it declines when they differentiate toward endocrine cells (Jacquemin et al., 2003a; Zhang et al., 2009; Pierreux et al., 2010).

Specification

ONECUT1 is important for pancreatic specification. It enables the expression of PDX1, one of its direct targets. In its absence, fewer cells express PDX1 in the prospective ventral and dorsal pancreas and therefore commit to a pancreatic fate, even though other specification markers, such as *Foxa2*, are unaffected. *Onecut1* KO pancreata are consequently hypoplastic (Jacquemin et al., 2003a).

Bipotent progenitors

Early endocrine cells expressing GCG do not require ONECUT1 but it is important for the commitment of pancreatic progenitors towards all endocrine progenitors at later stages. After the secondary transition has started, few endocrine progenitors with low levels of *Neurog3* are produced as it is a direct target of ONECUT1. This defect causes a nearly complete loss of endocrine cells (Jacquemin et al., 2000; Zhang et al., 2009).

Ductal cells

In the absence of ONECUT1, ducts become cystic from E15.5 (see also p 64). Cysts may be lined by a multilayer epithelium instead of a cuboidal epithelium, and endocrine cells can also be detected in this epithelium (Pierreux et al., 2006; Zhang et al., 2009). Aberrant proliferation and disturbed WNT signaling, which are associated with cyst formation, are not detected (Pierreux et al., 2006). Nevertheless, primary cilia, whose lack or malfunction can cause cysts, are absent. HNF1B expression is also altered. *Pkhd1*, and *Cyst1*, two cyst-associated genes, are downregulated while *Pkd1*, *Pkd2* and *Ift88* are unaffected, suggesting that SOX9, HNF1B, and ONECUT1 regulate ductal homeostasis in parallel (Maestro et al., 2003; Pierreux et al., 2006; Shih et al., 2012; De Vas et al., 2015).

ONECUT2

Onecut2 is a paralog of *Onecut1* (Jacquemin et al., 2003b). It starts to be expressed after ONECUT1 in the prospective liver and pancreatic epithelium (Jacquemin et al., 2003b; Pierreux et al., 2004). In the liver, they act redundantly (Clotman et al., 2005). In the pancreas, *Onecut2* deletion does not lead to an obvious phenotype. Moreover, ONECUT2 does not compensate for *Onecut1* deletion as the phenotype of *Onecut1*; *Onecut2* double KOs is only slightly enhanced as compared to *Onecut1* KOs. However, *in vitro* studies have showed that ONECUT2 is able to activate the *Neurog3* promoter (Vanhorenbeeck et al., 2007).

6.2.3.6 FOXA2

FOXA2 is already expressed in the definitive endoderm (Ang et al., 1993). It continue to be expressed in all cells of the developing and adult pancreatic epithelium (Ahlgren et al., 1996; Sund et al., 2001; Besnard et al., 2004; Lee et al., 2005). *Foxa2* is also expressed in the node, and its deletion precludes node and, therefore, notochord formation. *Foxa2* KO embryos die around E10 (Ang et al., 1993; Ang and Rossant, 1994; Weinstein et al., 1994)

Pancreatic progenitors

Although endoderm specific deletions of *Foxa2* or *Foxa1* do not cause pancreatic morphogenesis defects, the double deletion of *Foxa2* and *Foxa1* in the pancreatic epithelium causes a similar phenotype as *Pdx1* KOs (Kaestner et al., 1999; Lee et al., 2005; Gao et al., 2008). The pancreas is hypoplastic and cystic. The remnant epithelium lacks endocrine and acinar cells. Furthermore, PDX1 is absent of the pancreatic epithelium already at E10.5 arguing that FOXA2 and FOXA1 are major activators of the *Pdx1* promoter (Gao et al., 2008). FOXA2 is also able to induce *Sox9* expression while *Foxa2* is activated by SOX9, PDX1, and HFN1B (Lynn et al., 2007; Oliver-Krasinski et al., 2009). They therefore form a feedforward loop to maintain progenitor identity (Fig. 4). In addition, FOXA2 is able to activate *Neurog3* promoter. It can also synergize with NEUROG3 to promote *Neurog3* expression (Lee et al., 2001; Ejarque et al., 2013).

Endocrine cells

Endoderm deletion of *Foxa2* causes a specific loss of alpha cells (Lee et al., 2005). Nevertheless, FOXA2 is necessary to maintain the beta cell identity. Beta cell deletion of *Foxa2* causes hypoglycemia due to hyperinsulinemia. FOXA2 activates *Pdx1* expression in beta cells, as well as the expression of *Kcjn11* and *Abcc8*, two genes involved in insulin release regulation (Wu et al., 1997; Sund et al., 2001; Lee et al., 2002; Lantz et al., 2004).

6.2.3.7 GLIS3

GLIS3 is a C_2H_2 krüppel-like zinc finger transcription factor (Kim et al., 2003). It has a role in the kidney homeostasis as its absence causes cyst formation (Kang et al., 2009a). It is expressed in the pancreatic epithelium from E11.5. It is restricted to the bipotent progenitors. At birth it is expressed in beta cells as well as in the ducts (Kang et al., 2009b).

Bipotent progenitors

Bipotent progenitors do not seem to be affected by *Glis3* deletion. However, in its absence, the commitment toward endocrine progenitor fate is affected. *Glis3* KO pancreata thus have less endocrine cells. GLIS3

promotes endocrine progenitor differentiation by activating *Neurog3* promoter either alone or synergistically with ONECUT1 or FOX2A (Kang et al., 2009b; Yang et al., 2011; Kim et al., 2012).

Beta cells

GLIS3 is also able to activate *Ins* promoter. The more extensive reduction of beta cells as compared to the other endocrine cells in *Glis3* KOs may be linked to a lower INS production, and therefore, the inability to detect beta cells (Kang et al., 2009b; ZeRuth et al., 2013).

Ductal cells

Glis3 KOs also develop pancreatic cysts. They are associated with less primary cilia in the cystic ducts but not in the non-cystic ducts of Glis3 KOs, arguing for a secondary effect rather than the initial cause of cyst formation (Kang et al., 2009b).

6.2.3.8 NKX6.1 and NKX6.2

NKX6.1 and NKX6.2 are expressed in the multipotent progenitors at E10.5 and E12.5. At E14.5 NKX6.1 is excluded from the distal domain while NKX6.2 becomes restricted to the distal domain. Contrary to NKX6.2, NKX6.1 is also expressed in the endocrine progenitors and some cells differentiating toward endocrine cells (Sander et al., 2000; Henseleit et al., 2005). At E18.5 and in the adult, NKX6.1 is expressed in the beta cells (Sander et al., 2000; Nelson et al., 2007).

Multipotent and bipotent progenitors

NKX6.1 and NKX6.2 act redundantly in the multipotent progenitors. Inactivation of both *Nkx6* factors causes a drastic decrease of alpha and beta cells while the other endocrine cells are not affected (Henseleit et al., 2005). This is due to a reduction of endocrine progenitors at E10.5 and E12.5 while their number is normal afterward (Schaffer et al., 2010). The deficient multipotent progenitors express more *Ptf1a*, and are more prone to differentiate into acinar progenitors, leading to an increase of the acinar compartment after the proximal-distal domains have been segregated. Indeed the overexpression of PTF1A converts the pancreatic

epithelium into acinar cells at E14.5. The overexpression of NKX6.1 in the pancreatic epithelium has the opposite effect, the acinar compartment is reduced and more cells adopt an endocrine fate (Schaffer et al., 2010).

Differentiation toward endocrine lineage and beta cells

Deletion of *Nkx6.1* in endocrine progenitors causes beta cell underrepresentation in the islet. Conversely, overexpression of *Nkx6.1* in NEUROG3^{+} cells has the opposite effect. As no cell death or proliferation defects in beta cells are observed, it suggests the importance of NKX6.1 for beta cell production. Indeed NKX6.1 is able to directly inhibit the expression of *Arx*, a transcription factor important for alpha cell production. NKX6.1 is also important for maintaining the beta cell identity as beta cells convert into SST-expressing cells in the absence of *Nkx6.1* (Schaffer et al., 2013).

6.2.3.9 NEUROG3

NEUROG3 is a bHLH transcription factor expressed in cells scattered in the pancreatic epithelium (Sommer et al., 1996). The pancreatic expression pattern of NEUROG3 is biphasic. It is first observed in a few cells from E8.25. NEUROG3^{+} cells increase until E10.5. At E11.25, no more cells express NEUROG3. Cells expressing NEUROG3 reappear at E12. Their number peaks at E15.5 and decreases thereafter. At E18.5, only a few NEUROG3^{+} cells are still in the ducts or in their vicinity (Schwitzgebel et al., 2000; Villasenor et al., 2008). NEUROG3 is also detected at low level in the islets after birth (Wang, S. et al., 2009).

Endocrine progenitors

NEUROG3 is a major regulator of endocrine progenitors, and is used to identify them. It is the only gene absolutely required for endocrine cell generation, as no endocrine cells or factors associated with endocrine differentiation are present in *Neurog3* KO pancreata (Gradwohl et al., 2000). It is sufficient to induce endocrine cell differentiation, as its overexpression in pancreatic cells differentiates them all into endocrine cell (Apelqvist et al., 1999; Schwitzgebel et al., 2000). It is noteworthy that, contrary to mice, NEUROG3 is not absolutely required for endocrine cell differentiation in humans and in zebrafish (Flasse et al., 2013;

Rubio-Cabezas et al., 2014). It is to put in line with the presence of a few GCG^+ cells in *Neurog3* KO pancreata before E15.5 (Wang, S. et al., 2008).

Several transcription factors, *i. e.* PDX1, SOX9, HNF1B, ONECUT1, GLIS3 HNF1A, ONECUT2, and FOXA2, have been identified as inducers of *Neurog3* expression. In addition, NEUROG3 itself is able to induce its own expression (Jacquemin et al., 2000; Lee et al., 2001; Lynn et al., 2007; Vanhorenbeeck et al., 2007; Yang et al., 2011; Ejarque et al., 2013). *Neurog3* is repressed by the transcription factor HES1 (Jensen et al., 2000b). After NEUROG3 expression starts, it represses *Sox9* expression (Magenheim et al., 2011a; Shih et al., 2013). On the contrary, ONECUT1 is required for the differentiation of $NEUROG3^+$ cells towards the endocrine lineage, as less endocrine cells are observed when *Onecut1* is deleted in $NEUROG3^+$ cells (Zhang et al., 2009). NEUROG3 expression is also reinforced by endocrine differentiation factors. MYT1 and NKX2.2 are able to promote its expression, although it is not clear if they are able to directly activate *Neurog3*. Moreover, INSM1 is able to promote the splicing of *Neurog3* into its coding mRNA (Osipovich et al., 2014).

The expression level of NEUROG3 is critical to elicit the endocrine differentiation program. In *Neurog3* heterozygote animals the amount of NEUROG3 per cell is reduced, and the number of endocrine cells is also reduced, while more cells are prompted to commit towards an endocrine fate (Wang et al., 2010). The *Neurog3*-expressing cells that fail to further differentiate into endocrine cells are redirected toward an acinar or ductal fate (Schonhoff, S. E. et al., 2004; Wang et al., 2010). The ability to adopt one or the other depends on the potency of the cells of origin. Before E12.5, the endocrine progenitors arise from multipotent progenitors, and have the capacity to be redirected toward an acinar fate. Thereafter, they can only adopt a ductal fate (Beucher et al., 2012).

Ductal homeostasis

$NEUROG3^+$ cells feedback to the surrounding pancreatic progenitors to maintain ductal homeostasis. In *Neurog3* KOs, all cells activating the *Neurog3* promoter fail to become endocrine. The majority of these cells stays in the pancreatic proximal domain, and becomes ductal cells. They accumulate in the ducts

causing the formation of a poorly branched and dilated network (Wang et al., 2010; Magenheim et al., 2011a).

Endocrine cells

NEUROG3 has also been involved in endocrine cell function in the adult mouse. Indeed, deletion of *Neurog3* in beta cells impairs their function. Mutant mice have a higher fasting glucose and an impaired glucose tolerance. Mutant pancreata express less INS, MYT1, NEUROD1, PAX4, and PDX1 (Wang, S. et al., 2009).

6.2.3.10 Final steps toward endocrine cells

For the subsequent pancreatic differentiation steps, the hierarchy of the transcription factors involved in the completion of the endocrine differentiation program is difficult to establish. Nevertheless, the loss of ISL1, ARX, PAX4, PAX6, and NEUROD1 expression upon *Neurog3* deletion shows that they function downstream (Gradwohl et al., 2000; Collombat et al., 2003; Mastracci et al., 2011). The time sequence of gene expression is also informative. NEUROG3 is turned off after 24h of expression. It also has been reported that it only takes 10 hours for a cell to become endocrine after *Neurog3* has been switched off (Beucher et al., 2012). A subset of $NEUROG3^{+}$ cells expresses NEUROD1, INSM1, MYT1, and PAX4 These genes are directly activated by NEUROG3 (Huang et al., 2000; Jensen et al., 2000a; Schwitzgebel et al., 2000; Smith et al., 2003; Mellitzer et al., 2004; Wang et al., 2004; Wang et al., 2007). PAX6 is also expressed in a subpopulation of $NEUROG3^{+}$ cells even though it has not been reported as a direct NEUROG3 target (Maestro et al., 2003). On the contrary, no $NEUROG3^{+}$ cells express ISL1 (Schwitzgebel et al., 2000).

However, other factors such as NKX2.2 and NKX6.1 are first expressed in the multipotent or bipotent progenitors. They continue to be expressed in the cells adopting an endocrine cell fate, indicating their multiple roles during pancreas organogenesis (Sander et al., 1997; Sussel et al., 1998).

It is difficult to disentangle the function of each factor as they may play several roles in a redundant fashion. Moreover, no marker has been identified to highlight hierarchical precursors enabling the distinction between different populations. Nevertheless, single and compound KO analyses have provided cues to the mechanisms behind endocrine cell differentiation (Fig. 5).

The absence of NEUROD1, PAX6, or ISL1 causes a global and drastic reduction of endocrine cells (Ahlgren et al., 1997; Naya et al., 1997). NEUROD1 is also important for beta cell maturity while ISL1 is important for endocrine cell proliferation and survival (Du et al., 2009; Gu et al., 2010). *Insm1* deletion also causes a global endocrine cell reduction. *Insm1* KO cells accumulate in an immature state without expressing hormones (Gierl et al., 2006). Conversely, *Myt1* deletion does not cause a drastic endocrine cell decrease but endocrine cells are polyhormonal. The effect of the loss of function of *Myt1* is surprising, as its ectopic expression is sufficient to induce *Neurog3* expression and produce GCG^+ cells (Wang et al., 2007; Wang, S. et al., 2008).

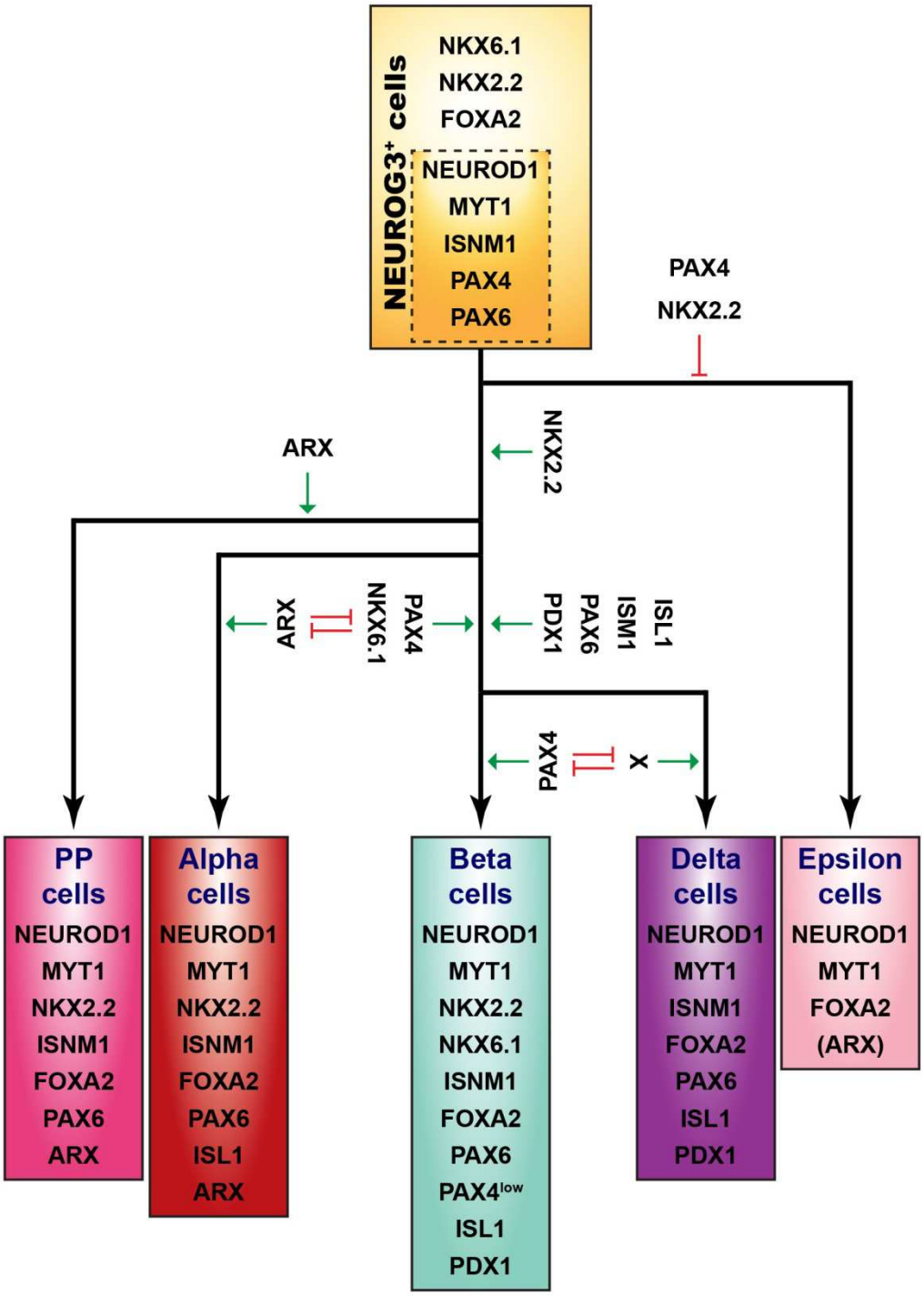

Fig. 5: endocrine progenitor differentiation toward endocrine cells.

Endocrine progenitor differentiation towards the different endocrine cell types is indicated by black arrows. Transcription factors present in the cells are contained in the color boxes referring to a given cell type (same color code as in Fig. 2). Some transcription factors (dashed box) are present only in a subset of the endocrine progenitors (NEUROG3^{+} cells). Fewer factors are present in epsilon cells due to poor description of these cells.

Green arrows indicate factors promoting a differentiation path while red arrows indicate factors repressing a differentiation path. Arrow length is not scaled with the differentiation duration. X represents unknown factors.

The absence of other transcription factors causes the decrease of specific populations, usually compensated by an increase in another endocrine cell type or the apparition of immature cells, suggesting bifurcations in the differentiation path. As previously mentioned, the deletion of *Nkx6.1* causes a beta cell decrease. The deletion of *Nkx2.2* causes beta, alpha and PP cell reductions with the apparition of GHR^+ cells expressing alpha and beta cell markers (Sussel et al., 1998; Kordowich et al., 2011; Schaffer et al., 2013). The absence of PAX4 leads to a beta and delta cell decrease with a GCG^+ GHR^+ cell increase (Sosa-Pineda et al., 1997; Collombat et al., 2005). Conversely, in *Arx* KO pancreata, alpha cells are decreased, and the delta cell population is increased. The effect of *Arx* deletion on the beta cell mass is controversial, as the beta cells are either unaffected or increased by the loss of *Arx* (Collombat et al., 2003; Kordowich et al., 2011). The opposing effects of the deletion of *Pax4* and of *Arx* are explained by the ability of the factors to repress each other (Collombat et al., 2003; Collombat et al., 2005). Ectopic expression of *Pax4* converts endocrine cells into beta cells, while ectopic expression of *Arx* causes beta and delta cell conversion into alpha and PP cells (Collombat et al., 2007; Collombat et al., 2009). PAX4 also directly represses *Ghr* expression (Fig. 5) (Wang, Q. et al., 2008).

A second layer of information is added by the study of double KO embryos. Double deletion of *Arx* and *Pax4* causes a drastic alpha and beta cell decrease. The cells adopt an immature delta cell fate coexpressing PPY (Collombat et al., 2005). Conjoint deletion of *Arx* and *Nkx2.2* causes an absence of beta and alpha cells. They are replaced by GHR^+ SST^+ cells also expressing alpha and beta cell markers (Kordowich et al., 2011). These studies suggest that cells adopt an epsilon cell fate in the absence of NKX2.2. Moreover, PAX4 and ARX antagonize each other. If the cell expresses ARX, the cell becomes either PPY or alpha, maybe depending on the stage of development. Otherwise, in the presence of PAX4, the cell adopts a beta-delta common precursor fate. The cell further differentiates toward a beta cell unless PAX4 is repressed (Fig. 5).

6.2.4 Signaling pathways involved in pancreas development

The organogenesis of the pancreas is coordinated with the development of the neighbouring organs. The proliferation and differentiation of the pancreatic cells also depend on the other cell types present in the

developing pancreas at a given time point. These interactions are mediated by extracellular signals, which activate several signaling pathways. As signaling pathways often interact, the outcome of an input can depend on other signaling cues, on the cell type that receives it, and the stage of development. Signaling pathways may also act redundantly making them more difficult to decipher.

6.2.4.1 NOTCH signaling regulates different aspects of pancreas development

This pathway is extremely important to balance pancreas expansion and differentiation. Signal sending cells express NOTCH ligands, DLL1 to DLL4, JAG1, and JAG2. The signal receiving cells express NOTCH receptors, NOTCH1 to NOTCH4. The ligands bind to NOTCH receptors, and, thereby, trigger a change in their conformation. It is followed by a series of cleavages of NOTCH receptor. The latter is mediated by gamma secretase. The intracellular domain of NOTCH is thereby released in the cytoplasm. NOTCH intracellular domain is exported to the nucleus, and associates with cofactors, such as RBPJ and MAML1. They then activate gene expression. Several NOTCH targets are transcriptional repressors of the HES family. HES family factors repress among others the expression of NOTCH ligands, forcing the cell into the dichotomic choice of being NOTCH-sending or NOTCH-receiving cell. This process of cell segregation is called lateral or trans- inhibition. In the absence of NOTCH, RBPJ interacts with co-repressors, and inhibits transcription (Fig. 6) (reviewed in Kandachar and Roegiers, 2012). Moreover, ligand-independent activation of NOTCH has been observed in *Drosophilae*. This mode of activation requires the endocytosis of NOTCH followed by its intracellular activation (reviewed in Hori et al., 2012).

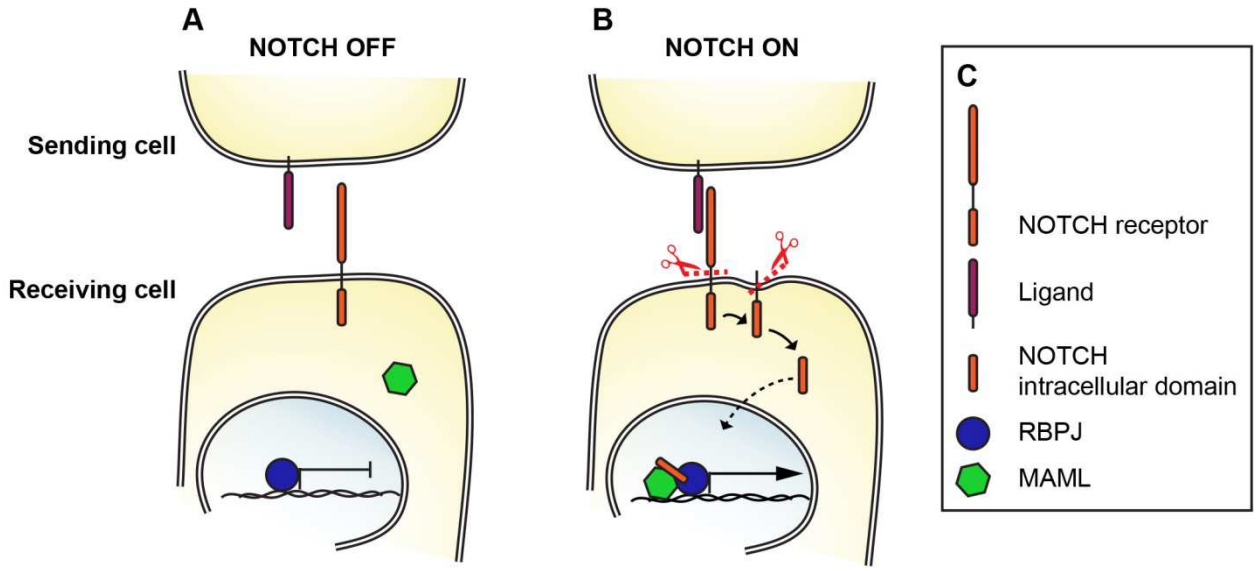

Fig. 6: Notch signaling pathway

(A) In absence of binding of NOTCH ligand to NOTCH receptor (NOTCH OFF), target genes of the NOTCH signaling pathway are repressed.

(B) When NOTCH ligand binds its receptor (NOTCH ON), the latter is cleaved and its intracellular domain is released in the cytoplasm. It migrates to the nucleus where it activates gene expression, such as *Hes1* with its cofactors such as MAML and RBPJ

(C) Legend of the different proteins depicted in the cartoons.

In the pancreas, the expression pattern of NOTCH signaling components is highly dynamic, highlighting the complexity of the pathway. The NOTCH ligand, *Dll1*, is first detected in a few cells of the dorsal pancreas at E9. Half a day later, it is expressed in a salt and pepper manner in the dorsal bud. At E10.5, *Dll1* starts to be expressed in the ventral bud (Ahnfelt-Rønne et al., 2012). *Dll1* expression then goes down but it is still present in acinar cells after E13.5 (Apelqvist et al., 1999). JAG1 becomes the major NOTCH ligand expressed in the pancreatic epithelium from E12.5. However, its expression pattern is unclear. It has been found to be progressively restricted to the ducts and beta cells at birth (Jensen et al., 2000b; Golson et al., 2009). On the contrary, other studies found that *Jag1* is detected in the endothelial cells from E15.5, (Lammert et al., 2000; Norgaard et al., 2003). Finally, Apelqvist and colleges reported that *Jag1* is present in the acini and not the trunk at E13.5 (Apelqvist et al., 1999).

NOTCH intracellular domain is already present in a few pancreatic cells at E9.0 indicating that the NOTCH signaling pathway is active at that stage (Jensen et al., 2000b), although *Notch1* and *Notch2* are first reported at E9.5 in a salt and paper manner (Apelqvist et al., 1999). They are broadly expressed at E10.5 in the pancreatic epithelium (Lammert et al., 2000). From E13.5, *Notch1* and *Notch2* are present in the progenitors which lined the ducts (Apelqvist et al., 1999).On the contrary, *Notch3* and *Notch4* are present in the surrounding mesenchyme at E10.5. Thereafter, they are localized in the endothelial cells (Lammert et al., 2000).

HES1, a NOTCH target gene, is expressed from E9.0 in the dorsal bud. HES1 colocalized with *Dll1* and PTF1A at E10.5. It is also present in the surrounding mesenchyme (Lammert et al., 2000; Ahnfelt-Rønne et al., 2012). At E15.5, HES1 is expressed in the bipotent progenitors, but is excluded from the endocrine progenitors (Shih et al., 2013). At E18.5, HES1 is only expressed in scattered ductal cells (Norgaard et al., 2003; Kopinke et al., 2011). However, Apelqvist and colleagues found *Hes1* in pancreatic tips at E13.5 (Apelqvist et al., 1999). Indeed, $HES1^{+}$ cells are still able to give rise to acinar cells at E15.5 (Kopinke et al., 2011).

Maintenance of progenitor identity by NOTCH signaling

NOTCH signaling is required to maintain the identity of the multipotent progenitors and, subsequently, of the bipotent progenitors. Indeed, inactivation of the NOTCH signaling pathway leads to the precocious differentiation of the multipotent progenitors into endocrine cells (Fig. 7) (Apelqvist et al., 1999; Jensen et al., 2000b; Ahnfelt-Rønne et al., 2012).

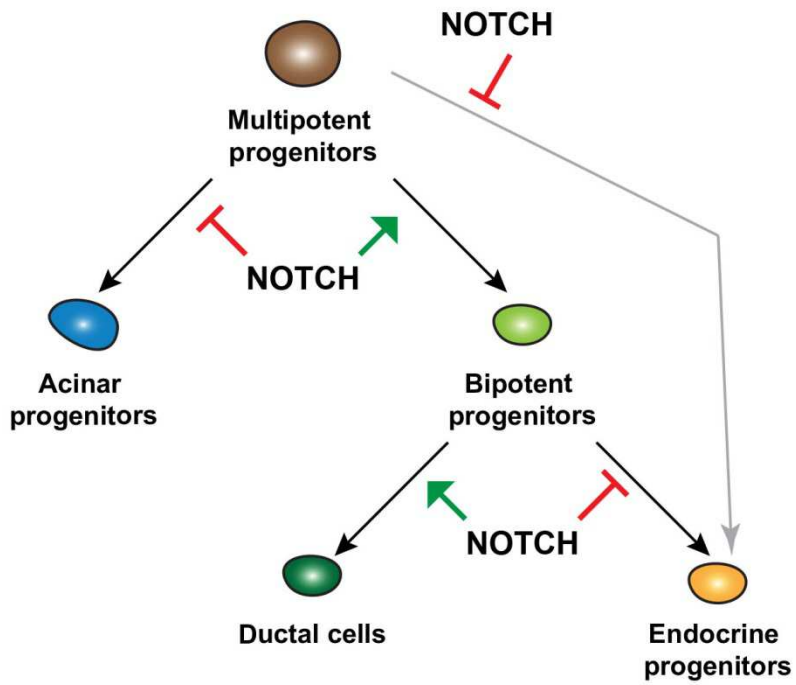

Fig. 7: Different roles of the Notch pathway during pancreas organogenesis
NOTCH signaling inhibits endocrine progenitor (orange) differentiation in multipotent progenitors (brown). During the tip trunk domain specification, around E12.5, NOTCH signaling inhibits acinar progenitor (blue) fate while it promotes bipotent progenitor (light green) fate. Thereafter, it inhibits endocrine progenitor differentiation and promotes ductal identity (dark green).

On the contrary, forced activation of NOTCH, by overexpressing its intracellular domain, causes the abrogation of endocrine cell differentiation. The epithelium remains immature. For example, it maintains PDX1 expression at late stages of development. It also reduces the ductal network branching and increases ductal cell proliferation (Hald et al., 2003; Murtaugh et al., 2003; Schaffer et al., 2010). Moreover, after the secondary transition has started, high NOTCH signaling induces both the expression of HES1 and SOX9. High NOTCH signaling therefore maintains the bipotent progenitor state, and precludes the differentiation toward endocrine cells. The cells expressing both HES1 and SOX9 then adopt a ductal fate (Fig. 7) (Shih et al., 2012)

Cis inhibition versus lateral inhibition

It is believed that lateral inhibition by NOTCH signaling is used to control the number of cells committing to the endocrine lineage (Apelqvist et al., 1999). It is hypothesized that when a cell starts to express

NEUROG3, it induces the expression of NOTCH ligand DLL1 (Shih et al., 2012). Then, NEUROG3^{+} cells signal to the neighbouring cells expressing NOTCH receptors. The receiving cells induce HES1 expression, and, thereby, inhibit the expression of *Neurog3*. Therefore the receiving cells maintain their progenitor identity (Lee et al., 2001). The hypothesis is mainly supported by the absence of HES1 expression in endocrine progenitors as well as the presence of DLL1 in these cells (Apelqvist et al., 1999; Shih et al., 2012). It is also based on the KO phenotypes of the different NOTCH components and the ectopic activation of NOTCH signaling (*cf.* above).

However, a recent study challenges the lateral inhibition mechanism (Ahnfelt-Rønne et al., 2012). DLL1 is initially expressed in all multipotent progenitors and not only in NEUROG3^{+} cells. Afterwards, it is also expressed in more cells than just NEUROG3^{+} cells. *Dll1* is induced by PTF1A and by HES1. If DLL1 was simply driving lateral inhibition, more endocrine cells would be expected in *Dll1* KOs. However, although *Dll1* KOs have more endocrine progenitor cells at E9, they have less at E9.5, contrary to other models of NOTCH signaling inactivation. This suggests that DLL1 plays an important role in endocrine progenitor production from E9.5. Consequently, a new picture emerges. In this model, NEUROG3 induces high levels of DLL1. High DLL1 then inhibits NOTCH receptors that are present in the same cell and not the neighbouring cells. Thereby the inhibition promotes endocrine differentiation program in a cell autonomous manner. This mechanism of inhibition is called cis-inhibition (Ahnfelt-Rønne et al., 2012).

Segregation of the proximal and distal domains by NOTCH signaling

The NOTCH pathway also has an important role in defining the boundaries between distal (acinar) and proximal (bipotent progenitors) domains. NOTCH inhibition models have an impaired acinar compartment due to the drastic and precocious endocrine differentiation, while NOTCH activation models also have defective or no acinar compartment (Apelqvist et al., 1999; Jensen et al., 2000b; Hald et al., 2003; Murtaugh et al., 2003). Two recent studies better decipher this role by studying the effects of NOTCH signaling impairment at later stages. Deletion of *Mib1*, a positive regulator of NOTCH signaling, causes a loss of beta cells and ductal cells, while the acinar compartment is increased. It is associated with an increase of the

NKX6.1$^-$ PTF1A$^+$ cell population, corresponding to the acinar or distal domain, at the expense of the NKX6.1$^+$ PTF1A$^-$ cells, which correspond to the bipotent progenitors, explaining why no endocrine progenitors or endocrine cells are generated at later stages (Horn et al., 2012). The imbalance between NKX6.1$^-$ PTF1A$^+$ cells and NKX6.1$^+$ PTF1A$^-$ cells was also observed in *Hes1* KOs and a model of ectopic expression of dominant negative *Maml1* (Horn et al., 2012). Upon NOTCH activation, the converse was seen. The whole pancreatic epithelium continued to express NKX6.1 at late stages, while it was devoid of PTF1A, even though HES1 is necessary for PTF1A expression at E9.5 (Schaffer et al., 2010; Ahnfelt-Rønne et al., 2012). It has thus been proposed that, in the absence of Notch signaling, multipotent progenitors adopt an acinar cell fate or distal domain fate (Horn et al., 2012).

The case of RBPJ, the cofactor of NOTCH intracellular domain

Contrary to other NOTCH inhibition models, *Rbpj* KOs have less endocrine cells. They also harbor no acinar cells at late stages and immature ducts. Depending of the promoter used to drive the Cre recombinase that delete *Rbpj* locus, *Rbpj* KO pancreata may recover (Fujikura et al., 2006; Fujikura et al., 2007). The *Rbpj* KO phenotype is similar to *Ptf1a* KOs and could be explained by the interaction between PTF1A and RBPJ in multipotent progenitors (Kawaguchi et al., 2002; Masui et al., 2007; Burlison et al., 2008).

6.2.4.2 FGF signaling promotes early pancreatic progenitor growth and identity

FGF signaling is also relevant to pancreas development. FGF ligands bind to FGFR, a family of tyrosine kinase receptors. They then activate different downstream signaling pathways such as the MAPK pathway, AKT pathway or PKC pathway (reviewed in Dorey and Amaya, 2010). Although FGF signaling plays an important role in pancreas development, little is known about its downstream effectors due to their redundancy.

FGF10 is expressed in the mesenchyme surrounding the pancreatic epithelium from E9.5. At E11.5, it is restricted to the mesenchyme between the stomach and the dorsal pancreas (Bhushan et al., 2001). Other FGF ligands have been detected by PCR but specific information on their expression pattern in different cell

types is scarce (Dichmann et al., 2003). FGFR2 is expressed in the pancreatic epithelium from E9.5 to E15.5 (Hart et al., 2003). *Fgfr4* and other *Fgf* receptors are also expressed in the pancreas (Dichmann et al., 2003; De Vas et al., 2015).

Mesenchymal-derived FGF10 promotes pancreas bud expansion. Indeed, deletion of either *Fgf10* or *Fgfr2* causes pancreatic hypoplasia due to a proliferation defect. The effect on endocrine or acinar differentiation is less clear, showing little impact in the case of *Fgfr2* KOs or a drastic reduction for *Fgf10* KOs, suggesting redundancy with other receptors (Bhushan et al., 2001; Pulkinnen et al., 2003). The loss of endocrine and acinar differentiation is associated with a conversion of the multipotent progenitors to a hepatic progenitor fate (Seymour et al., 2012). Conversely, when FGF10 is overexpressed, the pancreatic size is increased. The pancreata are also devoid of endocrine and acinar cells. Even at late stages, the pancreatic epithelial cells co-express multipotent progenitor markers including SOX9, PDX1, PTF1A, NKX6.1, and ONECUT1. NOTCH signaling is also upregulated (Hart et al., 2003; Norgaard et al., 2003; Kobberup et al., 2010). The inhibition of the ectopic expression of *Fgf10* at E13.5 rescues the endocrine cell production. However, the endocrine cell production is not rescued after E15.5, suggesting a loss of endocrine commitment after E15.5 upon FGF10 expression. The acinar compartment is rescued whenever the ectopic FGF10 expression is inhibited (Kobberup et al., 2010). Overexpression of *Fgf4* causes a similar phenotype. Although this FGF is not expressed in the pancreas, it may trigger the same response (Dichmann et al., 2003).

Interplay between transcription factors and Fgf signaling

The hypoplasia observed in *Hnf1b* KO pancreata has been associated with *Fgfr4* downregulation, although the role of Fgfr4 in the pancreas is unexplored. However, HNF1B is able to bind the *Fgfr4* promoter in the developing pancreas, suggestion a role of the latter in pancreas organogenesis (De Vas et al., 2015). Multipotent progenitors devoid of SOX9 adopt a liver fate, which is also observed in *Fgf10* KOs. It may be due to the ability of SOX9 to regulate FGFR2 (Seymour et al., 2012). Since both HNF1B and SOX9 are expressed in multipotent progenitors, this control may ensure that the progenitor cells respond to mesenchymal FGF10.

6.2.4.3 Role of canonical and non-canonical WNT signaling during pancreas development

Although there is evidence for the importance of several WNT signaling pathways in the pancreas, their activity remains quite obscure. WNT ligands can trigger different intracellular pathways depending on the type of WNTs and the components expressed in the receiving cell. The most studied is the canonical signaling pathway. In brief, in the absence of WNT ligand, CTNNB1, also called β-catenin, is phosphorylated by GSK3B, which is stabilized by APC and AXIN2. This phosphorylation leads to the degradation of CTNNB1 by the proteasome. When WNT ligands bind to the FZD receptor and the LRP5/6 co-receptor, it leads to the recruitment of DVL. DVL destabilizes the CTNNB1 - APC - AXIN2 - GSK3B complex, releasing CTNNB1. CTNNB1 migrates to the nucleus and activates transcription in the presence of cofactors such as TCF7 or LEF1. In the absence of CTNNB1, these cofactors are associated with repressors (Fig. 8) (reviewed in Niehrs, 2012).

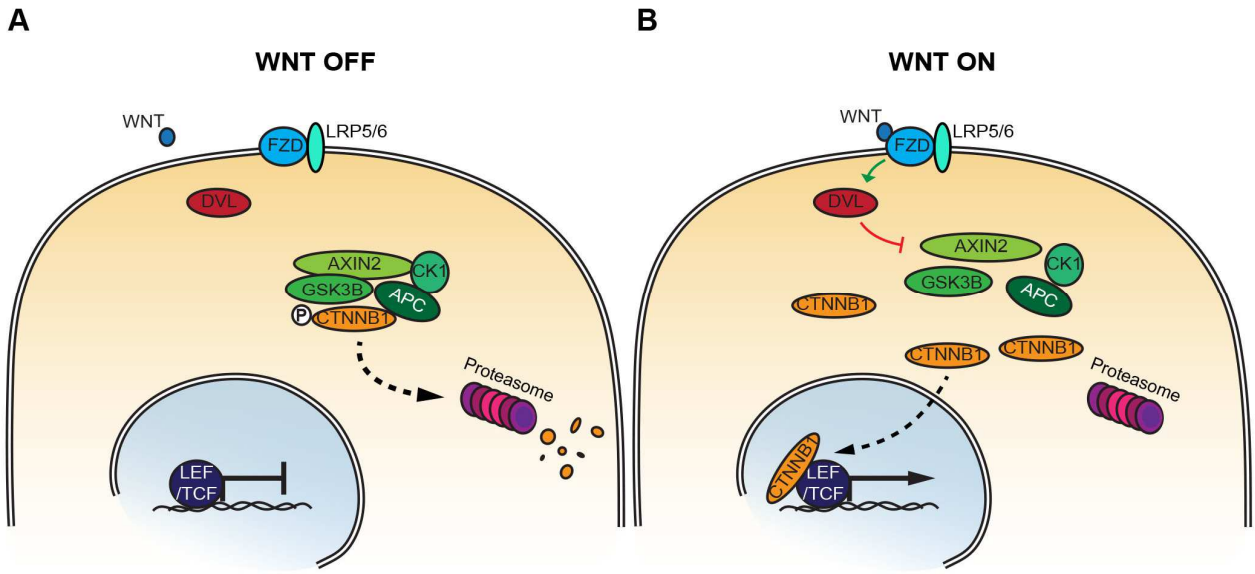

Fig. 8: canonical WNT signaling

(A) In absence of WNT, CTNNB1 is phosphorylated by the GSK3B complex and directed for degradation by the proteasome. Target genes are repressed by TCF or LEF.

(B) When WNTs binds to FZD, DVL is recruited and destabilizes GSK3B complex leading to the release and accumulation of CTNNB1. CTNNB1 is translocated to the nucleus, and activates gene expression together with the cofactors, TCF and LEF.

Non-canonical WNT signaling is induced by the binding of non-canonical WNT ligands to non-canonical FZD receptors. These FZD can also interact with VANGL receptors on neighbouring cells, an interaction that is stabilized by transmembrane proteins, CELSR1, CELSR2 or CELSR3. FZD then elicits a response that can either be transcriptional via the activation of MAPK8, also called JNK, or structural by modifying the actin cytoskeleton (reviewed in Seifert and Mlodzik, 2007; Niehrs, 2012).

Several WNT as well as FZD are detected during development pancreatic development such as *Wnt4, Wnt5b, Wnt7b*. *Fzd2*, *Fzd3* and *Fzd7* (Heller et al., 2002; Papadopoulou and Edlund, 2005; Afelik et al., 2015). Nevertheless, canonical WNT signaling activity patterns are controversial. Using mouse reporters, it is detected in the mesenchyme as well as in GCG^+ cells while immunostaining for active CTNNB1 suggests that it is active in the pancreatic epithelium. These discrepancies may be due to the different techniques used for the detection (Dessimoz et al., 2005; Murtaugh et al., 2005).

Canonical WNT signaling is involved in progenitor proliferation

Absence of CTNNB1 in the pancreatic epithelium causes pancreatic hypoplasia due to a proliferation defect. A dominant negative FZD8 inhibiting canonical WNT signaling confirms the involvement of WNT signaling in the proliferation of the pancreatic progenitors (Dessimoz et al., 2005; Murtaugh et al., 2005; Papadopoulou and Edlund, 2005; Wells et al., 2007; Baumgartner et al., 2014). In *Ctnnb1* mutant, only cells that do not have a recombined *Ctnnb1* locus are able to differentiate into acinar cells (Dessimoz et al., 2005; Murtaugh et al., 2005; Wells et al., 2007). A recent study has shown that CTNNB1 is necessary to maintain acinar identity, but their specification is not altered. Inhibition of NOTCH signaling rescues the acinar compartment, suggesting that CTNNB1 inhibits NOTCH signaling (Baumgartner et al., 2014). However, the outcome on endocrine differentiation is unclear. Only two studies report an absolute endocrine cell decrease, but are backed-up by FZD8 inhibiting canonical WNT signaling (Dessimoz et al., 2005; Papadopoulou and Edlund, 2005; Baumgartner et al., 2014). However, it cannot be excluded that endocrine cells require the adhesive function of CTNNB1 rather than its role in canonical WNT signaling. In addition, this difference may be due to the competitive disadvantage of the mutant cells or the strategy used to inactivate *Ctnnb1*

(Dessimoz et al., 2005; Murtaugh et al., 2005; Papadopoulou and Edlund, 2005; Wells et al., 2007). WNT7B is one of the WNTs acting on early pancreatic proliferation. Its deletion of *Wnt7b* causes pancreatic hypoplasia due to multipotent progenitor proliferation defects, while differentiation is not affected (Afelik et al., 2015).

It is noteworthy that stabilizing CTNNB1 before E11.5 or overexpressing *Wnt1* in the pancreatic epithelium also causes a hypoplastic phenotype (Heller et al., 2002; Heiser et al., 2006). The hypoplasia observed in stabilized *Ctnnb1* mutants is associated with decreased FGF10 in the mesenchyme and increased SHH signaling in the epithelium. Remnant pancreata are cystic and fibrotic while no acinar or endocrine cells are observed. Later CTNNB stabilization in pancreatic epithelium causes the converse phenotype. In mutant animals, pancreata are hyperplastic. Cell proliferation is globally increased, whereas acinar cells are the major contributor of hyperplasia (Heiser et al., 2006). The time-dependent WNT activity is reinforced by *Wnt7b* gain of function experiments. When *Wnt7b* is overexpressed until E11.5, pancreata are cystic, even though the size of the pancreatic epithelium does not seem affected. Multipotent progenitors of the mutant pancreata differentiate into ductal cells with loss of endocrine and acinar cells. However, when *Wnt7b* is overexpressed from E11.5, mutant pancreata are hypoplastic with a loss of acinar cells and gain of mesenchymal tissue (Afelik et al., 2015). The activity of the pathway is thus expected to be different at different phases and to be cell-context dependent.

Non canonical WNT signaling is important for endocrine cell formation

Deletions of *Celsr2* and *Celsr3* do not cause a pancreatic size defect or ductal cyst formation as could be expected with PCP mutants. Their absence causes a failure to produce half of the endocrine cells from the endocrine progenitors. These defects are associated with a decrease of MAPK8 activity, and inhibition of MAPK8 recapitulates the phenotype *in vitro* (Cortijo et al., 2012).

Two studies investigated the role of the WNT ligand, WNT5A, in pancreas development. The overexpression of *Wnt5a*, in pancreatic epithelium, induces hypoplasia. However as mentioned above, overexpression of WNT1, a canonical WNT, causes the same hypoplastic phenotype while the surrounding

organs are differently affected. It suggests therefore a toxic effect in the pancreas linked to the high transgene expression (Heller et al., 2002). Indeed, the analysis of *Wnt5a* KO pancreata does not show an effect on the size of the pancreas. However, the islets are closer to the ducts in *Wnt5a* KO pancreata compare to WTs, suggesting that the endocrine cell migration is impaired (Kim et al., 2005).

6.2.4.4 Role of TGFB in pancreas development and in adult pancreatic stroma homeostasis

TGFB signaling is poorly characterized during pancreas development. However, due to its major role in fibrosis, the role of the TGFB pathway in pancreas organogenesis is reviewed. TGFB signaling components are expressed in a dynamic pattern during pancreas development. TGFBR1 and TBFR2 are mainly expressed in the epithelium until E16.5. At E18.5, they are present in the blood vessels. ACVRL1 is expressed from E16.5 in the blood vessels (Tulachan et al., 2007).

It is difficult to extract a global picture from the experiments carried out so far on this pathway in the pancreas, because the inactivation of different ligands and receptors appear to have unrelated phenotypes. For example, expression of a dominant negative form of TGFBR2 causes an increase of endocrine cells associated with an increase of endocrine progenitors. Hyperplastic ducts and blood vessels are also observed (Wescott et al., 2009). However, deletion of *Gdf11*, a TGFB ligand, causes endocrine cell decrease associated with a partial replacement of beta cells by alpha cells, while endocrine progenitor number is increased. The control of the endocrine progenitor production is independent of NOTCH signaling, as HES1 is not affected in the mutant. *Smad2* heterozygotes partially recapitulate the phenotype, as beta cell mass is reduced, and endocrine progenitors production is enhanced (Harmon et al., 2004).

In the adult, stroma homeostasis requires tight regulation of TGFB signaling. Both inactivation and overactivation of the pathway cause fibrosis with immune cell infiltration, loss of acinar tissue, and its replacement by adipose tissue (Lee et al., 1995; Böttinger et al., 1997).

6.2.4.5 Other signaling pathways acting during pancreas development

BMP signaling components, another major branch of TGFB ligand superfamily, and BMP signaling activities are also detected during pancreas development (Lyons, K. M. et al., 1995; Dichmann et al., 2003; Ahnfelt-Rønne et al., 2010). However, their exact role is still unclear, as studies bring contradictory conclusions (Dichmann et al., 2003; Ahnfelt-Rønne et al., 2010).

The EGF pathway is involved in pancreas organogenesis. It promotes both pancreatic size and beta cell mass (Miettinen et al., 2000; Huotari et al., 2002).

Finally SHH signaling pathway inhibition is essential for pancreas specification (Apelqvist et al., 1997). Although some SHH compounds are present at later stages, inactivation of SHH signaling pathway does not cause any obvious phenotype, arguing that it is not essential during pancreas organogenesis, or that its components are redundant (Hebrok et al., 2000; Cervantes et al., 2010).

6.3 Cystic syndromes

Cyst is a broad term in biology and medicine that is used to define a closed pocket or pouch of tissue filled with air, fluid, or other material (http://www.ncbi.nlm.nih.gov/pubmedhealth). Cysts may arise in any kind of tissue, such as the skin, muscle, brain, liver, kidney.., and they have various origins, such as infection or duct obstruction. Cysts may be further defined as any fluid-filled closed cavity or sac lined by an epithelium. Moreover cyst may be formed of normal, abnormal or neoplastic tissues (http://www.ncbi.nlm.nih.gov/mesh). Such cyst may thus arise in any epithelium composed organs such as kidneys, ovaries, breast, liver, pancreas, lungs, and salivary glands. It is noteworthy that these definitions do not include any size criteria. Cysts in kidneys are largely studied as they cause renal failure. Pancreatic cysts are less studied, and they are often associated with neoplastic or pre-neoplastic lesions.

6.3.1 Human cystic kidney diseases and kidney dysplasia

Autosomal dominant polycystic kidney disease (ADPKD), which occurs in around 1:1000 births, is the major cystic kidney disease. Patients develop multiple cysts in both kidneys, and as many as half of these will develop end-stage renal disease (ESRD) that leads to kidney failure. ADPKD is caused in 85% of the cases by a mutation in PKD1 and in 15% by a mutation in PKD2. Autosomal recessive polycystic kidney disease (ARPKD) arises in 1:20000 births and is caused by a mutation in PKHD1. It differs from ADPKD in that it causes death at neonatal period in nearly half of the cases due to lung failure, and up to 45% of the patients develop ESRD in childhood (reviewed in Wilson and Goilav, 2007). Another major difference is the origin of the cysts, in ADPKD they start in foci in the nephron, while in ARPKD collecting ducts and nephrons dilate and become cystic (Ockenden and Blyth, 1971). Nephronophthisis are recessive diseases that are also characterized by cysts in the kidneys in association with other organ defects, depending of the affected gene that codes for ciliary proteins. Therefore, these diseases are called ciliopathies (reviewed in Wilson and Goilav, 2007). In rare monogenic syndromes renal dysplasia usually associated with other organ defects is observed. It is characterized by cysts and fibrosis, as in the case of renal-hepatic-pancreatic dysplasia or cystic renal dysplasia (Ivemark et al., 1959; Cole et al., 1976; Frank et al., 2013).

6.3.2 Cyst formation in polycystic kidney diseases

The study of patient's mutations, and also modeling of the disease in animals, combined with the use of patient cells have shed light on the genetic, molecular and cellular mechanisms of cyst formation. However, translating these findings into treatments has been achieved with relatively little success (reviewed in Riella et al., 2015).

6.3.2.1 Frequent genetic causes of polycystic kidney disease (PKD)

More than 1000 mutations have been reported in PKD1 and more than 200 in PKD2, causing ADPKD (http://pkdb.mayo.edu.). As only one allele is affected in patients, it has been suggested by Reeders that the second allele is mutated somatically in a nephric cell. Once the second allele is mutated, the nephric cell

expands clonally and form a cyst (Reeders, 1992). Indeed, loss of heterozygosity has been observed both for PKD1 and PKD2 in humans, although it may happen that the cells in the cyst do not carry all the same 2nd mutation (Qian et al., 1996; Torra et al., 1999). *Pkd2* KO mice develop kidney cysts from E15.5. They harbor cysts in other organs, and exhibit multiple developmental defects. They die *in utero,* or shortly after birth, mimicking the early lethality and organ defects, *e. g.* heart, that may be observed in ARPDK (Wu et al., 2000). The effect of *Pkd1* gene alteration is more complex. PKD1 is absent when the gene is disrupted in exon 1 or exon 4. The deletion of exon 34 leads to a smaller protein. The three homozygote mutants have a similar phenotype: they develop cysts, and *in utero* death is associated with edema (Lu et al., 1997; Lu et al., 2001; Wu et al., 2002). However, the deletion of the exon 17 to 21 causes earlier lethality due to cardiac defects precluding the observation of any renal cyst (Boulter et al., 2001). Aged *Pkd2* or *Pkd1* heterozygotes also develop renal cysts although mice are correspondingly older than human ADPKD onset average (Lu et al., 1999; Wu et al., 2000). In addition, the majority of the cysts formed in *Pkd2* heterozygote mice and some *Pkd1* heterozygotes mice are devoid of PKD2 or PKD1 respectively (Wu et al., 1998; Lu et al., 1999; Wu et al., 2002). Furthermore the pace of cyst formation in *Pkd2* heterozygotes is slower than in compound heterozygotes with an unstable allele and a null allele (Wu et al., 1998; Wu et al., 2000). Therefore, these mouse data support a 2-hit mutation theory in ADPKD (Reeders, 1992).

In contrast, it appears that even a severe reduction in *Pkd1* levels is sufficient to cause cysts. Mice expressing only 20% of normal PKD1 level develop cysts in both kidneys (Lantinga-van Leeuwen et al., 2004; Jiang et al., 2006). Cysts grow at a slower pace than in *Pkd1* KO and the mice survive more than a year. They also develop dilated pancreatic and liver bile ducts as well as other defects found in ADPKD patients (Lantinga-van Leeuwen et al., 2004; Jiang et al., 2006). Hypomorphic alleles likely exist in human since studies of ARPKD patients identified compound heterozygous PKD1 mutations correlating with early onset of the disease and *in utero* organ defects (Rossetti et al., 2009; Vujic et al., 2010). In good agreement, animals carrying one *Pkd1* null allele and a human mutation in the other *Pkd1* allele develop a rapid onset of the disease (Hopp et al., 2012). Conversely, mice overexpressing *Pkd1* or *Pkd2* develop cysts (Thivierge et al., 2006; Park et al., 2009). These findings highlight the tight level regulation of PKD1 and PKD2 required for

kidney homeostasis and suggest that the impact of any given PKD1 or PKD2 mutation on disease progression cannot be predicted a priori without detailed analysis.

The cystic outcome for different organs may also depend of the expression level of the affected gene. Indeed, while the *Pkhd1* KO is used as models of ARPKD, *Pkhd1* hypomorphs do not develop kidney cysts. They develop cysts and fibrosis in the pancreas and/or in the liver pancreas, highlighting again the importance of expression level in disease susceptibility (Moser et al., 2005; Gallagher et al., 2008; Williams et al., 2008).

Finally, the time of onset of the mutation is important. Indeed studies using different genetic models show that gene inactivation before postnatal day 14 (P14) causes massive cyst formation while after P14, the onset of the disease is much slower (Davenport et al., 2007; Piontek et al., 2007; Verdeguer et al., 2010). This developmental switch may be linked to the proliferative status of the kidney, as suggested by Verdeguer and colleagues (Verdeguer et al., 2010; Sharma et al., 2013). However forced proliferation is not sufficient to induce cyst formation in adult mice that do not have cilia (Verdeguer et al., 2010; Sharma et al., 2013). It has also been suggested that the acquisition of a more mature transcriptome, mainly linked to changes in metabolism, may switch the kidneys from a cystogenic state to a cyst refractory state (Menezes et al., 2012).

6.3.2.2 Cellular defects associated with cyst formation in PKD

PKDs have been associated with several perturbations. Cysts are usually surrounded by a fibrotic tissue especially at late stage of the disease. Cystic cells have been shown to proliferate more, and to secrete more fluid into the lumen. In some cystic models, the formation of cysts is associated with loss of primary cilia.

Cyst formation may be associated with primary cilia loss

Primary cilia are organelles that mediate the activity of multiple signaling pathways, in addition to other functions such as mechanical stress sensing (reviewed in Gerdes et al., 2009).

Murine mutants for ciliary proteins develop kidney cysts, as seen in *pcy/pcy* mice, where NPHP3 is inactivated, *cpk/cpk* mice, in which CYS is disrupted, *orpk/orpk* mice which lost IFT88 or *Kif3a* conditional KOs. However, the onset and the progression of the disease vary with an end-stage renal failure ranging from

a month to nearly a year (Takahashi et al., 1991; Moyer et al., 1994; Gattone et al., 1996; Pazour et al., 2000; Hou et al., 2002; Fangming et al., 2003; Olbrich et al., 2003). The number of cilia is also drastically reduced in other cystic mutants, such as *Glis3* KOs and conditional *Pkd2* KOs (Kang et al., 2009a; Kim et al., 2009). However, inactivation of *Inv*, the gene causing Nephronophthisis II that is localized at the cilia, does not affect cilia number (Otto et al., 2003). Nevertheless, it does not exclude that their function may be impaired (Watanabe et al., 2003). The exact role of cilia in cyst formation is still unclear.

Aberrant proliferation causes cyst expansion

Proliferation is a generally admitted mechanism for cyst growth. It is usually associated with increased apoptosis. Cystic kidney cells from patient with ADPKD proliferate more than normal epithelial cells (Hanaoka and Guggino, 2000). Overproliferation associated with increased cell death is also found in mouse mutants such as the *Pkd2* or *Kif3a* conditional KOs (Fangming et al., 2003; Kim et al., 2009).

However, it is difficult to assess if overproliferation is the cause of cyst formation or just expansion. Indeed, only cysts lining cells are overproliferating in *bpk/bpk* mouse model which have lost BICC1, while a global overproliferative phenotype is observed in a *Pkd2* haploinsufficiency model, both in cystic and non-cystic areas (Nauta et al., 1993; Cogswell et al., 2003; Chang et al., 2006). The latter is surprising, as it would suggest that proliferation does not always result in cyst formation, since kidneys at 9 months and upwards still have numerous non-cystic nephrons. It is supported by a report from Sharma and colleagues showing that proliferation alone is not sufficient to induce cyst formation in adults after cilia disruption (Sharma et al., 2013).

Moreover, proliferation is not increased upon *Pkd1* kidney-specific deletion in mice, either before or after the developmental switch (Piontek et al., 2007). It has been proposed that cysts may emerge only if the angle of division is affected (Fischer et al., 2006). Indeed, if cells divide in the longitudinal axis of the tubule it leads to tubule extension. On the contrary, if they divide perpendicularly, the tubule diameter expands and may lead to cyst formation (Fischer et al., 2006). Further experiments will be necessary to unravel the role of cell

division in cyst induction and expansion, and to determine if the major contributor of cyst expansion is the loss of oriented cell division.

Increase fluid secretion is associated with renal cyst formation

The other major contributor to cyst growth is the secretion of fluid into the lumen, which was mainly studied on ADPKD cystic cells in vitro (reviewed in Sullivan et al., 1998). Baso-lateral Na^+K^+ATPase and K^+ channels create an inward gradient of cations promoting the transepithelial flow of chloride via the $NaKCl_2$ transporter on the basal side and CFTR on the apical side. It is followed by a paracellular flow of Na^+ and water (reviewed in Sullivan et al., 1998). This mechanism is supported by the observation of less severe cysts harbored by patients with cystic fibrosis and ADPKD. Furthermore, cyst growth is decreased when CFTR is inhibited (O'Sullivan et al., 1998; Montesano et al., 2009). The aquaporin AQP2 is increased in different models of PKD, and is translocated to the apical membrane facilitating water exit into the lumen (Gresh et al., 2004; Jiang et al., 2006; Starremans et al., 2008). However, the contribution of CFTR-mediated fluid secretion to cyst formation does not appear to be necessary in all cystic models. For example, *bpk/bpk* mice show no reduction in cyst formation on a *cftr* null background, suggesting that other Cl^- channels or other mechanisms cause massive fluid secretion and implying different cysts may be caused by different mechanisms (Nakanishi et al., 2001).

Fibrosis and inflammation promote cyst expansion

Defects in the ductal cells that line the cysts are not the sole contributors to cyst formation. Interstitial fibrosis is observed in different models of cystic kidney diseases. Nevertheless fibrosis does not cause cyst formation as it is observed after cysts started to grow (Okada et al., 2000; Fangming et al., 2003; Chang et al., 2006; Jiang et al., 2006; Happé et al., 2013; Wallace et al., 2014). The TGFB signaling pathway may be involved in the fibrotic reaction. Indeed, phospho-SMAD2, a TGFB receptor intracellular target, is upregulated both in the cystic epithelium and in the mesenchyme surrounding the cysts (Hassane et al., 2010). Infiltration of inflammatory cells such as macrophages is also observed in cystic areas. These

inflammatory cells promote but do not initiate cyst growth and their inhibition slows down cyst growth (Karihaloo et al., 2011; Swenson-Fields et al., 2013; Ta et al., 2013).

Molecular pathways involved in cyst formation

Several pathways are altered during renal cyst formation. There are either strong evidence that they are downstream of the genetic cause of ADPKD, such as Ca^{2+} intracellular flow, cAMP signaling pathway, and MTOR pathway or they are associated to cyst formation, although but their role in the pathogenicity of the human disease is less clear, *e. g.* WNT signaling.

PKD1, PKD2 and Ca^{2+} intracellular flow defects in PKD

As discussed above, PKD1 and PKD2 mutations can cause cysts in the kidney. The complex formed by PKD1 and PKD2 acts as a mechanosensor at the cilia and translates mechanical stress into a Ca^{2+} influx (Hanaoka et al., 2000; Nauli et al., 2003). PKD1 is an integral protein with 11 transmembrane domains and a large extracellular domain (Hughes et al., 1995). PKD2 is a 6 transmembrane domain protein with both its C and N terminal domains in the cytoplasm (Mochizuki et al., 1996). PKD2 is mainly expressed in the endoplasmic reticulum. In the presence of PKD1, PKD2 is transported to the plasma membrane and the cilia. PKD2 is a nonselective cation channel with a higher permeability for Ca^{2+} than monovalent cations. Its Ca^{2+} channel permeability is stabilized by its interaction with PKD1 via its coiled-coiled intracellular domain (Cai et al., 1999; Foggensteiner et al., 2000; Hanaoka et al., 2000; González-Perrett et al., 2001; Vassilev et al., 2001; Koulen et al., 2002; Yoder et al., 2002; Grimm et al., 2003; Xu et al., 2003). Thus shear stress at the cilia leads to Ca^{2+} inward flow via PKD1-PKD2 complex (Fig. 9) (Hanaoka et al., 2000).

Elevated Ca^{2+} concentrations in the cilia are amplified by the release of Ca^{2+} from the endoplasmic reticulum through PKD2 and ITPR1, thus increasing the intracellular concentration of Ca^{2+} (Sammels et al., 2010). In the absence of functional PKD2 or PKD1, the intracellular concentration of Ca^{2+} is low (Koulen et al., 2002; Nauli et al., 2003). There are multiple consequences, but notably in the kidney low amount of Ca^{2+} leads to an increase of cAMP in the cells due to the loss of inhibition by Ca^{2+} of ADCY6 or ADCY5, the major Ca^{2+}-regulated adenylate cyclases in the renal epithelium. Ca^{2+} also activates PDE1, the main Ca^{2+}-regulated

phosphodiesterases in the renal epithelium. Therefore, in low concentration of Ca^{2+}, cAMP synthesis is increased while its degradation is reduced (Chabardès et al., 1999; Kakkar et al., 1999; Wang, X. et al., 2009; Rees et al., 2014). ADCY are also activated by the vasopressin receptor (Star et al., 1988), and are inhibited by somatostatin repressor, two potential drug targets in the treatment of ADPKD (Fig. 9) (reviewed in Riella et al., 2015).

Increase of cAMP signaling in cyst formation

cAMP stimulates both fluid secretion and proliferation (Mangoo-Karim et al., 1989; Hanaoka and Guggino, 2000). The activation of CFTR by cAMP contributes to the fluid secretion control (Morales et al., 1996; Wallace et al., 2001). Moreover it increases the transcellular Cl^- flow by activating basolateral K^+ channels (Albaqumi et al., 2008). Finally, it also promotes the translocation at the apical membrane of AQP2. The mechanism is unclear but most probably does not require PKA activity (Fig. 9) (Klussmann et al., 2001; Tamma et al., 2003; Umenishi et al., 2006; Kortenoeven et al., 2012).

Legend of Fig. 9

(A) In normal kidney cells, mechanical stress is sensed at the cilia by PKD1 and PKD2 and translated into an inward Ca^{2+} flux. It triggers the release of intracellular Ca^{2+} stock. Ca^{2+} inhibits the activity of ADCY6 and actives PDE1, leading to a low concentration of cAMP. Moreover the inhibition of BRAF by Ca^{2+} prevents proliferation.

(B) In ADPKD, PKD2 or PKD1 is mutated, leading to an impaired inward Ca^{2+} flux. ADCY6 is active while PDE1 is inhibited. The increase of cAMP concentration promotes a transepithelium Cl^- and water flux due to the activation of CFTR, to the translocation of AQP2 to the apical membrane and to the enhancement of K^+ channel. It also promotes proliferation via the MAPK pathway and the MTOR pathway that also promote aerobic glycolysis.

(C) Legend of the different proteins used in cartoons.

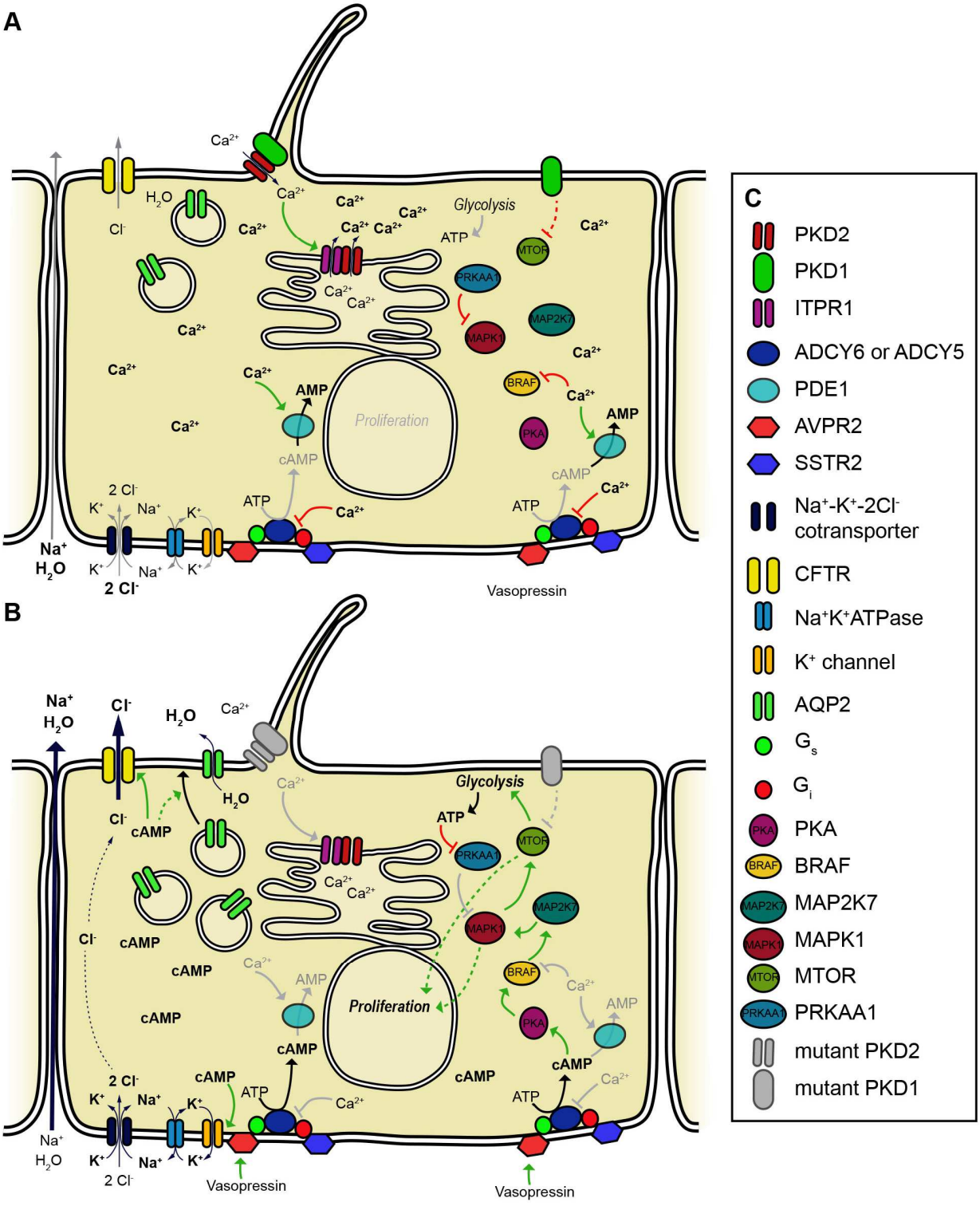

Fig. 9: Molecular defects causing ADPKD

Stimulation of proliferation requires both low concentration of Ca^{2+} and increase amount of cAMP. Ca^{2+} inhibits BRAF. In its absence, cAMP activated PKA activates BRAF triggering a cascade of activation of MAP2K7 and MAPK1, also called MEK and ERK respectively, which stimulates proliferation (Fig. 9) (Yamaguchi et al., 2000; Yamaguchi et al., 2003; Belibi et al., 2004; Yamaguchi et al., 2004).

Increased MTOR signaling pathway activity and aerobic glycolysis in renal cysts

The activity of the MTOR pathway in the cystic renal epithelial, but not in the non-cystic area, is elevated in different cystic mouse models and in ADPKD patients. The overactivation of the pathway may be direct as PKD1 interacts with TSC2, an activator of the MTOR pathway, or indirect, via an increase of MAPK1 activity (Shillingford et al., 2006; Gattone et al., 2009; Rowe et al., 2013). MTOR pathway inhibition slows down the progression of the disease in an ADKPD mouse model, and in *bpk/bpk* mice used as an ARPKD model, suggesting that it plays a role in cyst progression (Shillingford et al., 2006; Gattone et al., 2009). MTOR pathway activation also promotes aerobic glycolysis, which is used as the main source of energy in *Pkd1* conditional KO cells in contrast to WT cells. The increase of ATP promotes MAPK1 activity via the inhibition of PRKAA1, also called AMPK. MTOR and MAPK1 form thus a feedforward loop. The *Pkd1* conditional KO transcriptome also reflects its metabolic state by the upregulation of glycolytic enzymes. Cyst progression in murine models of ARPKD and ADPKD is thus inhibited by the inhibition of glycolysis (Rowe et al., 2013).

Aberrant canonical WNT signaling activity associated with renal cysts

Overactivation of canonical WNT signaling causes cyst formation in the kidneys (Saadi-Kheddouci et al., 2001; Chao-Nan et al., 2005). The epithelium lining the cysts is over-proliferative and often multilayered. In this model, only the dysplastic epithelium loses cilia. However no decrease of PKD1 or PKD2 was observed in these experiments, suggesting that PKD1/2 and the WNT pathway act either in parallel or that the WNT pathway acts downstream of these proteins (Chao-Nan et al., 2005). In agreement with the second hypothesis, overactive canonical Wnt signaling is also observed in the *Pkd2* and *Kif3a* conditional KOs, both models of ARPKD (Fangming et al., 2003; Kim et al., 2009). Moreover, two other proteins whose

inactivation causes renal cysts, INV and NPHP3, inhibit canonical Wnt signaling (Simons et al., 2005; Bergmann et al., 2008). However, it is unclear if changes in endogenous WNT signaling contribute to cyst formation or are a side effect of it.

6.3.3 Human pancreatic cyst and pancreatic dysplasia

Cysts can also be found in the pancreas. Cysts can be mistaken for pseudocysts that are not lined by an epithelium. Pseudocysts are the most frequent and are observed for example, in pancreatitis when fluid accumulation is surrounded by fibrotic tissue (reviewed in Demos et al., 2002). Cysts might be asymptomatic or without pathognomonic signs, and escape detection until they are incidentally discovered (Fernandez-del Castillo et al., 2003; Laffan et al., 2008; Lee et al., 2010).

Pancreatic cysts are divided into cystic neoplasms and congenital cysts. Cystic neoplasms are promoted by the accumulation of mucin, as seen in mucinous adenocarcinoma, mucinous cystic tumor and intraductal papillary tumor. Accumulation of glycogen is found in benign microcystic adenomas observed in patients with von Hippel Lindau disease (see below). Endocrine tumors in rare instances might also form cysts (reviewed in Demos et al., 2002).

Congenital pancreatic cysts are usually part of a multi-organ syndrome. The pancreas of cystic fibrosis patients is progressively replaced by a fibrotic and adipose tissue with microscopic cysts due to the obstruction of the ducts (reviewed in Agrons et al., 1996). Pancreatic cystosis, *i. e*. the presence of macroscopic cysts of more than 1 cm of diameter, is less common as it occurs only in 10% of the cystic fibrosis patients (Berrocal et al., 2005).

Von Hippel-Lindau syndrome is caused by a heterozygote mutation in *VHL*. The mutation predisposes to benign and malignant tumours and is associated with cysts in multiple organs such as kidneys and the pancreas (Lamiell et al., 1989).

Autosomal dominant polycystic kidney disease patients also develop pancreatic cysts. The frequency estimation turns around 5% (Nicolau et al., 2000). Pancreatic dysplasia, *i. e*. fibrosis associated or not with

cysts, may also be observed in ARPKD patients (Lundin and Olow, 1961). Other syndromes associate renal and pancreatic dysplasia such as renal-hepatic-pancreatic dysplasia and *situs inversus totalis* with cystic dysplasia of kidneys and pancreas. Loss of function of NEK8 or NPHP3, two ciliary proteins, has been identified in some cases of the former syndrome but the etiology of the latter is unknown (Ivemark et al., 1959; Balci et al., 1999; Bergmann et al., 2008; Frank et al., 2013).

6.3.3.1 The impairment of primary cilia causes cysts in murine pancreas

Pancreatic cysts have been found in murine mutants in which primary cilia are impaired. In the pancreas, primary cilia have been reported on bipotent progenitors lining the ducts, mature ductal cells, and endocrine cells (Munger, 1958; Boquist, 1968; Cano et al., 2004).

Two mutants show the importance of primary cilia in duct homeostasis. *orpk/orpk* mice have a mutation in *Ift88* precluding cilia formation (Pazour et al., 2000). Primary cilia are much smaller in o*rpk/orpk* mice and their frequency in ductal cells is drastically reduced. Mutants develop ductal cysts after birth combined to fibrosis and a progressive loss of acinar tissue. These defects are associated with increased PKD2 expression and WNT signaling activity. The second mutants, in which *Kif3a* was deleted in the pancreatic epithelium, have no cilia. Cyst formation starts slightly before birth. They are also associated with fibrosis and conversion of acinar cells into adipose tissue. It is noteworthy that these mutants do not have any reported endocrine cell defects in spite of the presence of cilia on the cells (Cano et al., 2004; Cano et al., 2006).

Mutants developing pancreatic cysts such as *Sox9* KOs, *Hnf6* KOs, *Glis3* KOs and *Hnf1b* KOs, also have cilia defects. However it is difficult to establish if it is the initiating cause of cyst formation or a consequence (Pierreux et al., 2006; Kang et al., 2009b; Shih et al., 2013; De Vas et al., 2015).

6.4 Bicaudal C1

Bicaudal C1 (*Bicc1*) is mutated in *bpk/bpk* mice and *jcpk/jcpk* mice, two models of ARPKD. BICC1 is an RNA binding protein found in several species, however, its mechanisms of action are poorly understood

(Gamberi and Lasko, 2012). The majority of BICC1 homologs possesses one SAM domain, are able to interact with proteins, and have several KH domains that bind RNA molecules (Mahone et al., 1995; Bouvrette et al., 2008; Jones et al., 2012). On the contrary, GLD-3, one of the poorly conserved homologs of *Bicc1* in *Caenorhabditis elegans,* that lacks the SAM domain interacts with proteins via its KH domains (Eckmann et al., 2002; Nakel et al., 2010).

6.4.1 Role of GLD-3 and BCC-1 in *Caenorhabditis elegans*

GLD-3 and BCC-1 are the homologs of BICC1 in *Caenorhabditis elegans* (Eckmann et al., 2002). GLD-3 controls sex determination and mitosis *vs* meiosis decision. It binds the polyA polymerase, GLD-2, and stimulates its activity to stabilize specific mRNAs. Thereby, it promotes their translation by polyA tail elongation (Wang et al., 2002). GLD-3 thus causes the cell to enter meiosis instead of mitosis (Eckmann et al., 2004). Through a distinct domain, GLD-3 can also sequester the fem3-binding factor (FBF-1) of the pumilio family of RNA-binding proteins, inhibiting its interaction with *fem* mRNA and, thereby promoting spermatogenesis at the expense of oogenesis (Eckmann et al., 2002; Eckmann et al., 2004). These observations suggest that GLD-3 can regulate mRNA polyA tail elongation and stability by associating with a variety of interacting partners. By comparison, little is known about the role of the Bicc1 ortholog BCC-1, except that its loss can suppress the loss-of-function phenotype of the receptor tyrosine kinase ROL-3 (Jones et al., 2012).

6.4.2 Role of BicC in *Drosophila Melanogaster*

BicC, the first homolog of *Bicc1* identified, was isolated during mutagenic screens. Its haploinsufficiency causes patterning defects, such as double abdomen embryos or headless embryos (Mohler and Wieschaus, 1986). They are associated with the mislocalization of *osk* mRNA, normally present at the posterior side of the oocyte, and its premature translation (Mahone et al., 1995; Saffman et al., 1998). The precise relationship between BicC and *osk* mRNA is unknown. BicC interacts with the CCR4-NOT complex, a deadenylase complex, and targets it to specific mRNAs such as its own mRNA, leading to a shortening of its polyA tail

(Chicoine et al., 2007). No such effect has been reported on *osk* mRNA, but BicC can instead inhibit osk mRNA polyadenylation and translation by sequestering the polyA polymerase *orb* (Castagnetti and Ephrussi, 2003; Chicoine et al., 2007).

BicC KO females are sterile due to an interruption of oogenesis. The follicle cells fail to migrate posteriorly and continue to cover nurse cells. The nurse cells then invade the space occupied by the oocyte. Oocyte and nurse cells degenerate resulting in an empty eggshell (Mohler and Wieschaus, 1986; Schüpbach and Wieschaus, 1991). Although the mechanism underlying the phenotype is unclear, it may be associated with cytoskeleton and trafficking defects. For instance, Grk, a protein that is normally secreted at the anteriodorsal side of the oocyte, accumulates in vesicles imbedded into actin cages in *BicC* KOs. BicC interacts with the Tral mRNP complex found on the endoplasmic reticulum membrane, and is important to maintain COPII coated vesicle exit sites. The cytoskeleton of the nurse cells is also affected in *BicC* KO females (Wilhelm et al., 2005; Kugler et al., 2009; Snee and Macdonald, 2009).

Beyond these defects, no other functions of BicC have been reported in flies. However, *BicC* mRNA is also expressed in males and at different stages in the embryos (Mahone et al., 1995).

6.4.3 Role of BICC1 in vertebrates

Bicc1 is able to induce endoderm formation when overexpressed in *Xenopus* embryo (Wessely and De Robertis, 2000). This ectopic capacity is maybe related to its ability to repress, in vegetal cells, mRNA translation, such as *tdgf1.3*, also called *cripto*, an important factor for neural development. This repression requires its N-terminal region containing its KH domains that bind *tdgf1.3* mRNA, and a region upstream of its SAM domain that inhibits the translation initiation machinery (Yabe et al., 2003; Zhang et al., 2013).

Bicc1 is also involved in the establishment of left-right asymmetry. While no defects have been reported in cilia formation in *Bicc1* KOs or knockdowns, motile cilia are dysfunctional (Tran et al., 2007; Maisonneuve et al., 2009; Bouvrette et al., 2010; Ryan et al., 2010; Piazzon et al., 2012). They are not oriented properly on node cells, and they are not able to generate the leftward fluid flow. In the node of *Bicc1* KOs, hyperactive

canonical Wnt signaling was also observed due to the ability of BICC1 to sequester DVL2 in P-bodies precluding the activation of canonical Wnt signaling (Maisonneuve et al., 2009).

6.4.3.1 BICC1 regulates epithelium homeostasis in kidneys

Bicc1 is expressed in the *Xenopus* and zebrafish pronephros as well as in the murine metanephros that give rise to the kidneys (Wessely and De Robertis, 2000; Wessely et al., 2001; Bouvrette et al., 2010). Its absence or its downregulation causes cyst formation in the three species (Nauta et al., 1993; Flaherty et al., 1995; Cogswell et al., 2003; Tran et al., 2007; Bouvrette et al., 2010; Tran et al., 2010; Piazzon et al., 2012). In humans, mutations of BICC1 have been associated with kidney dysplasia (Kraus et al., 2012). In mice, duct enlargement appears around E15.5 (Tran et al., 2010; Piazzon et al., 2012). Cysts are also observed in the pancreas as well as in the liver and extra-hepatic ducts (Nauta et al., 1993; Flaherty et al., 1995; Tran et al., 2010). Moreover kidney cysts have been observed in some aged *jcpk* heterozygote mice harboring a mutation in one of the *Bicc1* alleles (Flaherty et al., 1995; Cogswell et al., 2003).

The mechanism of cyst formation and initiation is still unclear. As in other polycystic kidney disease models, cysts are not caused by specification or early differentiation defects (Tran et al., 2007). As already mentioned, *bpk/bpk* cystic cells proliferate more, but overproliferation is not yet observed at early stages when cysts start to form (Nauta et al., 1993; Tran et al., 2010). Immotile cilia in kidneys and other organs are not affected by *Bicc1* deletion (Tran et al., 2007; Maisonneuve et al., 2009; Bouvrette et al., 2010; Ryan et al., 2010; Piazzon et al., 2012). However, studies with *bpk/bpk* mice show that EGFR is mislocalized on the apical membrane due to vesicle trafficking defects. The *bpk* mutation also leads to hyperactivation of the MAPK pathway (MacRae Dell et al., 2004; Ryan et al., 2010). The MTOR pathway may also be deregulated as its inhibition precludes cyst growth (Shillingford et al., 2006). Eventually, the major role of BICC1 in kidney homeostasis may be to promote PKD2 expression, and to regulate cAMP production via microRNA regulation (Tran et al., 2010; Piazzon et al., 2012).

6.4.3.2 Molecular mechanisms involving BICC1 in kidney homeostasis

Contrary to the ability of BICC1 to directly repress *tdgf1.3* translation in early *Xenopus* development, translation repression by BICC1 in kidneys requires specific microRNAs (Tran et al., 2010; Piazzon et al., 2012; Zhang et al., 2013). miRNA genes are transcribed into pri-miRNA, which are composed of a stem-loop structure with unpaired ends. In animal cells, unpaired ends are cleaved by the microprocessor containing DROSHA and DGCR8. Alternatively, pri-miRNA may be spliced by the spliceosome when they are part of an intron. The stem-loop structure is called pre-miRNA, and is exported to the cytoplasm where the loop is cleaved by DICER1. The double stranded miRNA is then unwound and one strand loaded onto the RISC complex formed by TNRC6A and AGO1 or AGO2. miRNAs are then able to repress translation by inhibiting translation initiation or elongation. They can also destabilize mRNA by inhibiting mRNA capping, or by promoting their degradation (Fig. 10) (reviewed in Carthew and Sontheimer, 2009).

BICC1 is able to target *Mir125a* to *Adcy6* mRNA and *MiR27a* to *Pkia* mRNA enabling translation repression without affecting mRNA stability or polyA tail length. ADCY6 and PKIA levels are thereby elevated in absence of *Bicc1*. The net impact is an excessive level of cAMP thought to cause cyst formation. However it should be mentioned that increased cAMP levels are observed when the cysts are already formed. One can therefore not rule out that this mechanism promotes cyst growth and not cyst initiation (Piazzon et al., 2012).

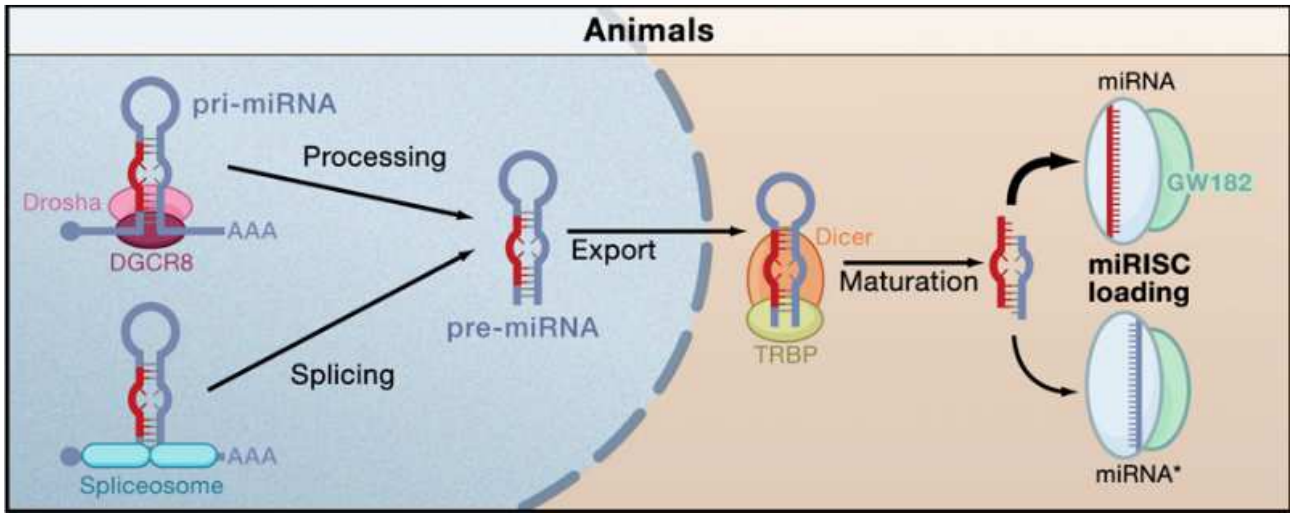

Fig. 10: Maturation of pri-miRNA into miRNA.

Pri-miRNA is processed into pre-miRNA by microprocessor containing Drosha and DGCR8 or by the spliceosome. Pre-miRNA is exported into the cytoplasm where it is further cleaved by Dicer1, and loaded onto the RISC complex. Then, it represses targeted mRNA (from the review of Carthew and Sontheimer, 2009).

BICC1 has also been involved in the regulation of PKD2 levels by inhibiting *Mir17* repression, although no direct binding between *Mir17* or *Pkd2* and BICC1 has been established (Tran et al., 2010). A role of the *MiR17* or *Mir17-92* cluster in kidney cyst formation has been confirmed by two other studies (Sun et al., 2010; Patel et al., 2013), although this likely involves multiple Bicc1-independent target mRNAs. In ARPKD mouse models, *Mir17-92* is upregulated and correlated with the severity of the disease. Its overexpression alone causes overproliferation while its deletion in ARPKD background limits cyst growth. *Mir17* is able to downregulate *Pkd2* and *Pkd1* translation (Patel et al., 2013). *Mir17* can also repress PKD2 in human cells (Sun et al., 2010). However, elucidating the precise roles of individual miRNAs and their potential as therapeutic targets in cyst formation will require further studies.

Not much is now know about the mechanism of action of BICC1 in different species and organs. Therefore, the lack of cohesion between the reported functions precludes a precise overview of its molecular nature. It requires miRNA in some but not others and, its functions may depend on its binding partners. Moreover few of its targets have been uncovered, and they do not seem conserved across species or systems, except *Pkd2* as it has been shown to also play a role downstream of BICC1 in osteoblastogenesis in mice (Mesner et al., 2014). Furthermore only one RNA sequence has been described as a binding site for BICC1 in Xenopus, and

none in mammals or invertebrates (Zhang et al., 2014). Finally BICC1 should have functions in other tissues as it is expressed broadly during development and in the adult (Wessely et al., 2001).

7 RESULTS

7.1 BICC1 is expressed in the pancreas progenitors and ducts during pancreas development

To investigate a possible role for BICC1 during embryonic pancreas formation, its expression was analyzed at different stages. *Bicc1* mRNA was already detected by Q-PCR at E10.5, whereas the protein was first detected at low levels at E11.5 in the whole $PDX1^+$ pancreatic epithelium. The expression level increased over time. It was still detected at E18.5 and after birth in ductal cells recognized by their positivity for Dolichos Biflorus Agglutinin (DBA), but not in beta cells (Fig. 11). As previously described in cell lines (Maisonneuve et al., 2009; Tran et al., 2010), BICC1 protein was present in the cytoplasm (Fig. 12A-C).

BICC1 is expressed in pancreatic bipotent progenitors

During the secondary transition, its expression was restricted to the pancreatic progenitors lining ducts and to a subset of $NEUROG3^+$ endocrine progenitors, mostly in those that had not yet delaminated to form endocrine clusters. It was excluded from the endocrine cells and acini (Fig. 12).

BICC1 is expressed in the extrahepatic duct

Contrary to what has been previously published in (Lian et al., 2014), BICC1 was expressed at E11.5 in hepatic ducts but not in the hepatoblasts (Fig. 13). However, the nature of the ducts have not been investigated.

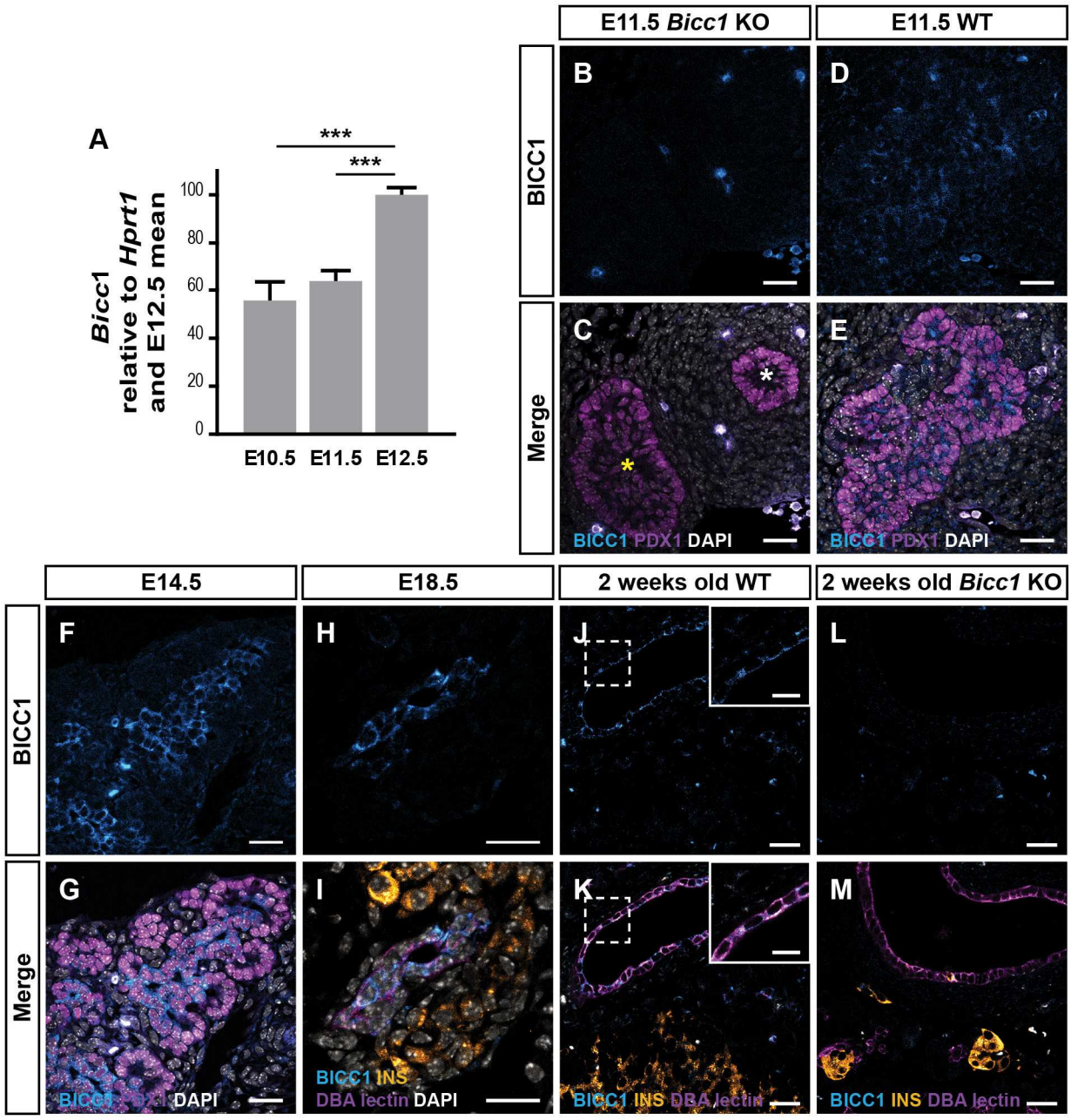

Fig. 11: BICC1 is expressed from E10.5 onward.

(A) Q-PCR analysis for *Bicc1* in E10.5, E11.5 and E12.5 dorsal pancreatic buds indicates that *Bicc1* mRNA is already present in E10.5 pancreas and its global expression level increases (n=3 for each stage; E10.5-E11.5 p=0.20; E11.5-E12.5 p=0.0003; E10.5-E12.5 p=0.0008). *Bicc1* mRNA level is normalized to *Hprt1* level. Results are represented as a percentage of *Bicc1* expression level at E12.5.

(B-G) Immunostaining for BICC1 (cyan) and PDX1 (magenta) is performed on E11.5 *Bicc1* KO and WT and E14.5 pancreatic sections. *Bicc1* KO is used to evaluate the specificity of the antibody. BICC1 is present in the whole pancreatic epithelium positive for PDX1 at E11.5 and in a subset of cells at E14.5.

Continuation of the legend of the Fig. 11

(H-M) E18.5, 2 weeks old WT and *Bicc1* KO pancreatic sections are immunostained for BICC1 (cyan), DBA lectin (magenta) and INS (orange). The specificity of the antibody is evaluated with sections of 2 weeks old KO. BICC1 is present in DBA lectin^{+} ducts but not in INS^{+} cells.

Sections are counterstained with DAPI (white). Scale bars B-G and G-M 25 µm, H-I 20 µm and insets in G-K 10 µm. See Table 12 in Appendix for further data

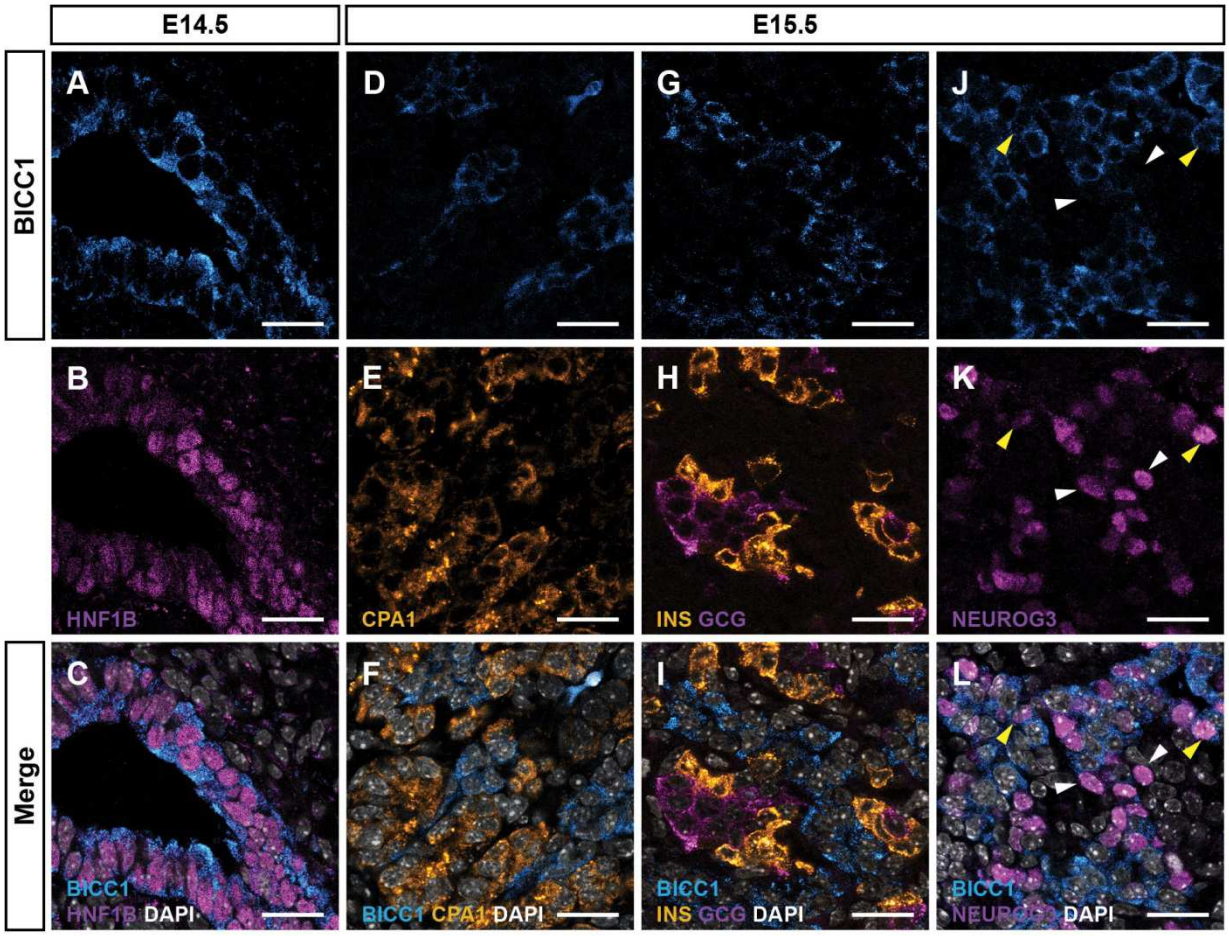

Fig. 12: BICC1 expression is restricted to progenitors during the secondary transition.

E14.5 and E15.5 pancreatic sections are immunostained and counterstained with DAPI (white).

(A-C) The BICC1 expression domain (cyan) co-localizes with the HNF1B expression domain (magenta) at E14.5, (D-F) but is excluded from the acinar cells stained by CPA1 (orange) at E15.5.

(G-I) It is also excluded from the beta cells expressing INS (orange) and from the alpha cells expressing GCG (magenta) at E15.5.

(J-L) A subset of NEUROG3^{+} cells (magenta) are positive for BICC1 (yellow arrowheads), while the others are negative (white arrowheads).

Scale bars A-L 20 µm.

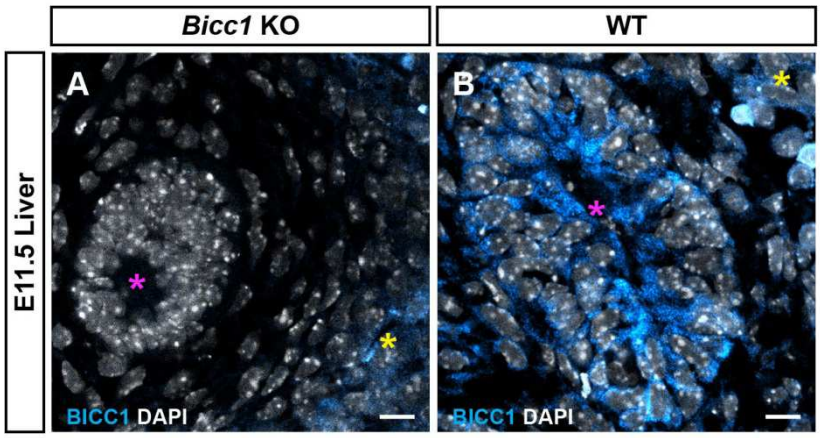

Fig. 13: BICC1 is expressed in hepatic ducts but not hepatocytes.

(A, B) Immunofluorescence staining performed on E11.5 *Bicc1* KO and WT liver sections indicates BICC1 expression (cyan) in the hepatic duct (magenta asterisk) but not in the hepatoblasts (yellow asterisk) as this staining is also present in *Bicc1* KO. Sections are counterstained with DAPI (white). Scale bars 10 µm

7.2 *Bicc1* KO progenitor-lined ducts expand and form cysts

To further analyze the function of BICC1 during pancreas development, the pancreas from *Bicc1* KO mice was analyzed at different stages of development..

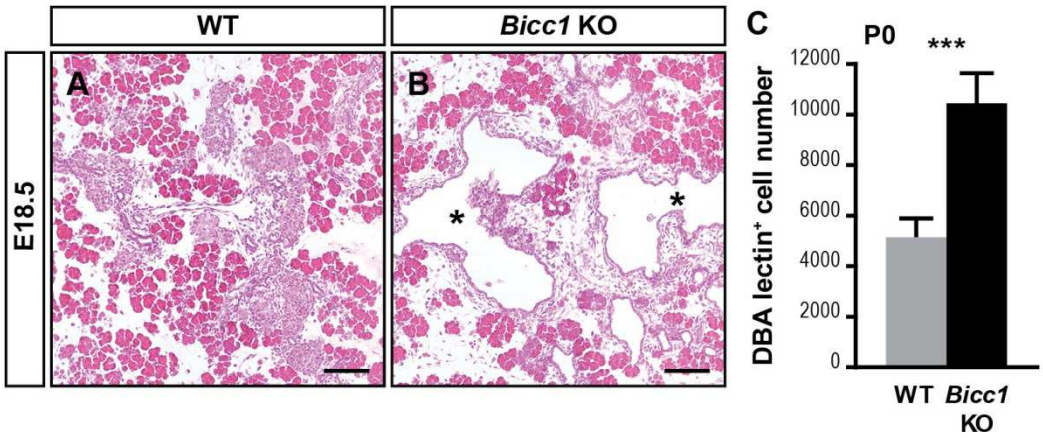

Fig. 14: Bicc1 KOs display cysts

(A, B) Haematoxylin eosin staining of E18.5 WT and *Bicc1* KO pancreatic sections shows cysts delineated by ductal cells in KO pancreata (asterisks).

(C) Quantification of pancreatic DBA lectin+ ductal cell numbers detected on immunofluorescence-stained sections at P0 shows that there are twice more ductal cells in *Bicc1* KO (n=4) than in WT (n=4, p= 0.0003).

Scale bars A-B 100 µm. See Table 12 in Appendix for further data.

Progressively expanding cysts lined by pancreatic progenitors were detected from E14.5 (Fig. 14A-B, 32A-B), confirming previous observations made at P1 in another *Bicc1* KO line and in *jcpk/jcpk* mouse model (Flaherty et al., 1995; Tran et al., 2010)

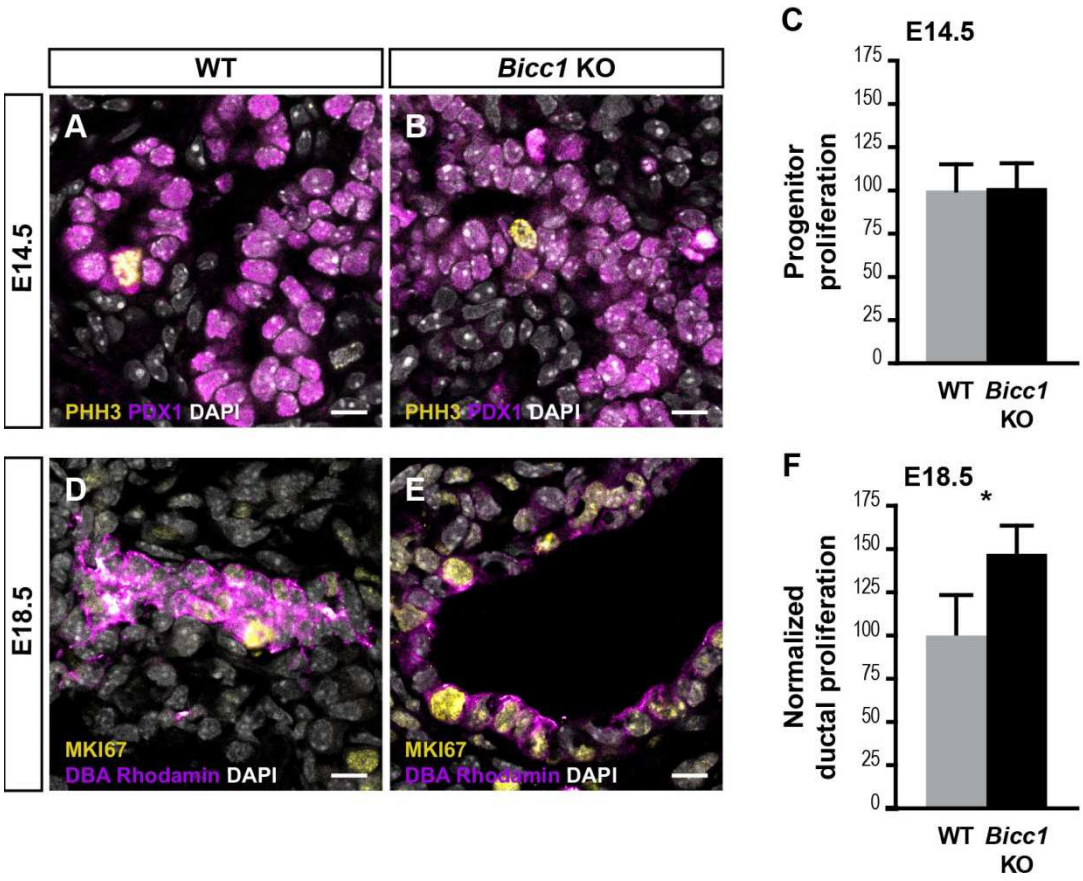

Fig. 15: Ductal proliferation at late developmental stages is increased in *Bicc1* KO.

(A, B) Immunofluorescence staining is performed on E14.5 WT and *Bicc1* KO pancreatic sections for PDX1 (magenta) and PHH3 (yellow)

(C) Percentage of $PDX1^+$ pancreatic progenitors expressing PHH3 among the E14.5 pancreatic progenitors detected on the immunostaining exemplified in (A, B). The proliferation is not affected in *Bicc1* KO (WT, n=4; *Bicc1* KO, n=3, p=0.9). The results are expressed as percentage of WT mean.

(D, E) Immunofluorescence staining for MKI67 (yellow), also known as Ki67, and DBA rhodamin (magenta), marking ductal cells, is performed on E18.5 *Bicc1* KO and WT pancreatic sections.

(F) Percentage of $MKI67^+$ cells among ductal cells detected on the sections exemplified in (D, E). The proliferation in *Bicc1* KO is increased 1.47-fold compared to WT. KO data are normalized to WT pancreas from the same background (WT, n=4; *Bicc1* KO, n=4, p=0.016).

Sections are counterstained with DAPI (white). Scale bars 10 µm. See Table 12 in Appendix for further data.

The cysts were not a consequence of the left/right asymmetry defects seen in *Bicc1* KO, since they occurred both in left- and right-turned pancreata. The cystic web arose in the main duct and interlobular ducts, while the intercalated ducts were not enlarged. Quantification of ductal cells expressing DBA at P0 revealed twice more cells in *Bicc1* KO pancreata than in wild type (WT) pancreata (Fig. 14C).

Proliferating ductal cell quantification at E18.5 revealed a 1.5-fold increase in proliferation index in *Bicc1* KO pancreata. However, it was not the primary cause of cyst formation as proliferation of pancreatic progenitors at E14.5 was not affected by *Bicc1* deletion (Fig. 15). Although rare, apoptotic cells were detected by terminal deoxynucleotidyl transferase-dUTP nick end labeling assay (TUNEL) in *Bicc1* KO ducts but not in WT ducts (Fig. 18).

Although sporadic cells positive for acinar markers and negative for ductal markers were found lining the cysts, we did not detect acinar to ductal metaplasia. The boundary between acinar and ductal compartments thus appears to be generally conserved (Fig. 16).

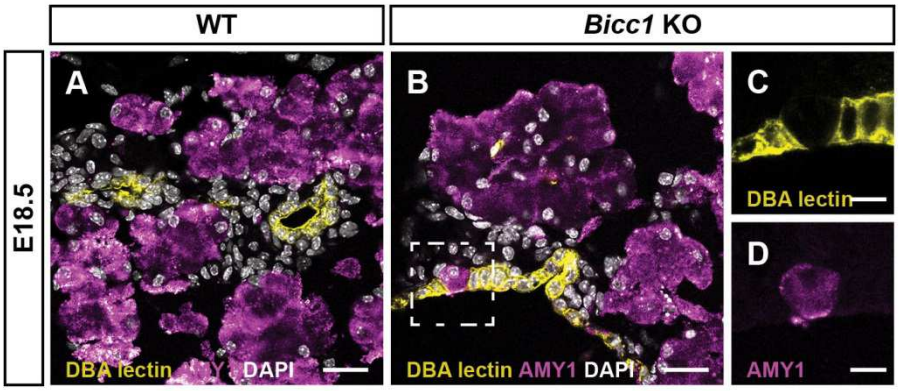

Fig. 16: No acinar to ductal or ductal to acinar metaplasia is observed in *Bicc1* KO

(A-D) Immunofluorescence staining on E18.5 WT and *Bicc1* KO pancreatic sections for amylase (AMY1, magenta) and DBA lectin (yellow) shows that there are few $AMY1^{+}$ cells in the ducts of *Bicc1* KO pancreas but their identity is not affected as they do not express DBA lectin (n = 4 for both genotype). C and D show a magnification of the dashed boxes in B.

Scale bars A-B 25 µm C-D 10 µm

7.2.1 The *Bicc1* KO does not exhibit a decrease in the number of cilia

Cilia mutants form ductal cysts in the pancreas (Cano et al., 2004; Cano et al., 2006), and other cystic mutants have cilia defects (Pierreux et al., 2006; Kang et al., 2009b), thus, propounding that cilia defects may contribute to cyst formation in *Bicc1* KOs. However, at the beginning of cyst formation, cilia were present at E14.5 in *Bicc1* KOs and did not show any obvious defects. Moreover, the number of cilia, in both *Bicc1* KO cystic and non-cystic ducts at E18.5, was not affected (Fig. 17).

Taken together, these results show that BICC1 deficiency leads to cyst formation during development, and it is associated with increased ductal proliferation at later stages.

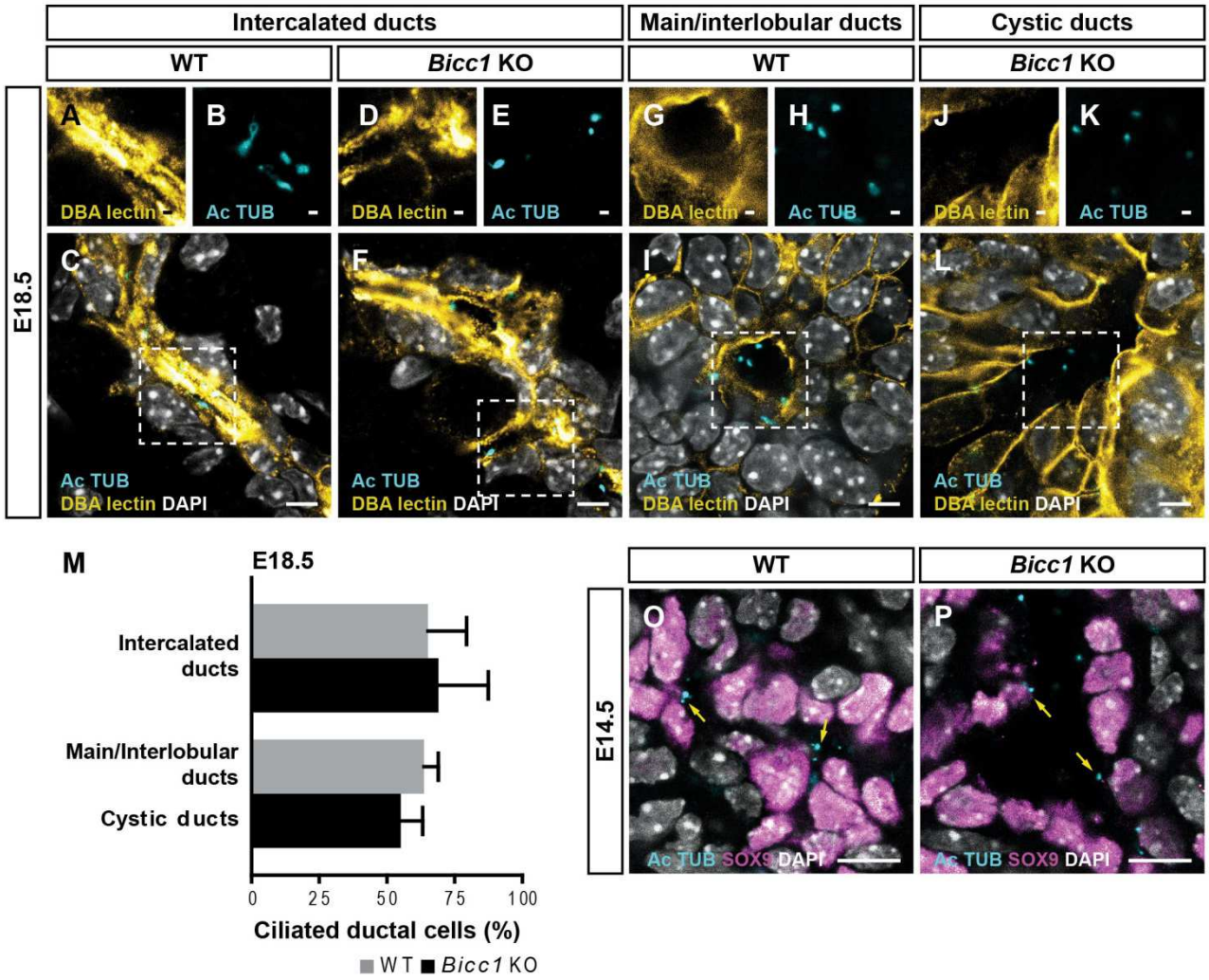

Fig. 17: Cilia are not decreased by *Bicc1* deletion either at E18.5 or E14.5

(A-L) Cilia on ductal cells are detected by immunofluorescence for acetylated tubulin (Ac TUB) (cyan) and DBA lectin (yellow) on E18.5 pancreatic sections. Insets show high magnification view of the dashed boxes in two separate channels. Cilia are present in both WT and *Bicc1* KO pancreata in intercalated ducts and main/interlobular ducts as shown on optical section.

(M) Percentage of DBA lectin$^+$ Ac TUB$^+$ cells among DBA lectin$^+$ ductal cells in intercalated and main/interlobular ducts in *Bicc1* KO and WT E18.5 pancreas quantified on 3D reconstructed images. Cilia are not affected by *Bicc1* deletion (n=4 for both genotypes: intercalated ducts, p=0.75; main/interlobular ducts vs cystic ducts, p=0.12).

(O, P) Cilia (yellow arrows) detected by immunofluorescence for Ac TUB (cyan) on E14.5 WT and *Bicc1* KO pancreatic sections are not obviously affected by *Bicc1* deletion as shown on an optical section. SOX9 antibody (magenta) is used to identify the ducts (n = 4 for both genotype).

Sections are counterstained with DAPI (white). Scale bars A-B, D-E, G-H, and J-K 1 µm; C, F, I and L 5 µm and O-P 10 µm. See Table 12 in Appendix for further data.

7.3 Endocrine cells are decreased in Bicc1 KO pancreata

To further explore the role of BICC1 in the pancreas, we investigated the differentiation of the endocrine cell types. In *Bicc1* KO, islet architecture was disturbed at P0. The islets, detected by their immmunoreactivity for INS, GCG, and SST, were visibly smaller. Many endocrine cells were scattered rather than clustered into islets. A higher number of endocrine cells had not delaminated from the duct (Fig. 18).

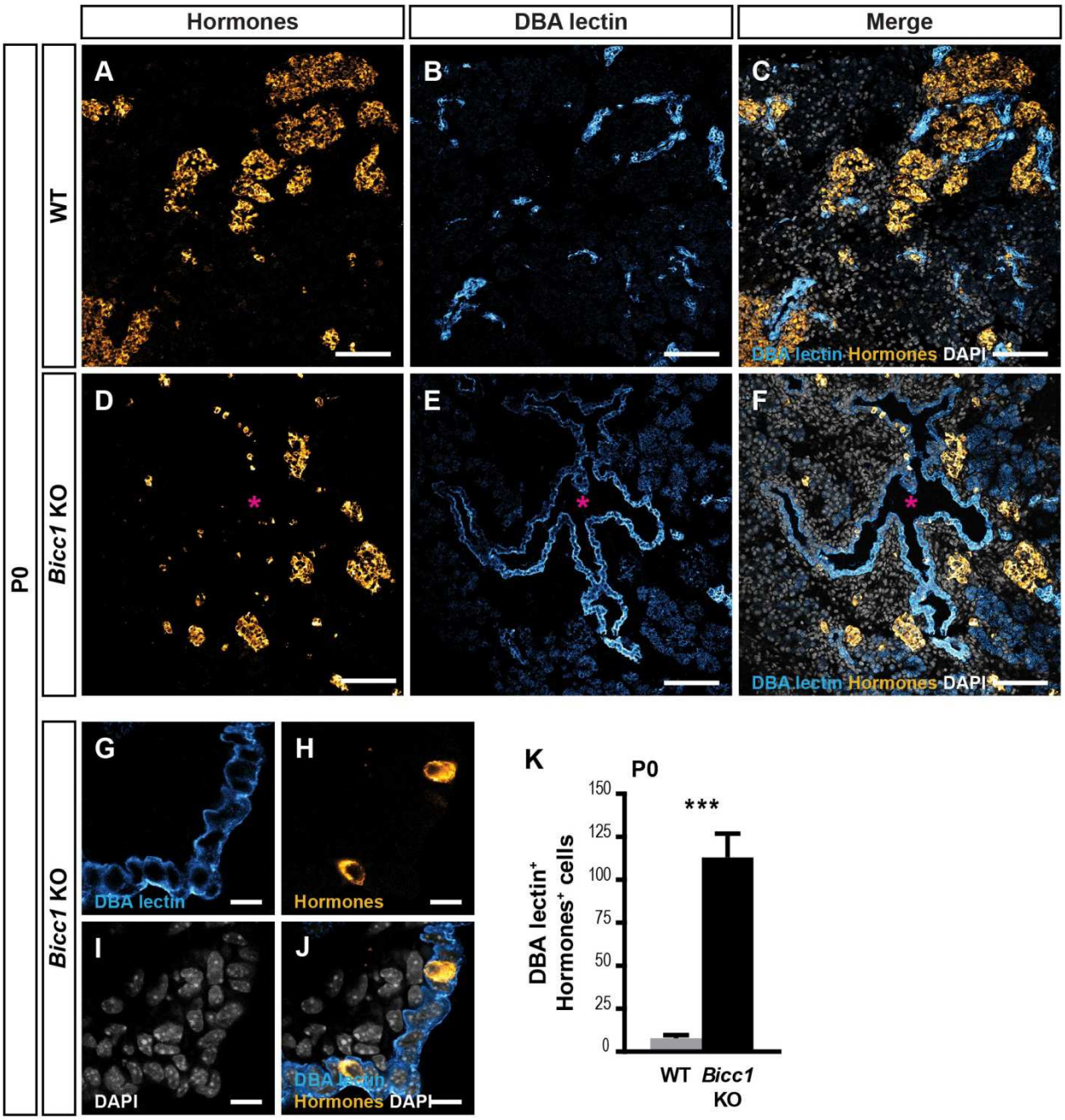

Fig. 18: The islet architecture is disturbed and endocrine cells are present in the ducts in *Bicc1* KOs

(A-F) Immunofluorescence staining on P0 WT and *Bicc1* KO pancreatic sections for GCG, INS, SST (hormones, orange) and DBA lectin (cyan) shows that endocrine cells are rather scattered and form smaller islets in *Bicc1*KO.

(G-J) A magnification of a *Bicc1* KO pancreatic section shows that some endocrine cells (orange) are in the ducts (cyan).

(K) Quantification of the endocrine cells present in the ducts identified by immunostaining. While there are only a few ductal endocrine cells in P0 WT pancreata, there are 14 times more in P0 *Bicc1* KO pancreata (n=4 for both genotype; n=4, p=0.0086).

Sections are counterstained with DAPI (white). Scale bars A-F 100 µm and G- J 10 µm. See Table 12 in Appendix for further data

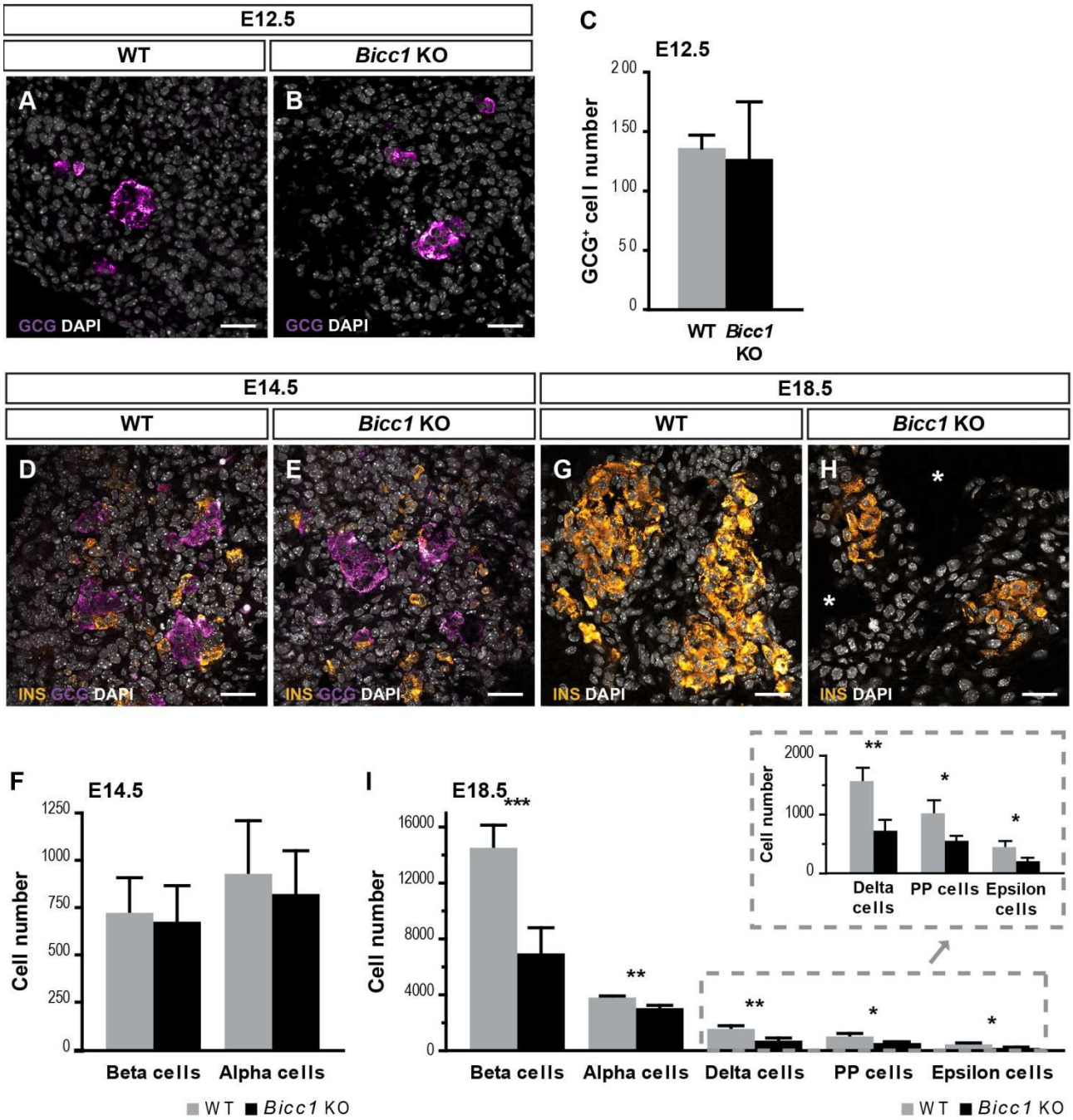

Fig. 19: Endocrine cells are reduced at E18.5 but not earlier in *Bicc1* KO.

(A, B) Immunofluorescence staining for GCG (magenta) performed on E12.5 WT and *Bicc1* KO pancreatic sections.

(C) Quantification of GCG^+ cells detected on the previous immunostaining shows no differences between WT and *Bicc1* KO pancreata (n=4 for both genotype, p=0.72)

(D, E) Immunofluorescence staining highlighting GCG^+ alpha cells (magenta) and INS^+ beta cells (orange) in E14.5 *Bicc1* KO and WT pancreatic sections.

(F) Quantification of INS^+ and GCG^+ cell number on the previous immunostainings shows no difference between *Bicc1* KO (INS^+ cells, n=4; GCG^+ cells, n=3) and WT (INS^+ cells, n=4, p=0.74; GCG^+ cells, n=4, p=0.62).

Continuation of the legend of Fig. 19

(G, H) Immunofluorescence staining for INS (orange) on E18.5 *Bicc1* KO and WT pancreatic sections reveals a marked decrease in KOs. White asterisks indicate cysts.

(I) Quantification of INS^+ beta cells, SST^+ delta cells, PPY^+ PP cells and $GHRL^+$ epsilon cells on E18.5 WT and *Bicc1* KO pancreatic sections reveals about 50% decrease (beta cells: n=4 for both genotype, p=0.0008; delta cells: WT, n=3; *Bicc1* KO, n=4, p=0.0029; PP cells: WT, n=3; *Bicc1* KO, n=4, p=0.012; epsilon cells: WT, n=3; *Bicc1* KO, n=4, p=0.011), while the GCG^+ alpha cell number is reduced by 20% (WT, n=3; *Bicc1* KO, n =4, p=0.0024).

Sections are counterstained with DAPI ((A-B) blue or (D-E) and (G-H) white). Scale bars 25 μm. See Table 12 in Appendix for further data

At E12.5, the number of cells expressing GCG, the first endocrine cells differentiating in the pancreas was not affected by *Bicc1* deletion (Fig. 19A-C). At E14.5, the number of both alpha and beta cells, identified by their secreted hormones GCG and INS, respectively, was not changed (Fig. 19D-F). As the other endocrine cell types form a rare population, they were only analyzed at a later stage. At the end of gestation, the number of beta cells was reduced by 50%. The number of ghrelin$^+$ ($GHRL^+$) cells (epsilon cells), SST^+ cells (delta cells) and PPY^+ cells (PP cells) were all significantly decreased in *Bicc1* KO pancreata, to the same extent as the beta cells. Finally, the alpha cell number was reduced by 20% (Fig. 19G-I). *Bicc1* deletion thus leads to a global but late endocrine cell decrease during pancreas development.

7.4 Cellular cause of the endocrine cell decrease in *Bicc1* KOs

The endocrine cell decrease might have different causes such as reduced proliferation, dying cells, global decrease of pancreatic progenitor pool or defective differentiation.

7.4.1 Endocrine cell proliferation and survival are not affected by *Bicc1* deletion

Beta cell proliferation was quantified at E18.5 as endocrine proliferation was too low to be reliably quantified earlier. The percentage of beta cells expressing MKI67 was not changed in *Bicc1* KO pancreata as compared to WTs. Moreover, TUNEL assay, performed at E18.5, showed no apoptosis in both WT and *Bicc1* KO beta cells (Fig. 20).

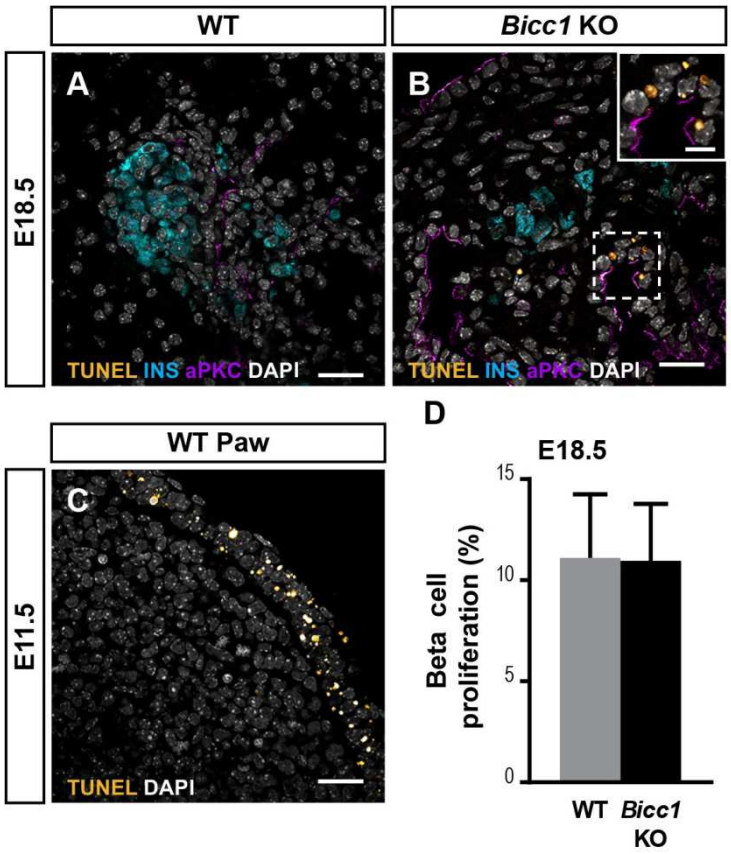

Fig. 20: Beta cell death and proliferation at E18.5 is not affected by *Bicc1* deletion

(A-C) TUNEL assay (orange) followed by immunofluorescence staining for INS (cyan) and aPKC, an apical marker (magenta), on E18.5 WT and *Bicc1* KO pancreatic sections shows no apoptotic death in INS^+ beta cells (n=4 for both genotypes). By contrast, $TUNEL^+$ nuclei are seen in the ducts delimited by aPKC (yellow arrowhead) in *Bicc1* KO pancreata. An E11.5 paw is used as a positive control for the TUNEL assay.

(D) Percentage of $MKI67^+$ INS^+ beta cell number among beta cells quantified on INS and MKI67 immunostained E18.5 *Bicc1* KO and WT pancreatic sections, shows no difference between E18.5 WT and Bicc1 KO pancreata (p=0.95).

Sections are counterstained with DAPI (white). (n=4 for both genotypes) Scale bars A-C 25 µm and insets 10 µm. See Table 12 in Appendix for further data.

7.4.2 Endocrine mass reduction in *Bicc1* KOs is not due to pancreatic hypoplasia

The endocrine cell decrease may be explained by a reduction of their progenitor pool, which was thus quantified at different stages. At E12.5, contrary to what might be expected based on the endocrine cell mass reduction, the number of $PDX1^+$ pancreatic was increased (Fig. 21A-C). However, at E14.5, the number of

pancreatic progenitors marked with PDX1 was back to normal (Fig. 21D). Finally at birth, there was again no difference between *Bicc1* KO and WT pancreata, as quantified by the number of nuclei present in pancreata (Fig. 21E). It thus suggests that there is a transient hyperplasia in *Bicc1* KO pancreata at early stages. At later stages, the size of the pancreas size is normal and cannot cause the observed endocrine cell reduction.

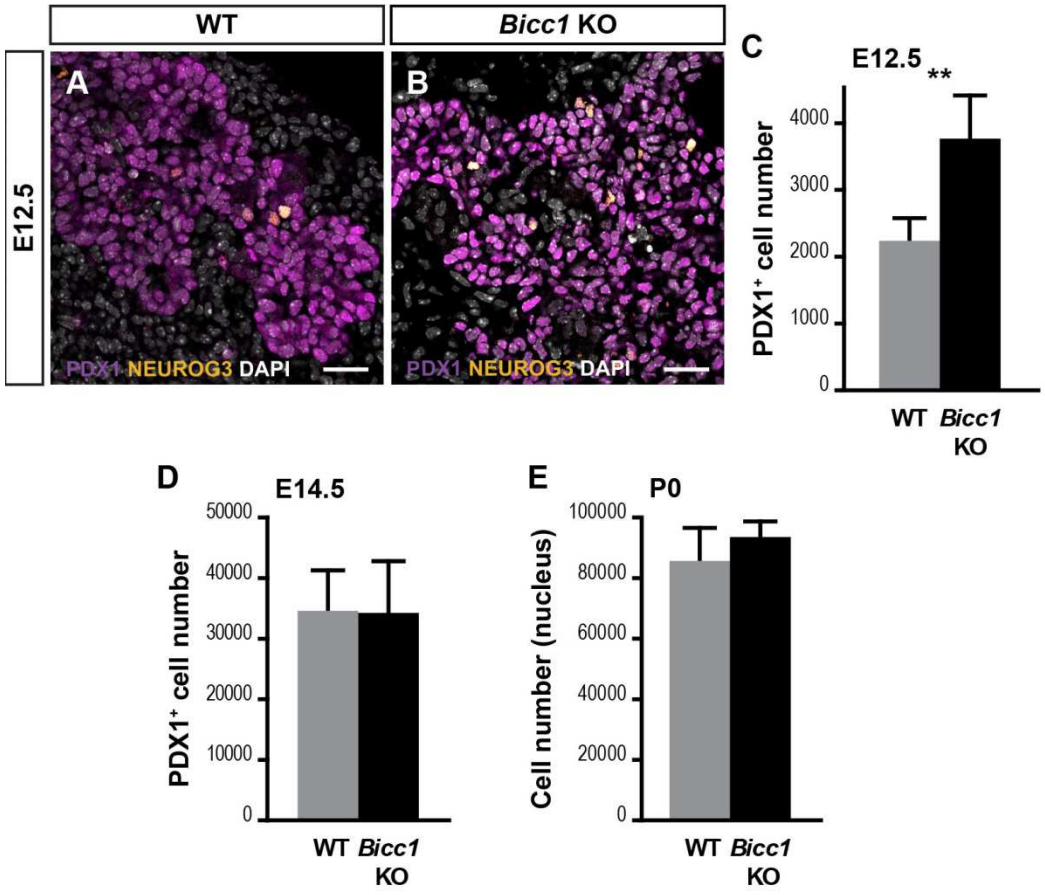

Fig. 21: Pancreatic size is increased at E12.5 but not at E14.5 or at P0 in *Bicc1* KOs

(A, B) Immunostaining for PDX1 (magenta) and NEUROG3 (Orange) was performed on E12.5 *Bicc1* KO and WT pancreatic sections.

(C) Quantification of the previous immunostaining shows an increase of 1.7-fold of PDX1 positive cells (n=4 for each genotype, p=0.0058).

(D) Quantification of the number of pancreatic progenitors immunoreactive for PDX1 on E14.5 pancreatic sections shows no difference between WT and *Bicc1* KO pancreata (n=4 for each genotype, p=0.95)

(E) Quantification of the number of nuclei stained by DAPI at P0 shows no difference between *Bicc1* KO and WT pancreata. (n=4 for each genotype, p=0.24).

Sections are counterstained with DAPI (white), scale bar 25 µm. See Table 12 in Appendix for further data.

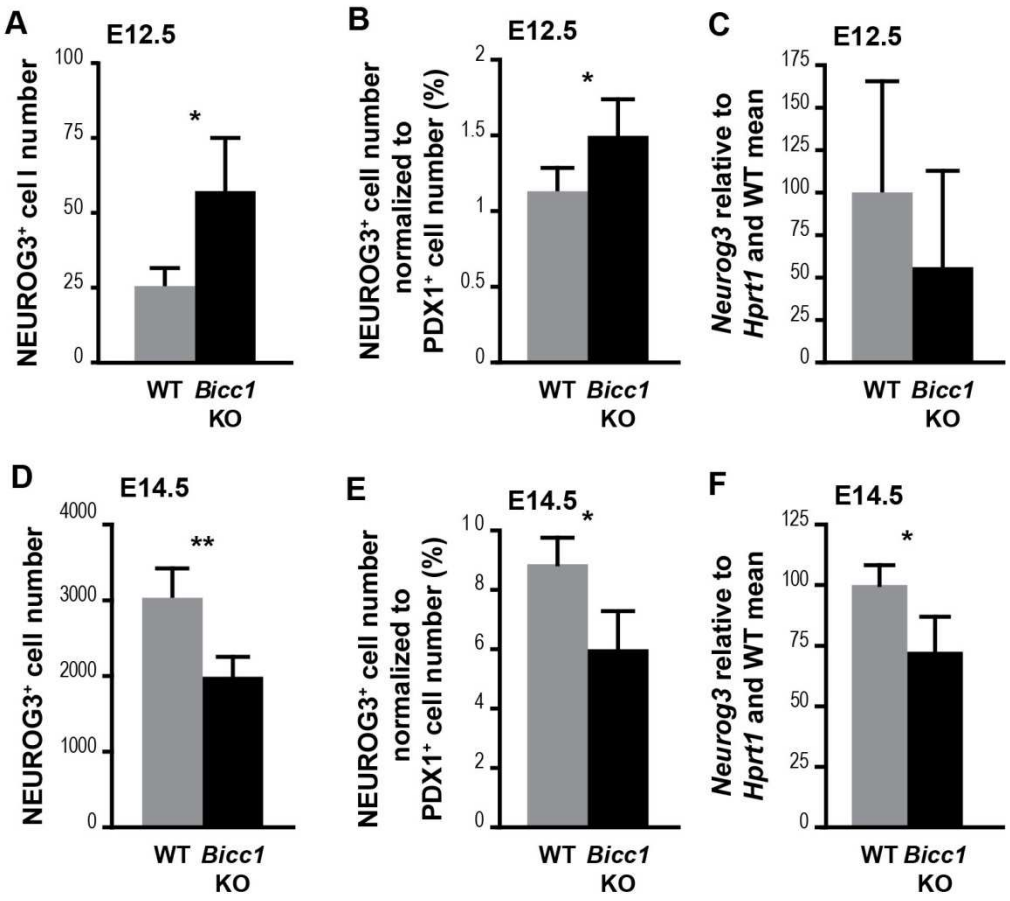

Fig. 22: Endocrine progenitor cells are decreased at E14.5 but not at E12.5 in *Bicc1* KOs

(A) Quantification of NEUROG3$^+$ cells detected on immunostained E12.5 *Bicc1* KO and WT pancreatic sections shows a 2.2-fold increase in *Bicc1* KO (n=4 for both genotypes, p=0.015).

(B) The quantification in (A) is normalized to the number of PDX1$^+$ pancreatic progenitors immunostained at the same time and indicated in percent (Fig. 21A, B). The proportion of NEUROG3$^+$ cells compared to PDX1$^+$ cells is increased 1.4-fold in *Bicc1* KO (n=4, for each genotype, p=0.043)

(C) Q-PCR analysis for *Neurog3* in E12.5 WT and *Bicc1* KO dorsal bud pancreata shows no difference and a very high variability (WT, n=6; *Bicc1* KO, n=5, p=0.27).

(D) Quantification of NEUROG3$^+$ cells detected on immunostained E14.5 *Bicc1* KO and WT pancreatic sections shows a decrease by 34% in *Bicc1* KO (n=4 for both genotype, p=0.0043).

(E) The quantification in (D) is normalized on the number of PDX1$^+$ pancreatic progenitors immunostained on adjacent sections (Fig. 21D), and indicated in percent. The proportion of NEUROG3$^+$ cells compared to PDX1$^+$ cells is still decreased to the same degree as in (D), by 32%, in *Bicc1* KOs (n=4, for each genotype, p=0.011)

(F) Q-PCR analysis for *Neurog3* in E14.5 WT and *Bicc1* KO dorsal bud pancreata shows a decrease by 27% in the KO (WT, n=4; *Bicc1* KO, n=5, p=0.012).

For Q-PCR analysis, expression levels are normalized to *Hprt1* mRNA level. Results are represented as a percentage of *Neurog3* level in WT. See Table 12 in Appendix for further data.

7.4.3 NEUROG3^{+} cells are reduced upon Bicc1 deletion

To explore the possibility of a defect in the differentiation pathway from pancreatic progenitors toward endocrine progenitors, we quantified the NEUROG3^{+} endocrine progenitor cells. At E12.5 the endocrine progenitors were also increased a little more than the multipotent progenitors (Compare Fig. 21C and Fig. 22A-B), suggestive of a slightly increased differentiation flux. However, it was not confirmed by Q-PCR arguing for a transient hyperplasia of the pancreas and no a specific increase of the endocrine progenitor pool (Fig. 22C).

At E14.5, the endocrine progenitor number was significantly decreased by 34% in *Bicc1* KOs. The same decrease was also observed if the endocrine progenitors were normalized to the PDX1^{+} pancreatic epithelium. It was consistent with a 30% decrease of *Neurog3* mRNA observed by Q-PCR at the same stage (Fig. 22D-F). Together, these results suggest that the endocrine progenitor deficiency observed at E14.5 causes the observed endocrine cell decrease.

7.4.3.1 NEUROG3^{+} cells do not undergo apoptosis

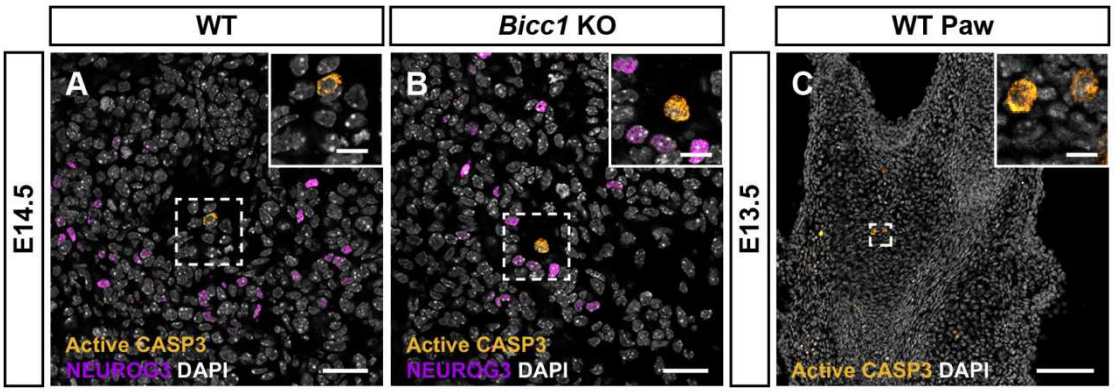

Fig. 23: Endocrine progenitor cells do not undergo apoptosis at E14.5 in *Bicc1* KO

(A-B) Immunofluorescence staining for active caspase3 (CASP3) (orange) and NEUROG3 (magenta) was performed on E14.5 WT and *Bicc1* KO pancreatic sections (n=4 for both genotypes). Insets show a magnified view of the dashed boxes. No apoptosis is observed in endocrine progenitor cells. An E13.5 paw is used as a positive control for active CASP3.

Sections are counterstained with DAPI (white). Scale bar 25 µm, insets 10 µm.

The decrease in NEUROG3$^+$ endocrine progenitors may be explained by a proliferation rate decrease, cell death or a generation rate reduction. It has already been shown that they hardly divide (Desgraz and Herrera, 2009). Moreover, no NEUROG3$^+$ cells were positive for active caspase3 (active CASP3$^+$) or TUNEL in *Bicc1* KO E14.5 pancreas arguing that there was no cell death (Fig. 23; data not shown). These results suggest that the production of NEUROG3$^+$ endocrine progenitors is affected by *Bicc1* deletion.

7.4.3.2 NEUROG3$^+$ progeny is not further affected by Bicc1 deletion

To investigate possible additional differentiation defects after endocrine progenitors had been produced, a short-term lineage tracing experiment was performed using the Neurog3-RFP reporter line (Kim et al., 2015) that marks NEUROG3 expression for about 48h after their emergence. It enabled us to follow the differentiation path from endocrine progenitors toward endocrine cells. Indeed, cells started to express NEUROG3 before expressing RFP. They then switched off NEUROG3, while RFP expression was switched off only after they became hormone-positive (Fig. 24).

To quantitatively follow this differentiation pipeline, different cell populations were quantified: NEUROG3$^+$RFP$^-$, NEUROG3$^+$RFP$^+$, NEUROG3$^-$INS$^-$GCG$^-$RFP$^+$ and INS$^+$ or GCG$^+$RFP$^+$. All of these populations were decreased in *Bicc1* KO pancreata at E14.5 (Fig. 24I). The similar ratio of the different populations in the *Bicc1* KO compared to control argues that the decrease of endocrine cells is mainly due to a decreased conversion of bipotent progenitors into endocrine progenitors that normally differentiate thereafter (Fig. 24J).

Continuation of the legend of Fig. 24

(J) Proportion of the different cell populations among RFP$^+$ cells identified in (A-H). There is no global ratio difference, indicating no slow-down in the differentiation path toward endocrine cells (NEUROG3$^+$RFP$^+$, p= 0.07; Hormones$^+$ RFP$^+$, p=0.80). However, the proportion of NEUROG3$^-$Hormone$^-$ RFP$^+$ in RFP$^+$ cells is slightly higher in *Bicc1* KO pancreas (p= 0.0078)

Sections are counterstained with DAPI (white). N=4 for both genotypes. Scale bars A-H 25 μm. See Table 12 in Appendix for further data.

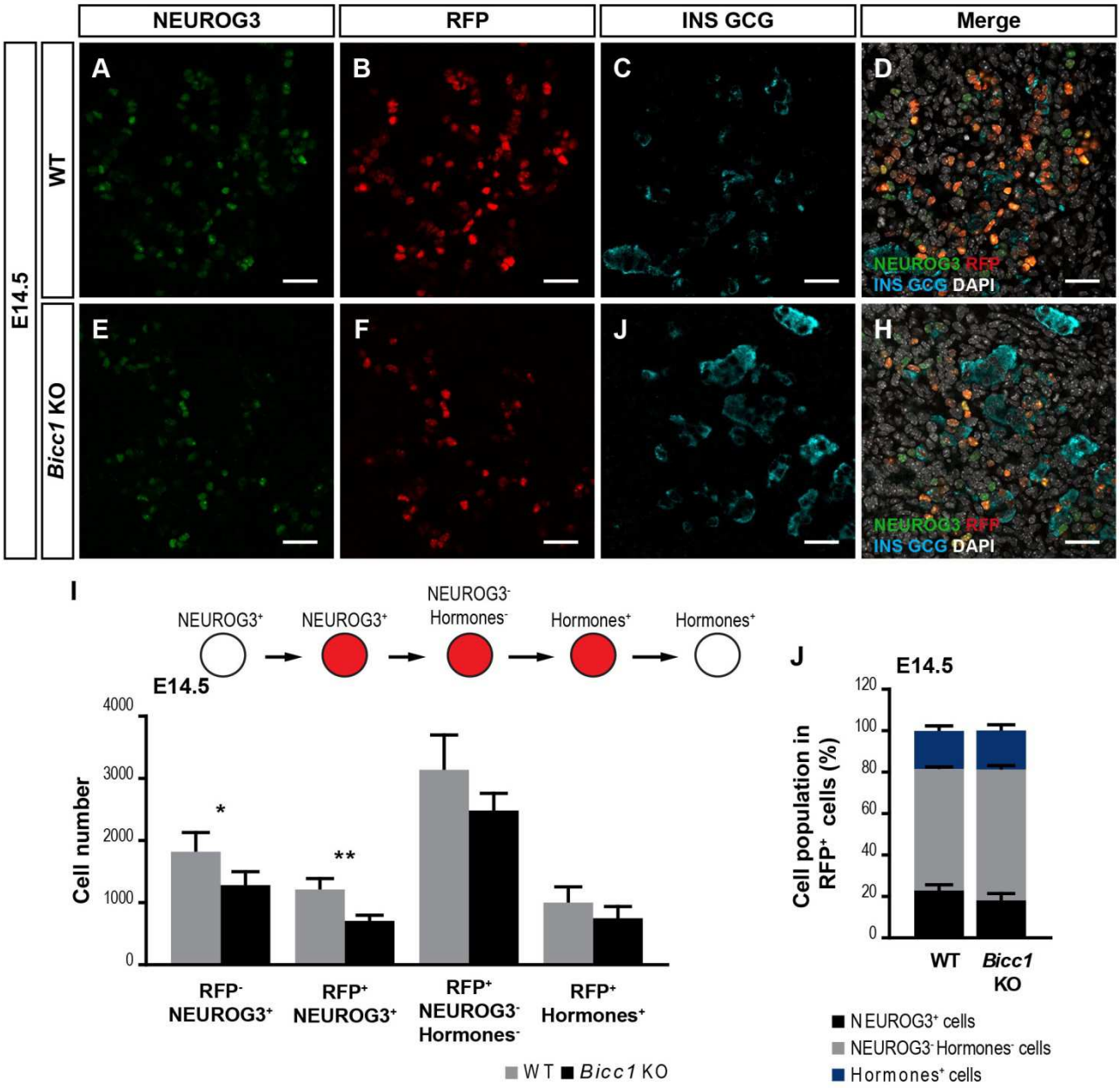

Fig. 24: The endocrine progenitor short-term progeny is decreased to the same extent as endocrine progenitors in *Bicc1* KO

(A-H) An RFP reporter under *Neurog3* promoter, Neurog3-RFP, was used to characterize the differentiation flux from NEUROG3$^+$ endocrine progenitors toward hormone$^+$ endocrine cells. Cells are first NEUROG3$^+$ (green) before becoming double positive for NEUROG3 and RFP (red). They switch off NEUROG3 and thereafter start to express hormones, INS or GCG (cyan), before switching off RFP, as exemplified in the immunofluorescence staining on sections at E14.5 in WT and *Bicc1* KO pancreas.

(I) Quantification of the different cell populations on sections reveals a similar decrease in both RFP$^-$ and RFP$^+$ fractions (NEUROG3$^+$RFP$^-$: p=0.029; NEUROG3$^+$RFP$^+$: p=0.0021). The two last populations, NEUROG3$^-$Hormone$^-$ RFP$^+$ cells and Neurog3$^-$Hormone$^+$RFP$^+$ cells, have a tendency to decrease that does not reach significance (Neurog3$^-$ Hormones$^-$RFP$^+$ cells: p=0.08; Neurog3$^-$Hormones$^+$RFP$^+$ cells: p=0.16).

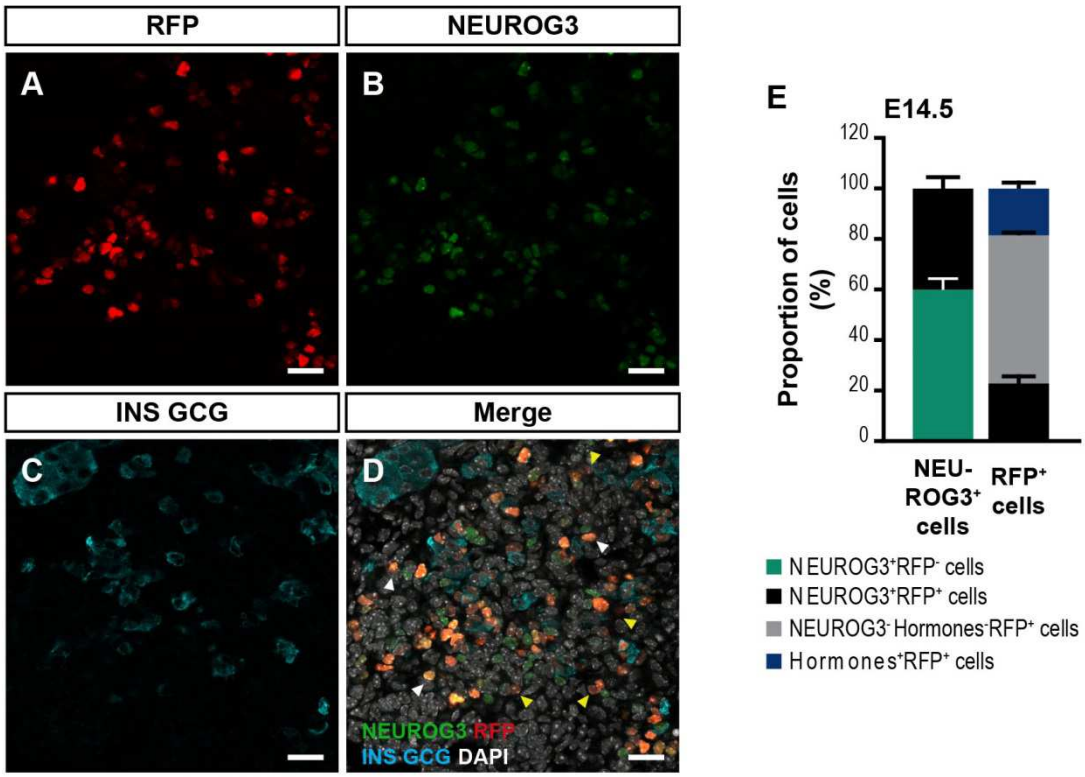

Fig. 25: Characterization of the Neurog3-RFP mouse line

(A-D) Optical section of E14.5 *Neurog3-RFP* pancreas, immunostained for NEUROG3 (cyan), RFP (Orange; immunostained for Myc), and INS and GCG (Magenta) shows that some RFP+ cells co-express NEUROG3 (white arrowhead) but not all (yellow arrowhead).

(E) Proportion of RFP^+ (green) and RFP^- (black) in $NEUROG3^+$ cells, and proportion of $NEUROG3^+$, $Hormones^+$ (identified by INS and GCG) (blue) and $NEUROG3^-/Hormones^-$ (gray) in RFP^+ cells.

Scale bars, 20 µm. See Table 12 in Appendix for further data.

The WT data obtained during these experiments were used to characterize the Neurog3-RFP mouse line (Kim et al., 2015). Only 40% of the $NEUROG3^+$ cells coexpressed RFP^+. The majority of the RFP^+ cells are not $NEUROG3^+$ and nearly 20% expressed either GCG or INS (Fig. 25).

7.4.3.3 The NEUROG3^{+} endocrine production defect is sustained after E14.5

Moreover, long-term lineage tracing using a Neurog3-Cre line crossed with Rosa26-YFP addressed whether NEUROG3^{+} cell differentiation was steadily defective until the end of gestation. The total number of recombined cells harboring the reporter was reduced in the same measure as the endocrine cells thus showing that the defect in endocrine progenitor cell production is sustained over the developmental period. No increase of NEUROG3 progeny in the acinar and ductal exocrine compartment was observed in *Bicc1* KOs, indicating that the cells expressing *Neurog3* are not diverted to a different developmental path (Fig. 26).

Together these data support that the endocrine cell defect observed in *Bicc1* KOs is due to an endocrine progenitor generation defect.

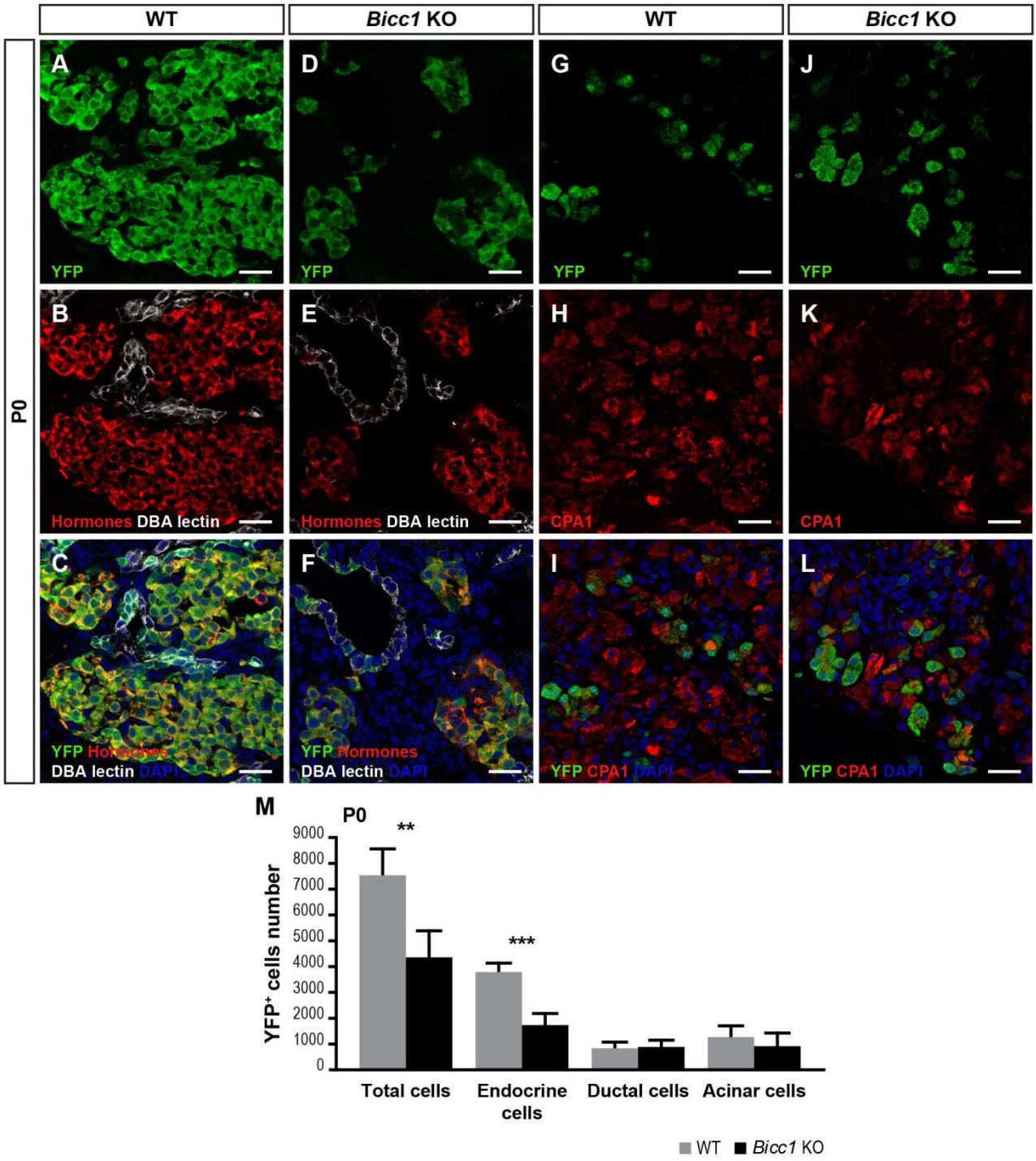

Fig. 26: The Endocrine progenitor long-term progeny is reduced similarly to the endocrine cells in *Bicc1* KO.

Legend of the Fig. 26

(A-L) Lineage tracing using the Neurog3-Cre mouse line crossed with the Rosa26 YFP mouse line. Immunofluorescence stainings for INS, GCG, SST (Hormones, red), DBA lectin (white) and YFP (green) or CPA1 (red) and YFP were done on P0 WT and *Bicc1* KO pancreatic sections.

(M) The total number of YFP^+ cells as well as YFP^+ cells among endocrine cells ($Hormones^+$) is decreased by half (Total cells, p=0.0046 and Endocrine cells, p=0.0003). YFP^+ cell numbers in acini is not significantly changed (p=0.49), and the number of $YFP^+DBA\ lectin^+$ cells in the ducts is unchanged either (p=0.78), reflecting the increased duct size in *Bicc1* KOs.

Sections were counterstained with Draq5 (blue). N=4 for each genotype Scale bars 25 μm. See Table 12 in Appendix for further data

7.5 Molecular causes of endocrine cell decrease in *Bicc1* KOs

The mechanism by which BICC1 controls $NEUROG3^+$ endocrine progenitors was further investigated. BICC1 binds to mRNAs and regulates positively or negatively their translation in mouse (Tran et al., 2010; Piazzon et al., 2012). A direct regulation of *Neurog3* mRNA by BICC1 is unlikely since *Neurog3* transcriptional reporters were affected by *Bicc1* deletion to the same degree as NEUROG3 protein. Instead, BICC1 may target activators or repressors of *Neurog3*.

7.5.1 BICC1 does not regulate NOTCH signaling pathway

$NEUROG3^+$ cell production is negatively regulated by the NOTCH pathway. HES1, expressed upon NOTCH pathway activation, is a repressor of *Neurog3*. Its deletion leads to massive $NEUROG3^+$ cell production and endocrine differentiation (Jensen et al., 2000b; Lee et al., 2001). However, HES1 protein levels were not changed in *Bicc1* KO pancreata at E15.5 (Fig. 27A, B). Its mRNA level was also unchanged one day earlier, as was the mRNA level of *Dll1* that activates the NOTCH pathway (Apelqvist et al., 1999) (Fig. 27C). In conclusion, the NOTCH pathway does not appear to be affected by *Bicc1* deletion in the pancreas.

7.5.2 BICC1 does not control SOX9, ONECUT1, FOXA2, PDX1, or HNF1B

We therefore asked whether the loss of *Bicc1* affects transcription factors that activate *Neurog3* such as SOX9, FOXA2, PDX1, HNF1B or ONECUT1 (Jacquemin et al., 2000; Lynn et al., 2007). The SOX9 expression pattern was indistinguishable between *Bicc1* KO and WT pancreata at E14.5 (Fig. 27D, E). Moreover, the protein levels of SOX9, FOXA2, PDX1, and HNF1B were not changed at E15.5 upon *Bicc1* deletion (Fig. 27A, B). Although *Onecut1* mRNA was increased by 34% in *Bicc1* KO compared to WT pancreas (Fig. 27F), its protein level was not changed one day later (Fig. 27A, B), and the localization of the protein was normal (Fig. 27H, I). In conclusion, NEUROG3^{+} cell reduction is not due to a decrease of its activators SOX9, FOXA2, PDX1, HNF1B and ONECUT1.

Legend of the Fig. 27

(A) Western blot performed for SOX9, HES1, HNF1B, FOXA2, PDX1, and ONECUT1 on E15.5 WT and *Bicc1* KO pancreata, and alpha tubulin (TUB) as a loading control.

(B) Quantification of the western blot shown in (A) is performed by normalizing band intensity to TUB intensity. Results are relative to WT mean. None of them are affected by *Bicc1* deletion (SOX9: WT, n=4; *Bicc1* KO, n=4, p= 0.30; HES1: WT, n=4; *Bicc1* KO, n=4, p=0.06; HNF1B: WT, n=4; *Bicc1* KO, n=4, p= 0.10; FOXA2: WT, n=4; *Bicc1* KO, n=4, p= 0.48; PDX1: WT, n=4; *Bicc1* KO, n=4, p= 0.37; ONECUT1: WT, n=7; *Bicc1* KO, n=8, p= 0.13).

(C) Q-PCR analysis for *Hes1* and *Dll1* performed on E14.5 WT and *Bicc1* KO dorsal pancreata does not show any differences (*Hes1*: WT, n=4; *Bicc1* KO, n=5, p=0.45; *Dll1*: WT, n=4; *Bicc1* KO, n=5, p=0.55).

(D-E) Immunofluorescence staining performed on E14.5 WT (n=4) and *Bicc*1 KO (n=4) pancreatic sections do not show SOX9 (orange) expression pattern differences between both genotypes.

(F) Q-PCR analysis of *Onecut1* in WT versus *Bicc1* KO E14.5 dorsal buds reveals a 34% increase in *Onecut1* transcript in the KO (WT, n=4; *Bicc1* KO, n=5, p=0.042).

(G) Q-PCR analysis of *Bicc1* in WT versus *Onecut1* KO E14.5 dorsal buds shows a decrease by 40% of *Bicc1* transcript in the *Onecut1* KO (WT, n=4; *Onecut1*, n=3, p=0.027).

(H-I) Immunofluorescence staining for ONECUT1 on E14.5 WT (n=2) and *Bicc1* KO (n=2) pancreatic sections shows no expression pattern difference. Q-PCR results are normalized to the housekeeping gene *Hprt1*. Results are represented in percent of WT mean.

Sections are counterstained with DAPI (white). Scale bars 25 μm. See Table 10 in Appendix for further data.

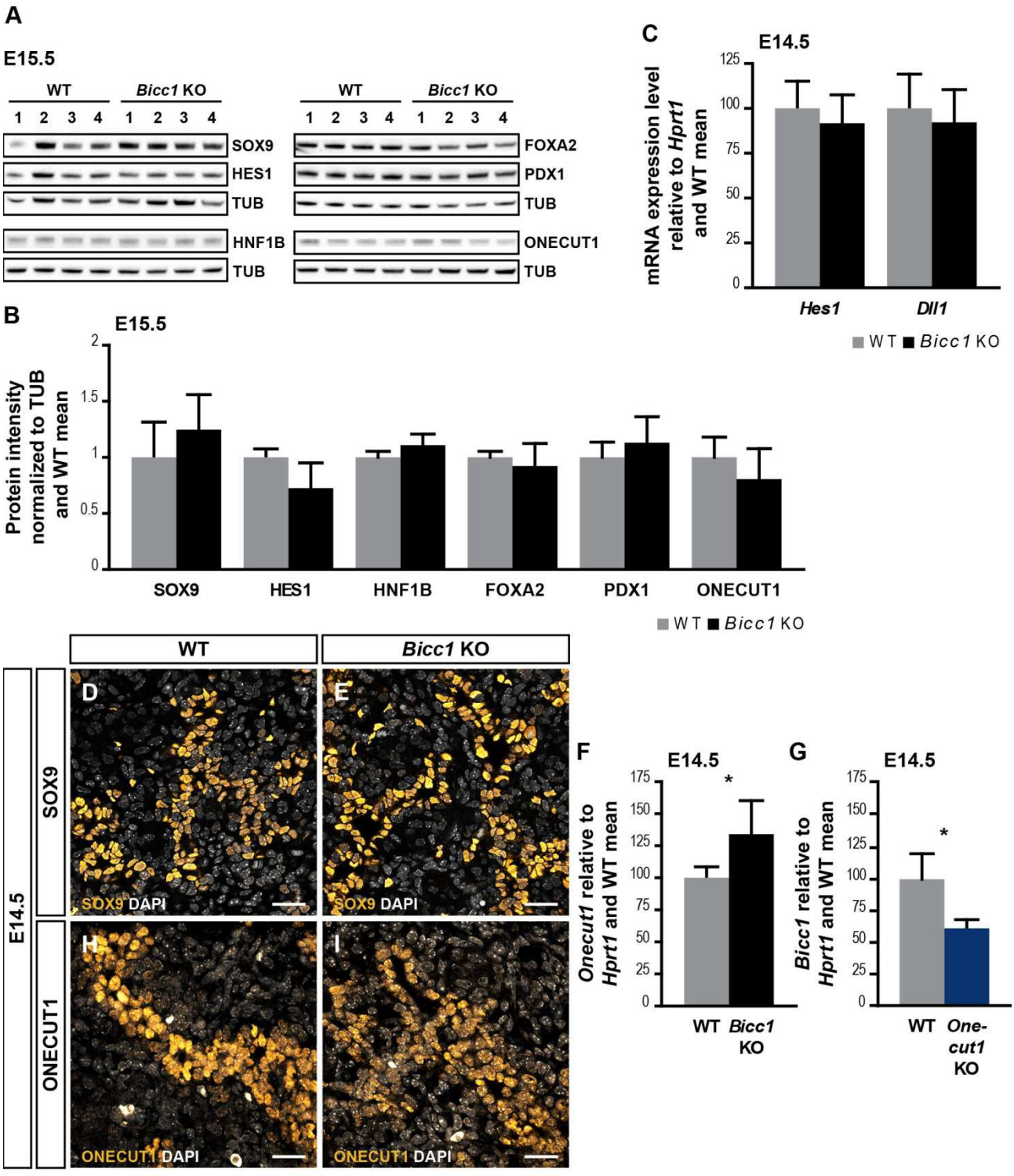

Fig. 27: BICC1 does not regulate the NOTCH pathway or known *Neurog3* transcriptional activators and functions downstream of ONECUT1.

7.5.3 Bicc1 acts downstream of ONECUT1

Onecut1 KO embryos also develop pancreatic cysts combined with a decrease in endocrine cells due to defective endocrine progenitor differentiation (Lynn et al., 2007). Since the experiments above showed that BICC1 does not promote ONECUT1 expression, we investigated whether BICC1 functions downstream of *Onecut1*. Indeed, we found that *Bicc1* mRNA was decreased by 40% in *Onecut1* KO pancreata (Fig. 27G), suggesting that ONECUT1 promotes *Bicc1* expression.

7.5.4 WNT signaling is not affected by Bicc1 deletion

Although BICC1 was previously shown to control WNT signaling in the node and in a cell line reporter assay (Maisonneuve et al., 2009), we did not detect any change in *Axin2* and *Tcf7*, two WNT targets, nor any alterations in the expression of the *Axin2-LacZ* reporter in the pancreata of *Bicc1* KOs at E14.5 (Fig. 28).

Taken together, these results show that *Neurog3* is transcriptionally regulated by BICC1 but this effect is likely to be indirect and we have not identified a direct target.

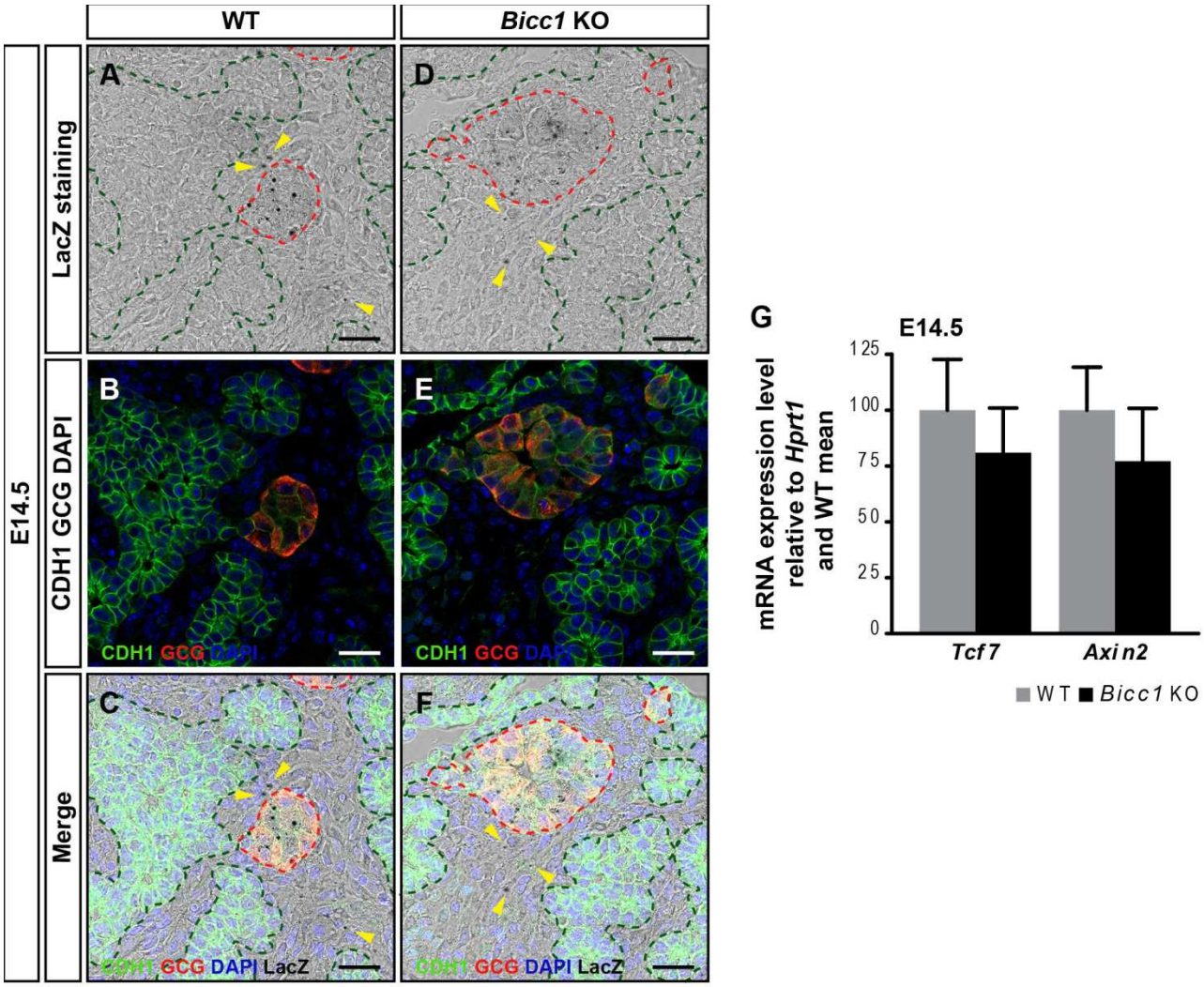

Fig. 28: Canonical WNT signaling is not affected by *Bicc1* deletion in the pancreas

(A-F) LacZ staining followed by fluorescence immunostaining on sections of the pancreas of WT; *Axin2* $^{LacZ/+}$ and *Bicc1* KO; *Axin2* $^{LacZ/+}$ embryos at E14.5. LacZ staining (black dots) is detected in GCG^{+} cells (red, red dashed lines) and in some mesenchymal cells (yellow arrowheads) but not in the pancreatic progenitor epithelium, stained by CDH1 (green, green dashed lines) both in WT (n=3) and in *Bicc1* KO (n=3).

(G) Q-PCR analysis for *Tcf7* and *Axin2* in E14.5 WT and *Bicc1* KO dorsal bud pancreata shows no alteration in KOs (WT, n=4; *Bicc1* KO, n=5: *Tcf7*, p=0.22; *Axin2*, p=16). Expression levels are normalized to *Hprt1* mRNA level. Results are represented as a percentage of mRNA level of WT mean.

Sections were counterstained with DAPI (blue). Scale bar 25 µm. See Table 12 in Appendix for further data.

7.6 Molecular mechanisms behind pancreatic cyst formation

7.6.1 Uncovering BICC1 targets by RNA sequencing

To decipher the molecular mechanisms underlying cyst formation in *Bicc1* KO pancreata, E13.5 *Bicc1* KO and WT pancreas transcriptomes were compared by RNA sequencing. At this stage, duct enlargement was not yet observed allowing us to detect expression changes prior to cyst formation rather than as a consequence of it. Moreover, the RNA sequencing data gave a clear idea of the genes expressed as well as their global expression level at E13.5 in dorsal pancreatic buds (Fig. 29).

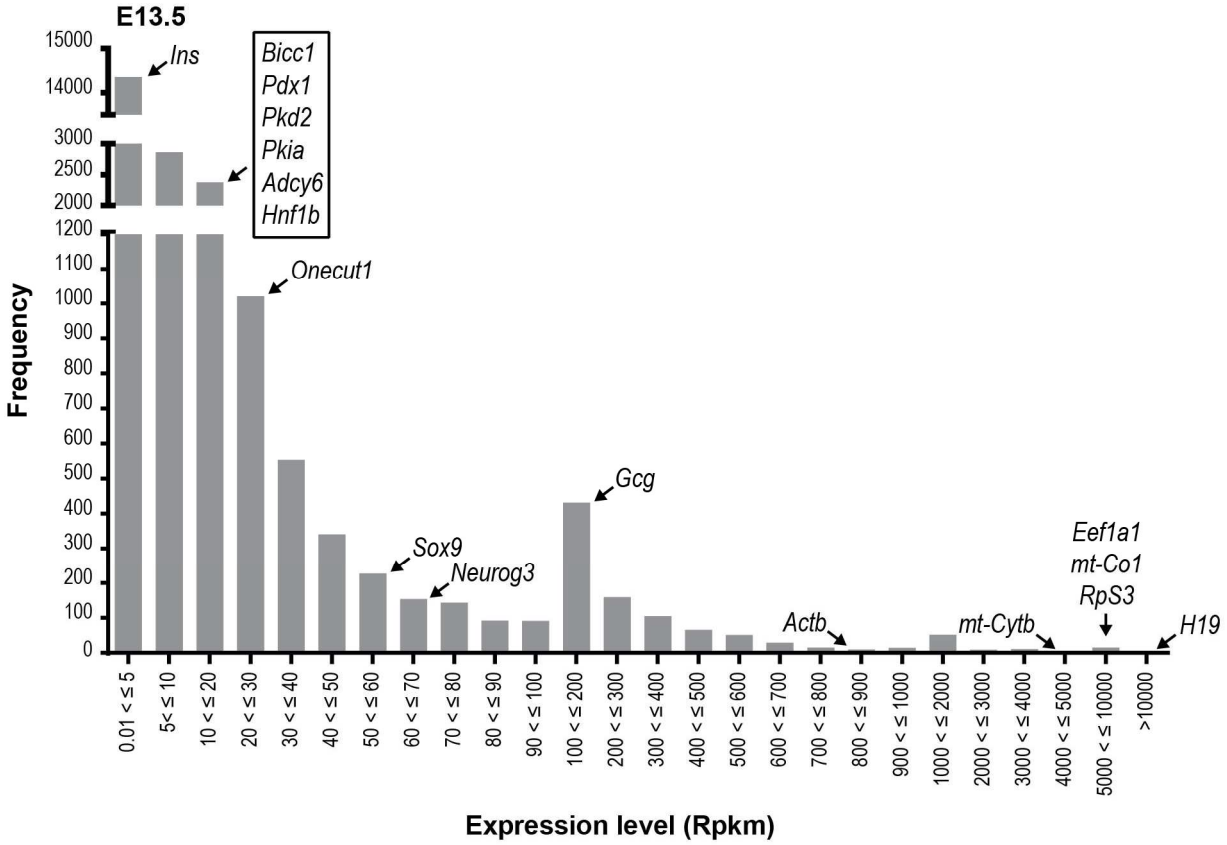

Fig. 29: Histogram of the number of genes in function of their expression level in E13.5 dorsal pancreatic buds. Expressed genes in E13.5 WT pancreatic dorsal buds are classified in function of their expression level in read per kilobase per million (rpkm). For clarity, genes which have an rpkm below 0.01 are not represented. Expression level of relevant landmark genes is indicated with an arrow.

The RNA sequencing data where first analyzed using the DESeq method (Anders and Huber, 2010). However, this method only gives p-value and no FDR rendering the analysis less stringent. With this

approach, the majority of genes significantly changed between *Bicc1* KO and WT pancreatic buds, were lowly expressed (Tables 13, 14 in Appendix). Fold Changes were important but may have little biological significance.

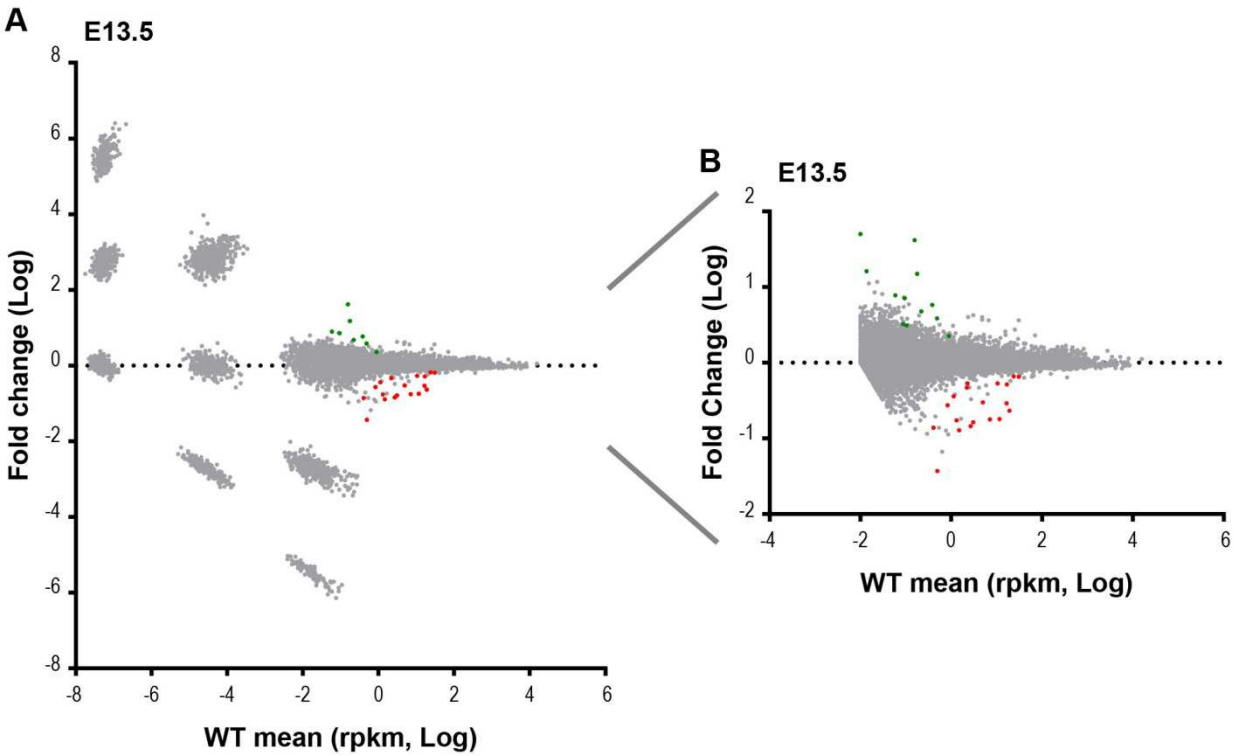

Fig. 30: E13.5 *Bicc1* KO and WT dorsal pancreatic bud transcriptome comparison using ANOVA

(A) Transcriptome analysis comparing E13.5 *Bicc1* KO and WT dorsal buds shows high amounts of lowly expressed genes. Only 8 and 18 genes were respectively significantly upregulated (green) and downregulated (red).

(B) The same analysis was performed without genes having an average rpkm below 0.01. 12 and 19 genes were respectively significantly upregulated (green) and downregulated (red).

Both plots represent the fold change in function of WT expression level mean in rpkm. Both axes have a logarithmic scale. Each dot represents a gene.

The analysis was repeated with a more stringent method based on ANOVA and calculating FDR (Sharov et al., 2005). For example, *Neurog3* was found downregulated in *Bicc1* KOs with a p value of 0.0027 while its FDR was more than 0.5 (Table 13). This example shows that some genes in this low-confidence category may be significant or may just begin to change and may become significant the day after.

Table 4: Upregulated mRNA in E13.5 *Bicc1* KO pancreas

Gene symbol	WT mean (rpkm)	*Bicc1* KO mean (rpkm)	fold change	FDR
Slc16a3	0.89	2.02	2.27	0.0049
Description	Proton-linked pyruvate and lactate transporter (reviewed in Halestrap, 2013)			
Gm15745	0.16	6.51	41.82	0.0006
Description	Predicted protein with a putative RNA binding domain[10,11]			
RP23-281E24.2	0.49	1.87	3.85	< 0.0001
Description	Predicted protein without predicted domain[10,11]			
Cma1	0.38	2.23	5.84	0.0009
Description	Secretory granule protease, expressed by mast cells (Reynolds et al., 1990)			
Six2	0.18	2.67	15.06	0.0004
Description	Transcription factor involved among other in kidney development (Oliver et al., 1995; Self et al., 2006)			
Fam162b	0.22	1.05	4.77	< 0.0001
Description	Predicted protein with a transmembrane domain[10,11]			
Hdc	0.10	0.32	3.12	0.0446
Description	Enzyme synthetizing histamine from histidine (Werle, 1936; first KO description in Ohtsu et al., 2001)			
Rpl30-ps5	0.09	0.28	3.24	0.0473
Description	Pseudogene[10]			
Myod1	0.09	0.67	7.14	< 0.0001
Description	Transcription factor involved among other in muscle differentiation (Davis et al., 1987; Lassar et al., 1989)			
Nkx2.5	0.06	0.46	7.83	0.0321
Description	Transcription factor involved among other in heart development (Komuro and Izumo, 1993; Lyons, I. et al., 1995)			
Mcpt4	0.01	0.22	16.23	< 0.0001
Description	Secretory granule protease, expressed by mast cells (Reynolds et al., 1990)			
1700023F06Rik	0.01	0.50	50.43	< 0.0001
Description	Predicted protein with 2 EF-hand motifs (calcium binding motif)[10,11]			

mRNAs found upregulated in *Bicc1* KO compared to WT pancreata are ordered according to NIA array analysis tool and after filtering of the data. The ordering is based on a combination of their expression level in rpkm, their fold change, and their FDR.

[10] Based on Ensembl genome browser
[11] Based on SMART tool

Table 5: Downregulated mRNA in E13.5 *Bicc1* KO pancreas

Gene symbol	WT mean (rpkm)	*Bicc1* KO mean (rpkm)	fold change	FDR
Bicc1	19.12	4.43	4.31	< 0.0001
S100a9	11.63	2.10	5.54	0.0083
Description	Calcium binding protein, it form a dimer with S100A8. They have different roles in inflammation (reviewed in Kerkhoff et al., 2012)			
Pah	16.42	4.78	3.43	0.0118
Description	Catabolizes phenylalanine into tyrosine (Mitoma, 1956)			
S100a8	7.10	1.26	5.62	0.0111
Description	Calcium binding protein, it form a dimer with S100A9. They have different roles in inflammation (reviewed in Kerkhoff et al., 2012)			
Calcr	16.85	8.74	1.93	< 0.0001
Description	Receptor for calcitonin, lowering blood calcium (Copp and Cheney, 1962; Yamin et al., 1994)			
2010107G23Rik	30.82	20.19	1.53	0.0321
Description	Predicted protein with one transmembrane domain[12,13]			
Pkd2	10.57	5.63	1.88	0.0001
Description	Calcium channel, see introduction p 59			
Crp	23.85	15.71	1.52	0.0092
Description	Activator of the immune acute phase (Bodmer and Siboo, 1977)			
4930533K18Rik	4.95	1.48	3.34	< 0.0001
Description	Predicted protein without predicted domain[12, 13]			
BC100530	3.07	0.50	6.10	0.0118
Description	Predicted protein with a cystatin-like domain[12, 13]			
Slc5a9	2.30	1.22	1.88	0.0481
Description	Sodium-dependent glucose transporter (Tazawa et al., 2005)			
Cer1	2.19	1.03	2.13	0.009
Description	BMP and Nodal antagonist (Belo et al., 2000)			
Ngp	2.69	0.39	6.88	0.0027
Description	Secreted protein, expressed during myeloid differentiation (Moscinski and Hill, 1995)			
Anxa9	1.13	0.41	2.77	0.0006
Description	Interacts with periplakin in the epidermis (Boczonadi and Määttä, 2012)			
Gm5483	1.31	0.23	5.77	0.0004
Description	Predicted protein with a cystatin-like domain[12, 13]			
Gm13305	0.84	0.23	3.66	< 0.0001
Description	Predicted protein coding from Il11ra2[12]			
Olfm4	1.48	0.19	7.83	0.0001
Description	Extracellular glycoprotein involved in innate cell immunity (Rosenbauer et al., 2004)			

[12] Based on Ensembl genome browser
[13] Based on SMART tool

Il11ra2	0.41	0.06	7.22	< 0.0001
Description	Alpha chain receptor for interleukin11, present in testis, lymph node and thymus (Robb et al., 1997)			
Gm2002	0.49	0.02	26.95	< 0.0001
Description	Predicted protein coding from Il11ra2[14]			

mRNAs found downregulated in *Bicc1* compared to WT pancreata are ordered according to NIA array analysis tool and after filtering of the data. The ordering is based on a combination of their expression level in rpkm, their fold change, and their FDR.

The RNA sequencing data were also filtered to remove the noise, *i. e.* genes with less than 0.01 rpkm representing more than 2000 genes (Fig. 29 and 30). Even so, only few genes were significantly upregulated or downregulated with a FDR below 0.05 (Tables 4, 5). All upregulated genes were expressed at low levels, with an rpkm below 1 in WT pancreata. These results suggest little changes at the mRNA levels in *Bicc1* KO pancreata compared to WTs prior cyst and endocrine progenitor defect onset.

7.6.2 MicroRNA sequencing

BICC1 regulates translation via miRNAs in vertebrates (Tran et al., 2010; Piazzon et al., 2012). To gain insight into the miRNAs expressed in the pancreas at E13.5the miRNA content of E13.5 WT and *Bicc1* KO dorsal pancreatic buds were sequenced. We could not collect enough material for multiple independent sequences and the data presented in (Fig. 31) thus represent the outcome of one WT sample, all consisting of several pancreatic buds. More than 800 microRNAs were uncovered. The range of microRNA expression level was very broad. The majority of them had high rpkm due to the small length of microRNAs and the high depth of the sequencing (Fig. 31).

[14] Based on Ensembl genome browser

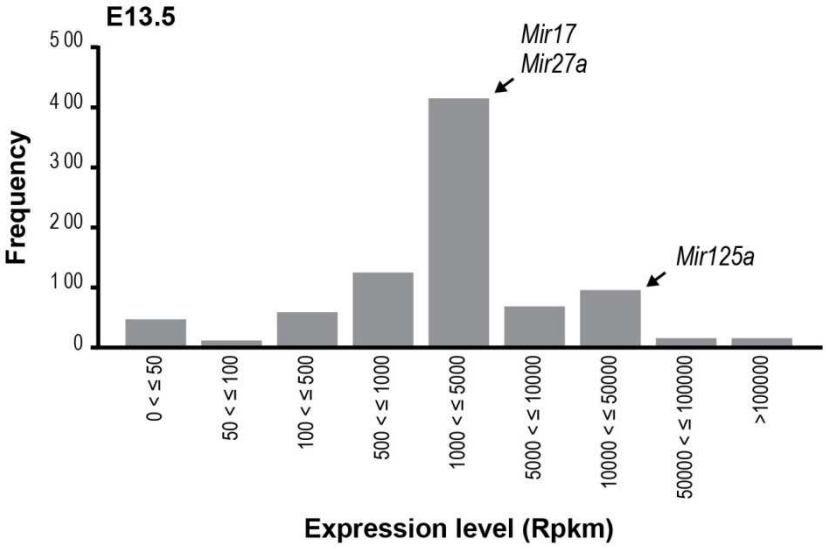

Fig. 31: Distribution of mircoRNAs found in E13.5 dorsal pancreatic buds by RNA sequencing

Expressed microRNAs in E13.5 WT pancreatic dorsal buds are classified in function of their expression level in rpkm. The expression level of microRNAs known to interact directly or not with BICC1 is indicated with an arrow.

Even though BICC1 was never shown to regulate miRNA half-life, miRNA content in WT and *Bicc1* KO pancreatic dorsal buds were compared using DESeq method. As no replicates were sequenced, miRNA fold changes were considered significant when their p-value was below 0.01. 10 miRNA were upregulated in *Bicc1* KO pancreatic buds and 1 was downregulated (Table 6).

Table 6: miRNA changed in E13.5 *Bicc1* KO pancreatic dorsal bud compared to WT

Gene symbol	WT (rpkm)	KO (rpkm)	fold change	p-value
Mir29b-1	299	812	2.72	< 0.0001
Mir875	821	1657	2.02	0.0001
Mir6243	4319	11616	2.69	0.0002
Mir6366	1650	3797	2.30	0.0003
Mir2183	1216	2306	1.90	0.0014
Mir494	1546	2989	1.93	0.0023
Mir5127	1074	1864	1.74	0.0038
Mir344c	8033	3941	0.49	0.0038
Mir804	346	599	1.73	0.0048
Mir3471-2	648	1058	1.63	0.0064
Mir23b	1586	2832	1.79	0.0068

Changed miRNAs in *Bicc1* KO dorsal pancreatic buds are ranked by p-value obtained with DESeq. n=1 per genotype

Targets for these miRNAs were then searched among the mRNAs down- or up-regulated upon BICC1 inactivation, using the DESeq analysis (Tables 13, 14 in Appendix). Based on seed discovery, only four upregulated genes were targeted by one of the differentially expressed miRNAs (Table 7).

Table 7: Putative mRNA targets of differentially expressed miRNA in *Bicc1* KOs at E13.5

Gene symbol	mean WT (rpkm)	Fold change	p-value	Targeted by
Slc2a1	10.71	1.57	0.0241	Mir374
Stard9	0.56	1.63	0.0304	Mir804
Robo2	2.59	2.75	< 0.0001	Mir494
Tnfrsf9	0.10	2.94	0.0176	Mir494

Putative targets, based on seed discovery by TargetScan, are ranked in function of their fold change.

As the genes uncovered were not present in the ANOVA analysis, this research line was not pursued. Moreover, if BICC1 behaves as previously reported (Dorey and Hill, 2006; Piazzon et al., 2012; Zhang et al., 2013), only the protein level of BICC1 pancreatic targets may change in absence of BICC1 without mRNA level modification. Changes in the levels of miRNAs and their putative targets could be secondary effects of *Bicc1* deletion and may not necessarily reflect direct interactions with BICC1.

7.6.3 *Bicc1* deletion is associated with PKD2 downregulation

Among the downregulated genes in the RNA sequencing, *Pkd2* was decreased by 1.9 fold in *Bicc1* KO compared to WT pancreata (Table 5). Since PKD2 deficiency results in pancreas and kidney cyst formation (Wu et al., 2000; Chang et al., 2006), we decided to validate whether its expression in *Bicc1* KO pancreata is also reduced at the protein level.

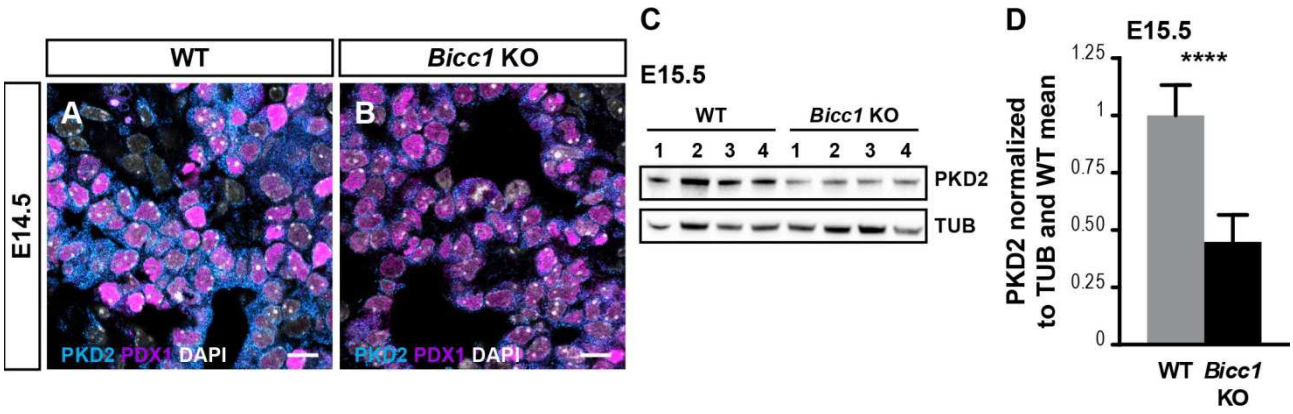

Fig. 32: PKD2 expression level is downregulated in *Bicc1* KO.

(A-B) E14.5 WT and *Bicc1* KO pancreatic sections were stained by immunofluorescence for PKD2 (cyan) and PDX1 (yellow) highlighting pancreatic epithelium. E14.5 *Bicc1* KO pancreata (n=4) have a marked PKD2 decrease in the epithelium compared to WT littermate pancreata (n=4)**.**

(C) Example of western Blot for PKD2 in E15.5 WT and *Bicc1* KO pancreata and TUB as a loading control.

(D) Quantification of the Western blot shown in (C). PKD2 intensity is normalized to TUB intensity, and results are relative to WT mean. PKD2 in *Bicc1* KO pancreata is decreased 2.1-fold (WT, n=8; *Bicc1* KO, n=8, $p<0.0001$)

Sections are counterstained with DAPI (white). Scale bars A-B 10 µm. See Table 12 in Appendix for further data.

Immunostaining detected PKD2 protein in pancreatic ducts, and this signal was significantly diminished in *Bicc1* KOs. Moreover, Western blot confirmed a 2.1-fold decrease in PKD2 protein levels in *Bicc1* KO pancreata at E15.5. Since this decrease is similar in magnitude to the one detected by RNA sequencing at the mRNA levels (1.9-fold), we conclude that BICC1 regulates PKD2 expression primarily before mRNA translation (Fig. 32).

7.6.4 *Bicc1* KO pancreata are characterized by an immune response and a stromal reaction

Due to the small number of differentially regulated genes uncovered by the ANOVA analysis, it was not possible to perform gene ontology analysis. Nevertheless an important proportion of both up and downregulated genes were related to the immune system such as *S100a8, S100a9, Crp, Cma1* arguing for an immune status change (Tables 4, 5).

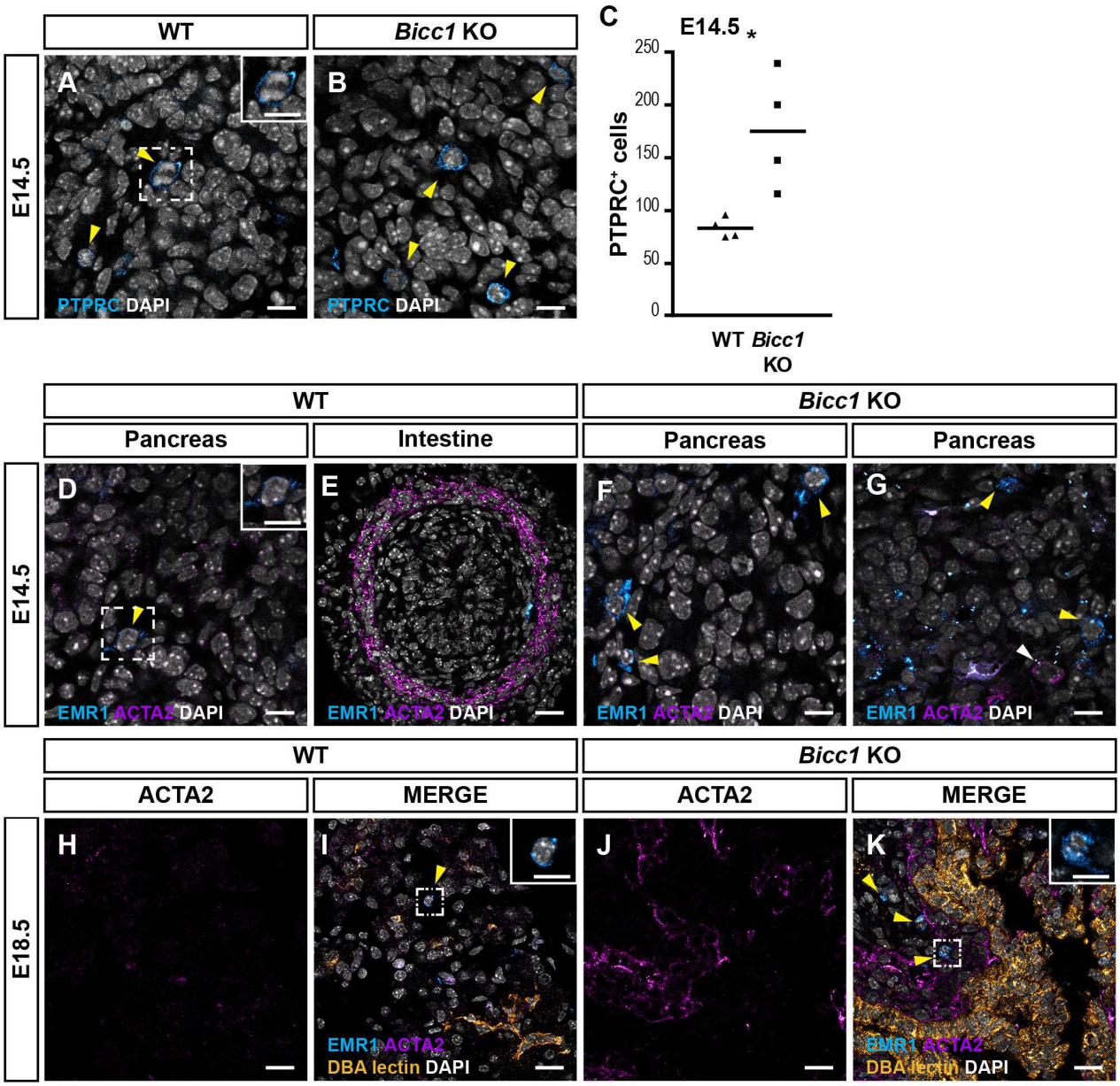

Fig. 33: Immune cell infiltration and stromal reaction are observed in *Bicc1* KO.

(A-B) Immunofluorescence staining for PTPRC (cyan), a pan-immune marker also called CD45 (yellow arrowheads), is performed on E14.5 WT and *Bicc1* KO pancreatic sections. The inset in (A) shows a high magnification of the dashed box.

(C) Quantification of the immunostaining shows a 2.1-fold increase of PTPRC^{+} cells in *Bicc1* KOs (WT, n=4; *Bicc1* KO, n=4, p=0.017).

(D-G) Immunofluorescence staining performed on E14.5 WT (n=5) and *Bicc1* KO (n=6) pancreata for EMR1 (cyan), a macrophage marker, and ACTA2 (magenta). E14.5 WT intestinal wall is used as a positive control for ACTA2. Both genotypes show EMR1^{+} macrophages in the pancreas. While ACTA2^{+} cells are not observed in E14.5 WT pancreata, they were present in a subset of *Bicc1* KO pancreata. Inset represents high magnifications of the dashed box.

Legend of the Fig. 33.

(H-K) Immunofluorescence staining for ACTA2 (magenta), EMR1 (cyan) and DBA lectin (orange) performed on E18.5 WT and *Bicc1* KO pancreatic sections. $ACTA2^+$ cells surround cysts (n=4), but not WT ducts (n=4). Macrophages (yellow arrowheads) are present around cystic ducts in E18.5 *Bicc1* KO pancreata (n=2), while there are only a few, scattered macrophages in WT pancreata (n= 4). Insets represent high magnifications of the dashed boxes. Sections are counterstained with DAPI (white). Scale bars, A-B, and insets 10 μm, and D-K, 20μm. See Table 12 in Appendix for further data.

To further investigate this observation, the number of cells stained for PTPRC, also called CD45, a pan-immune cell marker, was quantified in *Bicc1* KO and WT E14.5 pancreata. It revealed a 2-fold increase in the *Bicc1* KO (Fig. 33A-C). Moreover, the higher was the increase; larger was the dilation of the pancreatic ducts. Many of these cells were macrophages expressing EMR1, also called F4/80 (Fig. 33D-G). In addition, the tissue surrounding the cysts at E18.5 also exhibited numerous $PTPRC^+$ cells and $EMR1^+$ cells. The cysts at this stage were also surrounded by smooth muscle $actin^+$ ($ACTA2^+$) cells, suggestive of fibroblast activation (Apte et al., 1999; Haber et al., 1999) (Fig. 33H-K). $ACTA2^+$ cells were only present at E14.5 in a subset of *Bicc1* KO pancreata (Fig. 33D-G), which suggests a secondary effect of cyst formation and/or of immune cell recruitment. In conclusion, cysts arose in a context of PKD2 decrease and immune cell infiltration with stromal reaction.

7.6.5 Cyst formation is not associated with an increased ADCY6 or PKIA level

To start investigating direct targets, a candidate approach was initially used. In kidneys, BICC1 is able to repress the translation of ADCY6 and PKIA by respectively targeting *Mir125a* and *Mir27a* to their mRNA (Piazzon et al., 2012). Both ADCY6 and PKIA are expressed in E13.5 dorsal pancreatic buds based on the RNA sequencing. Their expression level is similar to PDX1, BICC1 or PKD2 (*Adcy6*: 10.71 rpkm and *Pkia*: 11.22 rpkm) (Fig. 29). Moreover both Mir125a and MiR27a are expressed in E13.5 dorsal pancreatic buds (*Mir125a*: 66793 rpkm and *Mir27a*: 2809) (Fig. 31). In the kidneys, neither these mRNAs nor their respective miRNAs are affected by *Bicc1* deletion. However, their protein level is. Therefore, the protein level of ADCY6 and PKIA was investigated in E15.5 *Bicc1* KO pancreata, and compared to WT littermates.

Contrary to kidneys, neither ADCY6 nor PKIA were affected by *Bicc1* deletion (Fig. 34). This thus suggests that ADCY6 and PKIA do not play a role in early cyst formation *Bicc1* KO pancreata.

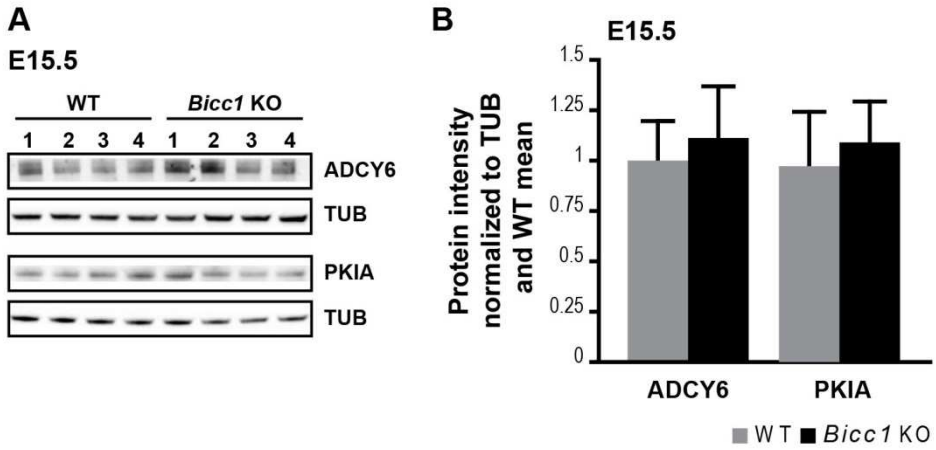

Fig. 34: ADCY6 and PKIA are not affected by *Bicc1* deletion in the pancreas

(A) Example of Western blot performed for ADCY6 and PKIA on E15.5 WT and *Bicc1* KO pancreata, and alpha tubulin (TUB) as a loading control.

(B) Quantification of the Western blot shown in (A) is performed by normalizing band intensity to TUB intensity. Results are relative to WT mean. ADCY6 and PKIA are not affected by *Bicc1* deletion (ADCY6: WT, n=8; *Bicc1* KO, n=8, p= 0.33; PKIA: WT, n=7; *Bicc1* KO, n=8, p=0.35).

See Table 12 in Appendix for further data.

7.7 WNT signaling inhibition is not affected by new *BICC1* human variants associated with cystic kidney diseases

In collaboration with the group of Dr. Bellané-Chantelot in Paris, *BICC1* mutations associated with kidney dysplasia were previously uncovered. They affect BICC1 ability to inhibit canonical WNT signaling (Kraus et al., 2012). Although the role of BICC1 in WNT signaling does not appear to be conserved in the pancreas, it appears to be relevant in the kidney for the former mutations. 5 new variants in *BICC1* were identified by the groups of Pr. Bingham, Pr. Ellard and Pr Hattersley in a cohort of 149 patients. They were associated with cystic kidneys and both oldest patients were also diabetic (Table 8 and Fig. 35A).

Table 8: BICC1 variants with kidney phenotype and diabetes onset time

Mutation	Age	Renal cyst diagnosis age	Diabetes	Family history of diabetes
D45G	55	42 years	Yes	Yes
V206M	4	Large echogenic kidneys		Yes
R800Q	32	21 years	Yes	Yes
G821K	4	8 months		Yes
T845K	22	3 years		

Since BICC1 is able to inhibit WNT signaling, the functionality of new BICC1 variants were evaluated with a TopFlash assay as previously performed (Maisonneuve et al., 2009; Kraus et al., 2012). Contrary to what had been observed with BICC1 Q87Stop and BICC1 E932G, the new variants do not inhibit canonical WNT signaling less effectively than WT BICC1 (Fig. 35B). This result suggests that kidney cysts observed in patients with new BICC1 variants are unlikely due to canonical WNT signaling up-regulation.

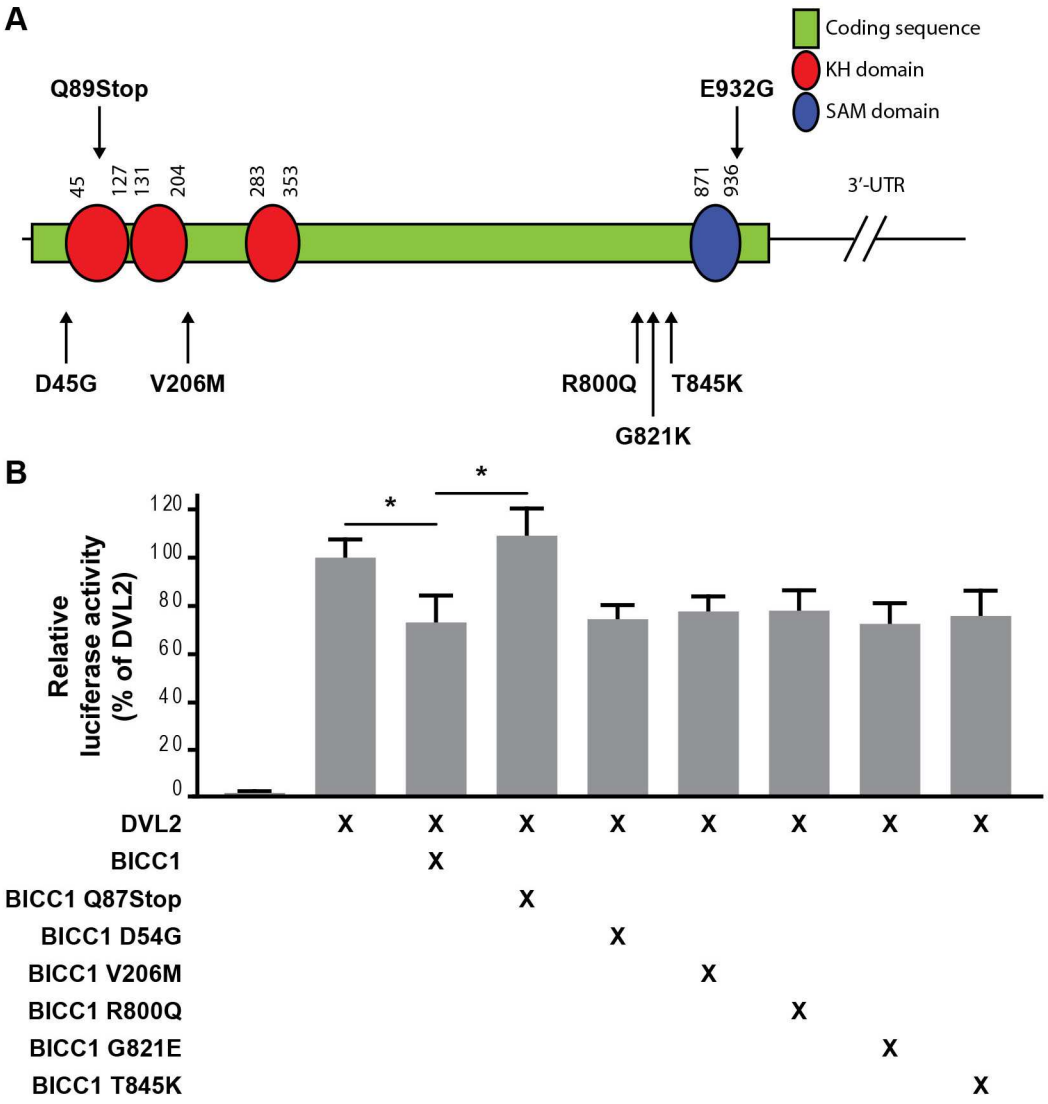

Fig. 35: New human BICC1variants inhibit canonical WNT signaling as strongly as WT BICC1.

(A) Cystic patient associated variations (arrow) are indicated below a schematic representation of human *BICC1* mRNA with its translated sequence shown in green, its KH domains in red and its SAM domain in blue (domain identification is based on SMART tool). The previously identified *BICC1* mutations are indicated on top of *BICC1* mRNA drawing.

(B) TopFlash assays were performed to assess canonical WNT signaling. HEK293T cells were transfected with TopFlash, *DVL2* to induce *firefly luciferase* expression, except for the negative control, and *Renilla luciferase* to normalize firefly luciferase activity. They were co-transfected with either *BICC1* or one of the *BICC1* variants. *BICC1 Q87Stop* was used as a positive control. The different transfection mix components are indicated by black crosses. Canonical WNT signaling was inhibited as effectively by BICC1 variants as BICC1 (n=10 for each assay, except negative control n=6: BICC1 *vs* DVL1, p<0.0001; BICC1 *vs* BICC1 Q87Stop, p<0.0001; BICC1 *vs* BICC1 D54G, p=0.74; BICC1 *vs* BICC1 V206M, p=0.27; BICC1 *vs* BICC1 R800Q, p=0.28; BICC1 *vs* BICC1 G821E, p=0.92; BICC1 *vs* BICC1 T845K, p=0.58). Results are represented as percentage of DVL2 induced relative luciferase activity. See Table 12 in Appendix for further data.

8 DISCUSSION

8.1 BICC1 integrates epithelial morphogenesis and differentiation

BICC1 is able to integrate appropriate pancreatic ductal tree morphogenesis and differentiation of endocrine cells originating from the progenitor-lined ducts. The absence of BICC1 causes cysts in both pancreatic and liver ducts, in addition to kidney dysplasia (Maisonneuve et al., 2009; Tran et al., 2010). Moreover, this work showed that BICC1 normally potentiates NEUROG3^{+} endocrine progenitor production leading to endocrine cell reduction in *Bicc1* KO pancreata (Fig. 36).

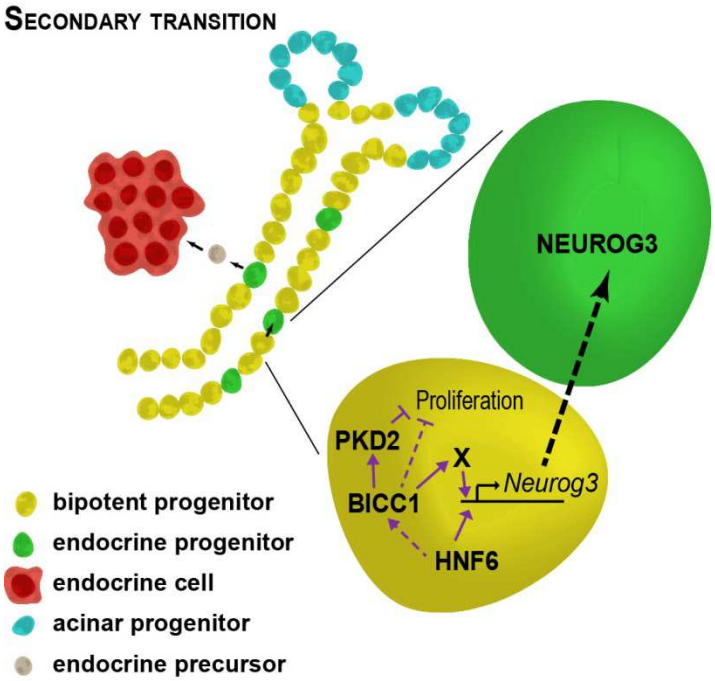

Fig 36: Proposed model of BICC1 function during pancreas development.
During the secondary transition, bipotent ductal progenitors (yellow) can differentiate into NEUROG3^{+} endocrine progenitors (green). These progenitors leave the ducts (grey cells) while differentiating into endocrine cells (red). After the onset of the secondary transition, BICC1 is present in bipotent ductal progenitors (yellow). It regulates PKD2 and thereby inhibits ductal overproliferation maintaining ductal homeostasis. BICC1 may also directly inhibit proliferation. It also promotes Neurog3 expression via an unknown factor enabling the differentiation toward endocrine progenitor (green). While ONECUT1 directly activates *Neurog3* (Jacquemin et al., 2000), it also promotes *Bicc1* expression.

During pancreas development, three distinct, stage dependent expression patterns of BICC1 were uncovered. Before E12.5, BICC1 was first expressed at low level in all PDX1 positive pancreatic progenitors. Then, its level increased, and BICC1 was restricted to the bipotent progenitors. Thereafter, BICC1 expressed in the ducts. The expression patterns highlighted different functions of BICC1: at early stages, BICC1 transiently controls pancreatic size and later, it promotes endocrine progenitor production and ductal homeostasis.

8.2 Transient hyperplasia at early stages

In the absence of BICC1, both the multipotent progenitors and the endocrine progenitors were hyperplastic at E12.5 (Fig. 21, 22). However, this effect was transient, as at E14.5 the pancreatic epithelium size was unaffected by *Bicc1* deletion. This suggests that the size control function is restricted to earlier stages of development, and compensatory mechanisms may restore the size later on. Two different mechanisms may cause hyperplasia: either more cells are specified, or proliferation is increased. Even though pancreatic size has not been assessed before E12.5, it is unlikely that BICC1 has a role during pancreas specification. Indeed, the absolute number of GCG^+ cells at E12.5 was not affected by *Bicc1* deletion. Endocrine cells come from endocrine progenitors and, therefore, pancreatic progenitors produced earlier. This argues strongly against an increase in endocrine progenitors and multipotent progenitors at earlier stages. In order to get more insight into the hyperplasia mechanism and the compensatory mechanism restoring pancreatic size later on, it would be interesting to estimate the mitotic index at E11.5 and at E13.5, but also the apoptotic index.

8.3 Endocrine progenitor production defect during the secondary transition

At E12.5, it was not clear if *Bicc1* deletion affected $NEUROG3^+$ cell production. Indeed, while the cell counting revealed a relative increase of $NEUROG3^+$ cells, Q-PCR data tended to indicate no changes in *Neurog3* transcript (Fig. 21A, B, 22A-C). The latter results had a great variability mainly due to the low

number of NEUROG3$^+$ cells representing only one percent of the total pancreatic epithelium. It should be noted that at this stage, the epithelium represents around half of the total pancreas (Landsman et al., 2011; and data not shown). Hence, NEUROG3$^+$ cells represent less than a percent of the total pancreas. Therefore if the cell number only slightly changes, a large variation in proportion is detected. Moreover the Cleaver laboratory has shown that *Neurog3* transcription is transiently inhibited at E11.25, and re-expressed at E12 (Villasenor et al., 2008). Delays between littermates may lead to relatively large variations around the time when *Neurog3* transcription is reinitiated. In *Bicc1* KO pancreata *Neurog3* was not yet significantly decreased at E13.5 based on RNA sequencing data. At E14.5, NEUROG3 was decreased (RNA and cell number). Therefore, the defect occurred after the secondary transition has started, *i. .e*. when the differentiation of bipotent progenitors toward endocrine cells, via NEUROG3$^+$ cells, is strongly enhanced (Mori and Haga, 1960; Rutter et al., 1968; Gradwohl et al., 2000). In *Bicc1* KOs the endocrine cell decrease followed the endocrine progenitor reduction, being detected at E18.5 but not yet at E14.5.

The analysis of the fate of NEUROG3$^+$ cell progeny, at E14.5 and E18.5, revealed a sustained decrease of 30-50% of endocrine cell production from E14.5 onwards (Fig. 24, 26). Since GCG$^+$ cells are produced in large numbers before E14.5 (Johansson et al., 2007), they were consequently less affected than the other endocrine cells in *Bicc1* KOs. Although most of NEUROG3-expressing cells become endocrine, a subset adopts an acinar or ductal fate (Schonhoff, S. et al., 2004; Wang et al., 2010; Beucher et al., 2012). Due to the general decrease in NEUROG3$^+$ cells, it might be expected that their small acinar and ductal progeny would also be decreased in *Bicc1* KOs (Fig. 26). However, acinar progenitors are segregated from bipotent progenitors before the regulation of endocrine progenitor production by BICC1, accounting for a normal size of the acinar progeny in *Bicc1* KOs. On the contrary, there is no time window restriction to NEUROG3$^+$ cell ability to adopt a ductal cell fate (Zhou et al., 2007; Beucher et al., 2012; Pan et al., 2013). Ductal *Neurog3*$^+$ progeny should thus be decreased in the *Bicc1* mutant, but duct expansion, due to increased proliferation, compensated for this defect. As *Neurog3*$^+$ progeny and endocrine cells were similarly reduced in *Bicc1* KOs, and BICC1 was absent of the differentiating endocrine cells, I conclude that BICC1 does not control endocrine cell production downstream of *Neurog3*.

8.4 Target(s) of BICC1 regulating endocrine progenitor production

In vertebrates, BICC1 is able to repress translation of target mRNAs either by facilitating miRNA binding (Piazzon et al., 2012) or by directly inhibiting the translation initiation machinery (Zhang et al., 2013). It is also able to enhance translation by inhibiting miRNA activity thus stabilizing protein levels of the targets even though no direct interaction between miRNA and BICC1 have been uncovered in this case (Tran et al., 2010; Gamberi and Lasko, 2012). The role of BICC1 in targeting mRNAs implies that its action may not be seen at the mRNA level (Dorey and Hill, 2006; Piazzon et al., 2012; Zhang et al., 2013)

It has not been reported that BICC1 regulates transcription. However, the transcription of *Neurog3* was affected by *Bicc1* deletion since we observed a similar reduction of the number of cells expressing transcriptional reporters, Neurog3-Cre and Neurog3-RFP, and of the number of cells expressing NEUROG3 protein (Fig. 22, 24, 26). Hence the direct regulation of *Neurog3* by BICC1 can be ruled out.

8.4.1 Known transcriptional regulators of *Neurog3* are not affected by *Bicc1* deletion

Since BICC1 do not control directly *Neurog3* transcription, BICC1 might either enhance a transcriptional activator of *Neurog3* or inhibit one of its transcriptional repressors. It has already been shown that expression level of transcriptional activator of *Neurog3* is important to produce the adequate number of endocrine progenitor cells. For instance, *Sox9* haploinsufficiency causes a decrease by 50% of endocrine progenitors (Seymour et al., 2008).

Nevertheless, the protein level of the different transcriptional regulators of Neurog3 tested in this study was unaffected by *Bicc1* deletion. HES1, a transcriptional repressor of *Neurog3,* was not changed in *Bicc1* KO pancreas, neither were SOX9, FOXA2, PDX1 and HNF1B, some of its transcriptional activators (Lee et al., 2001; Shih et al., 2012; Ejarque et al., 2013). ONECUT1 also activates *Neurog3* expression (Jacquemin et al., 2000), but, although *Onecut1* was upregulated at the mRNA level, its protein level was not changed, arguing against its being targeted by BICC1 (Fig. 27).

However, the ductal cell number has not been estimated at E15.5. If this cell population is expanded due to duct dilatation, the expansion may hide a decrease of the expression level of a given transcription factor. Indeed if the level of a transcription factor per cell is decreased in the same degree as the ductal population is increased, the global expression level detected by Western blot will be similar between WT and *Bicc1* KO pancreata. Nevertheless, such expansion is unlikely. For example, a 50% decrease of SOX9, corresponding to a 50% reduction of endocrine progenitors, would require a 50% increase of the bipotent progenitor cell population in order to get a similar expression level. Moreover, HES1 is not upregulated in *Bicc1* KO pancreata, contrary to what would be expected with an increased number of ductal cells (Fig. 27). In order to circumvent the potential ductal population increase, the expression of these transcription factors would have to be quantified in individual cells, *e.g*. using flow cytometry.

8.4.2 Putative BICC1 targets affecting endocrine progenitor cell production

ONECUT2, HNF1A and GLIS3 are able to activate *Neurog3* promoter (Lee et al., 2001; Vanhorenbeeck et al., 2007; Yang et al., 2011). As for the other transcription activators of *Neurog3*, their protein level would have to be assessed in order to evaluate if they are regulated by BICC1. However, there is little evidence that ONECUT1 and HNF1A have, *in vivo*, an important role in the generation of NEUROG3^{+} cells. ONECUT2 acts redundantly with ONECUT1, and its deletion does not cause an endocrine progenitor decrease (Vanhorenbeeck et al., 2007). In addition, HNF1A expression is excluded from the bipotent expression domain at E15.5 (Maestro et al., 2003). *Hnf1a* deletion causes neither a decrease of endocrine progenitor cell number nor the formation of cysts, although cyst formation and endocrine progenitor decrease may be uncoupled as discussed from p 116. The *Hnf1a* KO mice become glucose intolerant over time (Pontoglio et al., 1996; Pontoglio et al., 1998). Compared to ONECUT2 and HNF1A, GLIS3 is a more likely BICC1 target due to the phenotypic overlap between knockouts. A drastic decrease in pancreatic endocrine progenitors together with cyst formation is observed in *Glis3* KOs. *Glis3* KOs also develop cyst in the kidneys. Finally, based on seed prediction tool (TargetScan), seeds for *Mir17* involved in kidney cyst formation in *Bicc1* KOs (Tran et al., 2010) and for *Mir29b-1* found downregulated in the pancreas are

present in its 3'UTR. Unfortunately GLIS3 levels in *Bicc1* KO could not be tested due to poor antibody quality.

NEUROG3^{+} cell production is also inhibited by GDF11, a member of the TGFB family. The action of GDF11 is independent of the NOTCH signaling pathway (Nakashima et al., 1999; Harmon et al., 2004). More endocrine progenitors are observed in *Gdf11* KOs. However, it has additional effects on beta cell maturation which do not match *Bicc1* KO phenotype. SMAD2 haploinsufficiency causes the same phenotype as *Gdf11* KOs arguing that SMAD2 is the downstream effector of GDF11 (Harmon et al., 2004). It would be interesting to test the SMAD2 expression and activity levels in *Bicc1* KO pancreata.

Finally BICC1 may also target an unknown modulator of *Neurog3* promoter and therefore a more unbiased approach to identify BICC1 targets may be advisable, but rendered difficult by the heterogeneity and small size of the cell populations present in the developing pancreas.

A study to which I contributed is presented in the annex on page 151 and may be relevant to the mode of action of BICC1. We showed that bipotent progenitors have different modes of division. They can divide symmetrically, and generate either two bipotent progenitors or two endocrine progenitors. They also divide asymmetrically, and generate one bipotent progenitor and one endocrine progenitor. The choice to produce endocrine progenitors by symmetric or asymmetric cell division is hypothesized to be associated with the cell cycle. If the bipotent progenitor is primed for an endocrine progenitor fate before a certain time in the cell cycle, the cell exits the cell cycle and differentiates into endocrine progenitor. If the priming occurs after this restriction point, the bipotent progenitor continues the cell cycle and generates two endocrine progenitors after mitosis (Kim et al., 2015). It would be interesting to see if the deletion of *Bicc1* causes an imbalance between the asymmetric and symmetric cell division generating endocrine progenitor as it would indicate the involvement of different factors before and after the restriction point, or give insight on its molecular nature.

8.5 BICC1 controls pancreatic epithelial morphogenesis after the secondary transition as started

In *Bicc1* KO pancreata, ducts were dilated after the secondary transition has started. Cysts developed in the dilated ducts and formed a connected web rather than isolated foci (as shown by the movies in Lemaire et al., *in press*). In ARPKD patients, tube dilation also precedes cyst formation, reminiscent of what was observed in *Bicc1* KO pancreata (Ockenden and Blyth, 1971).

8.5.1 Endocrine cell defects are unlikely caused by cyst formation and *vice versa*

In addition to a complete loss of endocrine cells, *Neurog3* KOs harbor cysts smaller than those seen in *Bicc1* KOs (Gradwohl et al., 2000; Magenheim et al., 2011a). However, these cysts are thought to originate from an accumulation of progenitors failing to further differentiate into endocrine cells. This is not the case in *Bicc1* KOs where NEUROG3 progeny instead were reduced to the same extent as endocrine cells, arguing that the endocrine cell decrease observed in *Bicc1* KOs is not the cause of cyst formation (Fig. 27). On the contrary, it is also unlikely that the presence of cysts causes the endocrine defect since no pancreatic endocrine alterations have been reported in pancreatic cystic mutants, such as *Pkd2* KOs, *Pkd1* KOs, *Pkhd1* hypomorphs, or cilia defective mutants (Lu et al., 1997; Wu et al., 2000; Cano et al., 2004; Cano et al., 2006; Gallagher et al., 2008)

8.5.2 Aberrant proliferation *vs* cell shape defect as cause of cyst formation

In kidneys, proliferation is one of the major mechanisms of cyst expansion, although it is not sufficient to induce cyst formation (Hanaoka and Guggino, 2000; Fangming et al., 2003; Chang et al., 2006; Piontek et al., 2007; Kim et al., 2009; Sharma et al., 2013). In *Bicc1* KO pancreata, ductal proliferation was only increased at late stages, while at E14.5 it was unaffected (Fig. 15). A similar picture emerges from other pancreatic cystic mutants. The E15.5 *Hnf6* KO pancreatic epithelium does not over-proliferate, and neither do the pancreatic ducts of ciliary mutants (Cano et al., 2004; Cano et al., 2006; Pierreux et al., 2006).

Moreover, when cystic and non-cystic proliferation in *Bicc1* KO pancreata were considered separately, only the cystic cell mitotic index was increased compared to WT animals (data not shown). This result is in line with observations in kidneys where the mitotic index is increased in cysts but not in non-cystic areas (Nauta et al., 1993). In addition, uncontrolled proliferation is not observed in early renal cysts of *Bicc1* KOs (Tran et al., 2010). Overall, we conclude that while over-proliferation may contribute to late cyst expansion, it does not account for early duct dilation or cyst initiation in *Bicc1* KO pancreata.

It has been shown in several rodent models that kidney cyst formation is preceded by an impairment of oriented cell divisions parallel to the longitudinal axis of the nephron (Fischer et al., 2006). Pancreatic bipotent progenitors similarly divide mainly within the plane of the progenitor-lined duct at E14.5 (YH Kim, unpublished data). Ductal dilation observed in *Bicc1* KO pancreata may be caused by a loss of oriented cell division promoting more longitudinal and less circumferential divisions, especially if the number of bipotent progenitors is not increased. Although little is known about the shape of cyst-lining cells, a deformed shape with an increased width-over-height ratio may also be another mechanism causing duct dilation. It may also result in the misorientation of the cells in the ducts as observed in kidney of *Wnt9b* KOs (Karner et al., 2009). Therefore, the study of the shape of cells lining dilated ducts or cysts in *Bicc1* KO pancreata would give insight into the mechanisms of cyst initiation and expansion.

8.5.3 Cilia defects are not observed in the absence of Bicc1

Cyst formation is a shared feature of several mutants affecting pancreas development. Cilia mutants have cysts in the pancreas, although cysts also arise in intercalated duct and dilation is only observed at late gestational stages, contrary to what was observed in *Bicc1* KO pancreata. *Onecut1* KOs lack cilia at early stages while *Glis3* KOs and *Sox9* conditional KOs have less cilia in cyst-lining cells indicating an association between cilia and cysts formation (Cano et al., 2004; Cano et al., 2006; Pierreux et al., 2006; Kang et al., 2009b; Shih et al., 2012).

However, the presence of cilia has been reported in the cochlea and node of *Bicc1* KOs (Maisonneuve et al., 2009; Piazzon et al., 2012) and we also observed them in their pancreata (Fig. 17). Nevertheless, BICC1

affects cilia position on the cells and their ability to synergistically rotate in the node. These cilia normally generate a flow of extracellular signals creating left-right asymmetry in embryos. In *Bicc1* KOs the fluid flow randomization thus leads to left-right randomization (Maisonneuve et al., 2009). They might therefore also be altered in pancreatic ducts however, their position and function is difficult to assess in the tortuous pancreatic ductal network.

8.5.4 BICC1 acts downstream of ONECUT1

The *Bicc1* KO pancreatic phenotype partially recapitulates the *Onecut1* KO phenotype. Indeed in both cases there are ductal cysts and less endocrine cells due to a failure to produce endocrine progenitors (Jacquemin et al., 2000). I found that ONECUT1 regulated *Bicc1* transcript levels. ONECUT1 may activate *Bicc1* expression directly, but an indirect control via HNF1B is plausible. Indeed, ONECUT1 enhances *Hnf1b* expression and the latter is able to induce *Bicc1* expression in the kidney, although a direct binding as not been confirmed in E12.5 pancreata (Maestro et al., 2003; Verdeguer et al., 2010; De Vas et al., 2015).

8.5.5 BICC1 acts upstream of PKD2

PKD2 was downregulated at E13.5 (mRNA level, RNA sequencing) and at E15.5 (protein level) in *Bicc1 KO* pancreata (Table 5, Fig. 32). *Pkd2* KOs embryos and adult heterozygotes acquiring a spontaneous mutation of the second allele exhibit cysts in the pancreas and in kidneys (Wu et al., 1998; Wu et al., 2000; Chang et al., 2006). Moreover, if the expression level of PKD2 is as important as that of PKD1, a more than 2-fold decrease might lead to cyst formation (Lantinga-van Leeuwen et al., 2004; Jiang et al., 2006). In kidneys, BICC1 inhibits targeting of *Pkd2* by *Mir17*, thus stabilizing PKD2 (Tran et al., 2010). BICC1 does not affect *Mir17* expression level (Piazzon et al., 2012). In the pancreas, BICC1 may also repress *Mir17* without altering its stability since *Mir17* is present in E13.5 pancreata (Fig. 31). PKD2 also functions downstream of BICC1 in osteoblasts, and knock-down of *Bicc1* is rescued by overexpressing *Pkd2* (Mesner et al., 2014). Together, this argues that PKD2 is a major mediator of BICC1 activity in multiple organs.

PKD2 is also a major player of cyst formation in pancreata since its expression level is altered in several mutants. *Pkd2* is increased in *Hnf1b* conditional mutants, while *Bicc1* and several cyst associated genes are decreased, arguing that the inhibition of *Pkd2* expression by HNF1B is upstream or independent of BICC1, rather than downstream (De Vas et al., 2015). Late *Sox9* deletion in the pancreas also causes cyst formation. It is associated with *Pkd2* downregulation without affecting *Bicc1* expression (Shih et al., 2012). SOX9 is not affected in *Bicc1* KOs. Therefore, SOX9 and BICC1 appear to prevent cyst formation independently of each other by controlling *Pkd2* expression.

PKD2 is a Ca^{2+} channel allowing Ca^{2+} inward flow in response to shear stress at the primary cilia. Ca^{2+} intracellular level is decreased in cystic kidneys (Hanaoka et al., 2000; González-Perrett et al., 2001; Vassilev et al., 2001; Koulen et al., 2002). The role of Ca^{2+} associated signaling is relatively unknown in pancreas development. It would therefore be interesting to see if the Ca^{2+} concentration is reduced in *Bicc1* KO pancreata suggesting that initial mechanisms of cyst formation are conserved between kidney and pancreas and uncovering the importance of Ca^{2+} in ductal homeostasis.

8.5.6 BICC1 does not regulate ADCY6 or PKIA during pancreas development

Contrary to what has been described in the kidneys (Piazzon et al., 2012), ADCY6 and PKIA were not upregulated by BICC1 in E15.5 pancreata. It may be argued that the analyzed stages do not correspond to the same cyst enlargement in both organs. Indeed, ADCY6 and PKIA protein level are upregulated from E17.5 in the kidneys, when cysts are already clearly present (Piazzon et al., 2012), whereas the ducts of E15.5 *Bicc1* KO pancreata were normal to slightly cystic (Fig. 34).

In addition, BICC1 might target other genes involved in cAMP production regulation in the developing pancreas. Other $Ca2^{+}$-regulated proteins controlling cAMP level were expressed, but at low level, in the E13.5 pancreas, such as *Adcy5* (expression level < 1 rpkm by RNA sequencing), *Pde1a*, *Pde1b*, and *Pde1c* (around 1 rpkm by RNA sequencing) (Kakiuchi et al., 1973; Chabardès et al., 1999; Wang, X. et al., 2009). It might thus first be important to assess cAMP levels at different stages in *Bicc1* KO and WT pancreata to evaluate if pancreatic cyst formation is associated with cAMP dysregulation.

Increased levels of cAMP are known to both promote proliferation and fluid secretion, causing mainly cyst expansion (Hanaoka and Guggino, 2000; Tamma et al., 2003; Yamaguchi et al., 2003; Montesano et al., 2009). However, proliferation is not yet increased at cyst initiation stage in *Bicc1* KO pancreata. Furthermore, in E13.5 dorsal pancreatic buds, two major actors of cystic fluid secretion, CFTR and AQP2, are absent or only expressed at low level, respectively (*Cftr* mRNA < 1 rpkm by RNA sequencing). These data argue that cyst initiation and expansion mechanisms are not shared. Conversely, cyst formation mechanisms might be different in the pancreas and in kidneys. Alternatively, cyst formation in different models may rely on distinct mechanism. Indeed, patients with cystic fibrosis and ADPKD develop less severe cysts (O'Sullivan et al., 1998), while the absence of CFTR in *bpk/bpk* mice does not prevent cyst growth (Nakanishi et al., 2001).

8.5.7 Canonical WNT signaling is not altered in Bicc1 KO pancreatic cysts

Several pieces of evidence argue for a role of canonical WNT signaling in cyst formation both in kidneys and in the pancreas. Forced hyperactivation of canonical WNT signaling causes kidney cysts (Saadi-Kheddouci et al., 2001; Chao-Nan et al., 2005). Constitutively active WNT signaling also induces cysts in pancreata, but only if the activation starts before E12.5 (Heiser et al., 2006). Increased canonical WNT signaling combined with cysts in kidneys and the pancreas has also been reported in *inv/inv* mutants (Cano et al., 2004; Simons et al., 2005). Other cystic kidney mutants also have an increased WNT activity (Fangming et al., 2003; Kim et al., 2009). Finally, WNT signaling is more active in the pancreas of o*rpk/orpk* mutants (Cano et al., 2004). As BICC1 has been shown to inhibit canonical WNT signaling in the node (Maisonneuve et al., 2009), it could be expected that its deletion increases WNT signaling. However canonical WNT signaling is detected in the mesenchyme in E14.5 pancreata (Dessimoz et al., 2005), implying that a direct effect of BICC1 on canonical WNT signaling is unlikely. More importantly overactive WNT signaling was not detected with reporter mouse lines or gene readout (Fig. 28) suggesting that canonical WNT signaling is neither involved in cyst formation nor in endocrine cell decrease observed in *Bicc1* KO pancreata.

8.5.8 Role of apico-basal polarity defects in *Bicc1* KO cysts

Apico-basal polarity is globally unaffected in *bpk/bpk* kidneys (Ryan et al., 2010). Normal apico-basal polarity was also observed in *Bicc1* KO pancreata. Apical markers, such as aPKC and MUC1, were facing the lumens and not the basal side (Fig. 20, data not shown for MUC1). However, DBA and MUC1 had a tendency to be weaker in *Bicc1* KO pancreata (data not shown). Although the general apico-basal polarity machinery is conserved in the kidney of *jcpk/jcpk* mice and *bpk/bpk* mice, the EGFR receptor is not localized properly. The mislocalization causes an over-activation of the MAPK signaling pathway that may induce proliferation. EGFR mislocalization may be caused by a dysregulation of the endosome sorting pathway. Moreover, *bpk/bpk* renal cystic cells also secrete more EGF related ligands in the lumen, thereby, inducing proliferation (Sweeney and Avner, 1998; MacRae Dell et al., 2004; Ryan et al., 2010). Lastly pancreatic cysts of *Kif3a* conditional KOs also harbored increased phospho-MAPK1 without indication of EGFR mislocalization (Cano et al., 2006). The role of EGF/MAPK pathway may thus deserve further investigations.

EGFR localization and its contribution to cyst formation have not been assessed in *Bicc1* KO pancreata. It was expressed in E13.5 WT pancreata at relatively low level (around 1 rpkm, based on RNA sequencing data), while *Erbb2*, *Erbb3*, and *Erbb4* were expressed at higher level (around 10 rpkm, based on RNA sequencing data). Indeed, ERBB4 has been detected by immunostaining in duct at E12.5 (Huotari et al., 2002). Inactivation of EGFR causes slight hypoplasia with a higher relative reduction of beta cells, and BTC, an EGF ligand, promotes beta cell mass (Miettinen et al., 2000; Huotari et al., 2002). It should be noted that overexpression of TGFA causes ductal dilatation with interstitial fibrosis (Jhappan et al., 1990; Sandgren et al., 1990). TGFA, secreted by *bpk/bpk* renal cells, is also able to promote cyst expansion (MacRae Dell et al., 2004). This information may be valuable as EGFR receptor inhibition may reduce cyst growth.

8.5.9 Role of MTOR signaling pathway alterations in *Bicc1* KO cysts

MTOR inhibition in *bpk/bpk* mice represses kidney cyst growth (Shillingford et al., 2006). Moreover, in *Pkd1* KO cells, a upregulation of MTOR signaling has been associated to an increase of aerobic glycolysis,

the main source of energy of *Pkd1* KO cells (Rowe et al., 2013). The glycolytic enzymes, *Aldoa*, *Pfkl*, and *Eno1,* were upregulated in *Bicc1* KOs using the DESeq analysis even though the analysis is not stringent enough to reliably assess gene changes (Table 14). In the case of *Neurog*3, the downregulation observed at E13.5 was confirmed at later time points. Glycolytic enzymes may follow the same pattern and become reproducibly upregulated at a later time point. It would therefore be interesting to assess both MTOR pathway and aerobic glycolysis in *Bicc1* KO pancreata, and whether their inhibition may slow down cyst expansion.

8.6 An indirect and early mesenchymal contribution to cyst formation

A conserved feature of cyst formation in kidneys is its association with fibrosis and infiltrating macrophages (Okada et al., 2000; Fangming et al., 2003; Chang et al., 2006; Jiang et al., 2006; Happé et al., 2013). Activated macrophages have been shown to promote cyst formation in polycystic kidney disease models (Karihaloo et al., 2011; Swenson-Fields et al., 2013; Ta et al., 2013). However, macrophages are not sufficient to induce cyst formation in the fetal pancreas, and instead promote beta cell mass (Banaei-Bouchareb et al., 2004; Geutskens et al., 2005). Conversely, in adults, macrophages as well as other cell types are able to activate pancreatic stellate cells, a subset of fibroblasts present in the pancreas (Watari et al., 1982; Schmid-Kotsas et al., 1999). Once activated, stellate cells start to express ACTA2. They increase their production of extracellular matrix components and secrete cytokines that recruit inflammatory cells and sustain active pancreatic stellate cell state. If this positive feedback loop is not turned off, it leads to fibrosis (Apte et al., 1999; Masamune et al., 2009; Shi et al., 2014).

Although collagen accumulation, and therefore actual fibrosis, were not detected in E18.5 *Bicc1* KO pancreata, resident or infiltrating immune cells, such as macrophages, were increased in *Bicc1* KOs. The expansion occurred early, as immune associated genes are already affected in E13.5 *Bicc1* KOs, and an increase of immune cells was observed at E14.5. Immune cell increase was followed by the activation of fibroblasts, indicated by their positivity for $ACTA2^{+}$. Only some E14.5 *Bicc1* KO pancreata had $ACTA2^{+}$ fibroblasts, whereas at E18.5, all *Bicc1* KO pancreata had $ACTA2^{+}$ cells surrounding the largest cysts (Table

4, 5 Fig. 33). As for the kidneys, macrophages together with active fibroblasts, may thus promote cyst growth. Ongoing experiments using the organoid system developed in our laboratory are being performed to assess the role of the stroma and immune cells in cyst initiation. In this system, growth and branching of the pancreatic epithelium without its surrounding mesenchyme is observed (Greggio et al., 2013).

TGFB is able to activate pancreatic stellate cells and promote fibrosis (Apte et al., 1999). It is also associated with kidney cysts (Hassane et al., 2010). Moreover, in the RNA sequencing analysis using DESeq analysis several TGFB signaling pathway components were upregulated (Table 14), arguing that TGFB signaling could be altered at least at later stages. It would thus be interesting to inhibit TGFB signaling in explants or organoid cultures and see if the inhibition slower the stromal reaction or cyst growth.

8.7 Human cystic syndromes, diabetes, and BICC1

Heterozygous *BICC1* mutations in human have been identified and associated with kidney dysplasia (Kraus et al., 2012). The groups of Pr. Bingham, Pr. Ellard, and Pr Hattersley, identified 5 new heterozygote variants of *BICC1* in another cohort of patients having cystic kidneys and, for the oldest patients, diabetes. Our investigation suggests that pancreatic defects may be expected in these patients. Although these mutations are rare, it cannot be excluded that mutations occur in BICC1 introns or in its promoter changing its expression level. However, it suggests that these mutations act in a dominant manner.

8.7.1 Impact of the BICC1 variation on its protein

One of the previously characterized mutations disrupts the SAM domain of BICC1 while the other leads to a truncated form which includes the N-terminal part until the middle of the first KH domain (Fig. 35A) (Kraus et al., 2012). The effect of the new BICC1 variations on the protein structure is less clear. Only one of them (D54G) mutates a known BICC1 domain, its first KH domain. The others lie before or after the SAM domain (Fig. 35A). Therefore, if the new variations affect the functionality of BICC1, they may be useful in probing its molecular mechanisms.

8.7.2 Functionality assay of the new BICC1 variants

The precedent mutations affect the ability of BICC1 to inhibit canonical WNT signaling (Kraus et al., 2012). However, the new variants did not lose their ability to repress canonical WNT signaling, even partially. Loss of WNT signaling inhibition has not been associated to cyst formation in *Bicc1* KOs, even though constitutionally active WNT signaling causes kidney cysts (Saadi-Kheddouci et al., 2001; Chao-Nan et al., 2005; Maisonneuve et al., 2009). Other functions of BICC1 may be affected in the variants. They might affect BICC1 ability to localize to P bodies, as shown for human BICC1 E932G mutation (Kraus et al., 2012). Moreover, the Constam lab is investigating if the variants are still able to regulate ADCY6 and PKIA translation. Finally, variants might lose the ability to promote PKD2 expression. Addressing this would be interesting since PKD2 is a common target in the pancreas and the kidneys. Therefore, the mutation might associate kidney and pancreatic defects.

8.7.3 Association between BICC1 and diabetes

Kidney defects may be associated with diabetes in several human syndromes. For example, MODY5 syndrome, where *HNF1B* is mutated, is characterized by kidney cysts and diabetes (Bellanné-Chantelot et al., 2005). Both HNF1B and BICC1 prevent kidney cysts and control pancreas development. This might reflect a role of HFN1B in the transcriptional activation of *Bicc1* in the kidney (Haumaitre et al., 2006; Verdeguer et al., 2010). In the pancreas HNF1B also activates *Bicc1*, but the activation might be indirect (De Vas et al., 2015). It will be important to investigate whether *BICC1* mutations contribute to diseases combining kidney cysts and diabetes or to link *BICC1* with already identified genes in such pathologies. Other monogenic forms of diabetes may also be associated with kidney dysplasia. For example, *GLIS3* mutations can cause neonatal diabetes associated with cystic kidneys (Senée et al., 2006).

It might be argue that BICC1 is not expressed in beta cells and, therefore, its mutation could not cause diabetes. Indeed, BICC1 was neither expressed in beta cells at E18.5 nor in 2 weeks old animals (Fig. 11). However we cannot rule out that BICC1 is expressed in beta cells at later stages. BICC1 mRNA was also detected in low amounts in the beta cell-derived bTC cell line (not shown). Defects in endocrine progenitor

production in the long term may cause glucose intolerance, as observed in *Sox9* haploinsufficiency (Seymour et al., 2008; Dubois et al., 2011). It would also be interesting to evaluate if *Bicc1* KO pups, which have half less beta cells, are hyperglycemic or glucose intolerant, even though this remains difficult to determine due to embryonic and early postnatal lethality. Conditional deletion of *Bicc1* in the developing pancreas or in the endoderm, using *e. g.* $Sox17^{CreGFP}$, a tool I contributed to characterize (see Annex p150) , would address these issues as it circumvents the kidney lethality (Choi et al., 2012). Moreover, we could not identify stable glucose intolerance in *Bicc1* heterozygotes (data not show).

8.8 Putative role of BICC1 in endocrine cell differentiation

The analysis of the expression pattern of BICC1 might give cues on the possible roles of BICC1 in the production of endocrine cells in different organs (Wessely et al., 2001). Enteroendocrine cells are present in both the stomach and the intestines. While enteroendocrine cells in the stomach do not require NEUROG3, they are generated from $NEUROG3^{+}$ cells in the intestines (reviewed in May and Kaestner, 2010). BICC1 might thus be important for their production. Nevertheless BICC1 does not seem to be present in the intestines around E13.5-E14.5 as it does not in the stomach (Wessely et al., 2001; data not shown). Endocrine organs such as the pituitary gland, the pineal gland, the hypothalamus, the thyroid, parathyroids, and adrenal glands might also rely on BICC1 function for their development. However, the expression pattern of BICC1 in these organs and during their ontogeny is too poorly characterized to hypothesize any role (Wessely et al., 2001). Moreover, the early lethality of *Bicc1* KO precludes any physiological studies (Maisonneuve et al., 2009). On the contrary, both female and male gonads express *Bicc1* at high level. *Bicc1* is present in the stroma of the ovary as well as in the theca cells secreting androgen. It is also expressed at low level in the primary follicle giving rise to the granulosa secretin estrogen and later the corpus luteum secreting progestogen (Wessely et al., 2001; Norris and Carr, The Endocrinology of Mammalian Reproduction, in Vertebrate Endocrinology, 2013). The expression pattern in the developing and adult testes was not characterized by Wessely and colleagues (Wessely et al., 2001). However, the data in the ovaries suggest a role for BICC1 in the generation of the gonadal sex-hormones producing cells. The use of *Bicc1*

conditional deletion circumventing the early lethality will be necessary to assess the function of BICC1 in the different endocrine organs.

8.9 Conservation of BICC1 functions

The actions of BICC1, in different species, are still too poorly understood to establish the conservation of BICC1 functions. Until now, they are rather contracdictory. For example, BICC1 is able to regulate the length of polyA tail either positively in *Caenorhabditis elegans* or negatively in *Drosophila*, while BICC1 does not affect the polyA tail of PKD2, ADCY6 or PKIA in mice (Eckmann et al., 2004; Chicoine et al., 2007; Tran et al., 2010; Piazzon et al., 2012). Moreover only few mRNA targets have been identifed and validated (Chicoine et al., 2007; Piazzon et al., 2012; Zhang et al., 2013). Two screens have been performed to identified mRNA targets using RNA co-immunoprecipitation in stage 7 *Xenopus* embryos and in *Drosophila* ovarian extracts. However, the targets do not overlap. It could be mainly due to used of unrelated systems (Chicoine et al., 2007; Zhang et al., 2013). Thus, BICC1 functions may mainly rely on its binding partners and mRNA targets.

8.10 Concluding remarks

This study showed that BICC1 was important to produce adequate numbers of endocrine cells, and to promote ductal homeostasis during pancreas development. In its absence, endocrine progenitor cells were reduced due to a production defect. The ducts dilated, and became progressively cystic. A stromal reaction was then observed around the largest cysts. PKD2 is downregulated even before ducts start to enlarge. However, no target of BICC1 promoting endocrine progenitor production has been identified. Therefore, acquiring more knowledge on BICC1 binding partners and targets will be fundamental to understand its function in endocrine progenitor production. These studies may be relevant for the pathogeneicty of monogeneic diabetes as much as that of multifactorial type II diabetes. As *BICC1* muations are implicated in kidney dysplasia, it might be an important gene to screen in cystic kidney patients with unknown genetic

defects, both for genetic counselling and for the diagnosis as well as early managment of possible diabetes or impaired glucose tolerance.

9 MATERIALS AND METHODS

9.1.1 Association between BICC1 and pancreatic and/or renal dysplasia

We have also observed a stromal reaction in *Bicc1* KOs, which leads us to think that some patients with pancreatic dysplasia may bear *Bicc1* mutations. One of this syndromes is the renal-hepatic-pancreatic dysplasia in which kidneys are cystic and the pancreas fibrotic (Vankalakunti et al., 2007). In a subset of cases, the genetic cause has been identified. Mutations have been found in *NEK8* and, for the Ivemark syndrome, a subtype of the renal-hepatic-pancreatic dysplasia, in *NPHP3* (Bergmann et al., 2008; Fiskerstrand et al., 2010; Frank et al., 2013). *Situs inversus totalis* with cystic dysplasia of kidneys and pancreas, another autosomal recessive disease, is even more similar to *Bicc1* KO mice (Balci et al., 1999). Since no genetic cause has been identified for this rare syndrome, it would be interesting to look for *BICC1* mutations. These studies will be important for genetic counseling and patient management.

9.2 Mice and genotyping

Mice (*Mus Musculus)* were either housed at École Polytecnique Fédrérale de Lausanne, Switzerland, at the University of Copenhagen, Denmark or at Université Catholique de Louvain, Belgium. The Service de la consommation et des affaires vétérinaires, Vaud in Switzerland, the Commission d'Ethique d'Expérimentation Animale of the Université Catholique de Louvain in Belgium or the Dyreforsøgstilsynet in Denmark approved the mouse housing and experiments in the respective countries. The following mouse lines were used for this study: Bicc1tm1Bdc (*Bicc1*) (Maisonneuve et al., 2009), Tg(Ngn3-tRFP)AGB (*Neurog3-RFP*) (Kim et al, submitted), Gt(ROSA)26Sortm1(EYFP)Cos (*Rosa26 YFP*) (Srinivas et al., 2001), Tg(Neurog3-cre)C1Able Ngn3-Cre (*Neurog3-Cre*) (Schonhoff, S. et al., 2004) and *Onecut1* (Jacquemin et al., 2000) B6.129P2-Axin2tm1Wbm/J (*Axin2-LacZ*) (Lustig et al., 2002). Genotyping primers and conditions are listed in Table 9.

Table 9: Primer sequences and their annealing temperature.

Target	Forward primer	Reverse primer	Annealing temperature	Reference
Bicc1 locus WT allele	CCCAACACGGCATCTTTAGTC	GCACGGAAGCAGGGTTATGTC	58	(Maisonneuve et al., 2009)
Bicc1 locus KO allele	CAGGGTCGCTCGGTGTTC	GCACGGAAGCAGGGTTATGTC		
Neurog3-RFP locus	AAGCCTTCATCAACCACACC	GCGGGTTTCTTGGATCTGTA	60	
Rosa26 YFP locus	AAAGTCGCTCTGAGTTGTTAT	GCGAAGAGTTTGTCCTCAACC	50	(Soriano, 1999)
Rosa26 YFP locus recombined	AAAGTCGCTCTGAGTTGTTAT	GGAGCGGGAGAAATGGATATG		
Neurog3 Cre locus	TGCCACGACCAAGTGACAGC	CCAGGTTACGGATATAGTTCATG	58	
Axin2 locus WT allele	AGTCCATCTTCATTCCGCCTAGC	TGGTAATGCTGCAGTGGCTTG	60	(Yu et al., 2005)
Axin2 locus *LacZ* allele	AGTCCATCTTCATTCCGCCTAGC	AAGCTGCGTCGGATACTTGAGA		
*Hprt1*mRNA	GGCCAGACTTTGTTGGATTTG	TGCGCTCATCTTAGGCTTTGT	59.5	
Bicc1 mRNA	CCTAGGCAAATACACGGATGTCT	TGTGAGGGTGAGGAATGTCTGA	60	
Neurog3 mRNA	TGGCCCATAGATGATGTTCG	AGAAGGCAGATCACCTTCGTG	60	
Hes1 mRNA	ATAGCTCCCGGCATTCCAAG	TGTTGGGGAAATACCCGCC	59	
Dll1 mRNA	TCAATGGAGGACGATGTTCA	ACCGGCACAGGTAAGAGTTG	60	
Onecut1 mRNA	ACCCTTCACCAATGACTCCTATG	ATGATGACTGCAGCAAATCGC	60	
Tcf7 mRNA	GCTGCCATCAACCAGATCCT	GCTGCCATCAACCAGATCCT	59	
Axin2 mRNA	GGCAGTGATGGAGGAAAATG	TGGGTGAGAGTTTGCACTTG	60	

9.3 Specimen preparation

Guts, pancreas or dorsal pancreatic buds were dissected from mouse embryos at different stages or postnatally in phosphate buffer saline (PBS) (1.8 mM KH_2PO_4, 10 mM Na_2HPO_4, 137 mM NaCl, 2.7 mM KCl pH7.4). For embryonic tissue, midday after a vaginal plug was seen was considered as E0.5. Organs were either snap frozen or fixed. In the latter case, organs were fixed in 4% paraformaldehyde in PBS (4% PFA) for 30 minutes at room temperature or overnight at 4°C. Specimens were then washed in PBS, equilibrated in 0.12M phosphate buffer 15% sucrose overnight at 4°C. They were then soaked in 0.12M phosphate buffer 15% sucrose 7.5% gelatin warmed at 37°C. Afterward, organs were included in a gelatin

bloc and solidified at 4 degrees. Blocs were frozen in isopentane cooled down at -65°C by an ethanol-dry ice mix. Blocs were kept at -80°C. 7 µm thick cryostat sections were generally collected. If guts were stained with 3-12-beta-galactosidase staining (X-Gal staining), 10 µm thick cryostat sections were collected. In the case of cilia quantification on E18.5 pancreas, 15 µm thick sections were collected. For cell number quantification, systematic uniform random sampled sections (SUR sections) were collected every 5, 6, 10 sections for E12.5, E14.5, and E18.5/P0 respectively.

9.4 LacZ staining

Guts were dissected and fixed with 4% PFA for 10 minutes at room temperature. They were washed 3 times 5 minutes with X-Gal buffer (5 mM EGTA, 2 mM $MgCl_2$, 0.02% NP40, 0.01% Deoxycholate in PBS). They were then stained with X-Gal staining solution (5 mM $C_6FeK_3N_6$, 5 mM $C_6FeK_4N_63H_2O$, 0.05% X-Gal) for 5 hours 45 minutes at 37°C. Afterward they were washed 3 times 5 minutes in PBS, post-fixed 30 minutes at room temperature or overnight at 4 degrees and, processed normally for bloc embedding.

9.5 Histology, immunofluorescence, and TUNEL assay

Haematoxylin eosin staining was performed on cryosections. In case of immunofluorescence staining, cryosections were dried, rehydrated in 0.1% triton X-100 in tris buffer (50 mM Tris pH 7.5, 150 mM NaCl, 0.1% triton X-100) (TBST), permeabilized with 0.25% triton X-100 in tris buffer, blocked with 10% donkey serum (Sigma D9663) in TBST (blocking buffer) for 30 minutes to 4 hours and incubated overnight at 4°C with primary antibodies diluted in blocking buffer. The next day, sections were washed in TBST and incubated with secondary antibodies with DAPI or Draq5 as a nuclear counterstaining diluted in blocking buffer for 45 minutes at room temperature. They were subsequently washed in TBST and slides were mounted with a glass coverslip and 50% glycerol in PBS. They were sealed with nail polish. In case of biotin-streptavidin amplification, sections were incubated with Streptavidin Biotin blocking solution (Vector Laboratories, SP-2002) prior to primary antibody incubation following the manufacturer's protocol. After secondary antibody incubation and washes, slides were incubated with streptavidin-conjugated fluorophore

and DAPI diluted in blocking buffer. Slides were then washed in TBST and mounted. Antibodies and the dilution used in this study are listed in Table 10. TUNEL assay was performed with the ApopTag® Fluorescein Direct *In Situ* Apoptosis Detection Kit (Millipore, S7160). Cryosections were post-fixed 10 minutes in 1% PFA in PBS and permeabilized with 0.5% triton X-100 in PBS on ice. TUNEL assays were then carried out in accordance of the manufacturer's protocol followed by standard immunofluorescence staining, as described above.

Table 10: Antibodies, nuclear dyes and their dilution

Antibody	Company	Catalog number	Dilution
anti-Ac TUB	Sigma	T6793	1/500
anti-ACTA2	Sigma	A5228	1/400
anti-Active CASP3	Cell Signaling Technology	9664	1/500
Anti-ADCY6*	Protein Tech	14616-1-AP	1/500
anti-AMY1	Merk Millipore	171534	1/400
anti-aPKC	Santa Cruz	sc-216	1/500
anti-BICC1	Sigma	HPA045212	1/50
anti-chick Al488	InVitrogen	A-11039	1/1000
anti-EMR1	Serotec	MCA497	1/500
anti-FOXA2*	Abcam	ab40874	1/5000
anti-GFP	Abcam	AB13970	1/1000
anti-Ghrelin	Santa Cruz	sc-10368	1/800
anti-goat Al488	Life Technologies	A11055	1/1000
anti-goat Al568	Life Technologies	A11057	1/1000
anti-goat biotin	JIRE	705-065-1470	1/400
anti-goatAl488	Molecular Probes	A-11055	1/800
anti-guinea pig Al488	Life Technologies	A11073	1/2500
anti-guinea pig Al568	Life Technologies	A11075	1/800
anti-guinea pig Al568	Molecular Probes	A11075	1/600
anti-guinea pig biotin	JIRE	706-065-1480	1/400
anti-HES1*	Santa Cruz	sc-25392X	1/2000
anti-HNF1B	Santa Cruz	sc-7411	1/50
anti-HNF1B*	Santa Cruz	sc-22840	1/200
anti-ONECUT1	Santa Cruz	sc-13050	1/250
anti-ONECUT1*	Santa Cruz	sc-13050	1/200

anti-INS	Dako	A0564	1/50 or 1/100
anti-mouse Al568	Life Technologies	A10037	1/1000 or 1/2000
anti-mouse Al647	JIRE	715-605-1500	1/2000
anti-mouse biotin	JIRE	715-065-150	1/800
anti-myc	InVitrogen	13-2500	1/200
anti-PHH3	Merk Millipore	06-570	1/1000
anti-PDX1	Beta Cell Biology Consortium	ab2027	1/1000
anti-PDX1*	Beta Cell Biology Consortium	ab2027	1/2000
anti-PKD2	Santa Cruz	sc-2549	1/500
anti-PKD2*	Santa Cruz	sc-2549	1/1000
Anti-PKIA	Santa Cruz	sc-1943	1/200
anti-PP	peninsula lab (Bachem)	T-4088	1/400
anti-PTPRC	Becton Dickinson	550539	1/200
anti-rabbit Al488	JIRE	711-545-1520	1/200
anti-rabbit Al568	Life Technologies	A10042	1/500
anti-rabbit Al647	JIRE	711-605-1520	1/600
anti-rabbit HRP	JIRE	111-035-003	1/200
anti-Rabbit HRP*	Dako	P0048	1/2000
anti-Rat HRP*	JIRE	712-035-153	1/10000
anti-ratAl488	Life Technologies	A10042	1/600
anti-SOX9	Millipore	AB5535	1/500
anti-SOX9*	Millipore	AB5535	1/2000
anti-STS	Dako	A0556	1/800
anti-TUB	Abcam	sb6160	1/10000
DAPI	Sigma	D9542-1MG	1/10 000
DBA lectin	Vector	B1035	1/500 or 1/800
DBA rhodamin	Vector	RL-1032	1/500
draq5	Bionordika	4084	1/500
goat anti-CPA1	R&D	AF2765	1/500
goat anti-NEUROG3	Beta Cell Biology Consortium	AB2774	1/1000
guinea pig anti-GCG	Linco	4031-01F	1/400 or 1/800
mouse anti-GCG	Sigma	G2654	1/2000
mouse anti-MKI67	novocastra laboratories	NCL-L-Ki67-MM1	1/500
rabbit anti-CPA1	ANAWA	1810-006	1/800
rabbit anti-MKI67	Abcam	AB16667	1/100
rabbit anti-NEUROG3	Beta Cell Biology Consortium	AB2011 (2369B)	1/500

Streptavidin Al488	Molecular Probes	S-11223	1/800
Streptavidin Al647	JIRE	016-600-0840	1/1000

* Antibodies used for western blot

9.6 Images and image analyses

A Leica SP8 confocal, a Leica DM5500 upright wide-field microscope, and a 3DHISTECH panoramic MIDI slide scanner were used for imaging.

Cell number quantifications were performed on pictures from a Leica DM5500 upright wide-field microscope, and a 3DHISTECH panoramic MIDI slide scanner. Assuming a similar cell size distribution in WT and *Bicc1* KO, quantification was obtained by counting stained positive-cell profiles harboring a nucleus either manually or automatically with home-made Macros in Fiji software (Schindelin et al., 2012) on immunofluorescence-stained SUR sections. For E12.5 and E14.5 pancreata, cell profiles were counted on all the sampled sections or every 4^{th} section (progenitor proliferation). For E18.5 pancreata, quantifications were performed on every section (beta cells, automated quantification), every other section (other endocrine cell quantification) or every 8^{th} sections (ductal proliferation). P0 quantification was performed every 4^{th} section manually (ductal quantification) or automatically (lineage tracing and number of DAPI nucleus). Numbers per samples were then multiplied to get total cell profile numbers for all stained SUR sections except for P0 data. For cilia quantification, areas of 3801 μm^2 of immunostained 15µm-thick OCT sections of E18.5 pancreata were scanned by confocal microscopy. For WT animals (n=4), 4 main or interlobular ducts and 4 intercalated ducts were imaged while cystic areas were imaged instead of main or interlobular ducts in the case of KO animals (n=4). The number of cilia were quantified on 3D-reconstructed images and normalized to the total number of DBA $lectin^+$ cells present in the field.

9.7 Western blot

E15.5 pancreata were lysed in Laemmli buffer and sonicated (Bioruptor® Plus, Diagenode; intensity: high, [30 seconds ON-30 seconds OFF] x 2). Protein size separation on NuPage gel (Life Technologies, Novex,

NP0321) was achieved by voltage constant electrophoresis (Life Technologies, Novex, XCell Surelock™) in MES running buffer (Life Technologies, NP0002-02). Proteins were then wet-transferred on a nitrocellulose membrane (GE Heathlcare Life sciences, RPN303D; Biorad, Minipotrein tetrasystem) in transfer buffer (3.02 g/l Trizma Base, 14.4 g/l Glycine, 20% Methanol) using an intensity constant electric field of 400 mA for one hour and a half. Proteins on the gel were visualized by Coomassie Blue staining (Life Technologies, LC6065). After washing in Tris buffer saline Tween20 (2.42 g/l Trizma base, 8 g/l NaCl, 0.1% Tween20 pH7.6) (TBSTw), the membrane was blocked in 10% skimmed milk in TBSTw for 1 hour. It was incubated with a primary antibody diluted in 5% BSA in TBSTw overnight at 4°C. After washes with TBSTw, the membrane was incubated with HRP-conjugated secondary antibody diluted in 5% skimmed milk in TBSTw for 1 hour. It was then washed in TBSTw. ECL kit (GE Healthcare, RPN2232) was used for detection with Biorad Gel Doc™ following the manufacturer´s protocol. The antibody on the membrane could be stripped with stripping buffer (72.5 mM Tris pH 7.5, 2% SDS, 125 mM β-mercaptoethanol) at 65°C for 20 minutes. The membrane was then washed in TBSTw and used for another immunoblot. Antibodies and the dilution used in this study are listed in Table 10. For comparison, the protein of interest was normalized to alpha tubulin (TUB) level. Results are relative to WT mean.

9.8 RNA extraction and Q-PCR

RNA was extracted from E10.5, E11.5, E12.5 and E14.5 dorsal buds using RNeasy Mini Kit (QIAGEN, 74104) including a DNase treatment with RNase-free DNase (QIAGEN, Set 79254) following the manufacturer´s instructions. 100 ng to 500 ng of RNA was then reverse-transcribed into cDNA with SuperScript III Reverse Transcriptase (Life Technology, 18080-044) following the manufacturer's protocol. Q-PCRs were performed on 1/5 to 1/50 of the synthetized cDNA on the StepOnePlus™ Real-Time PCR system (Life Technology) using Power SYBR® Green as dye (Applied Biosystems, 4368577). Quantifications were normalized against standard curves of the respective genes. For comparison, the gene of interest was normalized to the housekeeping gene *Hprt1*. Results are indicated as percentage of WT mean. Primer sequences and annealing temperatures are listed in Table 9.

9.9 RNA and microRNA sequencing

RNA was extracted from E13.5 dorsal buds using the RNeasy Plus Micro Kit (QIAGEN, 74034) following the manufacturer´s protocol allowing small RNA elution. For RNA sequencing, three samples of the same genotype were then pooled together. TruSeq RNA libraries were synthetized from 500 ng of three WT and three *Bicc1* KO pools. Libraries were sequenced on an Illumina HiSeq 2500 platform (3 replicates per condition, 100nt single-end reads) at the genomic facility, University of Lausanne. Reads were mapped to the mm9 mouse genome with bowtie v0.12.7 (480M reads mapped in total) (Langmead et al., 2009). The data were first analyzed using the DESeq method by Solenne Carat at the Bioinformatics and Biostatistics Core Facility at Ecole Polytechnique Fédérale de Lausanne (Anders and Huber, 2010). The data were then reanalyzed. They were filtered to eliminate genes which had read per kilobase per million (rpkm) below 0.01 and analyzed using NIA array analysis tool (http://lgsun.grc.nia.nih.gov/ANOVA/). Differences with FDR below 0.05 were considered as statistically significant. RNA sequencing data are available on NCBI Gene Expression Omnibus (accession number: GSE58833).

For the microRNA sequencing, all E13.5 dorsal pancreatic bud RNA samples of the same genotype remaining after the synthesis of the TruSeqRNA libraries were pooled. TruSeq Small RNA libraries were then synthetized from 2.4 µg of RNA of WT and *Bicc1* KO. Libraries were sequenced on an Illumina HiSeq 2500 platform (1 replicate per condition, 100nt single-end reads) at the genomic facility, University of Lausanne. The sequences were mapped to the mm9 mouse genome using Eland_v2e. The data were than analyzed using DESeq method by Solenne Carat at Ecole Polytechnique Fédérale de Lausanne (Anders and Huber, 2010).

9.10 Human *BICC1* mutation

The Group of Pr. Bingham, Pr. Ellard and Pr. Hattersley sequenced the exons of BICC1 in 149 patients presenting cystic kidney disease with unknown genetic cause. 5 new variants of BICC1 were identified.

Yvan Pfister cloned the variants as well as WT BICC1 and BICC1Q87Stop into the pcDNA3.0 plasmid. Two HA epitopes were also inserted in BICC1 sequence.

9.11 Luciferase assay

HEK293T cells were plated in 48-well plates at a density of 80 000 cells/cm^2 and grown in DMEM medium with Glutamax (Life technologies, 31966021) supplemented with 10% fetal calf serum (Life Technologies, 10270-106). After one day, they were transfected using Transfast^{TM} (Promega, E2431) according to the manufacturer´s protocol except that the transfection medium was replaced by normal culture medium after 4 hours. The transfection mixes contained 252.5 ng of DNA: 50ng of pMegaTOPflash (gift of Dr. Fuerer), 2.5 ng of pGL3::RenillaTK (provided by the luciferase assay kit) combined with 50 ng of DVL2 (gift of Pr. Constam) and 150ng of pcDNA3.0 containing WT *BICC1* or one of the *BICC1* variants. In case of the negative control (no induction), 200ng of pcDNA3.0 plasmid were added and in the case of DVL2 alone, 150ng of pcDNA3.0 replaced the BICC1 plasmid. After two days, luciferase assays were performed using the Dual-Luciferase® Reporter Assay System (Promega, E1910) according to the manufacturer´s protocols. Every transfection was done in 5 replicates and the experiment was repeated once.

9.12 Statistical analysis

Statistical analyses were performed with GraphPad Prim4 and 6 softwares and Excel. Results were indicated by the mean ± standard deviation and graphically represented by the mean + standard deviation except in Fig. 30, 31, 32 and 34C, Fig. 30 and 32 show histograms. Fig. 31 shows scattered plots and Fig. 34C shows a dot plot with the mean. Differences assessed with a t test (assuming normal distribution) were considered as statistically significant when the p-value was below 0.05.

10 APPENDIX

10.1 Tables

Table 11: List of the gene symbol and their official name cited in this work.

Gene symbol	Official name
1700023F06-Rik	RIKEN cDNA 1700023F06 gene
2010107G23-Rik	RIKEN cDNA 2010107G23 gene
4930533K18-Rik	RIKEN cDNA 4930533K18 gene
Abcc8	ATP-binding cassette, sub-family C (CFTR/MRP), member 8
Acta2	actin, alpha 2, smooth muscle, aorta
Actb	actin beta
Acvrl1	activin A receptor type II-like 1
Adcy5	adenylate cyclase 5
Adcy6	adenylate cyclase6
Ago1	argonaute RISC catalytic subunit 1
Ago2	argonaute RISC catalytic subunit 2
Akt	thymoma viral proto-oncogene 1
Aldoa	aldolase A, fructose-bisphosphate
Alms1	Alstrom syndrome 1
Amy1	amylase 1, salivary
Anxa9	annexin A9
Apc	adenomatosis polyposis coli
Aqp2	aquaporin 2
Arx	aristaless related homeobox
Avpr2	arginine vasopressin receptor 2
Axin2	axin2
Bc100530	cDNA sequence BC100530
Bcc-1	protein BCC-1
BicC	Bicaudal C
Bicc1	bicaudal C homolog 1 (Drosophila)
Blk	B lymphoid kinase
bpk	Balb/c Polycystic Kidneys
Braf	Braf transforming gene
Btc	betacellulin, epidermal growth factor family member
Calcr	calcitonin receptor

Gene symbol	Official name
Casp3	caspase 3
Cdh1	cadherin 1
Cel	carboxyl ester lipase
Celsr1	cadherin, EGF LAG seven-pass G-type receptor 3 (flamingo homolog, Drosophila)
Celsr2	cadherin, EGF LAG seven-pass G-type receptor 2 (flamingo homolog, Drosophila)
Celsr3	cadherin, EGF LAG seven-pass G-type receptor 3 (flamingo homolog, Drosophila)
Cer1	cerberus 1 homolog (Xenopus laevis)
Cftr	cystic fibrosis transmembrane conductance regulator
Cma1	chymase 1, mast cell
Cpa1	carboxypeptidase A1, pancreatic
cpk	congenital polycystic kidney
Crp	C-reactive protein, pentraxin-related
Csf1	colony stimulating factor 1 (macrophage)
Ctnnb1	catenin (cadherin associated protein), beta 1
Cys1	cystin 1
Dgcr8	DiGeorge syndrome critical region gene 8
Dicer1	dicer 1, ribonuclease type III
Dll1	delta-like 1 (Drosophila)
Dll4	delta-like 4 (Drosophila)
Drosha	drosha, ribonuclease type III
Dvl2	dishevelled 2, dsh homolog (Drosophila)
Eef1a1	eukaryotic translation elongation factor 1 alpha 1
Egfr	epidermal growth factor receptor
Eif2ak3	eukaryotic translation initiation factor 2 alpha kinase 3
Emr1	EGF-like module containing, mucin-like, hormone receptor-like sequence 1

Gene symbol	Official name
Eno1	enolase 1, alpha non-neuron
Erbb2	v-erb-b2 erythroblastic leukemia viral oncogene homolog 2, neuro/glioblastoma derived oncogene homolog (avian)
Erbb3	v-erb-b2 erythroblastic leukemia viral oncogene homolog 3 (avian)
Erbb4	v-erb-a erythroblastic leukemia viral oncogene homolog 4 (avian)
Fam162b	family with sequence similarity 162, member B
fbf-1	Protein FBF-1
fem-3	Protein FEM-3
Fgf10	fibroblast growth factor 10
Fgf4	fibroblast growth factor 4
Fgfr2	fibroblast growth factor receptor 2
Fgfr4	fibroblast growth factor receptor 4
Foxa1	forkhead box A1
Foxa2	forkhead box A2
Foxp3	forkhead box P3
Fzd2	frizzled homolog 2 (Drosophila)
Fzd3	frizzled homolog 3 (Drosophila)
Fzd7	frizzled homolog 7 (Drosophila)
Fzd8	frizzled homolog 8 (Drosophila)
Gata4	GATA binding protein 4
Gata6	GATA binding protein 6
Gcg	glucagon
Gck	glucokinase
Gdf11	growth differentiation factor 11
Ghr	ghrelin
Gld2	Protein GLD-2
Gld3	Protein GLD-3
Glis3	GLIS family zinc finger 3
Gm13305	predicted gene 13305
Gm15745	predicted gene 15745
Gm2002	predicted gene 2002
Gm5483	predicted gene 5483
Grk	gurken
Gsk3b	glycogen synthase kinase 3 beta
H19	H19, imprinted maternally expressed transcript
Hdc	histidine decarboxylase
Hes1	hairy and enhancer of split 1 (Drosophila)

Gene symbol	Official name
Hnf1a	HNF1 homeobox A
Hnf1b	HNF1 homeobox B
Hnf4a	hepatic nuclear factor 4, alpha
Hprt	hypoxanthine guanine phosphoribosyl transferase
Ift88	intraflagellar transport 88
Il11ra2	interleukin 11 receptor, alpha chain 2
Ins	insulin
Insm1	insulinoma-associated 1
Inv	inversin
Isl1	ISL1 transcription factor, LIM/homeodomain
Itpr1	inositol 1,4,5-trisphosphate receptor 1
Jag1	jagged1
Jag2	jagged 2
jcpk	juvenile congenital polycystic kidney disease
Kcnj11	potassium inwardly rectifying channel, subfamily J, member 11
Kif3a	kinesin family member 3A
Klf11	Kruppel-like factor 11
lacZ	Beta-D-galactoxidase (E. coli)
Lef1	lymphoid enhancer binding factor 1
Lrp5	low density lipoprotein receptor-related protein 5
Lrp6	low density lipoprotein receptor-related protein 6
Maml1	mastermind like 1 (Drosophila)
Map2k7	mitogen-activated protein kinase kinase 7
Mapk1	mitogen-activated protein kinase 1
Mapk8	mitogen-activated protein kinase 8
Mapk8	mitogen-activated protein kinase 8
Mcpt4	mast cell protease 4
Mib1	mindbomb homolog 1 (Drosophila)
Mki67	antigen identified by monoclonal antibody Ki 67
Mnx1	motor neuron and pancreas homeobox 1
mt-Co1	mitochondrially encoded cytochrome c oxidase I
mt-Cytb	mitochondrially encoded cytochrome b
MtOR	mechanistic target of rapamycin (serine/threonine kinase)
Muc1	mucin 1, transmembrane
Myod1	myogenic differentiation 1

Gene symbol	Official name
Myt1	myelin transcription factor 1
Nek8	NIMA (never in mitosis gene a)-related expressed kinase 8
Neurod1	neurogenic differentiation 1
Neurog3	neurogenin 3
Ngp	neutrophilic granule protein
Nkx2.2	NK2 homeobox 2
Nkx2.5	NK2 homeobox 5
Nkx6.1	NK6 homeobox 1
Nkx6.2	NK6 homeobox 2
Noth1	notch 1
Noth2	notch 2
Noth3	notch 3
Noth4	notch 4
Nphp3	nephronophthisis 3 (adolescent)
Olfm4	olfactomedin 4
Onecut1	one cut domain, family member 1
Onecut2	one cut domain, family member 2
orb	oo18 RNA-binding protein
orpk	Oak Ridge Polycystic Kidney
osk	oskar
Pah	phenylalanine hydroxylase
Pax4	paired box 4
Pax6	paired box 6
pcy	polycystic
Pde1a	phosphodiesterase 1A, calmodulin-dependent
Pde1b	phosphodiesterase 1B, Ca2+-calmodulin dependent
Pde1c	phosphodiesterase 1C
Pdx1	pancreatic and duodenal homeobox 1
Pfkl	phosphofructokinase, liver, B-type
Pkd1	polycystic kidney disease 1 homolog
Pkd2	polycystic kidney disease 2
Pkhd1	polycystic kidney and hepatic disease 1
Ppy	pancreatic polypeptide
Prkaa1	protein kinase, AMP-activated, alpha 1 catalytic subunit
Ptf1a	pancreas specific transcription factor, 1a
Ptprc	protein tyrosine phosphatase, receptor type, C
Rbpj	recombination signal binding protein for immunoglobulin kappa J region

Gene symbol	Official name
Rbpjl	recombination signal binding protein for immunoglobulin kappa J region-like
Rfx6	regulatory factor X, 6
Robo2	roundabout homolog 2 (Drosophila)
rol-3	Protein ROL-3
Rpl30-ps5	ribosomal protein L30, pseudogene 5
Rps3	ribosomal protein S3
S100a8	S100 calcium binding protein A8 (calgranulin A)
S100a9	S100 calcium binding protein A9 (calgranulin A)
Shh	sonic hedgehog
Six2	sine oculis-related homeobox 2
Slc16a3	solute carrier family 16 (monocarboxylic acid transporters), member 3
Slc19a2	solute carrier family 19 (thiamine transporter), member 2
Slc2a1	solute carrier family 2 (facilitated glucose transporter), member 1
Slc5a9	solute carrier family 5 (sodium/glucose cotransporter), member 9
Smad2	SMAD family member 2
Sox9	SRY (sex determining region Y)-box 9
Sst	somatostatin
Sstr2	somatostatin receptor 2
Stard9	START domain containing 9
Tcf7	transcription factor 7, T cell specific
tdgf1.3	teratocarcinoma-derived growth factor 1
Tgfa	transforming growth factor alpha
Tgfb	trasnforming growth factor beta
Tgfbr1	transforming growth factor, beta receptor I
Tgfbr2	transforming growth factor, beta receptor II
Tnfrsf9	tumor necrosis factor receptor superfamily, member 9
Tnrc6a	trinucleotide repeat containing 6a
tral	trailer hitch
Tsc2	tuberous sclerosis 2
Tub	alpha tubulin
Vhl	von Hippel-Lindau tumor suppressor
Wfs1	Wolfram syndrome 1 (wolframin)
Wnt1	wingless-type MMTV integration site family, member 1

Gene symbol	Official name
Wnt4	wingless-type MMTV integration site family, member 4
Wnt5a	wingless-type MMTV integration site family, member 5a
Wnt5b	wingless-type MMTV integration site family, member 5b

Gene symbol	Official name
Wnt7b	wingless-type MMTV integration site family, member 7B
Wnt9b	wingless-type MMTV integration site family, member 9b

Official name corresponds to mouse name with the exception of the genes in blue that are *Caenorhabditis elegans* genes and the red-color genes that are from *Drosophila melanoblaster*

Table 12: Average, standard deviation, number of samples (n) and t test p value from the different figures.

			Average	Standard deviation	n	T test p value
Fig. 9	**Q-PCR quantification**					
	Bicc1/*Hprt1* (% of E12.5 mean)	E10.5	55	7	3	E10.5 vs E11.5: 0.20
		E11.5	64	5	3	E11.5 vs E12.5: 0.0003
		E12.5	100	3	3	E10.5 vs E12.5: 0.0008
Fig. 12	**Ductal cell number at P0**					
	DBA lectin$^+$ cell number	WT	5151	742	4	0.0003
		Bicc1 KO	10451	1188	4	
Fig. 13	**Pancreatic progenitor proliferation at E14.5**					
	PHH3$^+$PDX1$^+$cells/PDX1$^+$cells (% of WT mean)	WT	100	15	4	0.90
		Bicc1 KO	101	14	3	
	Ductal proliferation at E18.5					
	MKI67$^+$DBA lectin$^+$ cells/DBA lectin$^+$ cells (% of WT mean)	WT	100	23	4	0.016
		Bicc1 KO	147	16	4	
Fig. 15	**Cilia at E18.5**					
	Intercalated ducts					
	Ac TUB$^+$DBAlectin$^+$cells / DBAlectin$^+$cells (%)	WT	65	14	4	0.75
		Bicc1 KO	69	18	4	
	Main/inter-/intralobular ducts vs cystic ducts					
	Ac TUB$^+$DBAlectin$^+$cells/DBAlectin$^+$cells (%)	WT	64	5	4	0.12
		Bicc1 KO	55	8	4	
Fig. 16	**Endocrine cells in the duct at P0**					

	Hormones$^+$DBAlectin$^+$ cell number	WT	8	4	4	0.0086
		Bicc1 KO	113	28	4	
Fig. 17	**Endocrine cells at E12.5**					
	Alpha GCG$^+$ cell number	WT	136	11	4	0.72
		Bicc1 KO	127	48	4	
	Endocrine cells at E14.5					
	Beta INS$^+$ cell number	WT	679	189	4	0.74
		Bicc1 KO	725	185	4	
	Alpha GCG$^+$ cell number	WT	824	228	3	0.62
		Bicc1 KO	930	280	4	
	Endocrine cells at E18.5					
	Beta INS$^+$ cell number	WT	14515	1624	4	0.0008
		Bicc1 KO	6964	1833	4	
	Alpha GCG$^+$ cell number	WT	3807	115	3	0.0024
		Bicc1 KO	3047	206	4	
	Delat STS$^+$ cell number	WT	1567	223	3	0.0029
		Bicc1 KO	726	185	4	
	PP PP$^+$ cell number	WT	1022	221	3	0.012
		Bicc1 KO	560	91	4	
	Epsilon GRH$^+$ cell number	WT	449	102	3	0.011
		Bicc1 KO	208	59	4	
Fig. 18	**Beta cell proliferation at E18.5**					
	MKI67$^+$INS$^+$ cells/INS$^+$ cells (%)	WT	11.1	3.2	4	
		Bicc1 KO	11	2.8	4	0.95
Fig. 19	**Pancreatic progenitor number at E12.5**					
	PDX1$^+$ cell number	WT	2237	341	4	
		Bicc1 KO	3767	648	4	0.0058
	Pancreatic progenitor number at E14.5					
	PDX1$^+$ cell number	WT	34600	6690	4	
		Bicc1 KO	34271	8532	4	0.95
	Pancreatic size at P0					
	DAPI nucleus number	WT	85612	10986	4	
		Bicc1 KO	93573	5126	4	0.24
Fig. 20	**Endocrine progenitor number at E12.5**					
	NEUROG3$^+$ cell number	WT	26	6	4	
		Bicc1 KO	57	18	4	0.015
	Relative endocrine progenitor number at E12.5					
	NEUROG3$^+$ cell number/PDX1$^+$ cell number (%)	WT	1.1	0.16	4	0.043
		Bicc1 KO	1.5	0.24	4	

	Q-PCR quantification *Neurog3* at E12.5					
	Neurog3/*Hprt1* (% of WT mean)	WT	100	66	6	0.27
		Bicc1 KO	56	57	5	
	Endocrine progenitor E14.5					
	NEUROG3$^+$ cell number	WT	3032	388	4	0.0043
		Bicc1 KO	1989	262	4	
	Relative endocrine progenitor number at E14.5					
	NEUROG3$^+$ cell number/PDX1$^+$ cell number (%)	WT	8.9	0.90	4	
		Bicc1 KO	6.0	1.29	4	0.011
	Q-PCR quantification *Neurog3* at E14.5					
	Neurog3/*Hprt1* (% of WT mean)	WT	100	8	4	0.012
		Bicc1 KO	72	14	5	
Fig. 22	**Lineage tracing with Neurog3-RFP**					
	NEUROG3$^+$RFP$^-$ cell number	WT	1820	308	4	
		Bicc1 KO	1281	216	4	0.029
	NEUROG3$^+$RFP$^+$ cell number	WT	1212	174	4	
		Bicc1 KO	708	88	4	0.0021
	NEUROG3$^-$Hormones$^-$RFP$^+$ cell number	WT	3136	562	4	
		Bicc1 KO	2482	277	4	0.08
	NEUROG3$^-$Hormones$^+$RFP$^+$ cell number	WT	1001	253	4	
		Bicc1 KO	751	188	4	0.16
	Lineage tracing with Neurog3-RFP: proportion to total RFP cells					
	NEUROG3$^+$RFP$^+$ cells/RFP$^+$ cells (%)	WT	23	3	4	0.07
		Bicc1 KO	18	3	4	
	NEUROG3$^-$Hormones$^-$RFP$^+$ cells/RFP$^+$ cells (%)	WT	59	1	4	0.0078
		Bicc1 KO	63	2	4	
	Hormones$^+$RFP$^+$ cells/RFP$^+$ cells (%)	WT	18	2	4	0.80
		Bicc1 KO	19	3	4	
Fig. 23	**Characterization of Neurog3-RFP**					
	NEUROG3$^+$RFP$^-$ cells/NEUROG$^+$ cells (%)	WT	60	4.5	4	
	NEUROG3$^+$RFP$^+$ cells/NEUROG$^+$ cells (%)	WT	40	4.5	4	
	NEUROG3$^+$RFP$^+$ cells/RFP$^+$ cells (%)	WT	23	3	4	
	NEUROG3$^-$Hormones$^-$RFP$^+$ cells/RFP$^+$ cells (%)	WT	59	1	4	
	Hormones$^+$RFP$^+$ cells/RFP$^+$ cells (%)	WT	18	2	4	
Fig. 24	**Lineage tracing with Neurog3-Cre**					
	YFP$^+$ cell number	WT	7539	1022	4	0.0046
		Bicc1 KO	4364	1024	4	
	Hormones$^+$ YFP$^+$ cell number (endocrine cells)	WT	3791	344	4	0.0003

		Bicc1 KO	1740	444	4	
	$CPA1^+YFP^+$ cell number (acinar cells)	WT	1268	440	4	0.49
		Bicc1 KO	921	505	4	
	DBA $lectin^+$ YFP^+ cell number (ductal cells)	WT	835	239	4	0.78
		Bicc1 KO	886	263	4	
Fig. 25	**Western blot quantification**					
	SOX9/TUB (relative to WT mean)	WT	1	0.31	4	0.30
		Bicc1 KO	1.25	0.31	4	
	HES1/TUB (relative to WT mean)	WT	1	0.08	4	0.06
		Bicc1 KO	0.73	0.23	4	
	HFN1B/TUB (relative to WT mean)	WT	1	0.05	4	0.10
		Bicc1 KO	1.11	0.10	4	
	FOXA2/TUB (relative to WT mean)	WT	1	0.05	4	0.48
		Bicc1 KO	0.92	0.20	4	
	PDX1/TUB (relative to WT mean)	WT	1	0.14	4	0.37
		Bicc1 KO	1.13	0.23	4	
	ONECUT1/TUB (relative to WT mean)	WT	1	0.18	7	0.13
		Bicc1 KO	0.81	0.27	8	
	Q-PCR quantification					
	Hes1/*Hprt1* (% of WT mean)	WT	100	15	4	0.45
		Bicc1 KO	92	16	5	
	Dll1/*Hprt1* (% of WT mean)	WT	100	19	4	0.55
		Bicc1 KO	92	18	5	
	Onecut1/*Hprt1* (% of WT mean)	WT	100	8	4	0.042
		Bicc1 KO	134	26	5	
	Bicc1/*Hprt1* (% of WT mean)	WT	100	20	4	0.027
		Onecut1 KO	61	6	3	
Fig. 26	**Q-PCR quantification**					
	Tcf7/*Hprt1* (% of WT mean)	WT	100	22.71	4	0.22
		Bicc1 KO	80.97	20.01	5	
	Axin2/*Hprt1* (% of WT mean)	WT	100	19.25	4	0.16
		Bicc1 KO	77.15	23.65	5	
Fig. 28	**Western blot quantification**					
	PKD2/TUB (relative to WT mean)	WT	1	0.13	8	<0.0001
		Bicc1 KO	0.45	0.12	8	
Fig. 29	**Immune cells**					
	$PTPRC^+$ cells	WT	84	10	4	0.017
		Bicc1 KO	175	55	4	
Fig. 30	**Western blot quantification**					
	ADCY6/TUB (relative to WT mean)	WT	1	0.20	8	0.33

		Bicc1 KO	1.11	0.26	8	
	PKIA/TUB (relative to WT mean)	WT	1	0.28	7	0.35
		Bicc1 KO	1.12	0.21	8	
Fig. 31	**Luciferase assay quantification**					
	TopFlash assay normalized on Renilla luciferase chemiluminescence (% of DVL1)	Negative control	2	1	6	
		DVL1	100	8	10	
		BICC1	73	11	10	BICC1 *vs* DVL1, p<0.0001
		BICC1 Q87Stop	109	11	10	BICC1 *vs* BICC1 Q87Stop, p<0.0001
		BICC1 D54G	74	6	10	BICC1 *vs* BICC1 D54G, p=0.74
		BICC1 V206M	78	6	10	BICC1 *vs* BICC1 V206M, p=0.27
		BICC1 R800Q	78	8	10	BICC1 *vs* BICC1 R800Q, p=0.28
		BICC1 G821E	73	8	10	BICC1 *vs* BICC1 G821E, p=0.92
		T845K	76	11	10	BICC1 *vs* BICC1 T845K, p=0.58

Table 13: Downregulated mRNA in E13.5 Bicc1 KO pancreas using DESeq

Gene Symbol	WT mean (rpkm)	KO mean (rpkm)	Fold change	p value
Gm2002	0.52	0.02	28.23	3.9E-19
Gm1082	0.05	0.00	22.46	0.0003
Fcnb	0.09	0.01	16.52	0.0015
Stfa2	0.74	0.07	11.29	3.2E-08
Camp	1.02	0.10	9.71	1.7E-09
Prap1	0.51	0.06	8.83	0.0003
Olfm4	1.66	0.20	8.45	2.2E-22
Stfa3	0.96	0.12	7.96	4.5E-06
Stfa1	2.39	0.30	7.88	5E-11
Ngp	3.10	0.40	7.82	1.1E-19

Ifitm6	0.32	0.04	7.59	0.0039
Il11ra2	0.43	0.06	7.51	4.9E-10
BC100530	3.58	0.51	6.96	2.1E-16
Xlr5c	0.07	0.01	6.82	0.0402
Xlr5a	0.19	0.03	6.64	0.0002
S100a8	8.19	1.28	6.40	1.3E-15
Gm5483	1.46	0.23	6.30	1.2E-06
Xlr5b	0.16	0.03	6.19	0.0013
Stfa2l1	0.65	0.11	6.13	0.0009
S100a9	13.09	2.16	6.05	8.8E-21
Ltf	0.52	0.09	5.43	3.5E-09
Gm15845	0.26	0.06	4.72	0.0437
Bicc1	19.13	4.45	4.30	9.3E-47
Lcn2	0.38	0.10	3.88	4.5E-05
Gm13305	0.86	0.23	3.75	6E-08
Mmp8	0.13	0.03	3.63	0.0255
4930533K18-Rik	4.97	1.49	3.35	9.9E-08
Pah	16.63	5.12	3.25	7.4E-21
Tbx18	0.11	0.04	3.13	0.0208
Anxa9	1.14	0.42	2.73	0.0004
Chi3l1	0.29	0.12	2.53	0.0310
Prodh2	0.77	0.34	2.25	0.0179
Cer1	2.20	1.05	2.10	0.0092
Adamts18	0.58	0.28	2.05	0.0215
Adamts16	5.86	3.03	1.93	1.1E-06
Calcr	16.85	8.79	1.92	0.0011
Slc5a9	2.32	1.23	1.89	0.0011
Ppp1r1b	2.54	1.34	1.89	0.0103
Pkd2	10.61	5.64	1.88	2.5E-08
Cmah	2.23	1.23	1.81	0.0004
Pappa	1.05	0.63	1.68	0.0385
Serpini2	20.50	13.05	1.57	0.0084
2010107G23-Rik	30.91	20.29	1.52	0.0017
Serpina6	381.90	251.75	1.52	6E-05
Crp	23.87	15.79	1.51	0.0158
Neurog3	60.02	39.99	1.50	0.0027

Table 14: Upregulated mRNA in E13.5 *Bicc1* KO pancreas using DESeq

Gene Symbol	WT mean (rpkm)	KO mean (rpkm)	Fold change	p value
Mcpt4	0.01	0.26	25.51	4E-07

Mcpt2	0.01	0.30	20.78	1.7E-07
Six2	0.21	3.00	14.32	7.7E-34
Gm10055	0.00	0.04	14.27	0.01173
Myod1	0.10	0.70	7.23	4.3E-10
Nkx2.5	0.07	0.50	7.02	2.1E-07
Cma1	0.39	2.45	6.28	2E-12
Gm12733	0.07	0.42	6.25	0.0039
Tpsab1	0.02	0.09	5.19	0.0121
Fam162b	0.22	1.08	4.82	0.0001
Gm2214	0.16	0.70	4.49	0.0405
Gm12798	0.15	0.68	4.44	0.0060
Myh3	0.05	0.19	3.97	9E-05
Myog	0.23	0.91	3.94	9.6E-05
RP23-281E24.2	0.49	1.88	3.81	3.2E-10
Trhde	0.02	0.08	3.43	0.0026
3110047P20Rik	0.30	1.01	3.32	2.1E-07
Rpl9-ps3	0.21	0.68	3.27	0.04387
Hdc	0.11	0.34	3.25	4.2E-05
3110047P20Rik	0.35	1.10	3.17	7E-08
Rpl21-ps5	0.42	1.34	3.17	0.0243
Actc1	0.60	1.90	3.15	5E-05
Hoxa6	0.18	0.56	3.02	0.0183
Tnfrsf9	0.10	0.28	2.94	0.0176
Robo2	2.59	7.11	2.75	4.1E-12
Lor	0.16	0.44	2.72	0.0366
Hecw1	0.17	0.46	2.67	0.0004
Kazald1	1.99	5.13	2.57	2.5E-05
Cpa3	1.15	2.95	2.57	0.0002
Gm13239	0.46	1.14	2.47	0.0215
Frzb	0.83	2.04	2.45	0.0003
Itga8	3.86	9.44	2.44	7.7E-13
Bai2	0.23	0.55	2.40	0.0033
Gm13155	0.52	1.26	2.40	0.0274
Gm8178	0.52	1.26	2.40	0.0274
CT030724.1	31.93	74.96	2.35	5.9E-07
Frmpd4	0.11	0.25	2.34	0.0057
Nkx3-2	0.98	2.29	2.33	0.0041
Mme	0.88	2.01	2.27	0.0002
Oit3	0.42	0.94	2.27	0.0276
Gm10169	20.41	45.49	2.23	4.7E-05
Slc16a3	0.91	2.03	2.23	0.0002
Kcne3	0.94	2.08	2.22	0.0354
E030013I19Rik	0.47	1.04	2.22	0.0215

Hoxa7	0.97	2.13	2.20	0.0023
Fibin	1.44	3.11	2.16	0.0020
Cyp26b1	1.57	3.36	2.13	0.0001
CT025683.1	82.47	172.63	2.09	2.1E-07
Htr7	0.77	1.60	2.09	0.0056
Barx1	1.78	3.69	2.08	0.0192
Gm13611	20.56	42.77	2.08	0.0003
Rpl36-ps3	7.61	15.71	2.06	0.0215
RP23-52O21.2	10.36	21.00	2.03	0.0112
Fabp4	8.56	17.21	2.01	0.0025
Pfkl	3.54	7.11	2.01	1.4E-05
Gm16379	14.70	29.13	1.98	0.00155
Ltbp4	2.43	4.80	1.98	3.3E-05
AL928940.2	34.51	68.10	1.97	0.0145
Rps8-ps1	8.61	16.88	1.96	0.0061
Tlx1	2.43	4.75	1.95	0.0139
Arhgef4	0.47	0.90	1.92	0.0430
Tnc	0.81	1.54	1.90	0.0032
Hoxb8	1.67	3.15	1.89	0.0183
Xist	1.69	3.20	1.89	0.0002
Rusc2	0.57	1.07	1.87	0.0221
Gm5121	14.12	26.35	1.87	0.0062
Chpf	3.32	6.18	1.86	0.0013
Emilin1	10.41	19.28	1.85	4E-06
Gm14303	70.11	127.09	1.81	0.0067
Slc40a1	19.97	35.86	1.80	9.5E-06
Ntm	20.34	35.74	1.76	0.0009
BC005764	2.82	4.81	1.70	0.0417
Rpl35	45.33	75.95	1.68	0.0009
Lrp1	3.44	5.75	1.67	0.0001
Gm12481	47.77	79.77	1.67	0.0154
Ptms	19.88	33.09	1.66	0.0060
Gadl1	12.82	21.11	1.65	0.0020
Igfbp2	16.30	26.70	1.64	0.0048
Fzr1	3.69	6.00	1.63	0.0304
Stard9	0.56	0.91	1.63	0.0304
Dchs1	9.55	15.36	1.61	0.0003
Hspg2	3.29	5.25	1.60	0.0032
Mbd3	17.96	28.55	1.59	0.0159
Ftl1	366.04	580.07	1.58	0.0005
Btbd2	6.14	9.66	1.57	0.0448
Gm11539	64.93	102.05	1.57	0.0241
Slc2a1	10.71	16.82	1.57	0.0241

Gm10736	297.16	465.70	1.57	0.0080
Ak4	5.12	7.94	1.55	0.0241
Tcf21	16.30	25.15	1.54	0.0435
Kcnj8	16.16	24.92	1.54	0.0174
Ptov1	8.15	12.56	1.54	0.0353
Rpl28-ps3	117.87	181.03	1.54	0.0179
Rpl8	106.07	162.57	1.53	0.0122
Gm10116	241.13	368.70	1.53	0.0043
Pkd1	16.29	24.80	1.52	0.0279
Gm15501	81.93	124.63	1.52	0.0304
Gsn	16.67	25.27	1.52	0.0255
Eno1	60.54	91.66	1.51	0.0016
Gm13699	309.53	467.28	1.51	0.0024
Kif26b	4.65	7.01	1.51	0.0327
Gm15590	512.61	771.19	1.50	0.0074
Aldoa	84.25	126.18	1.50	0.0040
Bat2	303.27	453.77	1.50	0.0121

10.2 Articles

10.2.1 Dual lineage-specific expression of Sox17 during mouse embryogenesis.

Authors: Eunyoung Choi; Marine R Kraus; Laurence A Lemaire; Momoko Yoshimoto; Sasidhar Vemula; Leah A Potter; Elisabetta Manduchi; Christian J Stoeckert; Anne Grapin-Botton; Mark A Magnuson

Contribution: I have performed the characterization of the Sox17 ^{CreGFP} mouse line (Supplemental Figure 2). Sox17 ^{CreGFP} mice were crossed with Rosa26 ^{LacZ} reporter mice. The embryos were collected at E12.5. LacZ staining was performed as described in the material and method on sections. The sections were counterstained with eosin.

STEM CELLS®

TISSUE-SPECIFIC STEM CELLS

Dual Lineage-specific Expression of Sox17 During Mouse Embryogenesis

Eunyoung Choi[1], Marine R-C. Kraus[2], Laurence A. Lemaire[2,3], Momoko Yoshimoto[4], Sasidhar Vemula[4], Leah A. Potter[1], Elisabetta Manduchi[5], Christian J. Stoeckert Jr.[5], Anne Grapin-Botton[2,3], Mark A. Magnuson[1,*]

[1]Center for Stem Cell Biology and Department of Molecular Physiology and Biophysics, Vanderbilt University, Nashville, TN; [2]Swiss Institute for Experimental Cancer Research, School of Life Sciences, Ecole Polytechnique Fédérale de Lausanne, Lausanne, Switzerland; [3]DanStem, University of Copenhagen, 3B Blegdamsvej, DK-2200 Copenhagen N, Denmark; [4]Department of Pediatrics, Wells Center for Pediatric Research, Indiana University School of Medicine, Indianapolis, IN; [5]Penn Center for Bioinformatics and Department of Genetics, University of Pennsylvania School of Medicine, Philadelphia, PA

Key words. Endoderm • mesoderm • Ventral pancreas • Hemogenic endothelium • Sox17

ABSTRACT

Sox17 is essential for both endoderm development and fetal hematopoietic stem cell (HSC) maintenance. While endoderm-derived organs are well known to originate from Sox17-expressing cells it is less certain whether fetal HSCs also originate from Sox17-expressing cells. By generating a *Sox17*^{GFPCre} allele and using it to assess the fate of Sox17-expressing cells during embryogenesis we confirmed that both endodermal and a part of definitive hematopoietic cells are derived from Sox17-positive cells. Prior to E9.5 the expression of Sox17 is restricted to the endoderm lineage. However, at E9.5 Sox17 is expressed in the endothelial cells (ECs) at the para-aortic splanchnopleural (P-Sp) region that contribute to the formation of HSCs at a later stage. The identification of two distinct progenitor cell populations that express Sox17 at E9.5 was confirmed using FACS together with RNA-Seq to determine the gene expression profiles of the two cell populations. Interestingly, this analysis revealed differences in the RNA processing of the *Sox17* mRNA during embryogenesis. Taken together, these results indicate that Sox17 is expressed in progenitor cells derived from two different germ layers, further demonstrating the complex expression pattern of this gene and suggesting caution when using Sox17 as a lineage-specific marker.

INTRODUCTION

Sox17, a member of the Sry-related high mobility group box (Sox) transcription factors, plays an essential role in the differentiation of many types cells [1-4]. During mouse embryogenesis, Sox17 is first detected in extraembryonic visceral endoderm at embryonic

Author contributions: E.C.: conception and design, collection and assembly of data, data analysis and interpretation, manuscript writing; M.R-C.K.,L.A.L., M.Y. and S.V.: collection and assembly of data; L.A.P.: data analysis and manuscript writing; E.M. and C.J.S.: data analysis and interpretation, manuscript evaluation; A.G-B.: provision of study material, financial support, manuscript evaluation; M.A.M: conception and design, data analysis, financial support, manuscript writing, final approval of manuscript.

*Corresponding author: 9465 MRB-IV, 2213 Garland Avenue, Vanderbilt University School of Medicine, Nashville, TN 37232-0494, Tel: 615.322.7006, Fax: 615.332.6645, Email: mark.magnuson@vanderbilt.edu; These studies were supported by NIH grants DK72473 and DK89523 to MAM and DK072495 to AGB; CA68485 and DK58404 to the Vanderbilt Flow Cytometry Shared Resource; CA68485 and DK20593 to the Vanderbilt Transgenic Mouse/ES Cell Shared Resource; and CA68485 to the Vanderbilt Genome Sciences Resource.; Received March 13, 2012; accepted for publication July 17, 2012; available online without subscription through the open access option. 1066-5099/2012/$30.00/0 doi: 10.1002/stem.1192

This article has been accepted for publication and undergone full peer review but has not been through the copyediting, typesetting, pagination and proofreading process which may lead to differences between this version and the Version of Record. Please cite this article as doi: 10.1002/stem.1192

day (E) 6.0 and in the endoderm of mid- to late-gastrula stage embryos (e.g. around E7.5) where it plays an essential role in organ formation [5]. Epithelial cells of the gut tube endoderm maintain Sox17 expression until approximately E8.5 as they undergo specification into distinct endoderm-derived organs [5-8]. Expression of Sox17 in endoderm, albeit transient, has led to this gene being widely used as a marker for definitive endoderm in studies using embryonic stem (ES) cells [9-12].

Within the developing endoderm, Sox17 is critical for specifying pancreatic progenitors in the ventral foregut endoderm. Mice that are globally deficient in *Sox17* fail to undergo axis rotation at E8.5 and exhibit a severe defect of the posterior region of the embryo [5, 13]. Moreover, while *Sox17*-null embryos express Hnf3a/b and other endoderm derived organ-specific markers such as Hhex and Cdx2, they do not express Pdx1, an essential factor for pancreatic outgrowth and development [5, 14]. Interestingly, Sox17 is expressed in a ventral foregut endoderm region from which the ventral pancreas and extrahepatobiliary ducts emerge where it appears to be essential for the segregation between liver and pancreatibiliary systems [15].

Sox17 also plays a crucial role in the maintenance of fetal and neonatal hematopoietic stem cell (HSC) identity [13, 16]. During vascular system development, *Sox17* expression begins at approximately E8.5 [17]. However, the precise time at which *Sox17* is expressed during embryonic hematopoiesis has not been as thoroughly investigated [18]. During embryogenesis, HSCs originate from the hemogenic endothelial cells (ECs) located on the aortic floor at E10.5, and migrate to the liver to expand in number [19-24]. Utilizing Tie2-Cre to conditionally eliminate *Sox17* expression, Kim et al. investigated the role of Sox17 in HSC development post-migration and found a marked impairment in the number of HSCs in the liver at E11.5 [13]. A role for Sox17 in fetal HSC maintenance was further supported by He et al. who reported that the transient expression of Sox17 in adult bone marrow (BM) caused adult hematopoietic cells to adopt characteristics of fetal HSCs [16]. However, while both of these studies demonstrated the importance of Sox17 in the maintenance of the fetal HSCs, neither explored whether Sox17- expressing ECs can give rise to hematopoietic cells or not.

In this study, we generated mice with a $Sox17^{GFPCre}$ allele and used it to identify Sox17-expressing cells and their progeny. At E9.5, we identified two distinct progenitor populations of Sox17-expressing cells, both an endoderm-derived ventral pancreatic epithelial cell population and a mesoderm-derived endothelial cell population that has hemogenic potential. Furthermore, we show that the two populations exhibit distinct gene expression signatures as assessed by whole transcriptome profiling.

MATERIALS AND METHODS

Gene targeting and RMCE. Mice containing a $Sox17^{GFPCre}$ allele were derived using both gene targeting and recombinase-mediated cassette exchange (RMCE). First, a *Sox17* loxed cassette acceptor (LCA) allele was made by gene targeting. The targeting vector made by BAC recombineering replaced a 3.793 kb region of the gene containing exons 3-5 with a *puromycin resistance-Δthymidine kinase* (*puΔTK*) fusion gene driven by the mouse *phosphoglycerol kinase* (*PGK*) promoter and a *kanamycin resistance* gene driven by the bacterial EM7 promoter. The selection cassettes were flanked by tandemly-oriented lox71 and lox2272 sites, two homology arms, and a *PGK-diphtheria toxin A* (*DT-A*) cassette for negative selection. After linearization using NotI, a 129S6-derived mouse ES cell line was electroporated with the targeting vector, and puromycin-resistant clones were isolated. Homologous recombination was verified by Southern hybridization with 5' and 3' probes following digestion with either SphI or SpeI. Second, an exchange cassette flanked by tandem lox66 and lox2272 sites was made with an enhanced green fluorescent protein (GFP) and

Cre fusion gene in place of the coding sequences of *Sox17* and replace the selectable markers in the $Sox17^{LCA}$ allele. In addition, the vector contained a *PGK-hygromycin resistance* ($Hygro^{R}$) cassette flanked by tandem flippase recognition target (FRT) sites. Following co-electroporation of the exchange vector and a Cre-expression plasmid, positively exchanged clones were identified by a staggered positive-negative selection strategy using both hygromycin and gancyclovir [25]. To identify correctly exchanged clones, PCR was performed using the following primers: 5'-ACAGTCTTACACGCTACGGAT and 5'-CAAGACCTCTTGGGGAAATAG on the 5' end (a); 5'-CAGAGGTATGCAGATCTCTGT and 5'-CATTCTGGTCAACATGTAAGGT on the 3' end (b).

Mouse strains. Chimeric mice containing the $Sox17^{GFPCre}$ allele were derived by the microinjection of clone 1G3:1C10 ES cells into blastocysts of C57BL/6J mice. After germline transmission, the $Hygro^{R}$ cassette was removed by cross breeding with *ACTB:FLPe* mice [26]. The $Sox17^{GFPCre}$ allele was maintained within a CD1 background for experiments. Mice with the $R26R^{eYFP}$ and $R26R^{LacZ}$ (*Rosa26:LacZ* (*Gt(ROSA)26Sor*^{tm1Sor})) alleles were previously described [27]. Embryos were considered to be E0.5 at noon on the day a vaginal plug was detected. All experimental protocols were approved by the Vanderbilt Institutional Animal Care and Use Committee.

Immunohistochemistry. Five micron frozen sections were preincubated with 5% normal donkey serum (NDS) for 30 mins at room temperature, incubated with primary antibodies at 4°C overnight, and washed in phosphate buffered saline (PBS) with 0.1% Tween 20. Secondary antibodies were incubated at room temperature for 1 hour then washed in PBS containing 0.1% Tween 20. All antibodies were diluted in PBS containing 5% NDS and 0.1% Tween 20. The sources of the antibodies used are listed in Table S3. Images were acquired using either a Zeiss LSM510 or LSM710 inverted confocal microscope at the Vanderbilt Cell Imaging Shared Resource.

ß-D-Galactosidase staining. $Sox17^{GFPCre/+}$;$R26R^{LacZ/+}$ embryos were harvested at E7.5, E9.5, or E12.5 and fixed at room temperature for 10 mins in 4% paraformaldehyde. 5-bromo-4-chloro-3-indolyl β-D-Galactosidase staining was performed on 10 µm-thick serial transversal sections for 4 hours at 37°C (Thompson et al., 2012). Images were acquired with a Leica DM5500B microscope equipped with a DFC 320 color camera.

FACS analysis. $Sox17^{GFPCre/+}$ embryos were identified by direct fluorescence using a Leica MZ 16 FA stereoscope. The pooled embryos, containing five to seven embryos, were dissociated with AccuMax (Sigma) and 5 µg/ml DNase I (Sigma) and passed through a 35 µm mesh filter into FACS tubes (BD). After centrifugation, the cells were resuspended with FACS staining buffer (R&D Systems), blocked using 1 µg/ml of mouse IgG at room temperature for 15 min, then immunolabeled with PE conjugated-EpCAM (G8.8) antibody (Santa Cruz) at room temperature for 30 mins. The cells were washed three times in FACS staining buffer, centrifuged, and resuspended with FACS staining buffer with 10mM HEPES, 1mg/ml BSA and 1% penicillin/streptomycin. 7-aminoactinomycin D (7-AAD, Molecular Probes) was added at a dilution of 1:1000 to assess cell viability, and cells were analyzed using an LSRII (BD Biosciences). To isolate the Sox17-expressing cell populations, the midgut regions from 26 to 29 $Sox17^{GFPCre/+}$ embryos at E9.5 were dissected (Fig. S5C) and pooled prior to cellular dissociation. Samples were prepared as described above, and cells were isolated using either an Aria II or III (BD Biosciences).

Fetal liver cells were obtained from dissected E12.5 embryo livers then dissociated into a single cell suspension using a 200 µl large orifice tip pipette. Bone marrow was collected from the tibias and femurs of 6 week old mice. The cells were flushed using 1X PBS through a 21G

needle more than 10 times then filtered with a 100□µm cell strainer. Red blood cells were lysed using ACK lysis buffer (0.15 M NH_4Cl, 1 mM $KHCO_3$, 0.1 mM Na_2EDTA, pH 7.4, sterilized using 0.2 mm filter). The following antibodies were used for immunolabeling: anti-CD41 (MWReg30), anti-VE-Cad (BV13), anti-CD45 (30-F11), anti-CD19 (1D3), anti-CD11b/Mac1 (M1/70), anti-CD3 (17A2) and anti-Ter119. DAPI (1 µg/ml) was added to assess cell viability.

Hemogenic endothelial cell culture. $GFPCre^+$ or $GFPCre^-$ endothelial cells ($CD45^-Ter119^-CD41^-VE\text{-}cad^+CD31^+$ cells) from the YS and P-Sp region of E9.5 *Sox17*$^{GFPCre/+}$ embryos were sorted and 3,000 cells were plated onto an OP9 stromal cell layer in 6 well plates with SCF (10 ng/ml), Flit3-ligand (10 ng/ml), IL3 (10 ng/ml), IL7 (10 ng/ml), and TPO (10 ng/ml). Endothelial cells from wild-type YS and P-Sp were also plated as a positive control. Floating cells in the co-culture were collected every 3-4 days and analyzed by flow cytometry using anti-TER119 and Mac1 antibodies.

Total RNA isolation, amplification, library construction, RNA-Seq and analysis. Total RNA was isolated using TRIzol LS (Invitrogen) containing 40 µg/ml mussel glycogen (Sigma). Following treatment with DNase (Ambion), total RNA was column-purified using a DNA-Free RNA kit (Zymo Research). RNA integrity was assessed using an Agilent 2100 Bioanalyzer (Agilent Technologies, CA), and RNAs with an RNA Integrity Number (RIN) > 7.0 were processed for RNA-Seq. Total RNA (10 ng) was amplified using the Ovation RNA-Seq system (NuGen, CA), and amplified cDNA (750 ng) was sheared using Covaris S2 system (Covaris, MA) and used to construct the cDNA library using the Illumina TruSeq DNA prep kit (Illumina, CA). The libraries were used to generate ≥110 base reads as single-end tags using an Illumina HiSeq 2000, and the HiSeq Control Software (HCS 1.4.8/RTA 1.12) was used for image analysis. Reads were mapped to mm9 genome with RNA-Seq unified mapper (RUM, v1.09, http://www.cbil.upenn.edu/RUM/) [28]. Expression was quantified as reads per kilobase of exon model per million mapped reads (RPKM). A summary of the mapped reads is in Table S4, and confidence values were determined by PaGE (http://www.cbil.upenn.edu/PaGE/) [29]. Differentially expressed genes were selected as those displaying at least a 4-fold change in RPKM, ≥ 4 RPKM in one sample, and ≥ 80% confidence value, and these genes were clustered using Cluster program [30]. Gene Ontology analysis was performed using PANTHER (v7.0) [31].

Meta-data and processed data for the RNA-Seq are available at http://genomics.betacell.org. The RNA-Seq data has been deposited at ArrayExpress (accession number E-MTAB-970) and the Sequence Read Archive (accession number ERP001235).

Semiquantitative RT-PCR. RT-PCR was performed using 50 ng of amplified cDNA template used for RNA-Seq. *Sox17* transcript variants were detected using the following primers: 5' -GGATACGCCAGTGACGACCA with 5' -CGTTCGTCTTTGGCCCACAC (a) or 5' -TCATGCGCTTCACCTGCTTG (b); 5'-ATGGCCCACTCACACTGCTG with 5' -ATGTAGCTCTCCTGCCTCTC (c) or 5' -CGTTCGTCTTTGGCCCACAC (d).

RESULTS

Derivation of mice with a *Sox17*^{GFPCre} allele

To explore the stage-specific expression and lineage of Sox17-expressing cells, we derived mice that express a GFPCre fusion protein under control of the endogenous *Sox17* gene locus through gene targeting and recombinase-mediated cassette exchange (RMCE) [32] (Fig. 1A). First, we performed gene targeting to generate mouse ES cells containing a *Sox17*^{LCA} allele. Two of 84 mouse ES cell clones that survived puromycin selection were correctly targeted as confirmed by Southern hybridization (Fig. 1B). Second, we generated an exchange

cassette that replaced coding sequences in the *Sox17* gene with a GFPCre fusion protein. Following RMCE into the $Sox17^{LCA}$ allele, the exchange was confirmed using PCR across both the lox66/71 and lox2272 sites, and one clone (1G3:1C10) was used to generate mice containing the $Sox17^{GFPCre\ (+HygroR)}$ allele (Fig. 1C). After germline transmission, mice containing the $Sox17^{GFPCre(+HygroR)}$ allele were bred with FLPe-expressing mice to delete the FRT-flanked hygromycin resistance cassette, thereby establishing the $Sox17^{GFPCre}$ line.

To determine whether expression of the $Sox17^{GFPCre}$ reporter allele faithfully recapitulates that of the wild type *Sox17* allele, we first performed whole mount fluorescence microscopy of $Sox17^{GFPCre/+}$ mouse embryos. In agreement with previous reports [5, 15], we observed fluorescence in the extra-embryonic region beginning at E6.5 (Fig. 2A-a,b) and in the intra-embryonic region beginning at E7.5 (Fig. 2A-c,d). A three-dimensional reconstruction of E7.5 embryo images revealed that GFPCre-expressing cells were highly abundant and clustered together in the definitive endoderm rather than the visceral endoderm (Fig. S1). At E8.5, between the fourth and ninth somite (S) stage, fluorescence was localized to the foregut endoderm (Fig. 2A-e,f), and histological analysis revealed co-expression with Sox17 (Fig. 2B-a). At E9.5 (> 20S), fluorescence throughout the endoderm was greatly diminished, but localized expression was evident in the ventral pancreas region (Fig. 2A-g,h and 2B-b) At E9.5, we also observed cells expressing both GFPCre and Sox17 in the dorsal aorta (Fig. 2B-c). This finding indicates that Sox17 is not only expressed in the ventral pancreatic epithelium at E9.5 but is also present in cells in the dorsal aorta.

Two types of $Sox17^{GFPCre}$-expressing cells during organogenesis in the mouse embryo

At E9.5, Sox17 was detected primarily in the ventral pancreatic epithelium but not in the liver epithelium (Fig. 3A). GFPCre was strongly expressed in the tip area of the ventral pancreatic epithelium (Fig. 3A, left arrow) and at a lower level in the Pdx1-high area of ventral pancreatic epithelium (Fig. 3A, right arrow) [15]. Several GFPCre-expressing cells were also located in the region of the liver epithelium; however, they were not co-localized with the liver marker Hnf4a, indicating that these GFPCre-expressing cells were separate but intermingled with the developing liver epithelium at this stage (Fig. 3A). We also observed GFPCre-expressing cells localized within the dorsal aorta (Fig. 3B [17]) and in the vicinity of the neural tube area (Fig. 3C). While these GFPCre-expressing cells were not co-localized with Sox2, an ectoderm marker, Foxa2, a floor plate marker, or Sox10, a marker of neural crest cells, they were co-localized with PECAM, an endothelial cell marker (Fig. 3E, arrow [17]). Conversely, the GFPCre-expressing cells in the ventral pancreatobiliary epithelium co-localized with epithelial cell adhesion molecule (EpCAM), an epithelial cell marker (Fig. 3D, arrow). These data indicate that Sox17 is expressed in two distinct progenitor cell populations at E9.5: 1) an epithelial cell population found in the ventral foregut epithelium that gives rise to the ventral pancreas, extrahepatic ducts and gall bladder and 2) an endothelial cell population found in the P-Sp area, which includes the dorsal aorta.

Two distinct cell populations expressing Sox17 are alternatively derived from two different origins

To trace the lineage of Sox17-expressing cells the $Sox17^{GFPCre}$ mice were crossed with either a $Gt(ROSA)26Sor^{tm1Sor}$ $(R26R^{LacZ})$ or *ROSA26-eYFP* $(R26R^{eYFP})$ cre-reporter line [27, 33] and the locations of either LacZ or YFP, repectively, were determined (Fig. 4 and S2). Consistent with previous studies, LacZ was detected as early as E7.5 in extraembryonic and embryonic visceral endoderm, as well as the definitive endoderm where it was detected primarily in the proximal endoderm (data not shown) [34]. Previous studies have also shown that Sox17 plays a key role in determining endoderm and pancreas fates [5, 35]. Consistent with this [15, 34, 36], we found that at E9.5 all endoderm-derived

epithelial cells, from the branchial arch endoderm to the hindgut, were derived from cells that once expressed Sox17 (Fig. S2A-D). At E9.5, YFP was co-expressed with EpCAM or Foxa2 within the gut endoderm and the pancreatic epithelium (Figs. 4A and S3A). At E12.5, we confirmed that endoderm-derived organs, including the thyroid, thymus, parathyroid, esophagus, trachea, lungs, stomach, liver epithelium and endothelium (but not blood cells), dorsal and ventral pancreas, small intestine, cecum, and large intestine were labeled by LacZ (Fig. S2 E-G). We also observed YFP labeling in Ptf1a-expressing pancreatic multipotent progenitor cells (MPCs) at E11.5. Additionally, as observed at E15.5, acinar, ductal, endocrine progenitor, and insulin-expressing cells were derived from a Sox17-expressing lineage (Fig. S3B).

In addition to contributing to endoderm-derived lineages, we observed YFP-expressing cells in the endothelia, such as dorsal aorta and veins at E9.5 (Fig. 4B and S4A). An analysis of YFP-positive cells in the heart, which is comprised of both endothelial cells and mesenchymal cells, showed that YFP was selectively observed in the PECAM-positive endothelial cells (Fig. 4C, arrow) but not in the VCAM-positive cardiac myocytes, representing cells of the mesenchymal lineage [37] (Fig. 4C, arrowheads). These findings indicate that Sox17 is not expressed in mesoderm progenitor cells that gives rise to both heart endothelium and mesenchyme [38], but is expressed after the mesoderm is specified into either the mesenchymal or endothelial lineage.

Sox17 is expressed in hemogenic endothelial cells at E9.5

While it has been previously shown that Sox17 has a role in the maintenance of fetal and neonatal HSCs [13], it is not clear from these studies whether Sox17 is expressed in the hemogenic ECs in the YS and in the P-Sp region. Given that Sox17 was detected in the ECs of P-Sp region, we sought to determine whether the Sox17-expressing cells were hematopoietic in nature. At E9.5, many GFPCre-expressing cells along the aortic wall co-expressed c-Kit (Fig. 5A, arrows). However, GFP was not co-localized in $CD41^+$c-Kit^+ HPCs [39] (Fig. 5A, arrowheads), indicating that Sox17 expression occurs only in the endothelial stage and is not sustained as the cells differentiate into HPCs. In contrast, some Sox17-derived cells, as indicated by YFP expression, were detected in $CD41^+$c-Kit^+ HPCs (Fig. 5B, arrowheads), indicating that $CD41^+$c-Kit^+ HPCs were derived from Sox17 expressing cells. Consistent with this, a few $CD41^+$c-Kit^+ cells (~1%) were produced when $GFPCre^+$ EC cells were cultured on OP9 cells (data not shown). To determine whether Sox17-expressing ECs have hemogenic potential we sorted $GFPCre^+$ EC cells ($CD45^-CD41^-Ter119^-CD31^+$ or $VEcad^+$ cells), which accounted for around 40-50% of the EC cells, from E9.5 YS and P-Sp and plated them on an OP9 stromal cell layer along with stimulatory cytokines. After 8 days of co-culture, large cobblestone-appearing areas were observed that were proven to be $Ter119^+$ or $Mac1^+$ erythro-myeloid colonies by FACS (Fig. 5C). Of note, $GFPCre^-$ EC also produced erythro-myeloid cells in the OP9 co-culture (data not shown). Taken together, these data indicates that Sox17 is expressed in the hemogenic ECs.

Use of Sox17 lineage tracing to show the development of definitive hematopoiesis *in vivo*

We next sought to determine how many hematopoietic cells are derived from Sox17-expressing cells *in vivo*. To do so, we determined the number of Sox17-lineaged cells in E9.5 embryos, E12.0 fetal liver (FL) and in adult bone marrow (BM) (Fig. 5D). While only 25.1 ± 12.3% of $CD41^+$ cells, 9.5±2% of $Ter119^+$ cells, and 21.4±11.1% of $Mac1^+$ cells were YFP^+ in the E9.5 embryos (Fig. 5D upper panel), the number of YFP^+ cells was dramatically increased in the E12.5 FL. Indeed, up to 81.9 ± 2.2 of the $CD41^+$ cells, 39.5 ± 5.5% of the $Ter119^+$ cells and 81.6 ± 4.1% the $Mac1^+$ cells were lineage-labeled (Fig. 5D middle panel). Furthermore, YFP^+ cells were also detected among $CD19^+$ cells (55.8% ± 10.4%) and $CD3^+$ cells (58.9 ±

1.1%), representing lymphocytes. YFP^+ cells were also detected in the VE-cad^+ cells (81.9 ± 2.2%). These results suggest that Sox17 is expressed in VE-cad^+ endothelial cells and is linked to the production of definitive hematopoietic cells, perhaps through hemogenic ECs, based on the previous reports [40-42]. In adult BM, all $CD45^+$ hematopoietic cells were YFP^+, clearly demonstrating that all the blood cells in the adult BM are derived from Sox17-expressing cells. This is consistent with the previous report that HSCs in the FL express Sox17 [13], and that FL HSCs migrate into the BM and support hematopoiesis, as is commonly considered. However, the low percentage of YFP^+ cells among $Ter119^+$ cells were detected in adult BM, likewise in E12.5 FL. Since definitive erythroid cells are enucleated, these cells may lose the expression of YFP as they mature. Also, about 17% of the $CD3^+$ cells were YFP^-. While this may suggest that T cell lymphopoiesis occurs in $Sox17^-$ hemogenic EC cells in the YS and P-Sp before emergence of HSCs [42], this finding could also be due to a low amount of GFPCre in the hemogenic ECs resulting in only partial recombination of the $R26R^{eYFP}$ reporter allele. In either case, Sox17 marks a part of hemogenic ECs and Sox17 lineage tracing shows the progression of definitive hematopoiesis in the embryo.

Sox17-expressing endothelial and epithelial cells exhibit transcriptional differences in distinct protein classes

To further demonstrate differences in the two Sox17-expressing populations, we isolated both cell populations using fluorescence-activated cells sorting (FACS) and performed whole transcriptome sequencing (RNA-Seq). Using E9.5 $Sox17^{GFPCre/+}$ mouse embryos, the epithelial and endothelial cells were separated based on expression of EpCAM, an epithelial cell marker (Fig. S5A). From whole embryos, we obtained less than one percent GFPCre-expressing cells (Fig. S5A) of which only 7.0% ± 3.2% were Sox17-expressing epithelial cells based on the expression of both GFP and EpCAM (Fig. S5B). Since endodermal expression becomes restricted to the ventral posterior foregut at E9.5, we dissected the mid region of the embryo to increase the yield of Sox17-expressing cells (Figs. S5C and 6A). Even so, the total number of cells was low, thereby requiring RNA amplification prior to sequencing. As summarized in Table S1, 62.5% - 75.6% of the RNA-Seq reads obtained were aligned to the mouse genome (mm9) [28]. Each profile from three biological replicates showed high reproducibility (Table S2). Interestingly, the profiles between $EpCAM^+$ and $EpCAM^-$ Sox17-expressing cells were also highly correlated, simply implying that the global gene expression profiles for the two populations are similar.

To identify differentially expressed transcripts within the two populations, we examined the transcriptional levels of 28,683 genes. While the overall gene expression profiles were similar (Table S2), the two populations were distinguished by many differentially-expressed genes with high confidence values (Table S4). To more clearly illustrate the differences we selected 321 genes that displayed a four-fold or greater change in expression (Table S5) and performed a cluster analysis. By doing so, differences between the epithelial and endothelial cells became readily apparent (Fig. 6B). Furthermore, many of the differentially-expressed genes are important for ventral foregut development, hematopoiesis and/or the regulation of cell fate and signal transduction based on their gene ontology annotations in PANTHER [43].

In the transcription factor cluster (PC00218), there were 11 up- and 26 down-regulated genes in Sox17-expressing epithelial cells compared to the endothelial cells (Fig. 6C). The up-regulated transcripts primarily consisted of endoderm and pancreas development-related genes, such as *Onecut1*, *Foxa3*, *Foxa2*, *Hnf1b*, *Sox9*, and *Prox1*. However, other transcription factors, including *Cited1*, *Tcea3*, *ID2*, *Lin28a* and *Aes*, were also highly expressed in the Sox17-expressing epithelial cells. Conversely, most of the down-regulated genes, including *Gata2*,

Ets1, *Elk3*, *Lmo2*, *Kef2c*, *Klf2*, *Sox7*, *Tal1* and *Sox18,* are known to play a role in endothelial and HSC development. In the receptor (PC00197) and cell adhesion molecule (PC00070) clusters, we found 11 up- and 19 down-regulated genes in Sox17-expressing epithelial cells as compared to the endothelial cells (Fig. 6C). *Tacstd1* (*EpCAM*), which was used to isolate the two Sox17-expressing cell populations, was one of the most abundant genes in epithelial cells, and several epithelial cell-related genes, such as *Cdh1*, *Tmprss2*, *Emb* and *Bcam,* were also abundant. *Paqr9*, a member of the progestin and adipoQ receptor family, and *Dlk1*, a member of the EGF-like family, were also highly expressed; however, their role in pancreas development has not been elucidated. Conversely, in the Sox17-expressing endothelial cells, many genes important for endothelial cell development or hematopoiesis, such as *Kdr*, *Eltd1*, *Eng*, *Cd97*, *Cd34*, *Esam*, *Nid1*, were highly expressed. In the signaling molecule cluster (PC00207), we found 13 up- and 13 down-regulated genes in Sox17-expressing epithelial cells as compared to the endothelial cells (Fig. 6C). In agreement with studies highlighting the roles of Wnt and TGFβ signaling in pancreas development [44-45], we found that Wnt signaling-related genes, *Fzd7* and *Sfrp5*, and TGFβ signaling-related genes, such as *Npnt* and *Bmp7*, were abundant in epithelial cells. Similarly, *Habp2*, a hepatocyte growth factor activator-like protein and endoderm-enriched gene, and *Sdc4*, which is involved in organogenesis of the kidney, were highly expressed.These data not only confirm the existence of two distinct Sox17-expressing progenitor populations at E9.5, but they also reveal numerous transcription factors and cell surface molecules that may be useful for distinguishing the two populations.

Alternative splicing variant of *Sox17* gene is expressed in two populations

Previously, tissue-specific splicing variants of *Sox17* were identified in mouse adult testis and lung [46], and the presence of alternative transcription start sites has been suggested during embryonic development [34, 36]. An analysis of the RNA-Seq reads mapped to the *Sox17* locus revealed differences in exon abundance (Fig. S6). Thus, to further explore whether the Sox17-expressing epithelial and endothelial cells express unique *Sox17* mRNA transcripts (Fig. 7A), we performed exon-specific RT-PCR (Fig. 7B). We found that the fourth and fifth exons, which contain the coding sequences, were amplified from cDNA from both Sox17-expressing epithelial and endothelial cells (Fig. 7B-a,b). However, sequences in exons one, two and three were amplified only in the Sox17-expressing endothelial cDNA (Fig. 7B-c,d). This data indicates that the *Sox17* pre-mRNA is alternatively processed in the two different cell types.

DISCUSSION

Our study indicates the existence of two distinct Sox17-expressing cell lineages in the P-Sp region of the mouse at E9.5. The first population of Sox17-expressing cells, DE (Fig. 2), goes on to form endoderm-derived organs, such as lung, stomach, pancreas, liver, and intestine. The second population is mesoderm-derived endothelium, which go on to contribute to the derivation of HPC. While the expression of Sox17 in the ECs and fetal HSCs has been previously reported using reporter mouse lines [13, 34, 47], it has not been clear when Sox17-expressing ECs and fetal HSCs begin to emerge.

Most mature blood cells at E9.5 are considered to be primitive erythro-myeloid cells derived directly from mesoderm, not ECs [48-49]. Thus, the YFP^+ hematopoietic cells detected in this study may reflect definitive hematopoiesis from hemogenic ECs, although there is a possibility that primitive hematopoietic cells are derived from $Sox17^-$ hemogenic ECs. At E12.5, when definitive hematopoiesis is increased, YFP^+ cells were not only detected in erythro-myeloid cells, but also in both $CD19^+$ and $CD3^+$ cells. This indicates that Sox17 also gives rise to lymphocyte cells. However, the fact that half of the $CD19^+$ and $CD3^+$ cells were YFP^- in the

lineage tracing experiment suggest the need for further, even more detailed studies of the biological potential of Sox17-expressing ECs. Nonetheless, when taken together, our findings indicate that Sox17-expressing ECs have, at a minimum, the potential to form erythro-myeloid cells.

To better understand the characteristics of the two populations, we utilized EpCAM immunolabeling to isolate Sox17-expressing epithelial and endothelial cells from dissected mouse embryos. Using whole transcriptome profiling, we determined that the gene signatures for the epithelial and endothelial cells exhibit specific differences and that the *Sox17* mRNA in these two populations is alternatively processed (Fig. 7). However, the coding sequences for Sox17 in the two variants are unaffected. While it is well known that alternative splicing occurs in many genes during embryonic development [50] and is an important means of regulating gene expression, it is not known whether the two different *Sox17* mRNAs that distinguish the ventral foregut progenitor and hemogenic endothelial cell populations have any functional significance.

Previous studies have reported the failure of normal gut tube and blood cell formation due to *Sox17*-deficiency [5, 13]. While some endoderm-derived organs such as the liver and thyroid are not dependent on *Sox17* for development, the specification of other organs, such as the pancreas is dependent on *Sox17* [5]. The transcriptome profiling we performed revealed the expression of many different genes, in addition to *Sox17*, known to be involved in endoderm and foregut development in the ventral pancreatobiliary epithelium at E9.5 (Fig. 6C). In endothelial development, previous studies have shown that the vascular system is unaffected in *Sox17*-null embryos at E8.25 [17]; however, at E11.5 there is a significant impairment in the number of HSCs in *Sox17*-null embryos [13].

In our analysis of differentially expressed genes, we found that Sox7 and Sox18, other members of Sox-F family, are more abundant in the Sox17-expressing endothelial cells at E9.5 (Fig. 6C). While these Sox-F members have a redundant role in vascular development [17], it has been suggested that Sox7 and Sox18 have no impact in the generation of HSCs by zebrafish experiments performed with morpholinos to inhibit translation of *Sox7* and *Sox18* [51]. However, little is known about the role of Sox-F family members in HSC generation in mice. Our lineage tracing study shows that Sox17 is expressed in hemogenic ECs that give rise to definitive HPCs. To date, no in-depth studies have been performed to assess the role of the other Sox-F members in intra- or extra-embryonic hematopoiesis. Here, our study reveals that Sox17, one Sox-F member, contributes to embryonic HPC generation.

In spite of the highly similar global expression profiles for the two Sox17-expressing populations, the transcriptional profiles clearly revealed distinct differences as would be expected for two distinct cellular lineages. Many pancreatic and hematopoietic cell-type specific genes distinguish the two populations, suggesting that combinatorial expression of tissue-specific transcription factors is crucial for the fate decision of Sox17-expressing cells. First, numerous pancreas-related genes are highly expressed in Sox17-expressing epithelial cells (Fig. 6C). Specifically, these cells express not only *Onecut1* and *Sox9,* genes important for the continuance of pancreatic progenitor cell fate, but also *Lin28a*, a gene important for cell pluripotency [52-54]. The combinatorial expression of these transcription factors with Sox17 in the epithelial cells may be crucial for the specification of pancreatic progenitor cells. Furthermore, we identified high expression of *Fzd7* (*Frizzled-7*), a Wnt receptor, in the Sox17-expressing epithelial cells. Given that Sox17 regulates transcription of endodermal target genes through the beta-catenin pathway and Wnt/beta-catenin signaling is required for the proliferation of pancreatic progenitor cells [55-

56], Fzd7 may mediate the Wnt/beta-catenin signaling pathway during the pancreas segregation from the gut and biliary system within the Sox17-expressing epithelium. Second, a different set of genes is expressed in the Sox17-expressing endothelial cells. Specifically, we observed the expression of transcription factors such as *Gata2*, *Lmo2*, *Tal1* and *Mef2c*, all of which have roles in both vascular and HSC development [57-60], further supporting our identification of a novel Sox17-expressing hemogenic ECs during embryogenesis. The expression of *CD34* and *Kdr* confirms endothelial phenotype. Indeed, given that multiple markers currently need to be used in combination to identify early HSC populations [61], the *Sox17*^{GFPCre} mice we have derived may be useful in future studies that seek to identify and isolate HSC-producing hemogenic ECs.

In conclusion, our study indicates the existence of two lineage-specific, Sox17-expressing progenitor cell populations during early mouse development. Given that Sox17 is widely used to identify endoderm-like cells during embryonic stem cell directed differentiation, our results suggests that Sox17 is not solely an endoderm-specific marker but that it identifies both ventral pancreatic MPCs and a part of hemogenic ECs at E9.5.

ACKNOWLEDGMENTS

We thank Drs. Stacey S. Huppert and Mervin C. Yoder for critically reviewing the manuscript and other helpful suggestions; Susan B. Hipkens and Rama Gangula for establishing and maintaining the mouse line; Travis Clark for RNA amplification and library construction; Anna Osipovich, Judsen D. Schneider and Anil Laxman for helpful suggestions; the Vanderbilt Transgenic Mouse/Embryonic Stem Cell Shared Resource for performing blastocyst injections; the Vanderbilt Flow Cytometry Shared Resource for assistance with FACS and the Vanderbilt Genome Sciences Resource for performing the RNA-Seq.

Disclosure of Potential Conflicts of Interest
No potential conflicts of interest.

REFERENCES

1. Foster JW, Dominguez-Steglich MA, Guioli S, et al. Campomelic dysplasia and autosomal sex reversal caused by mutations in an SRY-related gene. Nature. 1994;372:525-530.
2. Kamachi Y, Uchikawa M, Collignon J, et al. Involvement of Sox1, 2 and 3 in the early and subsequent molecular events of lens induction. Development. 1998;125:2521-2532.
3. Schilham MW, Oosterwegel MA, Moerer P, et al. Defects in cardiac outflow tract formation and pro-B-lymphocyte expansion in mice lacking Sox-4. Nature. 1996;380:711-714.
4. Pingault V, Bondurand N, Kuhlbrodt K, et al. SOX10 mutations in patients with Waardenburg-Hirschsprung disease. Nat Genet. 1998;18:171-173.
5. Kanai-Azuma M, Kanai Y, Gad JM, et al. Depletion of definitive gut endoderm in Sox17-null mutant mice. Development. 2002;129:2367-2379.
6. Zorn AM, Wells JM. Vertebrate endoderm development and organ formation. Annu Rev Cell Dev Biol. 2009;25:221-251.
7. Beck F, Erler T, Russell A, et al. Expression of Cdx-2 in the mouse embryo and placenta: possible role in patterning of the extra-embryonic membranes. Dev Dyn. 1995;204:219-227.
8. Bogue CW, Ganea GR, Sturm E, et al. Hex expression suggests a role in the development and function of organs derived from foregut endoderm. Dev Dyn. 2000;219:84-89.
9. Peterslund JM, Serup P. Activation of FGFR(IIIc) isoforms promotes activin-induced mesendoderm development in mouse embryonic stem cells and reduces Sox17 coexpression in EpCAM+ cells. Stem Cell Res. 2011;6:262-275.
10. D'Amour KA, Bang AG, Eliazer S, et al. Production of pancreatic hormone-expressing endocrine cells from human embryonic stem cells. Nat Biotechnol. 2006;24:1392-1401.
11. D'Amour KA, Agulnick AD, Eliazer S, et al. Efficient differentiation of human embryonic stem cells to definitive endoderm. Nat Biotechnol. 2005;23:1534-1541.
12. Borowiak M, Maehr R, Chen S, et al. Small molecules efficiently direct endodermal differentiation of mouse

and human embryonic stem cells. Cell Stem Cell. 2009;4:348-358.
13. Kim I, Saunders TL, Morrison SJ. Sox17 dependence distinguishes the transcriptional regulation of fetal from adult hematopoietic stem cells. Cell. 2007;130:470-483.
14. Fujitani Y, Fujitani S, Boyer DF, et al. Targeted deletion of a cis-regulatory region reveals differential gene dosage requirements for Pdx1 in foregut organ differentiation and pancreas formation. Genes Dev. 2006;20:253-266.
15. Spence JR, Lange AW, Lin SC, et al. Sox17 regulates organ lineage segregation of ventral foregut progenitor cells. Dev Cell. 2009;17:62-74.
16. He S, Kim I, Lim MS, et al. Sox17 expression confers self-renewal potential and fetal stem cell characteristics upon adult hematopoietic progenitors. Genes Dev. 2011;25:1613-1627.
17. Sakamoto Y, Hara K, Kanai-Azuma M, et al. Redundant roles of Sox17 and Sox18 in early cardiovascular development of mouse embryos. Biochem Biophys Res Commun. 2007;360:539-544.
18. Jang YY, Sharkis SJ. Fetal to adult stem cell transition: knocking Sox17 off. Cell. 2007;130:403-404.
19. Jaffredo T, Gautier R, Eichmann A, et al. Intraaortic hemopoietic cells are derived from endothelial cells during ontogeny. Development. 1998;125:4575-4583.
20. Zovein AC, Hofmann JJ, Lynch M, et al. Fate tracing reveals the endothelial origin of hematopoietic stem cells. Cell Stem Cell. 2008;3:625-636.
21. Kissa K, Herbomel P. Blood stem cells emerge from aortic endothelium by a novel type of cell transition. Nature. 2010;464:112-115.
22. Bertrand JY, Chi NC, Santoso B, et al. Haematopoietic stem cells derive directly from aortic endothelium during development. Nature. 2010;464:108-111.
23. Boisset JC, van Cappellen W, Andrieu-Soler C, et al. In vivo imaging of haematopoietic cells emerging from the mouse aortic endothelium. Nature. 2010;464:116-120.
24. Mikkola HK, Orkin SH. The journey of developing hematopoietic stem cells. Development. 2006;133:3733-3744.
25. Long Q, Shelton KD, Lindner J, et al. Efficient DNA cassette exchange in mouse embryonic stem cells by staggered positive-negative selection. Genesis. 2004;39:256-262.
26. Rodriguez CI, Buchholz F, Galloway J, et al. High-efficiency deleter mice show that FLPe is an alternative to Cre-loxP. Nat Genet. 2000;25:139-140.
27. Srinivas S, Watanabe T, Lin CS, et al. Cre reporter strains produced by targeted insertion of EYFP and ECFP into the ROSA26 locus. BMC Dev Biol. 2001;1:4.
28. Grant GR, Farkas MH, Pizarro AD, et al. Comparative analysis of RNA-Seq alignment algorithms and the RNA-Seq unified mapper (RUM). Bioinformatics. 2011;27:2518-2528.
29. Grant GR, Liu J, Stoeckert CJ, Jr. A practical false discovery rate approach to identifying patterns of differential expression in microarray data. Bioinformatics. 2005;21:2684-2690.
30. Eisen MB, Spellman PT, Brown PO, et al. Cluster analysis and display of genome-wide expression patterns. Proc Natl Acad Sci U S A. 1998;95:14863-14868.
31. Ashburner M, Ball CA, Blake JA, et al. Gene ontology: tool for the unification of biology. The Gene Ontology Consortium. Nat Genet. 2000;25:25-29.
32. Chen SX, Osipovich AB, Ustione A, et al. Quantification of factors influencing fluorescent protein expression using RMCE to generate an allelic series in the ROSA26 locus in mice. Dis Model Mech. 2011;4:537-547.
33. Soriano P. Generalized lacZ expression with the ROSA26 Cre reporter strain. Nat Genet. 1999;21:70-71.
34. Engert S, Liao WP, Burtscher I, et al. Sox17-2A-iCre: a knock-in mouse line expressing Cre recombinase in endoderm and vascular endothelial cells. Genesis. 2009;47:603-610.
35. Hudson C, Clements D, Friday RV, et al. Xsox17alpha and -beta mediate endoderm formation in Xenopus. Cell. 1997;91:397-405.
36. Liao WP, Uetzmann L, Burtscher I, et al. Generation of a mouse line expressing Sox17-driven Cre recombinase with specific activity in arteries. Genesis. 2009;47:476-483.
37. Grogan SP, Miyaki S, Asahara H, et al. Mesenchymal progenitor cell markers in human articular cartilage: normal distribution and changes in osteoarthritis. Arthritis Res Ther. 2009;11:R85.
38. Garry DJ, Olson EN. A common progenitor at the heart of development. Cell. 2006;127:1101-1104.
39. Ferkowicz MJ, Starr M, Xie X, et al. CD41 expression defines the onset of primitive and definitive hematopoiesis in the murine embryo. Development. 2003;130:4393-4403.
40. Nishikawa SI, Nishikawa S, Kawamoto H, et al. In vitro generation of lymphohematopoietic cells from endothelial cells purified from murine embryos. Immunity. 1998;8:761-769.
41. Yoshimoto M, Montecino-Rodriguez E, Ferkowicz MJ, et al. Embryonic day 9 yolk sac and intra-embryonic hemogenic endothelium independently generate a B-1 and marginal zone progenitor lacking B-2 potential. Proc Natl Acad Sci U S A. 2011;108:1468-1473.
42. Yoshimoto M, Porayette P, Glosson NL, et al. Autonomous murine T cell progenitor production in the extra-embryonic yolk sac prior to HSC emergence. Blood. 2012.
43. Mi H, Dong Q, Muruganujan A, et al. PANTHER version 7: improved phylogenetic trees, orthologs and collaboration with the Gene Ontology Consortium. Nucleic Acids Res. 2010;38:D204-210.

44. Heller RS, Dichmann DS, Jensen J, et al. Expression patterns of Wnts, Frizzleds, sFRPs, and misexpression in transgenic mice suggesting a role for Wnts in pancreas and foregut pattern formation. Dev Dyn. 2002;225:260-270.
45. Wandzioch E, Zaret KS. Dynamic signaling network for the specification of embryonic pancreas and liver progenitors. Science. 2009;324:1707-1710.
46. Kanai Y, Kanai-Azuma M, Noce T, et al. Identification of two Sox17 messenger RNA isoforms, with and without the high mobility group box region, and their differential expression in mouse spermatogenesis. J Cell Biol. 1996;133:667-681.
47. Burtscher I, Barkey W, Schwarzfischer M, et al. The Sox17-mCherry fusion mouse line allows visualization of endoderm and vascular endothelial development. Genesis. 2011.
48. Baron MH, Isern J, Fraser ST. The embryonic origins of erythropoiesis in mammals. Blood. 2012;119:4828-4837.
49. Fraser ST, Isern J, Baron MH. Maturation and enucleation of primitive erythroblasts during mouse embryogenesis is accompanied by changes in cell-surface antigen expression. Blood. 2007;109:343-352.
50. Kalsotra A, Cooper TA. Functional consequences of developmentally regulated alternative splicing. Nat Rev Genet. 2011;12:715-729.
51. Pendeville H, Winandy M, Manfroid I, et al. Zebrafish Sox7 and Sox18 function together to control arterial-venous identity. Dev Biol. 2008;317:405-416.
52. Patterson M, Chan DN, Ha I, et al. Defining the nature of human pluripotent stem cell progeny. Cell Res. 2011.
53. Seymour PA, Freude KK, Tran MN, et al. SOX9 is required for maintenance of the pancreatic progenitor cell pool. Proc Natl Acad Sci U S A. 2007;104:1865-1870.
54. Furuyama K, Kawaguchi Y, Akiyama H, et al. Continuous cell supply from a Sox9-expressing progenitor zone in adult liver, exocrine pancreas and intestine. Nat Genet. 2011;43:34-41.
55. Dessimoz J, Bonnard C, Huelsken J, et al. Pancreas-specific deletion of beta-catenin reveals Wnt-dependent and Wnt-independent functions during development. Curr Biol. 2005;15:1677-1683.
56. Sinner D, Rankin S, Lee M, et al. Sox17 and beta-catenin cooperate to regulate the transcription of endodermal genes. Development. 2004;131:3069-3080.
57. De Val S, Black BL. Transcriptional control of endothelial cell development. Dev Cell. 2009;16:180-195.
58. Reynaud D, Ravet E, Titeux M, et al. SCL/TAL1 expression level regulates human hematopoietic stem cell self-renewal and engraftment. Blood. 2005;106:2318-2328.
59. Gerstein RM. Deciding the decider: Mef2c in hematopoiesis. Nat Immunol. 2009;10:235-236.
60. Ling KW, Ottersbach K, van Hamburg JP, et al. GATA-2 plays two functionally distinct roles during the ontogeny of hematopoietic stem cells. J Exp Med. 2004;200:871-882.
61. Medvinsky A, Rybtsov S, Taoudi S. Embryonic origin of the adult hematopoietic system: advances and questions. Development. 2011;138:1017-1031.
62. Zhang H, Ables ET, Pope CF, et al. Multiple, temporal-specific roles for HNF6 in pancreatic endocrine and ductal differentiation. Mech Dev. 2009;126:958-973.

See www.StemCells.com for supporting information available online.

Figure 1. Generation the *Sox17^{GFPCre}* allele

A) Diagram of the *Sox17* locus, targeting vector, *Sox17^{LCA}* allele, GFPCre exchange cassette, *Sox17$^{GFPCre(+HygroR)}$*, and *Sox17^{GFPCre}* allele. A targeting vector for the mouse *Sox17* gene was constructed where sequence including exons 3 to 5, which contain the coding region of *Sox17*, was replaced with a *puromycin resistance-Δ-thymidine kinase* fusion gene (*puΔTK*) and an EM7-driven *kanamycin resistance* gene (*Kan^R*) flanked by lox66 (open triangle) and lox2272 (black triangle) sites. The GFPCre exchange cassette was flanked by lox71 (grey triangle) and lox2272 sites and contained a *PGK*-driven *hygromycin resistance* gene (*Hygro^R*) flanked by FRT sites (open circles). Following exchange into *Sox17^{LCA}*-containing mouse ES cells by RMCE, mice containing the *Sox17$^{GFPCre(+HygroR)}$* allele were bred with FLPe-expressing transgenic mice, thereby generating the final *Sox17^{GFPCre}* allele. PCR amplifications for 5' and 3' screening of *Sox17$^{GFPCre(+HygroR)}$* allele depicted as a and b. SA, short arm. LA, long arm. B) Southern blot analysis of genomic DNA from puromycin-resistant *Sox17^{LCA}* ES cells. DNA was digested with SphI or SpeI and hybridized with a 5' or 3' probe as indicated in panel A. Clones 1C1 and 1G3 were correctly targeted by presence of a 12.3 kb and 11.1 kb band on the 5' and 3' ends, respectively. Clone 1G3 was used for RMCE. C) PCR screening of *Sox17$^{GFPCre(+HygroR)}$* exchanged clones. The proper exchange of clone 1C10 was identified by 660 and 1,006 basepair (bp) bands on the 5' and 3' ends, respectively.

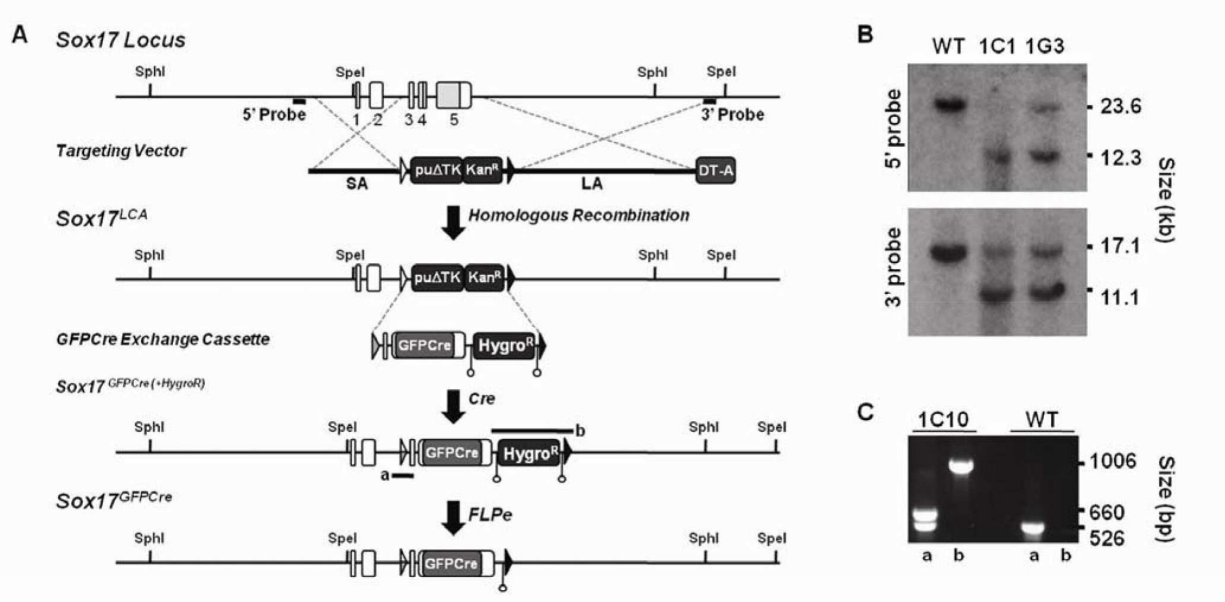

Figure 2. Expression pattern of *Sox17*$^{GFPCre/+}$ during development
A) GFPCre expression was observed from E6.5 to E9.5 in *Sox17*$^{GFPCre/+}$ embryos. At E6.5, GFPCre was observed only in the extra-embryonic region (a&b). Conversely, at E7.5, it was seen in the embryonic region (c&d), specially the definitive endoderm area (arrow). At E8.5, GFPCre was observed in the gut tube area (e&f) with expression in the foregut region marked (arrow). At E9.5, the expression was diminished in the gut (g&h) but was still seen in the ventral pancreatic bud (arrow). Scale bar = 100 μm. Anterior (A), posterior (P), proximal (Pr), distal (Di), dorsal (D), ventral (V). B) Immunolabeling revealed co-localization of both GFPCre and Sox17 in E8.5 and E9.5 *Sox17*$^{GFPCre/+}$ mouse embryos. At E8.5, GFPCre and Sox17 were co-expressed in the foregut endoderm (a) and at E9.5 in the ventral pancreatic bud (b) and the para-aortic splanchnopleural area (c). White boxed areas depict regions enlarged. Scale bar = 50 μm. Foregut (FG), ventral pancreatic bud (VP), para-aortic splanchnopleural (P-Sp).

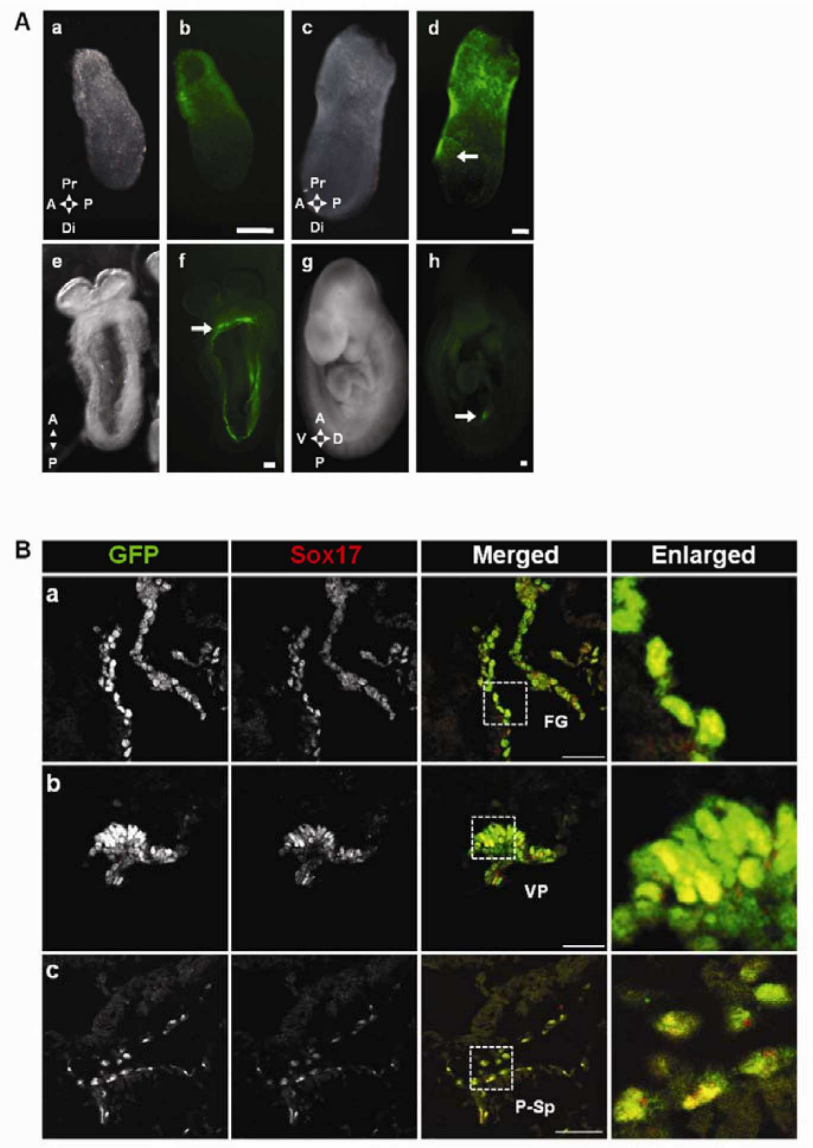

Figure 3. Two distinct types of *Sox17*^{GFPCre}-expressing cells at E9.5
A) Immunolabeling revealed that GFP expression at E9.5 in the ventral pancreatic bud (VP) was co-localized with Pdx1 (arrows). Several GFPCre-expressing cells were found in the liver bud region (Li) but did not co-localize with Hnf4α (arrowheads). B) GFP was detected in the dorsal aorta (DA); however, it did not co-localize with Sox2, an early ectoderm marker, or Foxa2, a floor plate marker, (arrow). C) GFP was detected in the neural tube (NT); however, it did not co-localize either Sox2 or Sox10, a neural crest cell marker (arrow). D) GFP in the ventral pancreatic bud co-localized with EpCAM (arrow) but not with PECAM (arrowheads). E) GFP in the neural tube co-localized with PECAM (arrow). White boxed areas depict regions enlarged. Scale bar = 50 μm. Floor plate (FP), neural crest cells (NC).

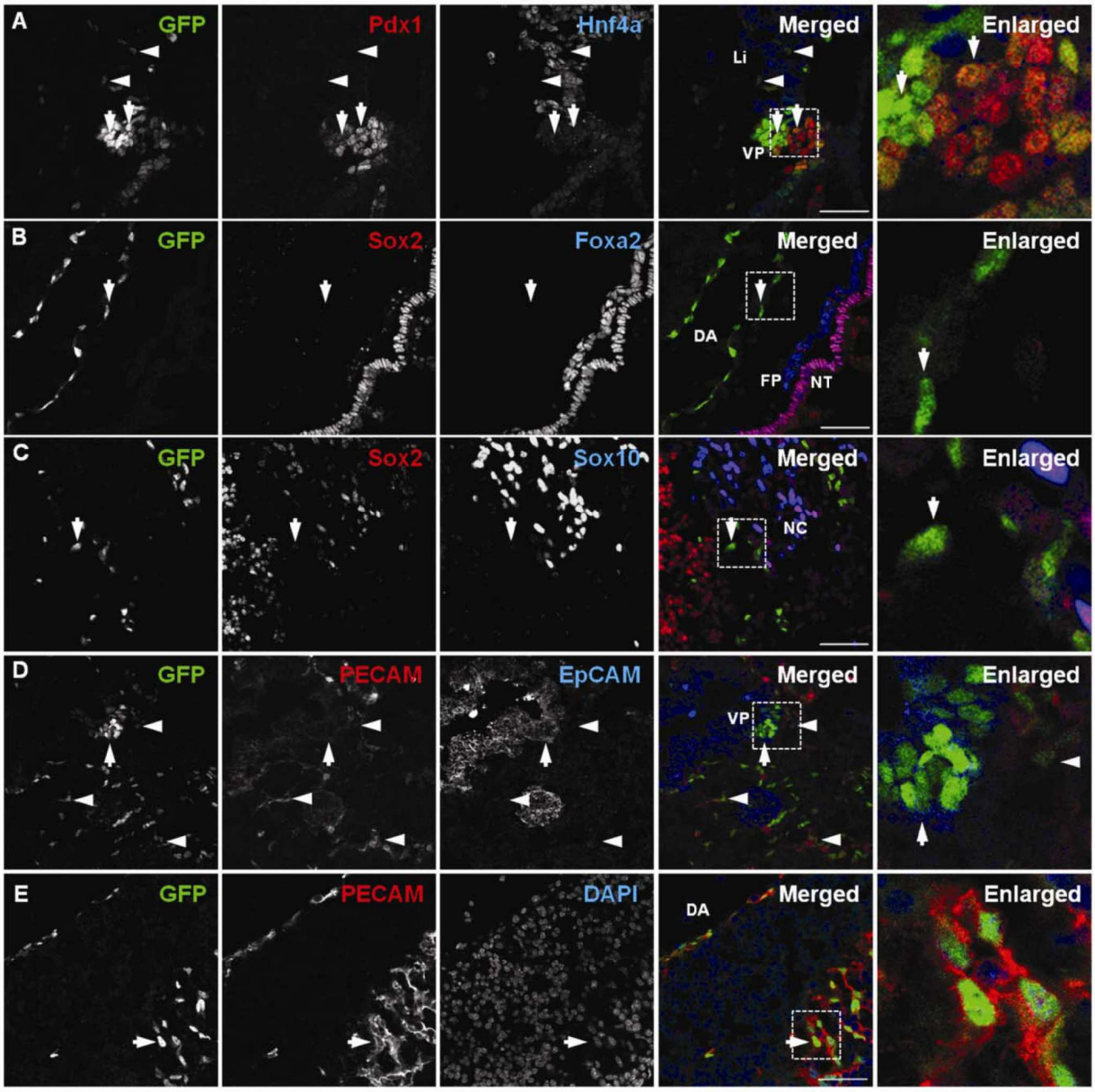

Figure 4. Fate tracing of Sox17-expressing cells at E9.5
A) In E9.5 *R26R*^{eYFP};*Sox17*^{GFPCre} mouse embryos, YFP was detected in the ventral pancreatic bud (VP) and gut tube [62] and displayed co-localization with EpCAM. YFP also co-localized with *Sox17*^{GFPCre}-expressing cells in the ventral pancreatic bud (arrow). B) YFP was detected in the dorsal aorta (DA) and co-localized with PECAM. Some YFP-positive cells also co-localized with Sox17 (arrow). C) YFP co-localized with PECAM in the endocardium of heart (H) (arrow); however, it did not co-localize with VCAM in the myocardium (arrowheads). White boxed areas depict regions enlarged. Scale bar = 50 μm.

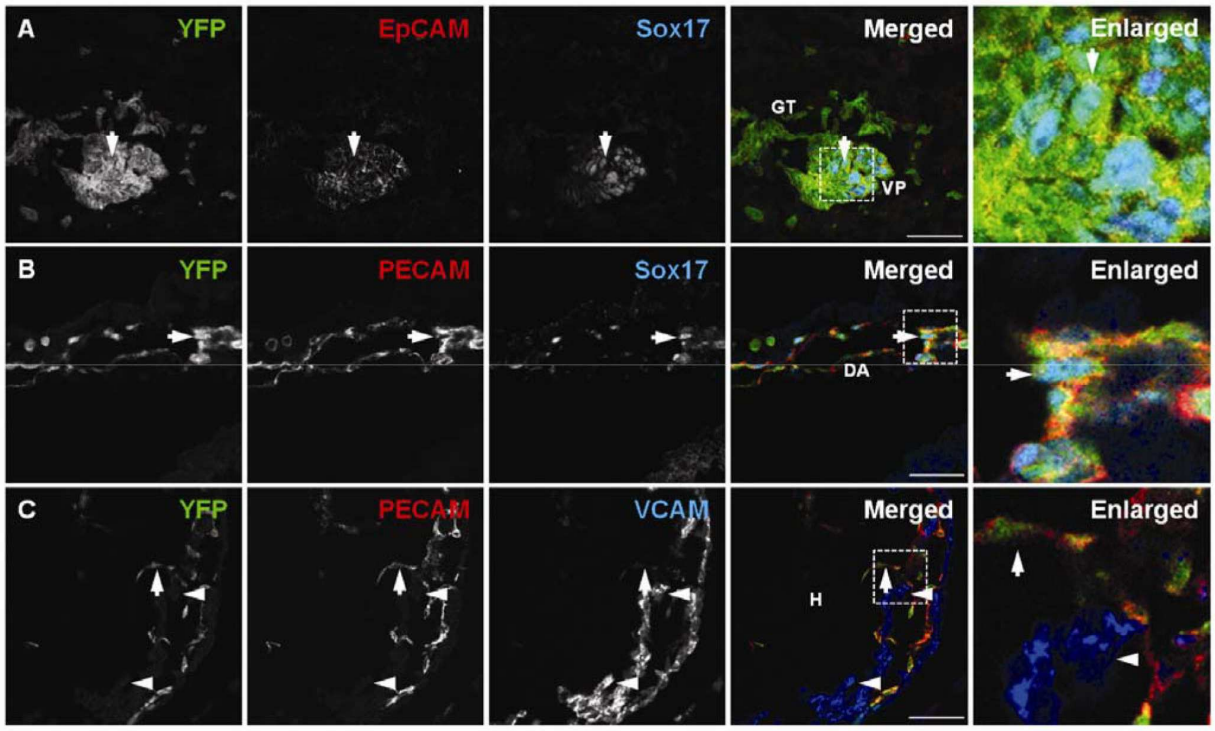

Figure 5. Sox17-expressing endothelial cells exhibit hemogenic potential
A) In E9.5 *Sox17*$^{GFPCre/+}$ embryos, GFP was detected in the para-aortic splanchnopleural (P-Sp) area. GFP co-localized with c-Kit-positive cells in the aortic floor (arrows); however, GFP was diminished or not detected in CD41-positive and/or c-Kit positive hematopoietic cells (arrowheads). White boxed areas depict regions enlarged. Scale bar = 50 μm. B) In E9.5 *R26R*^{eYFP};*Sox17*^{GFPCre} embryos, YFP was detected in the para-aortic splanchnopleural (P-Sp) area. YFP co-localized with c-Kit- and CD41-positive cells (arrowheads). C) Both erythrocytes and myeloid (Ter119+ or Mac1+) cells were differentiated from wild type and Sox17-expressing ECs obtained from E9.5 YS and P-Sp. D) YFP expression in hematopoietic cells from E9.5 embryos, E12.5 fetal liver (FL), and adult mouse BM of *R26R*^{eYFP};*Sox17*^{GFPCre} mice (n≥3). YFP-expression was analyzed with hematopoietic cell marker-gated cells.

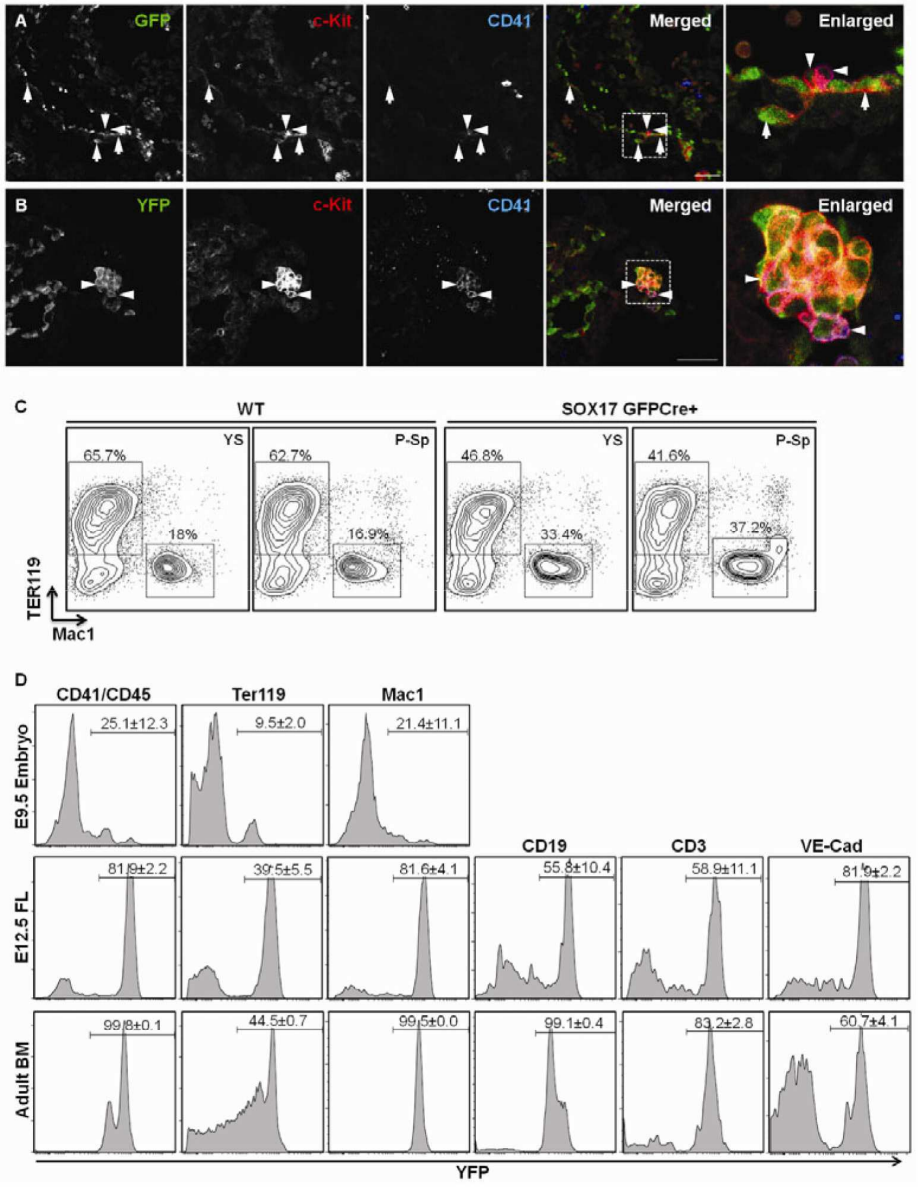

Figure 6. Comparison of differentially expressed genes in two populations

A) Fluorescence-activated cell sorting (FACS) was used to isolate GFP/EpCAM co-positive cells representing ventral pancreatic epithelial cells (EpCAM$^+$) and GFP$^+$/EpCAM$^-$ cells representing hemogenic ECs (EpCAM$^-$) from dissected E9.5 *Sox17*$^{GFPCre/+}$ embryo midguts. B) The distinct difference between the EpCAM$^+$ and EpCAM$^-$ cell populations is evident in the heat map which displays the RPKM values for 321 genes from three biological replicates for either EpCAM$^+$ or EpCAM$^-$. Black color corresponds to an RPKM value of 0, and the brightest red corresponds to ≥ 100 RPKM value. C) The selected transcripts were clustered according to protein class, and the fold change (natural log scale) indicating gene expression in EpCAM$^+$ cells as compared to EpCAM$^-$ cells is shown. ** > 0.9 and * > 0.85 confidence value.

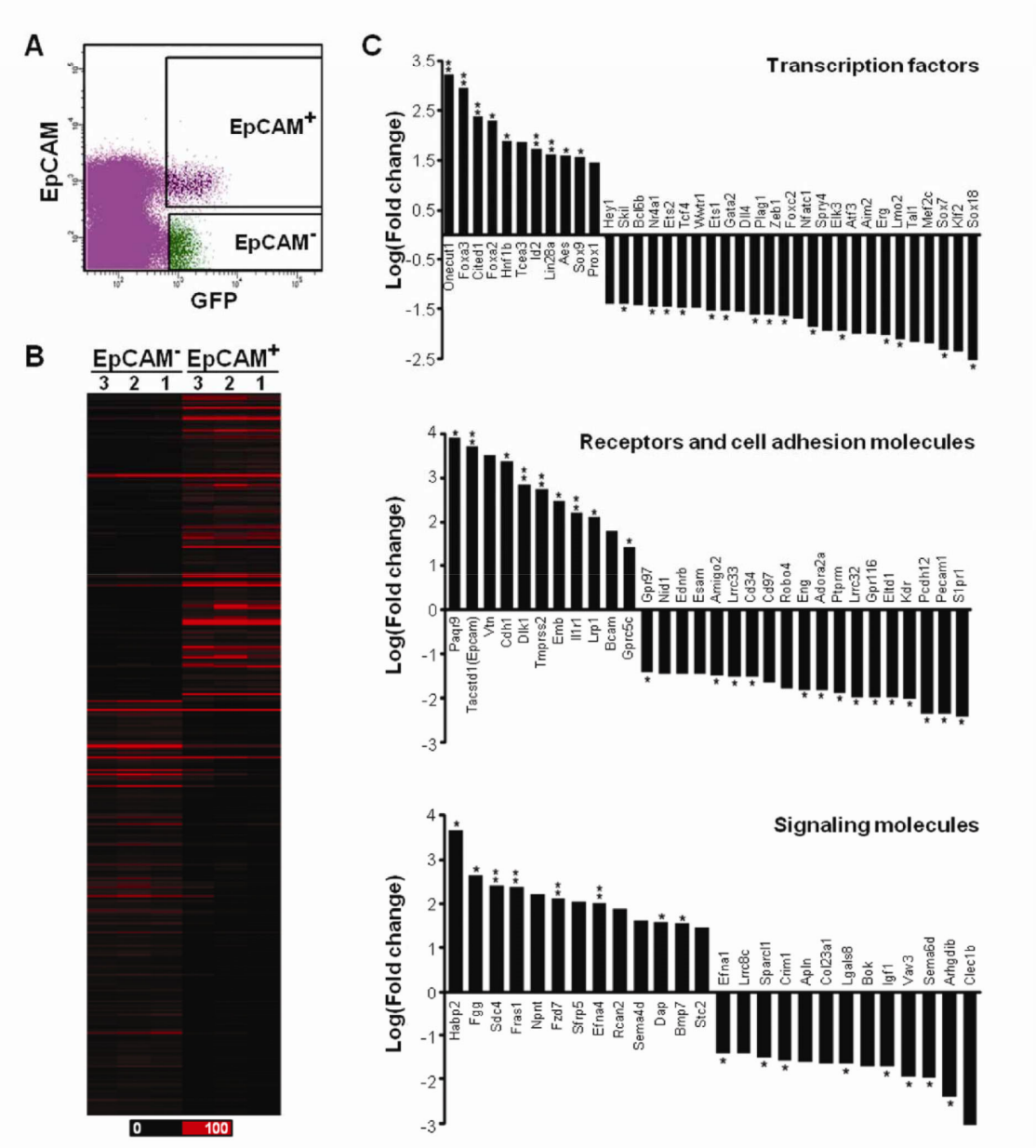

Figure 7. Isolation of Sox17-expressing cells and identification of alternative variants of *Sox17* transcript in EpCAM$^+$ and EpCAM$^-$ cells

A) Schematic of two transcript variants of *Sox17* (T1 & T2). Dark gray box shows coding regions. Black lines (a – d) indicate the amplified regions for PCR. B) Both EpCAM$^+$ and EpCAM$^-$ cells samples amplified sequence within the coding regions (a and b); however, only the EpCAM$^-$ sample amplified regions spanning the first three exons. The band in the EpCAM+ lane in d is non-specific (expected band size = 316 bp) (c and d).

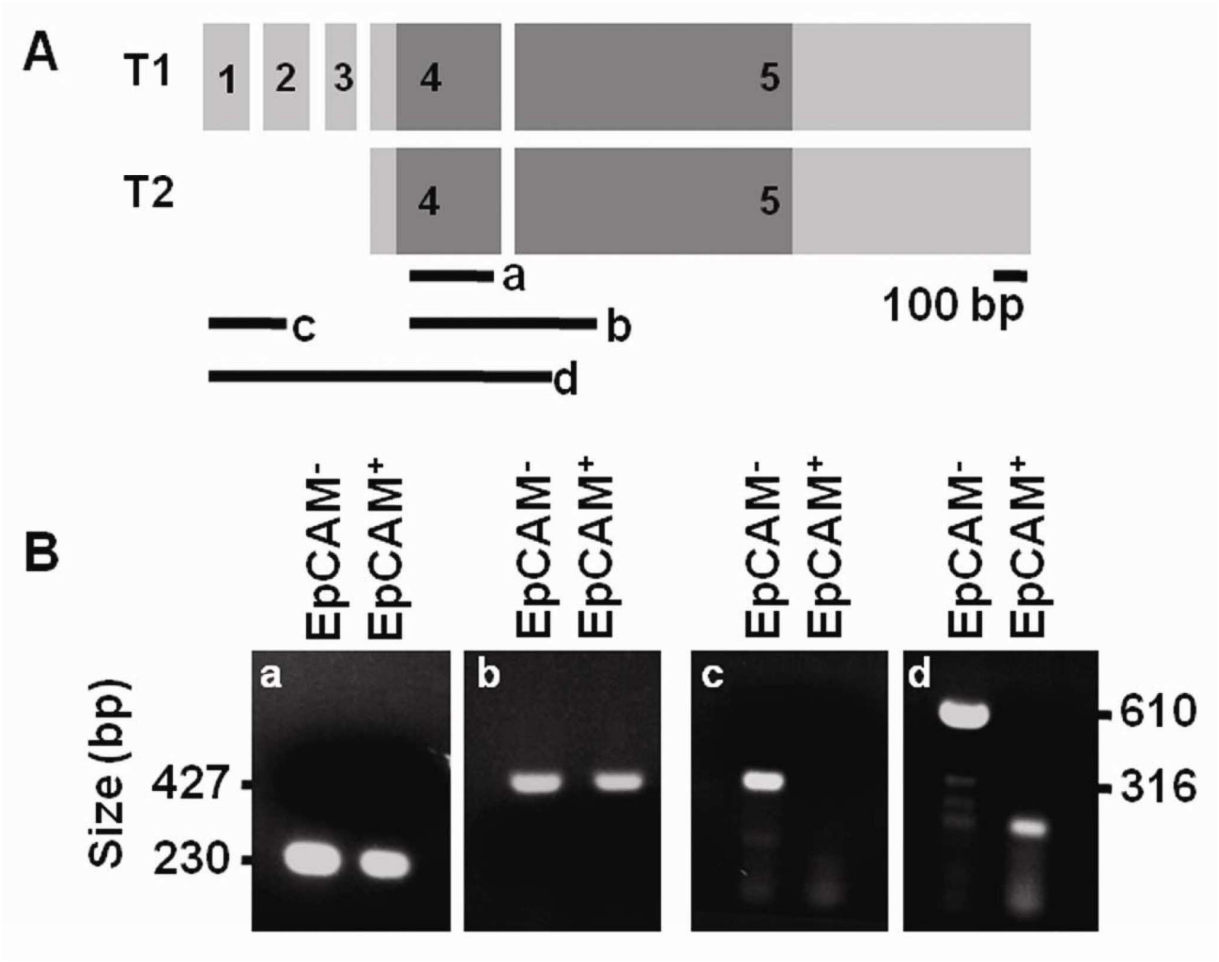

Supplementary Figures

Supplemental Figure 1. Expression pattern of Sox17GFPCre/+ at E7.5

A) 3D reconstruction of an E7.5 Sox17GFPCre/+ embryo. Intense GFP fluorescence was observed in the definitive endoderm area (arrow) and weaker expression seen in visceral endoderm area (arrowhead). Anterior (A), posterior (P), proximal (Pr), distal (Di). Scale bar = 100 μm.

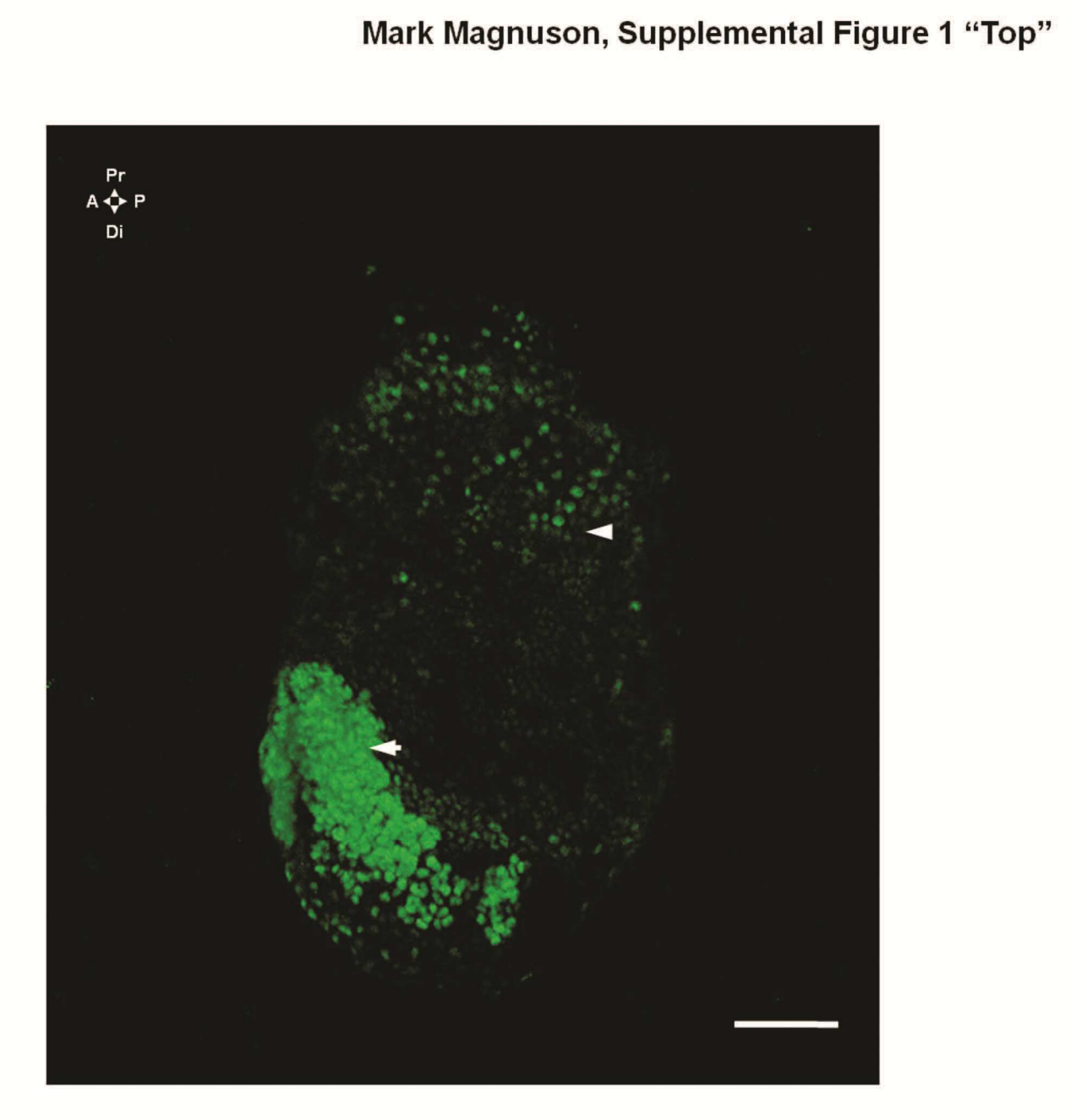

Supplemental Figure 2. Cre recombinase efficiency assessment

A-D) β -D-Galactosidase staining of E9.5 Sox17GFPCre/+;R26RLacZ/+ embryo sections showed LacZ activity in all endoderm-derived cells such as (A) the first branchial pouch (BP1) (B) the second branchial pouch (BP2) (C) the foregut (Fg), the hepatic primordium (HP) and (D) in the hindgut (Hg). It was also present in endothelia as illustrated for the dorsal aorta endothelium (DA). E-F) β -D-Galactosidase staining was performed on E12.5 Sox17GFPCre/+;R26RLacZ/+ embryo sections. The recombination of the Rosa26 locus was detected in (E) the endocardium (heart, H) as well as in the endothelia, such as in the aorta (A). The enzyme activity was also present in all endoderm-derived organs, such as the liver (Li), the stomach (St), the dorsal and ventral pancreas (DP and VP), the small intestine (It) (F), as well as the colon and the caecum (G). Scale bar = 100 μ m (A-D, F-G), 200 μ m (E). Magnification insert scale bar = 20 μ m

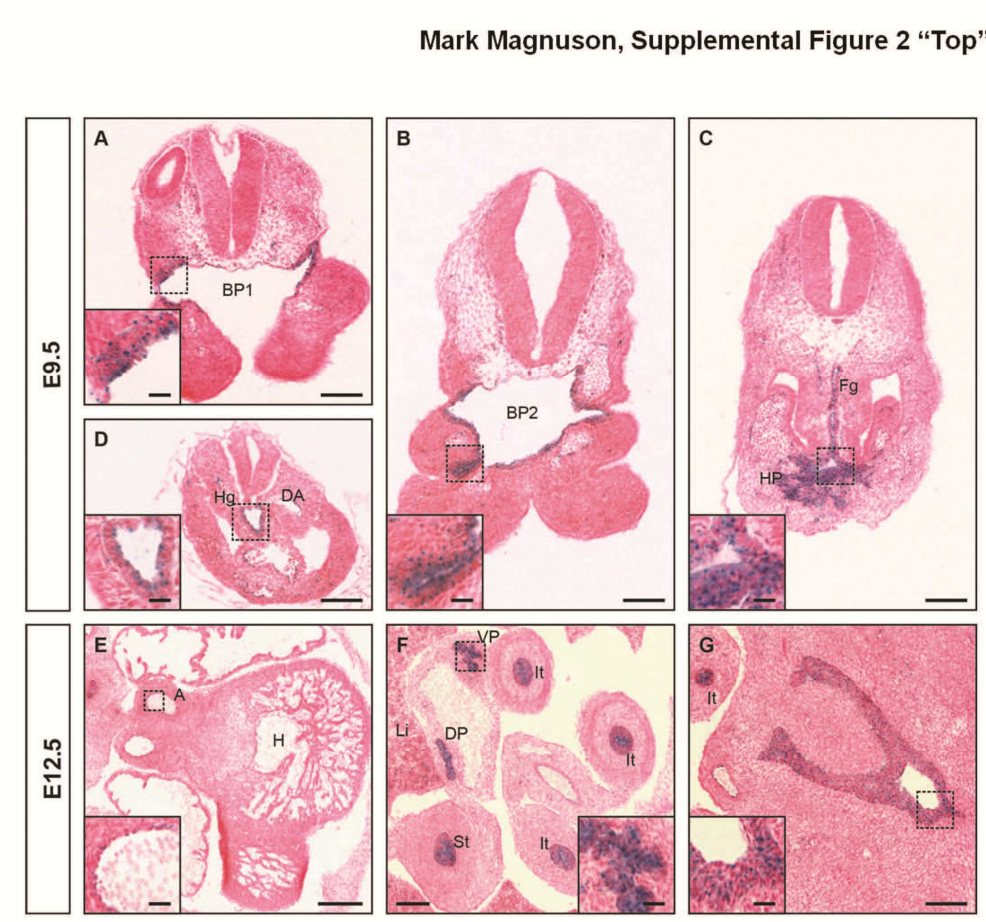

Supplemental Figure 3. Fate tracing of Sox17-expressing cells at multiple stages

A) Immunolabeling of E9.5 R26ReYFP ;Sox17GFPCre embryos revealed YFP and Foxa2 colocalization in the gut tube (GT), ventral pancreas (VP), and liver (Li). However, Foxa2 is not detected in YFP-positive endothelial cells (arrows). Scale bar = 50 μm. B) Immunolabeling of E11.5 and E15.5 R26ReYFP;Sox17GFPCre pancreata revealed YFP co-localization with pancreatic markers, such as Ptf1a, Ngn3, Ins, and the ductal stain, Dolichos biflorus agglutinin (DBA). Scale bar = 50 μm.

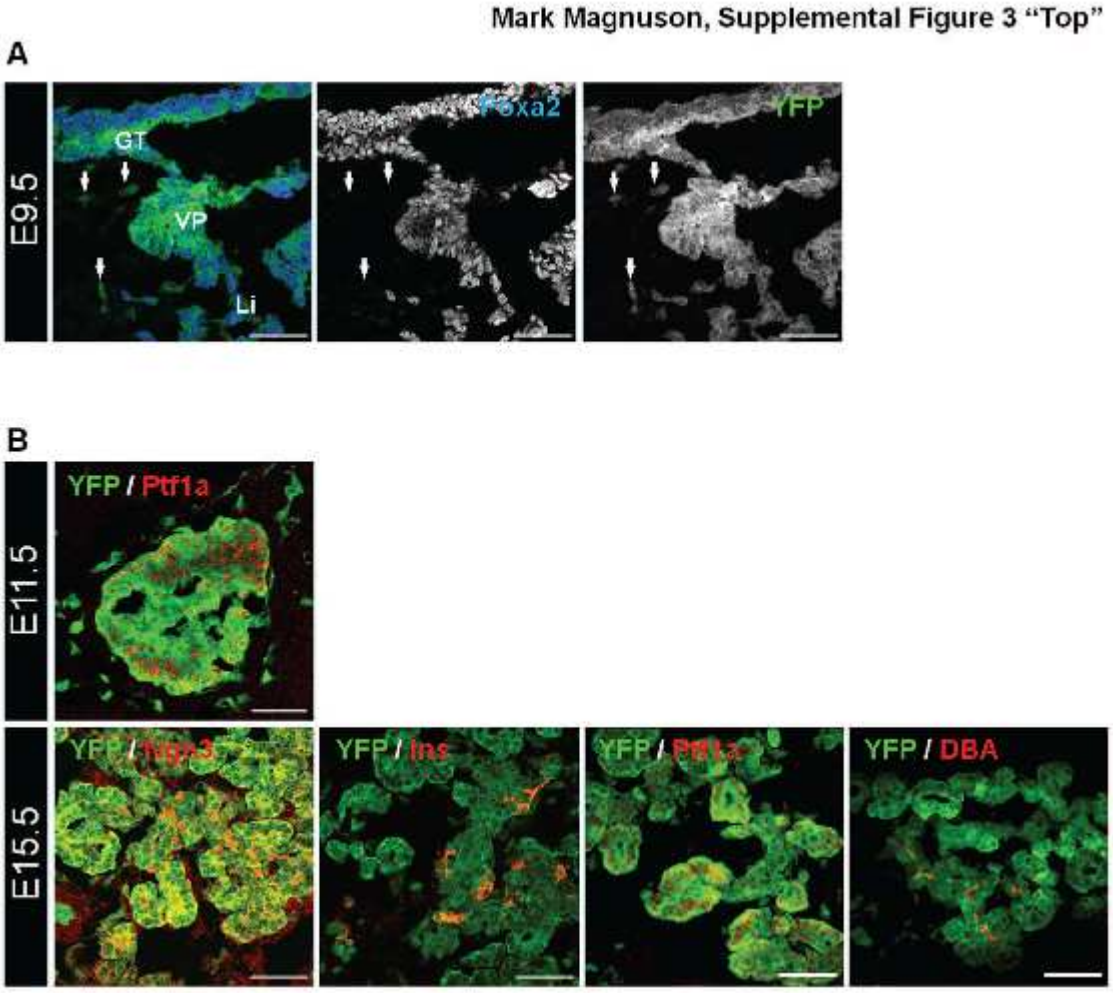

Supplemental Figure 4. Fate tracing of Sox17-expressing cells in different organs

A) Immunolabeling of E15.5 R26ReYFP;Sox17GFPCre embryos revealed YFP and PECAM colocalization in the vein (V), liver (Li), pancreas (P), and hepatic vein (HV). B) Immunolabeling of E9.5 R26ReYFP;Sox17GFPCre embryos revealed YFP and pre-HSC markers co-localization in the blood island of yolk sac.

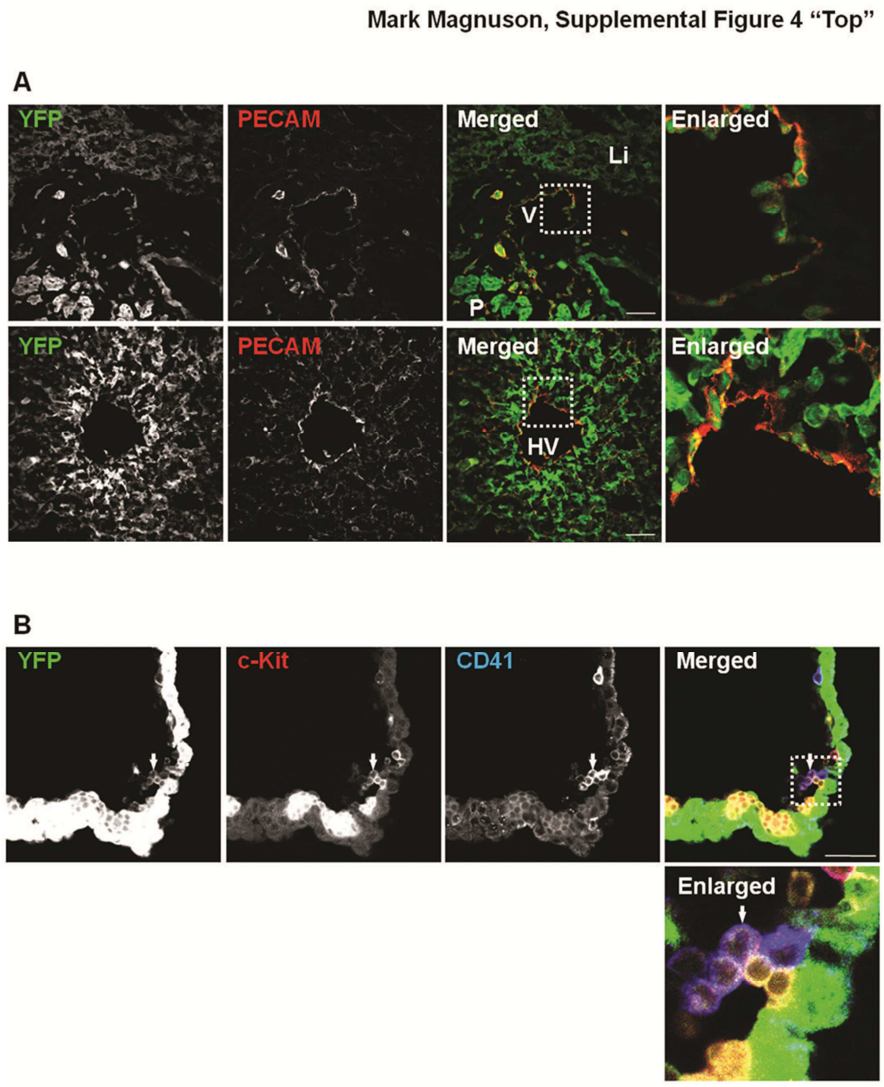

Supplemental Figure 5. Analysis of the two Sox17-expressing cell populations

A) EpCAM immunolabeling was used to analyze the number of EpCAM+ and EpCAM- cells present in E9.5 Sox17GFPCre/+ whole mouse embryos. GFP/EpCAM co-positive cells represent ventral pancreatic cells (EpCAM+), and GFP-positive/EpCAM-negative cells represent hemogenic endothelial cells (EpCAM-). Percentages indicate the mean percentage of EpCAM+ or EpCAM- cells which are GFP-positive (n=4). B) Quantification of EpCAM+ and EpCAM- cells analyzed by FACS from all GFP-positive cells identified in E9.5 Sox17GFPCre/+ whole mouse embryos. C) The mid region including ventral pancreas (red box) was dissected from whole embryos to increase sorting efficiency. Immunohistochemistry on E9.5 Sox17GFPCre/+ whole mount embryo cryo-sections showed that GFPCre was expressed in the ventral pancreatic bud (VP) with weaker expression in the dorsal aorta (DA) in P-Sp area. Image was acquired using AZ100 multizoom microscope, Nikon. Zoom = 5.7x. Scale bar = 100 μm

Mark Magnuson, Supplemental Figure 5 "Top"

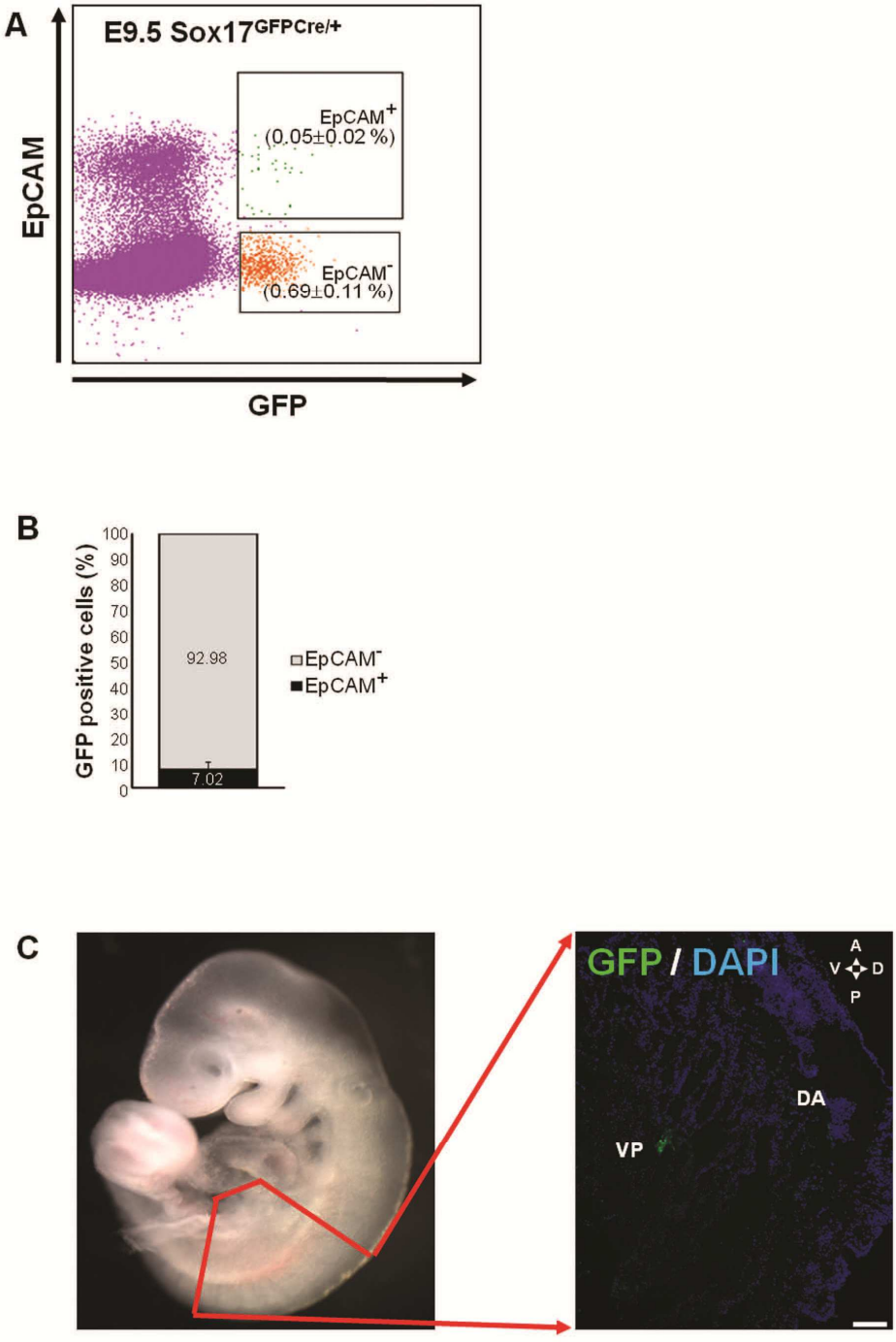

Supplemental Figure 6.

Comparison of coverage plots on mouse Sox17 gene locus Coverage plot of uniquely mapped sequence reads (red) from EpCAM- and EpCAM+ samples following RNA-Seq. Predicted Sox17 transcripts taken from either the UCSC database (Sox17 (UCSC)) or RefSeq and EMBL/GenBank databases (Sox17 (TROMER)) are shown below mapped reads. Exons 1 – 5 are noted, and a CpG island spanning exons 4 – 5 is indicated. Blue box indicates exon 2 region which contains mapped reads for EpCAM- sample.

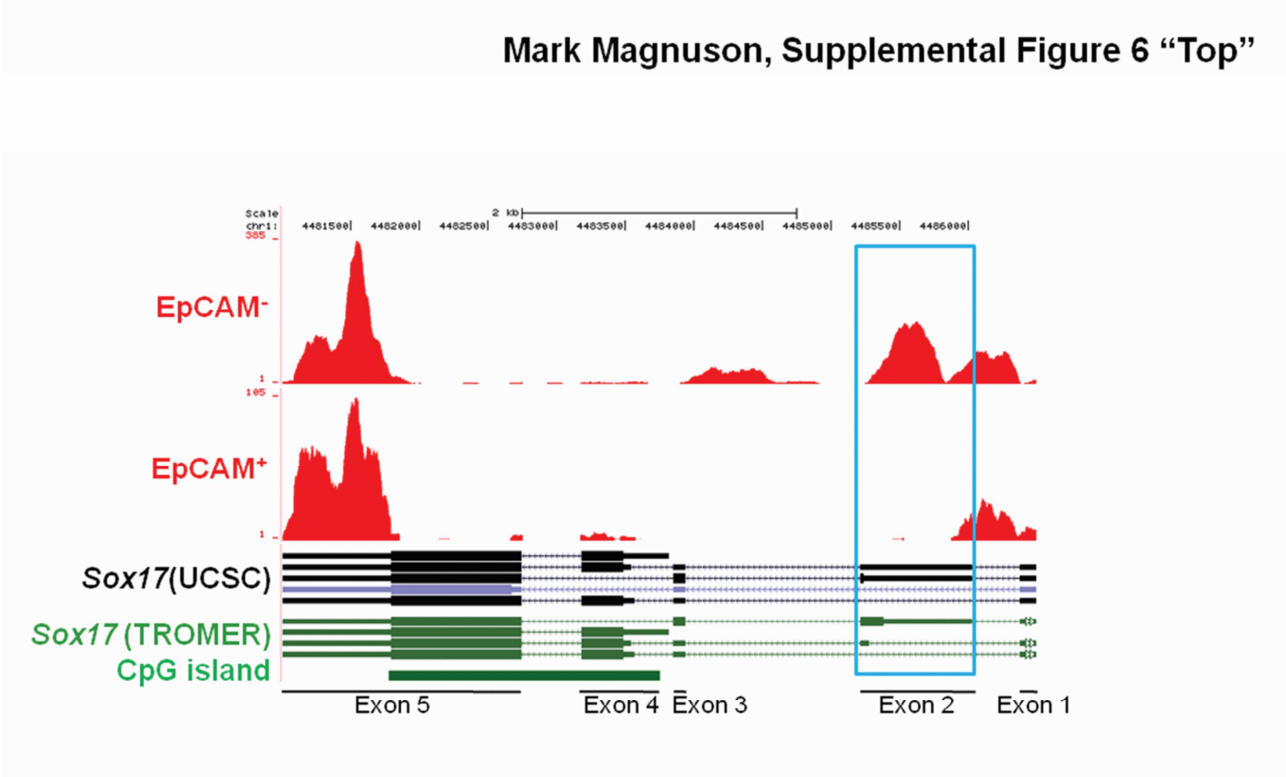

Supplementary Tables

Mark Magnuson, Supplemental Table 2 "Top"

	EpCAM$^-$-1	EpCAM$^-$-2	EpCAM$^-$-3	EpCAM$^+$-1	EpCAM$^+$-2	EpCAM$^+$-3
EpCAM$^-$-1	1	0.981623	0.985769	0.970455	0.977042	0.945636
EpCAM$^-$-2	0.981623	1	0.974057	0.956915	0.981355	0.946997
EpCAM$^-$-3	0.985769	0.974057	1	0.950457	0.974453	0.950186
EpCAM$^+$-1	0.970455	0.956915	0.950457	1	0.976534	0.971136
EpCAM$^+$-2	0.977042	0.981355	0.974453	0.976534	1	0.976611
EpCAM$^+$-3	0.945636	0.946997	0.950186	0.971136	0.976611	1

(Pairwise Pearson correlation)

Mark Magnuson, Supplemental Table 1 "Top"

Sample	Num reads (total)	Unique mapped reads	Unique (%)	Non-unique mapped reads	Non-unique (%)	Total mapped reads	Total (%)
EpCAM$^-$-1	58,992,069	33,019,109	55.97	7,359,722	12.40	40,378,831	68.40
EpCAM$^-$-2	53,491,913	29,202,243	54.59	6,366,899	11.90	35,569,142	66.40
EpCAM$^-$-3	55,222,918	32,026,990	57.99	6,017,550	10.80	38,044,540	68.80
EpCAM$^+$-1	60,279,948	29,979,031	49.73	7,709,594	12.70	37,688,625	62.50
EpCAM$^+$-2	52,596,577	33,366,103	63.43	6,403,069	12.10	39,769,172	75.60
EpCAM$^+$-3	64,585,099	33,599,556	52.02	7,437,527	11.50	41,037,083	63.50

Mark Magnuson, Supplemental Table 3 "Top"

	Antibody	Source	Cat. No.	Dilution
Primary	Goat anti-Sox17	R&D Systems	AF1924	1:500
	Goat anti-Hnf4a	Santa Cruz	SC-6556	1:500
	Guinea pig anti-Pdx1	Chris Wright's lab		1:1,000
	Chicken anti-GFP	Invitrogen	A10262	1:500
	Goat anti-Hnf3b	Santa Cruz	SC-6554	1:100
	Rat anti-EpCAM	Santa Cruz	SC-53532	1:50
	Rabbit anti-Sox2	Chemicon	AB5603	1:1000
	Rabbit anti-ECAD	Cell Signaling	#4065	1:200
	Goat anti-Sox10	Santa Cruz	SC-17342	1:50
	Rabbit anti-VCAM-1	Santa Cruz	SC-8304	1:100
	Rat anti-CD31/PECAM	BD Pharmingen	550274	1:1000
	PE-conjugated Rat anti-CD31/PECAM	BD Pharmingen	561073	1:100
	Rat anti-CD41	BD Pharmingen	553847	1:200
	Rabbit anti-c-Kit	Cell Signaling	#3074	1:400
	Goat anti-Ngn3	BCBC	AB2774	1:2,000
	Guinea pig anti-Insulin	Linco	4011-01	1:1,000
	Rabbit anti-Ptf1a	BCBC	AB2153	1:1000
	Biotinylated DBA	Vector	B-1035	1:5,000
Secondary	Donkey anti chicken-Dylight488	Jackson ImmunoResearch		1:500
	Donkey anti rabbit-Alexa fluor 555	Invitrogen		1:1,000
	Donkey anti rabbit-Alexa fluor 680	Invitrogen		1:1000
	Donkey anti guinea pig-Cy3	Jackson ImmunoResearch		1:500
	Donkey anti Rat-Cy3	Jackson ImmunoResearch		1:500
	Goat anti chicken-Alexa 488	Invitrogen		1:1,000
	Donkey anti goat-Alexa fluor 647	Invitrogen		1:1,000
	Goat anti rat-Alexa fluor 546	Invitrogen		1:1,000
	Donkey anti goat-Alexa fluor 546	Invitrogen		1:1,000
	Goat anti rabbit-Alexa fluor 647	Invitrogen		1:1,000
	Donkey anti rat-DyLight 649	Jackson ImmunoResearch		1:500
	TRITC-Streptavidin	Invitrogen		1:500

Supplementary Table 4 and 5 are available on the Stem Cell website

http://onlinelibrary.wiley.com/doi/10.1002/stem.1192/suppinfo

10.2.2 Cell cycle-dependent differentiation dynamics balances growth and endocrine differentiation in the pancreas

Authors: Yung Hae Kim, Hjalte List Larsen, Pau Rué, Laurence A. Lemaire, Jorge Ferrer, Anne Grapin-Botton

Contribution: I have characterized the *Neurog3-RFP* transgenic line mouse (Figure S3C and S3D). Guts were collected at E14.5. They were embedded in gelatin. Systematic uniform random sampled sections (SUR sections) were collected every 6 sections. Immunostainings for NEUROG3, Myc (recognizing RFP), and INS and GCG (Hormones) were performed. The number of RFP^+ cells were counted on all the immunostained sections as well as the subpopulations: $RFP^+NEUROG3^+$ and $RFP^+Hormones^+$. The number of $RFP^+NEUROG3^-Hormones^-$ cells was deduced from the quantified population. The number of $NEUROG3^+RFP^-$ cells was also quantified.

PLOS | BIOLOGY

RESEARCH ARTICLE

Cell Cycle–Dependent Differentiation Dynamics Balances Growth and Endocrine Differentiation in the Pancreas

Yung Hae Kim[1,2]*, Hjalte List Larsen[1], Pau Rué[3], Laurence A. Lemaire[1], Jorge Ferrer[4,5], Anne Grapin-Botton[1,2]*

1 DanStem, University of Copenhagen, Copenhagen, Denmark, **2** Ecole Polytechnique Fédérale de Lausanne, Life Sciences, Institute of Bioengineering, Lausanne, Switzerland, **3** Department of Genetics, University of Cambridge, Cambridge, United Kingdom, **4** Department of Medicine, Imperial College London, London, United Kingdom, **5** Institut d'Investigacions August Pi i Sunyer, CIBER de Diabetes y Enfermedades Metabólicas Asociadas, Barcelona, Spain

* yung.kim@sund.ku.dk (YHK); anne.grapin-botton@sund.ku.dk (AGB)

OPEN ACCESS

Citation: Kim YH, Larsen HL, Rué P, Lemaire LA, Ferrer J, Grapin-Botton A (2015) Cell Cycle–Dependent Differentiation Dynamics Balances Growth and Endocrine Differentiation in the Pancreas. PLoS Biol 13(3): e1002111. doi:10.1371/journal.pbio.1002111

Academic Editor: Brigid L. M. Hogan, Duke University Medical Center, UNITED STATES

Received: October 28, 2014

Accepted: February 16, 2015

Published: March 18, 2015

Data Availability Statement: All relevant data are within the paper and its Supporting Information files. All the files of mathematical model simulation are available from the Dryad repository (http://dx.doi.org/10.5061/dryad.4b58d). For complementary information on the mathematical model, a BioRxiv preprint is available at http://biorxiv.org/content/early/2014/10/28/010835.

Funding: This work was funded by the Ecole Polytechnique Fédérale de Lausanne (www.epfl.ch), the Novo Nordisk Foundation (www.novonordiskfonden.dk), and the NIDDK Beta Cell

Abstract

Organogenesis relies on the spatiotemporal balancing of differentiation and proliferation driven by an expanding pool of progenitor cells. In the mouse pancreas, lineage tracing at the population level has shown that the expanding pancreas progenitors can initially give rise to all endocrine, ductal, and acinar cells but become bipotent by embryonic day 13.5, giving rise to endocrine cells and ductal cells. However, the dynamics of individual progenitors balancing self-renewal and lineage-specific differentiation has never been described. Using three-dimensional live imaging and in vivo clonal analysis, we reveal the contribution of individual cells to the global behaviour and demonstrate three modes of progenitor divisions: symmetric renewing, symmetric endocrinogenic, and asymmetric generating a progenitor and an endocrine progenitor. Quantitative analysis shows that the endocrine differentiation process is consistent with a simple model of cell cycle–dependent stochastic priming of progenitors to endocrine fate. The findings provide insights to define control parameters to optimize the generation of β-cells in vitro.

Author Summary

In order to form organs of the right size and cell composition, progenitor cells must balance their proliferation and their differentiation into functional cell types. Here we study how individual progenitor cells in the developing pancreas execute their choices to either expand their pool or differentiate into hormone-producing endocrine cells. Using live microscopy to track the genetically marked progeny of single cells, we reveal that after they divide, individual cells generate either two progenitors, two cells on the endocrine path, or one progenitor and one cell on the endocrine path. Quantitative analysis shows that endocrine differentiation is largely stochastic and that the probability of progenitor cell differentiation by the end of mid-gestation is about 20%. We propose a model in which the

Biology Consortium Grant 1U01DK089570-01 (www.betacell.org). PR was supported by a Marie Curie IEF fellowship. The funders had no role in study design, data collection and analysis, decision to publish, or preparation of the manuscript.

Competing Interests: The authors have declared that no competing interests exist.

Abbreviations: 3-D, 3-dimensional; 4-OH, 4-hydroxy; BABB, benzyl alcohol to benzyl benzoate; bGH-PolyA, bovine growth hormone polyadenylation signal; E, embryonic day; EYFP, enhanced yellow fluorescent protein; GFP, green fluorescent protein; L, Neurog3-primed dividing cell; mG, membrane-localized green fluorescent protein; MPCs, multipotent pancreatic progenitor cells; mT, membrane-localized Tomato; N, NEUROG3 cell; NLS, nuclear localization signal; P, progenitor cell; PBS, phosphate buffered saline; PFA, paraformaldehyde; R, RFP cell; RFP, red fluorescent protein; Tx100, Triton X-100.

production of a progenitor and a differentiated cell in the pancreas results from the stochastic induction of differentiation in one daughter after cell division, rather than the unequal partitioning of molecules between two daughters at the time of division, as observed in the nervous system. Furthermore, when two daughters become endocrine cells, this results from the induction of differentiation followed by cell division—rather than two independent induction events. This model may be applicable to other organs and provides insights to optimize the generation of β-cells in vitro for diabetes therapy.

Introduction

The pancreas is an organ performing vital exocrine and endocrine roles in nutrient metabolism and glucose homeostasis. In the mouse, multipotent pancreatic progenitor cells (MPCs) emerge from the endoderm around embryonic day 9.0 (E9.0) [1]. This population, characterized by the expression of transcription factors PDX1 (GenBank NP_032840), SOX9 (GenBank NP_035578), and HNF1B (GenBank AAH25189), eventually gives rise to all three major cell lineages of the pancreas: endocrine, acinar, and ductal [2–4]. Following early progenitor expansion, three-dimensional (3-D) organization of the pancreatic epithelium leads to the generation of an apico-basally polarized [5–7], branched tubular network. By E13.5, it exhibits its final functional compartmentalization: the distal tip domains give rise to the acinar cells of the exocrine lineage [8], whereas the $SOX9^+/HNF1B^+$ proximal trunk domain is bipotent at the population level, giving rise to the ductal and endocrine cells [3]. The endocrine lineage arises from transient $NEUROG3^+$ (GenBank AAI04328.1) endocrine progenitors, as demonstrated by lineage tracing studies [2] and the absence of all pancreatic endocrine cells in *Neurog3*$^{-/-}$ mice [9]. $NEUROG3^+$ endocrine progenitors originate from pancreatic progenitors expressing PDX1/SOX9/HNF1B during the early phases of MPC expansion and during the secondary transition spanning E12.5–15.5, with specific endocrine subtypes being specified during discrete time windows [10]. Whereas the majority of $NEUROG3^+$ endocrine progenitors are post-mitotic [11] and unipotent, giving rise to only one endocrine subtype [12], we do not know whether individual PDX1/SOX9/HNF1B pancreatic progenitors give rise to both ductal and endocrine cells or are heterogeneous, encompassing cells with pre-specified lineage-restricted potentials. In this study, we ask how individual pancreas progenitors contribute to the population dynamics enabling organ expansion and endocrine differentiation.

Over the last few years cell-labelling and tracing methods have brought forth quantitative descriptions of cell differentiation. In homeostatic systems, for instance, the maintenance of a hierarchy of stem and differentiating cells can be accounted for by populations of equipotent progenitors exhibiting probabilistic fate choices [13–15]. An attempt to extrapolate these notions to developing systems has encountered some difficulties because, in these instances, the growth of the tissue needs to be taken into consideration. Notwithstanding these complications, lineage analysis of progenitor cells in the vertebrate retina indicates that, similarly to the abovementioned homeostatic systems, the distribution of clone sizes is compatible with a model in which progenitors stochastically divide in three modes: (1) symmetric self-renewing, (2) asymmetric, and (3) symmetric differentiating divisions [16–20]. Contrary to homeostatic systems, however, the probabilities of each division mode are not assumed to be fixed but to vary over time, following phases of proliferation and differentiation. These models have proven successful in explaining the distributions of clone sizes but do not explain the observed frequencies of each division type. Alternative models have been put forward that invoke deterministic asymmetric inheritance of differentiative cues at the time of division [21–24]. In

general, how decisions of single cells contribute to global organ growth and differentiation in developing organs remains an open question.

Here we test some of these notions in the context of the emergence of endocrine progenitor cells from uncommitted pancreatic progenitors in the embryonic pancreas. This developmental model has a simple lineage configuration, with a reduced number of fates over well-characterized time windows, and thus provides an optimal testing framework. We use 3-D live imaging of pancreatic explants ex vivo and in vivo, together with lineage tracing at a clonal density, to address the dynamics of the progenitors of the endocrine lineage. In addition to monitoring their lineage, we determined measurements for cell cycle length, synchrony, and differentiation dynamics of these progenitors. This revealed three types of pancreatic progenitor behaviours: (1) symmetric progenitor self-renewal, (2) symmetric endocrinogenic divisions leading to two NEUROG3$^+$ endocrine progenitors, and (3) asymmetric divisions generating a pancreatic progenitor and an endocrine progenitor. By live tracing individual cell fate specification events, we uncover the relationship between *Neurog3* expression timing and mitosis. We identify major differences in the onset of *Neurog3* transcription between cells stemming from symmetric and asymmetric divisions, and further show that this onset is highly synchronized between symmetrically generated sibling cells. Our analysis of such findings leads to a novel interpretation of the choice between symmetric and asymmetric cell divisions. We posit that asymmetric cell divisions are the result of the stochastic induction of endocrine fate in one of the progenitor daughters, rather than a decision made during cell division. Alternatively, if this progenitor divides a last time after induction, which is expected if the induction happens late in G1, the division will be seen as symmetric differentiative. These results argue against conventional views of asymmetric inheritance of differentiative cues at the time of division [21–24] and are instead consistent with a model of cell cycle–dependent stochastic specification of organ-specific progenitors.

Results

Time-Lapse Imaging Enables Pancreas Progenitor Tracking in Three Dimensions

To study how individual pancreatic progenitors contribute to pancreas expansion and to monitor their differentiation into endocrine progenitors, we conducted live imaging of explants of dorsal pancreatic buds from E12.5 *Pdx1*$^{tTA/+}$;*tetO-H2B-GFP* embryos (Fig. 1A). The buds were dissected and laid on a fibronectin-coated coverslip bottom plate, where they grew (Fig. 1B) [25,26]. After 24 h of settling time, we initiated high-magnification time-lapse live imaging in 3-D with 6-min intervals for up to 24 h. Nuclear H2B-GFP fusion protein enabled us to observe cell divisions and to track individual cell nuclei. At the end of the experiment, the explants were fixed and immunostained for markers of pancreatic progenitors (SOX9) and endocrine progenitors (NEUROG3) (S1F–I Fig.), while preserving the native green fluorescent protein (GFP) signal (S1G Fig.), which enabled us to match to the cells from the last frame of the time-lapse movies. The SOX9$^+$ cells constituted the majority of GFP$^+$ epithelial cells (S1I Fig.), and NEUROG3$^+$ cells were mainly observed in the middle trunk region of explant (S1H Fig.) [8]. In spite of the constant exposure to laser, explants grew, showed active cell movements, apicobasal polarization, branching, acini morphogenesis, and differentiation similarly to explants that were not subjected to imaging (S1A–E,J,N,O Fig. and S1 and S2 Movies). After 18–24 h of time-lapse imaging (42–48 h post-dissection), NEUROG3$^+$ cells were detected by immunostaining, showing that the differentiation process occurred ex vivo, albeit less efficiently than in vivo (S1 Table).

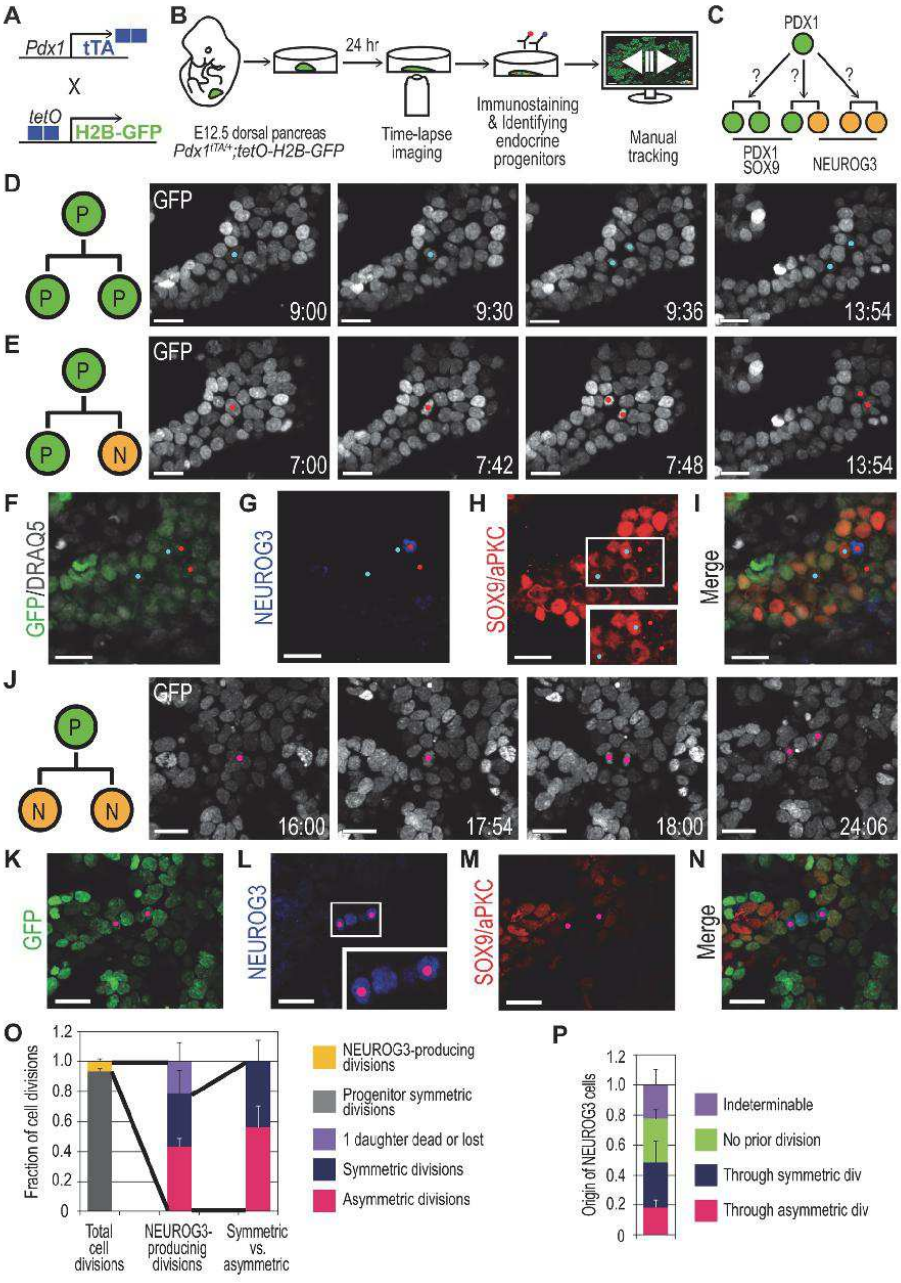
A
Pdx1 tTA
X
tetO H2B-GFP
B
E12.5 dorsal pancreas
Pdx1tTA/+;tetO-H2B-GFP
24 hr
Time-lapse imaging
Immunostaining & Identifying endocrine progenitors
Manual tracking
C
PDX1
?
?
?
PDX1 SOX9
NEUROG3
D
P
P
P
GFP
9:00
9:30
9:36
13:54
E
P
P
N
GFP
7:00
7:42
7:48
13:54
F
GFP/DRAQ5
G
NEUROG3
H
SOX9/aPKC
I
Merge
J
P
N
N
GFP
16:00
17:54
18:00
24:06
K
GFP
L
NEUROG3
M
SOX9/aPKC
N
Merge
O
Fraction of cell divisions
1.2
1.0
0.8
0.6
0.4
0.2
0
Total cell divisions
NEUROG3-producinig divisions
Symmetric vs. asymmetric
NEUROG3-producing divisions
Progenitor symmetric divisions
1 daughter dead or lost
Symmetric divisions
Asymmetric divisions
P
Origin of NEUROG3 cells
1.2
1.0
0.8
0.6
0.4
0.2
0
Indeterminable
No prior division
Through symmetric div
Through asymmetric div

Fig 1. Live imaging reveals both asymmetric and symmetric emergence of NEUROG3 cells. (A) Scheme summarizing the genetic strategy to visualize PDX1$^+$ pancreatic progenitors for live imaging. (B) Scheme of imaging and analysis. Pancreatic explants from E12.5 *Pdx1$^{tTA/+}$;tetO-H2B-GFP* embryos are cultured, and 3-D time-lapse imaging is done for 18–24 h. Then, the explants are immunostained for markers, and endocrine progenitor (NEUROG3) cells are back- and forward-tracked. (C) Model of pancreatic progenitor divisions. A PDX1$^+$ progenitor can produce two PDX1$^+$/SOX9$^+$ progenitor daughters, two NEUROG3$^+$ endocrine progenitor daughters, or one PDX1$^+$/SOX9$^+$ daughter and one NEUROG3$^+$ daughter. (D) Still images of live imaging in 3-D maximum intensity projection from S3 Movie, illustrating a symmetric (P/P) division producing two progenitor daughters (blue spots). White nuclei correspond to H2B-GFP signal in the cells originating from the pancreas epithelium. (E) Still images from S3 Movie, illustrating an asymmetric (P/N) division producing two daughters with different fates (red spots). (F-I) Images of fixed explant with native GFP and nuclear staining DRAQ5 overlay (F) and immunostained for NEUROG3 (G) and SOX9/aPKC (H). Blue spots correspond to cells in (D) and red spots to cells in (E). Inset in (H) shows high magnification image of SOX9 staining. Note both blue spotted cells are SOX9$^+$, but only one red spotted cell is SOX9^{low} (H), and the other red spotted cell is NEUROG3$^+$ (G). (J) Still images from S4 Movie, demonstrating a symmetric (N/N) division producing two daughters with the same fate (pink spots). (K–N) Images of fixed explant with native GFP (K) and immunostained for NEUROG3 (L) and SOX9/aPKC (M). Pink spots correspond to cells in (J), and both are NEUROG3$^+$/SOX9$^-$. Inset in (L) shows NEUROG3 staining (four NEUROG3$^+$ cells in a row) in high magnification. (O) Analysis of progenitor division patterns from live imaging. Total cell divisions are counted from four cropped positions from four live imaging movies, and fraction of NEUROG3-producing cell divisions is calculated from the corresponding positions (yellow bar over grey bar). NEUROG3-producing divisions (pink, blue, and purple bars) are counted from entire position of four movies. (P) Analysis of NEUROG3 emergence from four live imaging movies. 18.4% ± 5.0% cells emerge through P/N divisions, and 29.8% ± 14.2% through N/N divisions. 29.3% ± 5.9% do not exhibit prior division, and 22.4% ± 10.6% were either lost (17.5% ± 7.7%) or dead (8.9% ± 3.4%). Cells lost or gone out of frame were categorized as indeterminable (purple bar). Numbering denotes elapsed time in h:min, and in the cell division diagrams P indicates progenitor and N, NEUROG3 (D,E,J). Scale bars, 20 μm. Histograms and error bars represent the mean and standard deviation ($n = 4$). See S2 Table for further data.

doi:10.1371/journal.pbio.1002111.g001

Pancreatic Progenitors Divide in Three Different Modes That Differentially Contribute to Pancreas Expansion and Endocrine Differentiation

To determine how single progenitor cells contribute to balancing global pancreas expansion with endocrine progenitor generation (Fig. 1C), we systematically back-tracked NEUROG3$^+$ endocrine progenitors in 3-D, as well as a random subset of SOX9$^+$ pancreatic progenitors that were identified from immunostaining images and mapped onto the last frame of time-lapse movies. Once a cell division was observed through back-tracking, the sister cell was then forward-tracked, and its fate was determined by referring to the immunostaining. The tracking revealed that pancreatic progenitors divided in one of three different modes. The first type of division was symmetric, giving rise to two SOX9$^+$ progenitor cells (P/P division; S3 Movie and Fig. 1D,F–I). The second type was asymmetric, giving rise to a SOX9$^+$/NEUROG3$^-$ pancreatic progenitor and a NEUROG3$^+$ endocrine progenitor (P/N division; S3 Movie and Fig. 1E,F–I). The last type was symmetric endocrinogenic, producing two NEUROG3$^+$ cells (N/N division; S4 Movie and Fig. 1J–N). In order to quantitatively account for each division mode, we analysed 1,628 divisions comprising all observed division events of *Pdx1$^{tTA/+}$;tetO-H2B-GFP* cells from randomly selected positions from four time-lapse movies. Thus, non-NEUROG3-producing divisions include both bi-potent progenitors and acinar cells, since Pdx1$^+$ cells are multipotent at E13.5. This quantification revealed 6.6% ± 1.6% of divisions producing endocrine progenitors, and 93.4% ± 1.6% generating either progenitors or exocrine cells (Fig. 1O and S2 Table). Of all the divisions producing NEUROG3 cells that could be tracked, 56.3% ± 13.8% produced a SOX9$^+$ cell and a NEUROG3$^+$ cell (P/N division), and 43.7% ± 13.8% produced two NEUROG3$^+$ cells (N/N division; Fig. 1O). We could determine the origin of approximately half of NEUROG3$^+$ cells through P/N or N/N divisions in the past 24 h, while some NEUROG3$^+$ cells either did not exhibit prior division or were either lost or dead during tracking (Fig. 1P). Cell death might be a consequence of the explant culture since apoptosis is very rare in the pancreas epithelium in vivo [27]. Taken together, these results show that at E13.5–14.5 most progenitors undergo symmetric renewing divisions, accounting for pancreas size increase, while the remaining progenitors are approximately evenly split into those undergoing symmetric endocrinogenic division and asymmetric division.

Clonal Analysis Confirms the In Vivo Existence of Three Progenitor Division Types Based on Their Progeny

While ex vivo imaging enables constant monitoring of cell behaviours, it is performed in a somewhat artificial context. In order to determine whether pancreas progenitors undergo the same pattern of symmetric and asymmetric divisions in an in vivo context, we devised a clonal lineage tracing strategy (Fig. 2A) using *Hnf1bCreER* mice. Previously, this line was used to demonstrate that the E13.5 HNF1B$^+$ progenitor cells give rise to ductal and endocrine cells [3]. This could be accounted for either by individual cells giving rise to endocrine and ductal cells or by heterogeneity among HNF1B$^+$ cells, some giving rise to endocrine cells and others to ductal cells. To investigate this question, we subjected pregnant mice carrying E13.5 *Hnf1bCreER; mT/mG* embryos to a single low-dose intraperitoneal injection of 4-hydroxytamoxifen (Fig. 2B) to label pancreatic progenitors at a clonal density. We optimized conditions for clonal tracking leading to two-cell clones at E14.5 (Fig. 2B–G, S3 Table, and S5 Movie). Since we know from the time-lapse experiments that the majority of daughters from the same cell do not move more than 30 μm apart, we called labelled cells within 30 μm of each other a clone (S8 Fig.). Reiterations with a 60 μm radius led to similar outcomes. Whole-mount immunostaining of 22 pancreata and detection of 244 two-cell clones revealed that the majority of progenitors in which the fate could be determined divided symmetrically (P/P; Fig. 2E) into two SOX9$^+$ progenitors (59.8%; Fig. 2H). This proportion is lower than the 93.4% found in the explants, in part because the cells traced by HNF1B are a subgroup of PDX1$^+$ and SOX9$^+$ cells traced in the explants and some of the latter will give rise to acinar cells [2,4]. In vitro lineage tracing with *Hnf1bCreER;mT/mG* explants showed that 6.3% of clones became endocrine (S2 Fig. and S4 Table). This shows that the in vivo differentiation process is more efficient than in vitro differentiation. After the 24-h tracing period, we could not yet observe any INSULIN$^+$ clones in vivo, suggesting NEUROG3$^-$ or SOX9$^-$ clones might be in transition to endocrine differentiation. Of the NEUROG3-producing two-cell clones in which the fate of both daughters could be determined, 61.8% were asymmetric, generating one NEUROG3$^+$ daughter and a SOX9$^+$ progenitor (P/N; Fig. 2F,H), and the remaining were symmetric with two NEUROG3$^+$ daughters (N/N; Fig. 2G,H). As a consequence, more NEUROG3$^+$ cells originated from symmetric divisions (Fig. 2I). These results thus provide in vivo evidence of asymmetric and symmetric endocrinogenic progenitor divisions, as well as of symmetric renewal of progenitors, confirming the modes of divisions detected by the explant tracking data.

From the above data with regard to fate-determinable two-cell clones, we estimated expected ratios of P/P, P/N, and N/N divisions to be 69.9%, 18.6%, and 11.5%, respectively, after excluding indeterminable clones. Progenitors undergoing symmetric differentiating divisions will contribute all of their progeny to the differentiated pool, whereas asymmetrically dividing progenitors will contribute only one half of their progeny to this pool. We can therefore directly estimate the probability of differentiation of new-born cells to be 20.8% ([0.5 × 18.6] + 11.5)%, which is consistent with a net expansion of developing pancreas (S1.5 Text).

If sibling cells adopted their fate independently of each other, the expected fractions for each division type would be 62.7% for symmetric proliferative, 4.3% for symmetric differentiative, and 33% for asymmetric. Notably, these last two fractions deviate from the experimentally reported ones (Fig. 2H), contradicting the hypothesis of independent sibling fate allocation. This is further supported by statistical tests indicating a significant divergence from the independence ratios (S1.5 Text). Similar calculations can be made on the in vitro data leading to the same conclusion that a single conversion event leads to symmetric endocrine cell production (Fig. 1O and S1.5 Text).

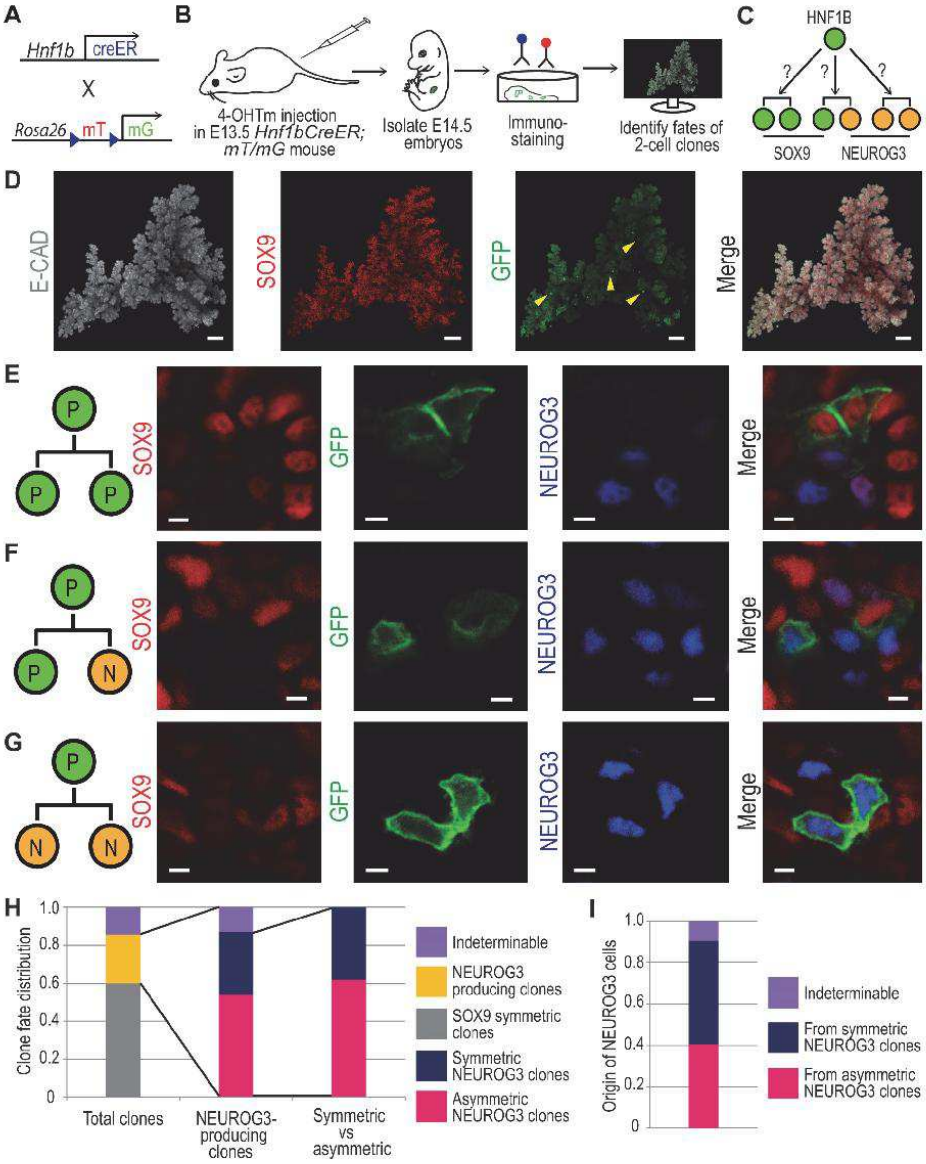

Fig 2. Asymmetric and symmetric divisions revealed by in vivo lineage tracing of progenitors at clonal density. (A) Scheme summarizing the genetic strategy to label HNF1B$^+$ pancreatic progenitors with membrane-localized GFP reporter (mG) for lineage tracing. Upon CRE recombination, membrane-localized Tomato (mT) is excised, allowing mG expression. (B) Schematic overview of the lineage tracing strategy used to trace the fate of progeny from single progenitor cells labelled at clonal density. E13.5 pregnant mice carrying *Hnf1bCreER;mT/mG* embryos received a single intraperitoneal injection of 0.175 mg 4-OH tamoxifen. After 24 h, pancreata were subjected to whole-mount immunostaining, imaging, and 3-D reconstruction to detect recombined two-cell clones. (C) Model of two-cell clone lineage tracing. A HNF1B$^+$ progenitor can produce two SOX9$^+$ progenitor clones, two NEUROG3$^+$ endocrine progenitor clones, or one PDX1$^+$/SOX9$^+$ and one NEUROG3$^+$ clones. (D) Maximum intensity projection of 3-D reconstructed E14.5 dorsal pancreas after

immunostaining for E-CADHERIN, SOX9, and GFP. Arrowheads indicate clones displaying recombination of the mT/mG reporter, detected by anti-GFP immunostaining, while membrane Tomato signal was diminished during staining process. (E) Optical sections from a whole-mount imaged dorsal pancreas demonstrating symmetric generation of SOX9$^+$ progeny (P/P) from a single dividing progenitor cell. (F) Optical sections demonstrating clonal progeny with asymmetric fates, generating one NEUROG3$^+$ and one SOX9$^+$ daughter (P/N). (G) Optical sections demonstrating clonal progeny with symmetric NEUROG3$^+$ fates (N/N). (H) Quantification of two-cell clone fate patterns after in vivo lineage tracing. 244 two-cell clones derived from 22 dorsal pancreata were scored according to SOX9 and NEUROG3 status. Indeterminable refers to clones that could not be categorized because of one or both daughters being both SOX9- and NEUROG3-negative after immunostaining. (I) Quantification of the number of NEUROG3$^+$ cells generated by the different clone patterns. 84 NEUROG3$^+$ cells were detected in 63 NEUROG3$^+$ two-cell clones. Indeterminable refers to clones in which the second daughter was neither NEUROG3- nor SOX9-positive. Scale bars, 100 μm (D) and 3 μm (E–G). Histograms represent the mean (n = 22). See S3 Table for further data.

doi:10.1371/journal.pbio.1002111.g002

A New Neurog3-RFP Reporter Reveals Synchrony in Differentiation and Differentiation Delays Suggestive of Cell Cycle–Dependent Priming

To investigate the dynamics of differentiation, we generated transgenic *Neurog3-RFP* reporter lines that can be used for live imaging together with H2B-GFP (Figs. 3A,B and S3A,B). Immunostaining for NEUROG3 and comparison with red fluorescent protein (RFP) from E14.5 *Neurog3-RFP* pancreas revealed that 40.1% ± 4.5% of NEUROG3$^+$ cells were co-expressing RFP, while the remaining NEUROG3$^+$ cells were RFP$^-$ (S3C,D Fig.). Some discrepancies may be expected because of the transient nature of *Neurog3* expression and the different onset and decay kinetics of the RFP protein compared to the NEUROG3 protein (S1.3 Text). Moreover, 77.1% ± 2.8% of RFP$^+$ cells were NEUROG3$^-$ due to probable delay and perdurance of RFP as compared to that of NEUROG3 [28], as also seen for other reporters [29–31]. This maintenance was attested by the detection of hormones in 18.5% ± 2.3% of RFP$^+$ cells. To further address the reliability of the reporter and assess its incidence in our analysis, we compared this line to the enhanced yellow fluorescent protein (EYFP) knock-add-on allele, which has been reported to show a greater overlap with NEUROG3 protein [29] and which is, in principle, less susceptible to exogenous chromatin environments, being in the endogenous locus. Our imaging of explants expressing one allele of EYFP and one of RFP (S4A,B Fig.) showed that all RFP$^+$ cells were also EYFP$^+$ (S4C Fig. and S5 Table), indicating no false positives due to genomic environment. Single cell tracing showed that RFP was turned on 4.7 ± 1.1 h after EYFP was detected (S4D Fig.); 11.6% ± 3.7% of EYFP$^+$ cells never became RFP$^+$, indicating the system was largely faithful.

From time-lapse imaging extended to 48 h, we could observe a dynamic change of RFP signal in single cells from the onset of fluorescence: gradual increase and a subsequent decrease, which reflects the transient expression of NEUROG3 [32]. Our analysis predicts a short half-life of 5–6 h for RFP in a cell, most probably due to continuous laser exposure. We estimate a "perdurance" of detectable fluorescence of more than 20 h (see S5 Fig. and S1.3 Text) and a minimum delay between cell priming and RFP onset of approximately 5 h. Monitoring all events of RFP onset (n = 323; Fig. 4A) initially suggested waves of cellular differentiation at the tissue level. However, statistical analysis of the timing of onset events showed that these are also compatible with a stochastic process of cell differentiation with homogeneous differentiation rate (i.e., a Poisson process) throughout the imaging period (S6 Fig. and S1.4 Text). While we cannot rule out a periodic process underpinning *Neurog3* expression, confirmation of this would require more data points.

Similar to earlier tracking, RFP$^+$ cells were back-tracked from the last time point in time-lapse movies, their prior division was monitored, and sister cells were forward-tracked. Quantifications (S6 Table) revealed that among the RFP-producing divisions where the fate of the two sisters was determinable, as follows: 60.2% ± 11.9% were asymmetric divisions producing a progenitor and a RFP$^+$ daughter (P/R; S6 Movie, and Fig. 3C–G,N), and 39.8% ± 11.9% were symmetric divisions producing two RFP$^+$ daughters (R/R; S7 Movie, and Fig. 3H–N). In these

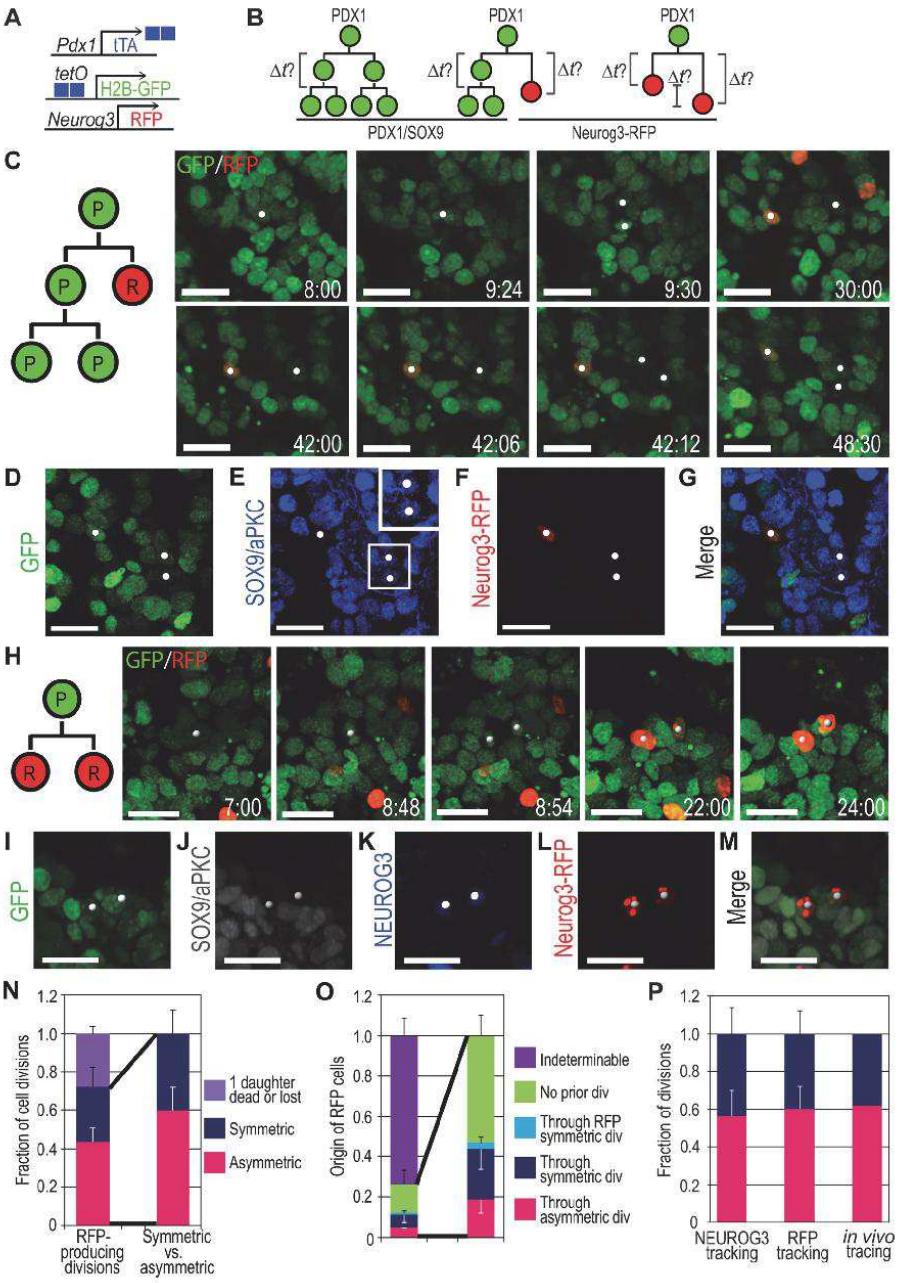
A
Pdx1 tTA
tetO H2B-GFP
Neurog3 RFP
B
PDX1
PDX1
PDX1
Δt?
Δt?
Δt?
Δt?
Δt?
PDX1/SOX9
Neurog3-RFP
C
GFP/RFP
8:00
9:24
9:30
30:00
42:00
42:06
42:12
48:30
P
P
R
P
P
D
GFP
E
SOX9/aPKC
F
Neurog3-RFP
G
Merge
H
GFP/RFP
7:00
8:48
8:54
22:00
24:00
P
R
R
I
GFP
J
SOX9/aPKC
K
NEUROG3
L
Neurog3-RFP
M
Merge
N
Fraction of cell divisions
1.2
1.0
0.8
0.6
0.4
0.2
0
1 daughter dead or lost
Symmetric
Asymmetric
RFP-producing divisions
Symmetric vs. asymmetric
O
Origin of RFP cells
Indeterminable
No prior div
Through RFP symmetric div
Through symmetric div
Through asymmetric div
P
Fraction of divisions
NEUROG3 tracking
RFP tracking
in vivo tracing

Fig 3. Extended live imaging with Neurog3-RFP reporter reveals the dynamics of progenitor cell cycle and differentiation. (A) Scheme summarizing the genetic strategy to visualize PDX1$^+$ pancreatic progenitors and *NEUROG3*$^+$ endocrine progenitors for live imaging. (B) Model of pancreatic progenitor divisions with a *Neurog3-RFP* reporter. After second division of self-renewing progenitors, cell cycle length can be obtained. Using the *Neurog3-RFP* reporter, endocrine differentiation timing and synchrony can be obtained. (C) Still images from S6 Movie, demonstrating an asymmetric (P/R) division producing one Neurog3-RFP$^+$ daughter and two other granddaughters (white spots) from a *Pdx1*$^{tTA/+}$*;tetO-H2B-GFP;Neurog3-RFP* explant. After the first division, one daughter turns on RFP (before elapsed time 30:00), and later the other daughter divides, producing two granddaughters (at elapsed time 42:12). (D-G) Images of fixed explant with native GFP (D) and immunostained for SOX9/aPKC (E) and Neurog3-RFP (F, staining for MYC-tag). White spots correspond to cells in (C), and one is RFP$^+$ and two granddaughters are SOX9$^+$ (E,F). Inset in (E) shows high magnification image of SOX9 staining. (H) Still images from S7 Movie, demonstrating a symmetric (R/R) division producing two Neurog3-RFP$^+$ daughters (grey spots). After the division, both daughters turn on RFP. (I–M) Images of fixed explant with native GFP (I) and immunostained for SOX9/aPKC (J), NEUROG3 (K), and Neurog3-RFP (L, staining for MYC-tag). Both daughters are NEUROG3$^+$/RFP$^+$. (N) Fraction of RFP-producing cell divisions. Each category (pink, blue, and purple bars) was counted from three movies. (O) Analysis of RFP emergence from three live imaging movies. In three cases, RFP$^+$ cells divided producing two RFP$^+$ cells each (cyan bar), and the majority of RFP$^+$ cells were either lost or moved out of frame during back-tracking (indeterminable, purple bar). (P) Fraction of asymmetric versus symmetric cell divisions from three different measurements: NEUROG3 tracking, Neurog3-RFP tracking, and in vivo clonal analysis. All three measurements exhibit equivalent rates of divisions. Numbering denotes elapsed time in h:min, and in the cell division diagrams P indicates progenitor and R, Neurog3-RFP (C, H). Scale bars, 20 μm. Histograms and error bars represent the mean and standard deviation (n = 3). See S6 Table for further data.

doi:10.1371/journal.pbio.1002111.g003

long time-lapse movies, many RFP$^+$ cells moved out of frame or were lost due to weak GFP signal before acquiring RFP expression (Fig. 3O and S6 Table). Excluding those indeterminable RFP cells, 18.8% ± 6.6% were generated through P/R division, 25.0% ± 10.0% through R/R division, and 3.2% ± 2.8% through RFP division, while no division was seen during the movie duration for 53.0% ± 10.3% of RFP cells (Fig. 3O). These RFP tracking results thus confirmed the calculated proportions of asymmetric versus symmetric divisions established from the previous live imaging and in vivo clonal analysis (Fig. 3P).

The dynamic reporter revealed highly synchronized differentiation after divisions producing two NEUROG3 cells, the RFP signal being detected in both daughters within 0.8 ± 0.4 h of each other (Fig. 4B, correlation coefficient between lag times 0.98 ± 0.002). This outstanding synchrony confirms that it is unlikely that the two daughters are induced by independent events and suggests that mother cells have been primed to differentiate into NEUROG3 cells prior to their division. This observation further suggests a defined time between priming and NEUROG3 expression (or its RFP proxy). In addition, asymmetrically generated NEUROG3 cells exhibited a significantly longer lag time between the division and RFP onset, as shown in Fig. 4C, further supporting an interplay between cell cycle, the differentiation priming event, and the division mode.

These results on the contrasting dynamics of differentiation between cells stemming from symmetric versus asymmetric division events are obtained with the RFP reporter, for which we have established a false negative rate of 11.6% (S4C Fig.). This implies that, far from amplifying the differences between the dynamics of differentiation between the two groups, we might be underestimating them. Specifically, our reporter may miss a subset of *Neurog3*-expressing cells, thus leading to mis-allocation of around 11.6% of symmetric events to asymmetric and therefore homogenizing the two categories and reducing the differences between them (See below).

A Model of Cell Cycle–Dependent Stochastic Priming of Progenitors Provides Quantitative Insight into the Dynamics of Cell Differentiation

To try to understand the mechanism underlying the emergence of endocrine progenitors, we devised a simple mathematical model [33] of cell proliferation dynamics based on the lineage and differentiation dynamics data. The model is based on the premise that proliferating progenitor cells primed for *Neurog3*-dependent differentiation might either exit the cell cycle and become terminally differentiated or commit to complete the cell cycle and produce two terminally differentiated cells via mitosis (Fig. 5A–C). Thus in this model there are three, rather than two, cell types: (i) NEUROG3-primed (*N*) cells, which are post-mitotic; (ii) cells primed for

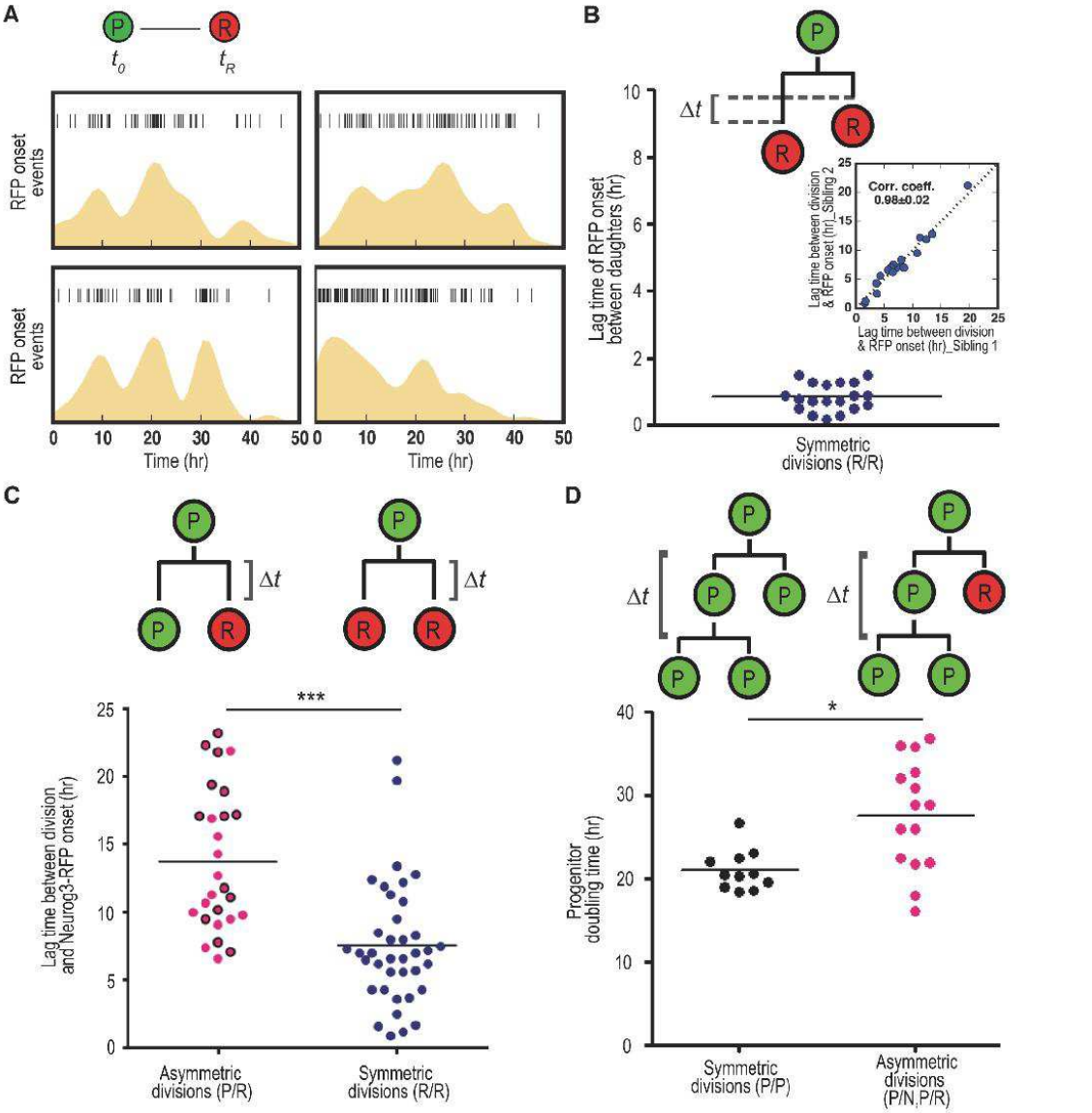

Fig 4. Analysis of differentiation and cell cycle dynamics from live imaging. (A) Analysis of Neurog3-RFP onset in four locations from three different time-lapse movies ($n = 56$, 89, 54, and 125, respectively). Each vertical bar symbol indicates an onset event, and the yellow area displays the probability, obtained by kernel density estimation, of an event occurring over time. These suggest that cell differentiation might not be a homogeneous process; however, further statistical analysis does not rule out this possibility (S1.4 Text). (B) Lag time of Neurog3-RFP onset between daughters derived from symmetric (R/R) divisions ($n = 19$). Symmetrically fated daughters exhibited synchronized expression of Neurog3-RFP, as pointed out by the highly correlated lag time between division and RFP onset (inset). (C) Lag time between division and Neurog3-RFP onset in asymmetric (P/R, $n = 27$) versus symmetric (R/R, $n = 38$) divisions. Note the data are pooled from three live imaging movies. RFP cells from P/R divisions took a significantly longer time to turn on RFP than cells from R/R divisions. Black-outlined red circles from P/R division ($n = 14$) indicate P/R divisions producing grand-daughters through progenitor daughter division. (D)

Doubling time of progenitors originating from either symmetric (P/P, black circle) or asymmetric (P/N and P/R, pink circle) divisions. Doubling time of asymmetrically generated progenitors took longer than symmetrically generated progenitors. Statistical analyses were done using two-tailed Mann-Whitney test. *** $p < 0.0001$ and * $p = 0.04$ (C,D).

doi:10.1371/journal.pbio.1002111.g004

differentiation but committed to cell cycle completion (L cells); and (iii) progenitor (*P*) cells, which will not differentiate (Fig. 5D). We assigned a probability *q* (the differentiation probability) for the differentiation of progenitors and a probability, θ, *for* primed cells to become N (1- θ to become L). Thus, the model describes the differentiation process in terms of two probabilities, which can be directly inferred from the lineage data (S1.6 Text), i.e. it has no free parameters. From the in vivo clonal analysis data, we estimate $\theta = 56.5\%$ and, as we have already seen, $q = 20.8\%$. This means that approximately one-half of the progenitors primed for differentiation become post-mitotic (P→N; 56.5%), while the other half (P→L[→N/N]; 43.5%) will undergo one last division before differentiating. Because this latter group of cells (L) is transient and contributes terminally differentiated cells (N), its expected abundance in the tissue is residuary. The model predicts that, at any given time, only 9.8% of cells in the developing tissue are primed progenitors committed to division-cycle completion (L), yet this small fraction accounts for 93.8% of the symmetric differentiative divisions (L→N/N) and might therefore explain our observation that the fates of sibling cells are linked (S1.6 Text). The remainder of symmetric differentiative divisions is interpreted to result from random, independent priming in two sister P cells.

The model also allows multiple interpretations for the probability of becoming L versus N (e.g., exposure to differentiation signals, gene expression noise, etc.). One such interpretation is the timing of the priming event after division (i.e., θ can be construed as accounting for a cell cycle restriction point). For instance, if a cell is primed early after division it might differentiate and halt the cell cycle, whereas if the priming event occurs late in G1, the cell might have already committed to cell cycle completion. Such specific reading of the model, which we adopt hereafter, leads to a few qualitative predictions on the dynamics of differentiation. First and foremost, the vast majority of sibling cells (93.8%) from symmetric divisions will have a perfectly synchronized differentiation program. According to the model, differentiated cells stemming from symmetric divisions shall turn on the differentiation program, on average, much earlier than those from asymmetric divisions (S1.6 Text). To quantitatively account for these predictions and compare them to the experimental data, we performed computational simulations of the model ($n = 10{,}000$ clones, S11 Fig.) including the observed variability in the cell cycle length as well as the dynamics of the fluorescent reporter (Figs. 5E–G, S9, S11 and S1.3, S1.4, and S1.6 Text; data deposited in the Dryad repository: http://dx.doi.org/10.5061/dryad.4b58d [34]). The simulations reproduced the differences in the onset of the reporter in cells stemming from symmetric versus asymmetric divisions (Figs. 5E,F, S6E,F, and S9) and also for the high degree of synchronization between sibling cells (Figs. 5G, S6G, and S9). Furthermore, when we included the 11.6% false negative rate in the reporter (S4C Fig.) of the model, the results were not significantly affected (S10 Fig. and S1.6 Text).

The results of the model led us to experimentally characterize the cell cycle. We used FACS-sorting of *Pdx1*$^{tTA/+}$;tetO-H2B-GFP^{+};Ngn3-RFP^{-} cells marking pancreatic progenitors at E14.5 to establish their cell cycle partition and observed that 69% were in G0/G1, 27% in S and 5% in G2/M, whereas 98% of Neurog3-RFP^{+} cells were in G0/G1 (S7 Fig.). The progenitors thus spend the majority of their time in G1. Our hypothesis is that priming in early G1 would lead to differentiation and exit of the cell cycle, and its mother would thus have an apparent asymmetric cell division. In contrast, priming in late G1 after the cell has committed to complete the

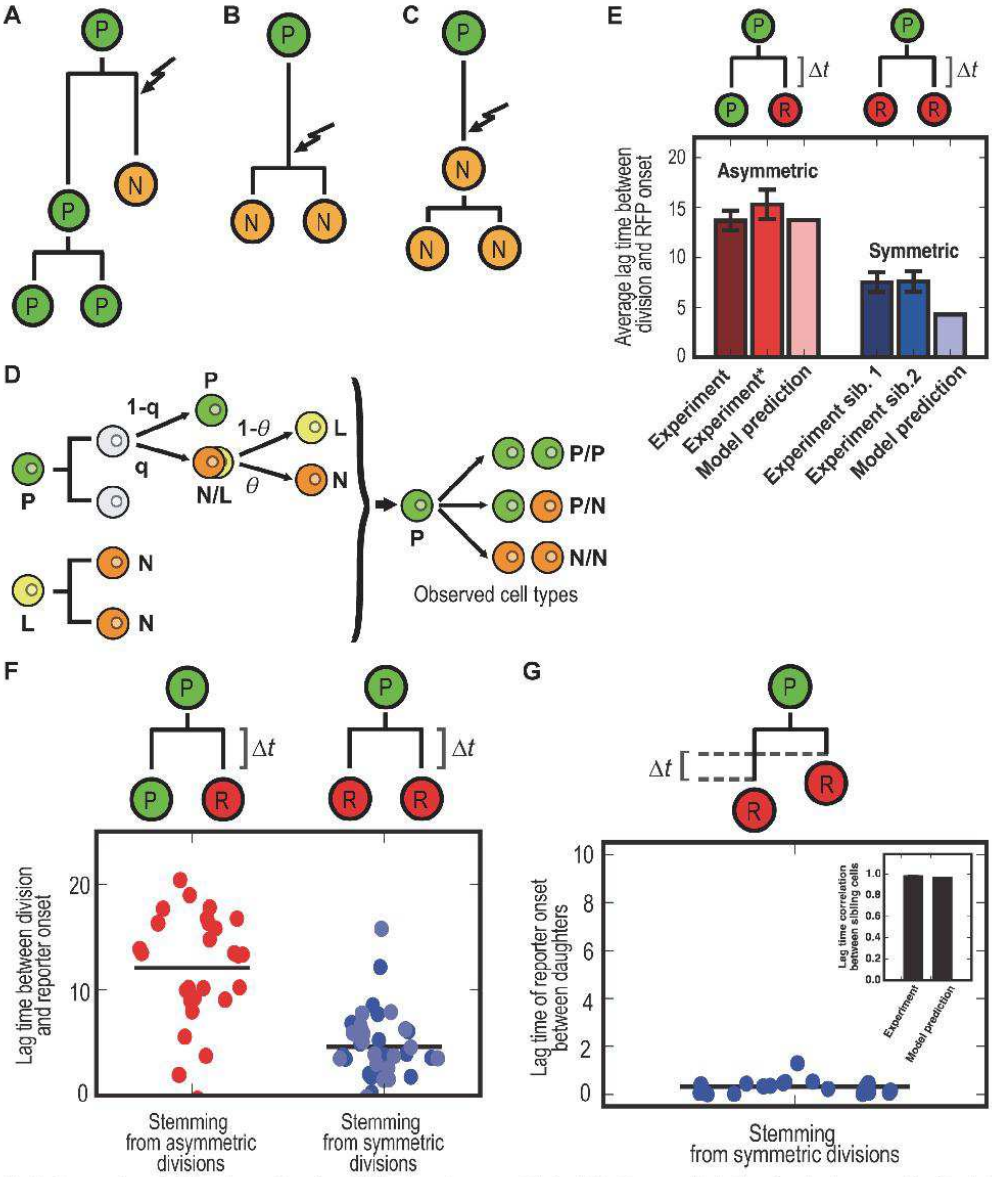

Fig 5. Proposed model. The observations from 3-D live imaging suggest that a distinct temporal induction of endocrine progenitor fate during the cell cycle may result in different fates of progenitors. As the majority of NEUROG3 cells are known to be largely post-mitotic [11], we propose models for three modes of cell division, resulting in NEUROG3 daughter differentiation according to a priming time point. (A) Asymmetrically fated daughter differentiation after progenitor cell division (P→P/N). Only one daughter may be induced (arrow) after the mother division, resulting in exit of cell cycle and its differentiation to NEUROG3, while the other daughter is fated as a progenitor, resulting in self-renewal. (B) Symmetrically fated daughter differentiation after progenitor cell division (P→N/N). Before mitosis, the progenitor may be induced to differentiate into an endocrine progenitor, complete the cell cycle, and divide, resulting in both daughters differentiating into NEUROG3. (C) Symmetrically fated daughters through symmetric division of endocrine progenitors (N→N/N). Considering

endocrine progenitors post-mitotic, the progenitor may be induced to differentiate into endocrine progenitor, but has not yet finished the cell cycle before the cell actually differentiates into an endocrine progenitor. Therefore, to complete the cell cycle, a recently differentiated NEUROG3 cell may divide and give rise to two NEUROG3 daughters. (D–F) We have developed a mathematical model of cell cycle–dependent stochastic priming of progenitors to endocrine fate. (D) Schematic of the model in which pancreatic progenitors (P, green circles) stochastically are primed for differentiation with probability *q*. Primed cells can either exit the cell cycle and differentiate into NEUROG3 (N) with probability *θ* or conclude the cycle (L) and give rise to two NEUROG3 cells. (E) The proposed model accounts for the observed frequencies of each division mode and predicts differential RFP onset dynamics in asymmetric and symmetric divisions. "Experiment*" bar in Asymmetric category denotes asymmetric divisions accounting for a RFP daughter and a self-renewing RFP$^-$ daughter (n = 14), whereas "Experiment" bar includes all the asymmetric divisions (refer to Fig. 4C). (F) The model with experiment-matching number of clones (out of 10,000 simulated clones) predicts a larger lag time between division and RFP onset in cells stemming from asymmetric divisions versus symmetric divisions. (G) Correlation of RFP lag times between sibling cells predicted by the model also matches that which was experimentally measured.

doi:10.1371/journal.pbio.1002111.g005

cell cycle through DNA replication and mitosis would lead to an apparent symmetric differentiative cell division.

Finally, simulations also predicted the existence of a residual fraction of primed cells that would turn on the reporter immediately before dividing. Noticeably, although most RFP$^+$ cells did not divide, we observed 3 cases of RFP$^+$ cell division producing six cells (Fig. 6, S8 Movie, and S6 Table) and thus accounting for 3.2% ± 2.8% of all tractable RFP cells. The average time between RFP signal acquisition and division was 1.7 ± 0.8 h. This result is in agreement with the previous estimations of the progression of NEUROG3 cells through S-phase (BrdU incorporation) [11] and further shows that the NEUROG3 cells can exceptionally progress through mitosis at an early stage of their life [29].

Analysis of the Expansion Potential of Progenitors

The longer movies enabled the observation of multiple rounds of division and the quantification of cell cycle parameters (Fig. 3B). They first confirmed that the daughter cells qualified as progenitors after asymmetric cell division based on SOX9 expression (Fig. 1H) were functionally behaving as progenitors. Indeed, among P/R divisions (n = 27), we observed 14 events where the RFP$^-$ daughter divided, producing second-generation progeny (S6 Movie and

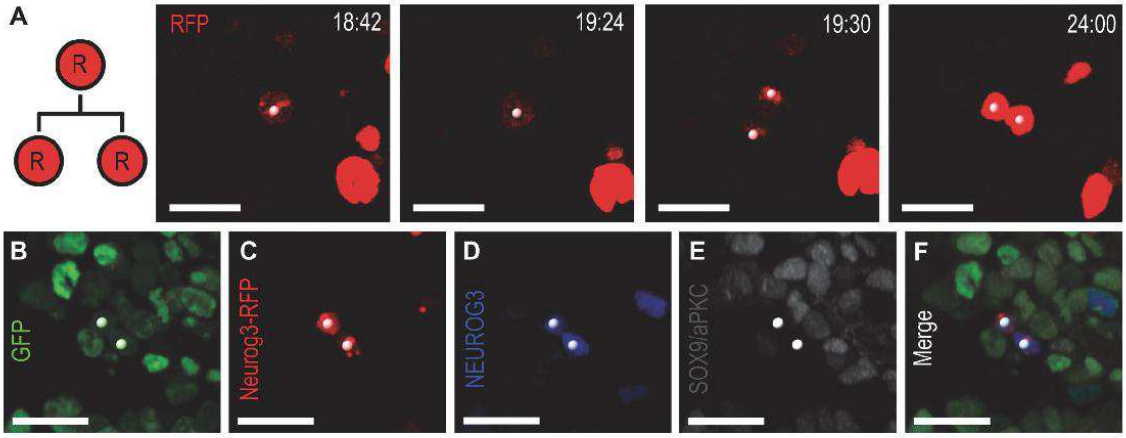

Fig 6. A small number of Neurog3-RFP cells divide into two NEUROG3$^+$ cells. (A) Still images from S8 Movie, demonstrating division of Neurog3-RFP cell (white spots) in RFP channel from a *Pdx1$^{(TA)/+}$;tetO-H2B-GFP;Neurog3-RFP* explant. (B–F) Images of fixed explant with native GFP (B) and immunostained for Neurog3-RFP (C, staining for Myc-tag), NEUROG3 (D) and Sox9/aPKC (E). Both daughters are NEUROG3$^+$/RFP$^+$. Numbering denotes elapsed time in h:min (A). Scale bars, 20 μm.

doi:10.1371/journal.pbio.1002111.g006

Fig. 3C). Of those 14 cases, we observed two events where one or both granddaughters divided again, producing third-generation progeny. For all of those, immunostaining at the end point revealed that the RFP^- progeny were $SOX9^+$ progenitors (Fig. 3E). In such cases, we could calculate the doubling time of daughter progenitor divisions, and we compared it between P/P and P/N or P/R divisions (Fig. 4D). The doubling time of self-renewing progenitors from P/P divisions was shorter than that from P/N or P/R divisions ($p = 0.04$, 21.0 ± 2.4 h and 26.5 ± 7.3 h, respectively). Moreover, the distribution of data points was greater in the asymmetric cell divisions. Finally, the time-lapse movies revealed that pancreatic epithelial cells were highly dynamic and that two daughters migrated to distances up to 64 μm apart from each other in the 24 h following division regardless of division mode (S8 Fig.).

Discussion

In this study, we elucidate the contribution of single cell decisions to the balance between expansion and differentiation in the pancreas. Our lineage analysis, combining in vivo genetic clonal tracing with dynamic imaging in explants, reveals the existence of three kinds of divisions: symmetric progenitor self-renewal, symmetric endocrinogenic divisions leading to two $NEUROG3^+$ endocrine progenitors, and asymmetric divisions generating a pancreatic progenitor and an endocrine progenitor. Furthermore, we show that progenitors are stochastically primed for endocrine differentiation, and that timing of induction in $NEUROG3^+$ cells within the cell cycle establishes the division mode. Whereas late-induced cells complete the cell cycle, resulting in a differentiative symmetric division, early induced cells exit the cell cycle, in which scenario their mother would have produced asymmetric progeny. The results can alternatively be interpreted as $HNF1B^+$ cells being a mix of three pre-determined populations, amongst which only one is truly bipotent. However, the clonal analysis performed in vitro shows different proportions of P/P, P/N, and N/N divisions as compared to in vivo, which would not be expected if the three $HNF1B^+$ subpopulations were predetermined (unless some would preferentially die, which was not observed). Our data is most consistent with a model in which all progenitors are similar, except for their cell cycle stage, and can be primed for endocrine specification with a differentiation probability of around 20% in vivo. Future studies should reveal how this probability changes with time. For example, how it evolves to the cessation of differentiation at the end of gestation, leading to homeostatic conditions that rely primarily on slow self-duplication of differentiated populations [35]. On the other hand, a first phase of symmetric progenitor expansion followed by an increase in the probability of differentiation minimizes the time to form mature organs [36] and may also be expected to occur in the pancreas. Analogous studies are also needed in the human pancreas, as the size of the organ and the length of the differentiation stage are much greater, and several parameters such as cell cycle length of progenitors, probability of differentiation, and ratio of symmetric and asymmetric differentiative divisions may differ.

The high correlation between our in vivo and in vitro results (Fig. 3P) rules out erroneous interpretations due to in vitro artefacts and biases caused by subpopulations of progenitors marked by HNF1B at low tamoxifen doses. Spatially, the endocrinogenic divisions were observed in the centre of the pancreas where the $HNF1B^+$ progenitors reside, but no areas of preferential symmetric or asymmetric division were observed.

Our dynamic data, including the synchrony in differentiation of symmetrically produced endocrine progenitor cells and their shorter lag from division to differentiation, argue that the specification event can occur at different phases in the cell cycle conditioning the ability to execute a final division or not (Fig. 5A,B). This is further supported by our analysis of the cell cycle–dependent priming model, which displays a good fit to the experimental results and

provides a causal understanding of the dynamics of the process. The model proposes parameters q and θ that can be measured in other systems to test its prevalence, and our analysis of previous data in other organs suggests that it may be more general rather than specific to the pancreas [33].

Although the molecular mechanisms of *Neurog3* priming remain to be elucidated, especially whether it is under cell-intrinsic or extrinsic control, our data provide information on the general principles. Intrinsic control may be based on asymmetric inheritance of molecular components during division [21–24] or incremental or oscillatory expression of transcriptional determinants [37]. Our results strongly argue against the iterative asymmetric inheritance of differentiation cues at the time of division, as seen in *Drosophila* neurogenesis and also reported in the mouse brain [24]. Indeed, if the specification was determined at the time of division, the differentiation should occur after the same lag time in symmetric and asymmetric cell divisions. Moreover, the lag time between division and Neurog3-RFP onset is very heterogeneous ranging from 0 to 20 h (Fig. 4C), which is difficult to reconcile with a specification occurring at the time of division. If either cumulative increase or oscillations of an intrinsic determinant promoting endocrine fate lead to differentiation, the progeny of progenitor daughters arising from asymmetric division may exhibit an endocrinogenic bias. On the contrary, these progeny were all $SOX9^{+}$ progenitors, which would rather suggest a negative bias. However, the movie duration might have been too short to observe differentiation after the second division. Moreover, we observe a slower doubling time of progenitor daughters from an asymmetric division, which may result from the inheritance of a factor that slows down the cell cycle [38–40]. Incremental specification could explain why the cell cycle time is also more heterogeneous in these progenitors. Our analyses are also compatible with extrinsic specification, for example, in the context of Notch-Delta-mediated lateral inhibition [41]. The apparent discrepancy with differentiation in the nervous system where uneven splitting of molecular cues at mitosis leads to asymmetric cell division requires further investigations in both systems. When quantified, the ratios of asymmetric and symmetric differentiation events are very similar in the pancreas and the nervous system [33], and our model would be compatible with the observation that lengthening of G1 impacts the cell division modes in the cortex [30]. Thus, an assessment of the differentiation dynamics in the nervous system similar to ours would be useful, and the possible existence of asymmetrically inherited of cues in mitotic cells in the pancreas can also be considered.

Our results reveal that the balance between expansion of progenitors and endocrine differentiation can potentially be regulated by either controlling the probability of endocrine cell induction or its timing in the cell cycle to boost the generation of endocrine cells in vitro for a cell therapy of diabetes. Our approach paves the way to establish how the frequency of division and the ratio of the different types of divisions vary over time and how their balance is controlled by signalling pathways such as Notch and FGF.

Materials and Methods

Mice

Genetically engineered mice used for this study were as follows: *Pdx1*$^{tTA/+}$ [42], *tetO-HIST1H2BJ/GFP* (*tetO-H2B-GFP*) [43], *Hnf1bCreER* [3], *Gt(ROSA)26Sortm4(ACTB-tdTomato,-EGFP)Luo/J* (*mT/mG*) [44], *N*eurog3-*EYFP* [29], and *N*eurog3-*RFP* (S3 Fig.). For embryonic stage, noon of the day when vaginal plug appeared was referred as E0.5.

The *N*eurog3-*RFP* transgenic construct (S3A Fig.) was generated by fusing 7.6 kb of the *Neurog3*-promoter [2] with a reporter construct composed of a chimeric intron; turbo RFP (Evrogen); a nuclear localization signal (NLS); a *Myc-tagC*; a bovine growth hormone

polyadenylation signal (bGH-PolyA). Transgenic mouse lines were obtained by pronuclear injection of the construct (Transgenic Core Facility, EPFL, Switzerland). Two different lines were obtained initially, exhibiting similar levels of RFP signal detectable by a wide-field fluorescent microscope, and one of the lines was used for this study. All animals were handled humanely according to the authorized protocols of Switzerland and Denmark.

3-D Live Imaging and Cell Tracking

Dorsal pancreata from E12.5 *Pdx1*$^{tTA/+}$;*tetO-H2B-GFP* or *Pdx1*$^{tTA/+}$;*tetO-H2B-GFP*;*Neurog3-RFP* were cultured on a fibronectin (Sigma)-coated coverslip, adapted from the previously published protocol [25]. GFP and RFP were readily detectable under wide-field fluorescent microscopes. We used a culture medium composed of Medium 199, 10% fetal calf serum, 1% Fungizone, and 1% penicillin/streptomycin (all from Gibco). After 24 h of culture that enabled stabilization of explant flattening to approximately 80 μm thick, pancreatic explants were imaged at a single-cell resolution using Leica SP5 or SP8 confocal microscopes with a 63X glycerol immersion objective in a humidified, heated, CO_2-controlled chamber. Tiled positions (9 [3x3] or 12 [3x4] tiles) were scanned in 256x256–280x280 format with around 40 μm Z-stack (voxel size, 0.506x0.506x1.3 μm^3–0.880x0.880x1.25 μm^3) every 6 min for 18–48 h. The GaAsP hybrid detection system (Leica HyD™) enabled a substantial reduction of laser power by 62.5% and increase in signal-to-noise ratio resulting in reduced scanning time, compared to conventional photomultiplier detectors. At each time point, it usually took approximately 5 min and 30 s to scan 9–12 tiled positions in 3-D. At the end point of image acquisition, the explants were fixed and prepared for whole-mount immunostaining.

Tiled images were stitched using either Leica AF6000 software or a custom-built Massive Stitcher plugin (Bioimaging and Optics Platform, EPFL, Switzerland) in Fiji. Imaris (Bitplane, Switzerland) software was used to track cells and their divisions in 3-D maximum intensity projection. Once immunostaining was done, NEUROG3$^+$ endocrine progenitor cells from staining images were manually identified on the last frame of time-lapse movies with *Pdx1*$^{tTA/+}$; *tetO-H2B-GFP* explants by GFP superimposition. The identified endocrine progenitors were first back-tracked to monitor their prior divisions. Once a division was observed, the other sister was forward-tracked to the final frame, and its fate was determined from the immunostaining images. For time-lapse movies from explants with *Ngn3-RFP* in addition to *Pdx1*$^{tTA/+}$; *tetO-H2B-GFP*, RFP$^+$ cells were back-tracked, and the fate of each sister was determined by immunostaining. For the quantification of total cell divisions, due to the technical difficulties in tracking all Sox9$^+$ cells from the immunostaining, we did not trace all the individual cells from those 1,628 divisions, but rather subtracted the tracked divisions that produced NEUROG3 cells from the total number of divisions.

In Vivo Clonal Analysis

Pregnant mice carrying *Hnf1bCreER;mT/mG* embryos were injected intraperitoneally with 0.175 mg 4-hydroxy (4-OH) tamoxifen (H6278, Sigma Aldrich) at E13.5. 4-OH tamoxifen was prepared as a 10 mg/mL stock in 90% corn oil and 10% ethanol and diluted to obtain the desired dose. Embryos were harvested at E14.5, and the dorsal pancreas was isolated and subjected to whole-mount immunostaining for GFP, SOX9, and NEUROG3, as indicated below. The fixation procedure eliminates native GFP and Tomato signals. After whole-mount immunostaining, dorsal pancreata were dehydrated through an ascending methanol series and subjected to clearing in a 1:2 solution of benzyl alcohol to benzyl benzoate (BABB). Cleared samples submerged in BABB were mounted on glass depression slides and imaged whole-mount using a Leica SP8 confocal microscope with a 20X oil objective at a 1024x1024 format.

3-D reconstruction of whole-mount imaged pancreata was performed using Imaris (Bitplane), enabling detection of recombined clones while preserving the spatial organization of the pancreas, thereby ensuring detection of clonal progeny by allowing interclone distance measurements. Two-cell clones were identified in 3-D space, and categorized according to SOX9 and NEUROG3 status. Recombined cells were only considered to be of clonal origin if the distance between recombined cells was less than 30 μm after the tracing period, based on live imaging data (S8 Fig.). The results were not sensitive to this parameter as using 60 μm as a maximal distance to be considered as a clone led to the same proportion of the three types of division (S2 Data).

Hnf1bCreER;mT/mG embryos were also used for in vitro clonal analysis by explanting pancreata at E13.5 and growing these at the air–liquid interface on 0.4 μm filters (Millipore). Explants were subjected to a 6 h pulse of 25 nM 4-OH tamoxifen in 100% ethanol to induce labelling at clonal density. Following tracing for 48 h, explants were fixed and subjected to whole-mount staining and imaging as indicated below.

Immunohistochemistry

Whole-mount immunostaining was performed after live imaging or for pancreata harvested from the lineage tracing. After fixation with 4% paraformaldehyde (PFA) for 5 min on ice, samples were washed in phosphate buffered saline (PBS) for 5 min three times. Then, they were dehydrated through 50% and 100% methanol, and could be stored at −20°C until later use. When ready, samples were rehydrated through 50% methanol and washing solution, PBS+0.5% Triton X-100 (Tx100). Throughout the procedure, all the solutions contained 0.5% Tx100, and all the incubation was undergone in 4°C. After blocking overnight in blocking solution (1% Bovine serum albumin+0.5% Tx100), samples were incubated with primary antibodies (S7 Table) in blocking solution for 24–48 h. After washing, secondary antibodies were applied overnight, followed by washing. Alexa fluorophore conjugated secondary antibodies (Invitrogen) were used. Stained explants were kept in PBS and imaged using a confocal microscope. For quantification from explants, NEUROG3^{+} cells were counted manually, and H2B-GFP^{+} cells were counted using a custom-made macro in Fiji.

Immunostaining of frozen sections from E14.5 *Neurog3-RFP* pancreata was performed as previously described [6], and images were taken with a Leica DM5500 microscope. Quantification was obtained by manually counting immunopositive cells on every sixth section.

Statistical Analysis and Probabilities

Statistical analyses were done by two-tailed Mann-Whitney U-test using GraphPad Prism software. Values were presented as the mean ± standard deviation.

Supporting Information

S1 Data. Excel spreadsheet containing, in separate sheets, the numerical data and statistical for Fig panels 1O, 1P, 2H, 2I, 3N, 3O, 3P, 4A, 4B, 4C, 4D, 5E, 5F, 5G, 6, and Model formulas.
(XLSX)

S2 Data. Excel spreadsheet containing, in separate sheets, the numerical data and statistical for Supplementary Fig panels S2, S3C, S4C, S4D, S4E, S5A, S5B, S6B, S7A, S7B, S7C, S7D, S8, and other data.
(XLSX)

S1 Fig. 3-D live imaging of dividing cells in pancreatic explants. (A–E) Still images of 24-h live imaging in 3-D maximum intensity projection from S1 Movie, showing an overall growth of explant and cell divisions. Numbering denotes elapsed time in h:min. (F–I) Images in 3-D projection of fixed explant with native GFP (G) and immunostained for NEUROG3 (H) and SOX9 (I). Inset shows NEUROG3$^+$ cells (H, nuclear signal; arrowheads) in high magnification. Channels in (H) and (I) are masked by native GFP channel (G) to exclude non-specific background in mesenchymal regions. (J–O) Images in 3-D maximum intensity projection of immunostained control explant without imaging and laser exposure. The overall morphology after 48 h of culture, equivalent to 24-h live imaging, reveals that the epithelium branches (J). The white square is an area zoomed in (K–O). Cells in the trunk region are differentiating into NEUROG3$^+$ endocrine progenitors (M, nuclear signal). The epithelium is intact as shown by E-CADHERIN staining (M), and branching ducts and acini are apically polarized as revealed by aPKC staining (O). Arrowheads in (K) indicate endocrine cell clusters. The blue channel (M) is masked by the native GFP channel (L) to exclude non-specific background in mesenchymal regions. A Z-stack is shown in S2 Movie (J–O). Scale bars, 50 μm.
(TIF)

S2 Fig. NEUROG3$^+$ endocrine progenitor generation is more efficient in vivo than in vitro. Comparison of two-cell clone frequency distribution from in vivo clonal analysis (left column, $n = 244$), and in vitro clonal analysis (right column, $n = 96$) using E13.5 *Hnf1bCreER;mTmG* explants cultured on filters.
(TIF)

S3 Fig. *Neurog3-RFP* transgenic line. (A) Construct. A 7.6 kb *Neurog3* promoter region is linked to an intron, open reading frame of turboRFP, which contains a nuclear localization signal (NLS) and a Myc-tagC (Myc), and a bGH-PolyA signal (PolyA). The transgenic construct injection resulted in two transgenic mouse lines. (B) Optical section of a pancreatic explant from a *Pdx1*$^{tTA/+}$*;tetO-H2B-GFP;Neurog3-RFP* embryo, immunostained for NEUROG3 (blue), SOX9 (white) and aPKC (white). The RFP (red) and GFP (green) channels are native signals from each fluorescent protein. (C) Characterization of Neurog3-RFP in the E14.5 pancreas: Proportion of RFP$^+$ (immunostained for Myc) (red) and RFP$^-$ (white) in NEUROG3$^+$ cells, and proportion of NEUROG3$^+$, Hormones$^+$ (identified by INSULIN [INS] and GLUCAGON [GCG]), and NEUROG3$^-$/Hormones$^-$ in RFP$^+$ cells. (D) Optical section of E14.5 *Neurog3-RFP* pancreas, immunostained for NEUROG3 (cyan), RFP (Orange; immnostained for Myc), and INS and GCG (Magenta). White arrowheads indicate RFP$^+$/NEUROG3$^+$ cells, and yellow arrowheads indicate RFP$^+$/NEUROG3$^-$ cells. Scale bars, 20 μm. Histograms and error bars represent the mean and standard deviation ($n = 4$).
(TIF)

S4 Fig. Comparison of *Neurog3-RFP* transgenic line to *Neurog3-EYFP* knock-add-on line. (A) Scheme summarizing the genetic strategy to evaluate *Neurog3-RFP* fidelity compared to *Neurog3-EYFP*. (B) Scheme of imaging and analysis. Pancreatic explants from E12.5 *Neurog3-EYFP*; *Neurog3-RFP* embryos are cultured, and 3-D time-lapse imaging is done for over 48 h. Then, EYFP- and RFP-expressing cells are tracked. (C) Quantification of EYFP and RFP cells at time 0 of time-lapse movies. Note that EYFP$^+$/RFP$^+$ bar (orange) includes cells that are initially RFP$^-$ but acquire RFP over time, whereas EYFP$^+$/RFP$^-$ bar indicates cells express EYFP only throughout the movie. All RFP$^+$ cells are EYFP$^+$ (brown bar). Histograms and error bars represent the mean and standard deviation ($n = 3$). (D) Lag time of RFP onset after EYFP onset. RFP expression is delayed by 4.7 (± 1.1) h in EYFP$^+$ cells. (E) Fluorescence intensity of EYFP and RFP in four cells in time-lapse movies. The green and red lines indicate EYFP and

RFP signals, respectively. Note RFP signal is delayed by several hours, and both EYFP and RFP signals have similar trend of increase and decrease over time. See S5 Table for further data.
(TIF)

S5 Fig. Dynamics of *Neurog3-RFP* during 48-hour time-lapse. (A) Fluorescence intensity of individual Neurog3-RFP cells over time. Different coloured lines indicate individual RFP cells. (B) Normalized fluorescence of all the RFP signals from (A) and aligned by 25% intensity to time 0. Black line indicates average intensity of all RFP signals. (C) Estimation of RFP half-life. Red line indicates the trend of exponential decay. RFP half-life is estimated as 5.3 h.
(TIF)

S6 Fig. Analysis of Neurog3-RFP onset from time-lapse movies. (A) RFP onset time distribution from four time-lapse movie positions (n = 56, 89, 54, and 125). Each circle indicates onset time of RFP cell. Red, blue, and yellow circles indicate RFP cells arising from asymmetric, symmetric, and RFP divisions, respectively. (B) Analyses of RFP onset Coefficient of Variance and sliding window for oscillatory patterns. The Coefficient of Variance of each time-lapse onset distribution is equivalent to a homogeneous process, which is equal to 1.
(TIF)

S7 Fig. Cell cycle analysis of e14.5 *Pdx1$^{tTA/+}$;tetO-H2B-GFP;Neurog3-RFP* pancreata. (A) Flow cytometry of dissociated pancreatic cells from pooled pancreata from a litter (10 embryos: 2 GFP$^+$/RFP$^+$, 1 GFP$^+$, 1 RFP$^+$, and 6 negative pancreata) for DNA content by DAPI staining. (B) Cell cycle analysis of pancreatic progenitors (Pdx1$^{tTA/+}$;tetO-H2B-GFP) by DAPI-stained DNA content. This panel shows 66.3% of cells in G1/G0 phase, 29.2% in S phase, and 4.5% in G2/M phase. (C) Cell cycle analysis of endocrine progenitors (Neurog3-RFP) by DAPI-stained DNA content. Note 97.2% of cells in G1/G0 phase, 1.6% in S phase and 1.2 in G2/M phase, as endocrine progenitors are mostly post-mitotic. (D) Average cell cycle of pancreatic progenitors (n = 3). 68.7% ± 2.1% of cells are in G0/G1, 26.6% ± 2.4% in S phase, and 4.7% ± 1.2% in G2/M phase.
(TIF)

S8 Fig. Distance between two daughters relative to time after division. The x-axis represents the time between division and NEUROG3 end-point immunostaining. White triangles show the distance between two progenitor daughters originating from symmetric divisions (P/P), pink triangles, distance between one progenitor and one NEUROG3 cell from asymmetric divisions (P/N), and blue triangles, distance between two NEUROG3 cells from symmetric divisions (N/N). Distance from P/P divisions was measured one frame prior to daughter divisions, which indicates doubling time between mother and daughter divisions. There is therefore no data point before 18 h. Regardless of the cell division mode, the distance between daughters increased, as time after division increased (Pearson's r, 0.81 [P/P], 0.33 [P/N], and 0.27 [N/N]). All three different modes of division showed statistically significant correlations between daughter distance and time: P/P division, p = 0.0025, P/N division, p = 0.0012, and N/N division, p = 0.016. The grey line indicates 30 μm threshold used for in vivo clonal analysis for two-cell clone boundaries. 90.2% of all data are under this threshold.
(TIF)

S9 Fig. A model of cell cycle–dependent stochastic priming of progenitors to endocrine fate accounts for the observed RFP onset dynamics. Monte Carlo simulations of clone expansion according to the model. Each newly born cell is randomly assigned a cell cycle length from a Gamma shifted (A) with mean and variance matching the experimentally measured. (B) Distribution of times from division to the priming event for cells stemming from P and L cells. Note

that in the latter the priming event occurs prior to division. (C) Distribution of times from division to the priming event for cells stemming from AD and SD divisions. (D) Distribution of set times for a reporter with constant delay. (E) Lag time between the reporter onset in sibling cells. The simulations anticipate a high degree of synchronization. (F–H) Effect of heterogeneity in the reporter delay. (F) The distribution of delays of the reporter onset is assumed Gaussian. Variability in the reporter delay has little impact in the distribution of lag times in ACD and SCD originated cells (G) and in the synchronization of sibling cells (H).
(TIF)

S10 Fig. Model results including cell misclassification. In order to account for the effect of possible misclassification biases in the distribution of lag times, we performed an in silico misclassification experiment. We randomly sampled 11.6% of simulated cells stemming from symmetric divisionand classified them as stemming from asymmetric division. The resulting distribution of reporter onset lag times for this latter group features a tail at low times that might partly account for the observed (cf. Fig. 4C). This tail in the distribution, however, does not substantially affect the average lag time.
(TIF)

S11 Fig. Representative in silico clone lineages generated. Temporal evolution of the expansion of five representative clones obtained with Monte-Carlo simulations of the model ($q = 0.2$, $\theta = 0.55$). *X*- axis indicates experimental time. All simulations start at time zero with one progenitor cell (P, green circle) whose cell cycle phase is set uniformly at random and run for 150 h. Progenitor cells continuously divide according to the distribution of cell cycles in S9A Fig. Stochastic priming events are indicated by red diamonds. Events occurring early following cell division lead to cells exiting the cell cycle and differentiating (N cells, orange circles). Events taking place later on lead to primed cells that are already committed to complete the cell cycle (L cells, yellow circles) and that will give rise to two differentiated post-mitotic cells (N cells).
(TIF)

S1 Movie. Time-lapse movie in 3-D maximum intensity projection of pancreatic epithelial cells. Pancreas from E12.5 *Pdx1*$^{tTA/+}$;*tetO-H2B-GFP* embryo was cultured on a fibronectin-coated coverslip plate for 24 h prior to live imaging. The explant was imaged in 3-D every 6 min in 12 positions (3x4 tiles), which were stitched after 24 h acquisition. This movie demonstrates overall expansion of explant and pancreatic progenitor divisions. Time indicates a time-lapse elapsed time in h:min:s. Frame rate: 10 frames per second (fps).
(MP4)

S2 Movie. Z-stack of stained pancreatic explant after 48 h of culture. The control explant was immunostained for endocrine progenitor, NEUROG3 (blue), epithelial membrane marker, E-CADHERIN (red), and apical membrane marker, aPKC (white). Green channel is native GFP signal. Lumenized branches of epithelium are visible, and nuclear signal of NEUROG3^{+} cell are found in the epithelium. Blue channel is masked by native GFP channel to exclude non-specific back-grounds in mesenchymal region. Frame rate: 10 fps.
(AVI)

S3 Movie. Time-lapse movie exhibiting symmetric (P/P) and asymmetric (P/N) pancreatic progenitor divisions. Two cell divisions are tracked in this movie (blue spots and red spots). One daughter of red spot (top; NEUROG3^{+} from immunostaining in Fig. 1G) was back-tracked from the last frame of the movie, and the other daughter was forward-tracked after the division was monitored. By referring to immunostaining at the end of the time-lapse imaging (Fig. 1), blue spotted daughters are symmetrically fated (P/P), as pancreatic progenitors

(SOX9$^+$), whereas red spotted daughters are asymmetrically fated (P/N), one as pancreatic progenitor (SOX9$^+$) and the other as endocrine progenitor (NEUROG3$^+$). *Pdx1$^{tTA/+}$*; *tetO-H2B-GFP* signal is presented in white channel. Time indicates a time-lapse elapsed time in h:min:s. Frame rate: 6 fps.
(MP4)

S4 Movie. Time-lapse movie exhibiting symmetric (N/N) cell division. At the last frame, one daughter (red spot; NEUROG3$^+$ from the immunostaining, Fig. 1L) was back-tracked and the other daughter was forward-tracked once the mother division was monitored. Referring back to immunostaining, the other daughter was NEUROG3$^+$, as well, demonstrating symmetric endocrinogenic division (N/N). *Pdx1$^{tTA/+}$;tetO-H2B-GFP* signal is presented in white channel. Time indicates a time-lapse elapsed time in h:min:s. Frame rate: 6 fps.
(MP4)

S5 Movie. 3-D reconstruction of whole-mount imaged *Hnf1bCreER;mT/mG* E14.5 dorsal pancreas after 24 h of in vivo lineage tracing at clonal density. Imaris software was used to perform a 3-D reconstruction of dorsal pancreas after masking of background signal in the surrounding mesenchyme. Staining for E-Cadherin (white) enables outlining of the pancreatic epithelium, while membrane GFP (green) represents labelled clones. After 360° spinning, a SOX9 symmetric two-cell clone is shown in high magnification with SOX9 in blue. Next, a NEUROG3 symmetric two-cell clone is displayed in high magnification, showing NEUROG3 in magenta. Frame rate: 15 fps.
(MP4)

S6 Movie. Time-lapse movie exhibiting asymmetric (P/R) cell division from *Pdx1$^{tTA/+}$;tetO-H2B-GFP;Ngn3-RFP* pancreatic explant. After the mother division at elapsed time 09:30:00.000 (white spots), one daughter acquires RFP signal at 19:42:00.000, whereas the other daughter divides at 42:12:00.000. Referring to immunostaining (Fig. 3E,F), the granddaughters are progenitors (SOX9$^+$), demonstrating asymmetric (P/R) division. Left panel, GFP/RFP channels and right panel, RFP channel. Time indicates h:min:s. Frame rate: 6 fps.
(MP4)

S7 Movie. Time-lapse movie exhibiting symmetric (R/R) cell division from *Pdx1$^{tTA/+}$;tetO-H2B-GFP;Ngn3-RFP* pancreatic explant. After the mother division at elapsed time 08:54:00.000 (white spots), and one daughter turned RFP on at 18:24:00.000 and the other at 20:54:00.000. Subsequent immunostaining revealed that both of RFP$^+$ daughters were still NEUROG3$^+$ but SOX9$^-$ (Fig. 3H). Left panel, GFP/RFP channels and right panel, RFP channel. Time indicates a time-lapse elapsed time in h:min:s. Frame rate: 10 fps.
(MP4)

S8 Movie. Time-lapse movie exhibiting symmetric cell division of Ngn3-RFP cell. In rare occasions, RFP$^+$ cell divides soon after acquiring RFP signal, producing two RFP$^+$ daughters (white spots). Referring to immunostaining, both daughter cells are fated as NEUROG3$^+$ (Fig. 6D). Left panel, RFP channel and right panel, GFP/RFP channels. Time indicates a time-lapse elapsed time in h:min:s. Frame rate: 10 fps.
(MP4)

S1 Table. Fraction of NEUROG3 over *Pdx1$^{tTA/+}$*;tetO-H2B-GFP cells from immunostaining images after time-lapse imaging.
(DOCX)

S2 Table. Data from NEUROG3+ cell tracking in time-lapse movies (Pdx1$^{tTA/+}$; tetO-H2B-GFP).
(DOCX)

S3 Table. Data from in vivo clonal analysis (Hnf1bCreER;mT/mG).
(DOCX)

S4 Table. Data from in vitro clonal analysis (*Hnf1bCreER;mT/mG*).
(DOCX)

S5 Table. Data from Neurog3-EYFP;Neurog3-RFP explant time-lapse.
(DOCX)

S6 Table. Data from RFP$^+$ cell tracking in time-lapse movies (*Pdx1$^{tTA/+}$;tetO-H2B-GFP; Neurog3-RFP*).
(DOCX)

S7 Table. Primary antibodies used for immunostainings.
(DOCX)

S1 Text. Supplemental methods.
(DOCX)

Author Contributions

Conceived and designed the experiments: YHK AGB HLL PR. Performed the experiments: YHK HLL LAL PR. Analyzed the data: YHK HLL LAL PR AGB. Contributed reagents/materials/analysis tools: JF. Wrote the paper: YHK HLL LAL PR AGB JF.

References

1. Jorgensen MC, Ahnfelt-Ronne J, Hald J, Madsen OD, Serup P, et al. (2007) An illustrated review of early pancreas development in the mouse. Endocr Rev 28: 685–705. PMID: 17881611
2. Gu G, Dubauskaite J, Melton DA (2002) Direct evidence for the pancreatic lineage: NGN3+ cells are islet progenitors and are distinct from duct progenitors. Development 129: 2447–2457. PMID: 11973276
3. Solar M, Cardalda C, Houbracken I, Martin M, Maestro MA, et al. (2009) Pancreatic exocrine duct cells give rise to insulin-producing beta cells during embryogenesis but not after birth. Dev Cell 17: 849–860. doi: 10.1016/j.devcel.2009.11.003 PMID: 20059954
4. Kopp JL, Dubois CL, Schaffer AE, Hao E, Shih HP, et al. (2011) Sox9+ ductal cells are multipotent progenitors throughout development but do not produce new endocrine cells in the normal or injured adult pancreas. Development 138: 653–665. doi: 10.1242/dev.056499 PMID: 21266405
5. Kesavan G, Sand FW, Greiner TU, Johansson JK, Kobberup S, et al. (2009) Cdc42-mediated tubulogenesis controls cell specification. Cell 139: 791–801. doi: 10.1016/j.cell.2009.08.049 PMID: 19914171
6. Cortijo C, Gouzi M, Tissir F, Grapin-Botton A (2012) Planar cell polarity controls pancreatic beta cell differentiation and glucose homeostasis. Cell Rep 2: 1593–1606. doi: 10.1016/j.celrep.2012.10.016 PMID: 23177622
7. Villasenor A, Chong DC, Henkemeyer M, Cleaver O (2010) Epithelial dynamics of pancreatic branching morphogenesis. Development 137: 4295–4305. doi: 10.1242/dev.052993 PMID: 21098570
8. Zhou Q, Law AC, Rajagopal J, Anderson WJ, Gray PA, et al. (2007) A multipotent progenitor domain guides pancreatic organogenesis. Dev Cell 13: 103–114. PMID: 17609113
9. Gradwohl G, Dierich A, LeMeur M, Guillemot F (2000) neurogenin3 is required for the development of the four endocrine cell lineages of the pancreas. Proc Natl Acad Sci U S A 97: 1607–1611. PMID: 10677506
10. Johansson KA, Dursun U, Jordan N, Gu G, Beermann F, et al. (2007) Temporal control of neurogenin3 activity in pancreas progenitors reveals competence windows for the generation of different endocrine cell types. Dev Cell 12: 457–465. PMID: 17336910

11. Miyatsuka T, Kosaka Y, Kim H, German MS (2011) Neurogenin3 inhibits proliferation in endocrine progenitors by inducing Cdkn1a. Proc Natl Acad Sci U S A 108: 185–190. doi: 10.1073/pnas.1004842108 PMID: 21173230

12. Desgraz R, Herrera PL (2009) Pancreatic neurogenin 3-expressing cells are unipotent islet precursors. Development 136: 3567–3574. doi: 10.1242/dev.039214 PMID: 19793886

13. Snippert HJ, van der Flier LG, Sato T, van Es JH, van den Born M, et al. (2010) Intestinal crypt homeostasis results from neutral competition between symmetrically dividing Lgr5 stem cells. Cell 143: 134–144. doi: 10.1016/j.cell.2010.09.016 PMID: 20887898

14. Clayton E, Doupe DP, Klein AM, Winton DJ, Simons BD, et al. (2007) A single type of progenitor cell maintains normal epidermis. Nature 446: 185–189. PMID: 17330052

15. Doupe DP, Klein AM, Simons BD, Jones PH (2010) The ordered architecture of murine ear epidermis is maintained by progenitor cells with random fate. Dev Cell 18: 317–323. doi: 10.1016/j.devcel.2009.12.016 PMID: 20159601

16. Miyata T, Kawaguchi A, Saito K, Kawano M, Muto T, et al. (2004) Asymmetric production of surface-dividing and non-surface-dividing cortical progenitor cells. Development 131: 3133–3145. PMID: 15175243

17. Noctor SC, Martinez-Cerdeno V, Ivic L, Kriegstein AR (2004) Cortical neurons arise in symmetric and asymmetric division zones and migrate through specific phases. Nat Neurosci 7: 136–144. PMID: 14703572

18. Dong Z, Yang N, Yeo SY, Chitnis A, Guo S (2012) Intralineage directional Notch signaling regulates self-renewal and differentiation of asymmetrically dividing radial glia. Neuron 74: 65–78. doi: 10.1016/j.neuron.2012.01.031 PMID: 22500631

19. Gomes FL, Zhang G, Carbonell F, Correa JA, Harris WA, et al. (2011) Reconstruction of rat retinal progenitor cell lineages in vitro reveals a surprising degree of stochasticity in cell fate decisions. Development 138: 227–235. doi: 10.1242/dev.059683 PMID: 21148186

20. He J, Zhang G, Almeida AD, Cayouette M, Simons BD, et al. (2012) How variable clones build an invariant retina. Neuron 75: 786–798. doi: 10.1016/j.neuron.2012.06.033 PMID: 22958820

21. Costa MR, Wen G, Lepier A, Schroeder T, Gotz M (2008) Par-complex proteins promote proliferative progenitor divisions in the developing mouse cerebral cortex. Development 135: 11–22. PMID: 18032449

22. Konno D, Shioi G, Shitamukai A, Mori A, Kiyonari H, et al. (2008) Neuroepithelial progenitors undergo LGN-dependent planar divisions to maintain self-renewability during mammalian neurogenesis. Nat Cell Biol 10: 93–101. PMID: 18084280

23. Schwamborn JC, Berezikov E, Knoblich JA (2009) The TRIM-NHL protein TRIM32 activates microRNAs and prevents self-renewal in mouse neural progenitors. Cell 136: 913–925. doi: 10.1016/j.cell.2008.12.024 PMID: 19269368

24. Gomez-Lopez S, Lerner RG, Petritsch C (2014) Asymmetric cell division of stem and progenitor cells during homeostasis and cancer. Cell Mol Life Sci 71: 575–597. doi: 10.1007/s00018-013-1386-1 PMID: 23771628

25. Burke ZD, Li WC, Slack JM, Tosh D (2010) Isolation and culture of embryonic pancreas and liver. Methods Mol Biol 633: 91–99. doi: 10.1007/978-1-59745-019-5_7 PMID: 20204622

26. Petzold KM, Spagnoli FM (2012) A system for ex vivo culturing of embryonic pancreas. J Vis Exp: e3979.

27. Georgia S, Kanji M, Bhushan A (2013) DNMT1 represses p53 to maintain progenitor cell survival during pancreatic organogenesis. Genes Dev 27: 372–377. doi: 10.1101/gad.207001.112 PMID: 23431054

28. Roark R, Itzhaki L, Philpott A (2012) Complex regulation controls Neurogenin3 proteolysis. Biol Open 1: 1264–1272. doi: 10.1242/bio.20121750 PMID: 23259061

29. Mellitzer G, Martin M, Sidhoum-Jenny M, Orvain C, Barths J, et al. (2004) Pancreatic islet progenitor cells in neurogenin 3-yellow fluorescent protein knock-add-on mice. Mol Endocrinol 18: 2765–2776. PMID: 15297605

30. Miyatsuka T, Li Z, German MS (2009) Chronology of islet differentiation revealed by temporal cell labeling. Diabetes 58: 1863–1868. doi: 10.2337/db09-0390 PMID: 19478145

31. Lee CS, Perreault N, Brestelli JE, Kaestner KH (2002) Neurogenin 3 is essential for the proper specification of gastric enteroendocrine cells and the maintenance of gastric epithelial cell identity. Genes Dev 16: 1488–1497. PMID: 12080087

32. Beucher A, Gjernes E, Collin C, Courtney M, Meunier A, et al. (2012) The homeodomain-containing transcription factors Arx and Pax4 control enteroendocrine subtype specification in mice. PLoS One 7: e36449. doi: 10.1371/journal.pone.0036449 PMID: 22570716

33. Rué P, Kim YH, Larsen HL, Grapin-Botton A, Martinez Arias A (2014) A framework for the analysis of symmetric and asymmetric divisions in developmental processes. Preprint. http://dx.doi.org/10.1101/010835. Accessed 28 October 2014.

34. Kim YH, Larsen HL, Rué P, Lemaire LA, Ferrer J, et al. (2015) Data from: Cell cycle-dependent differentiation dynamics balances growth and endocrine differentiation in the pancreas. Dryad Data Repository. http://dx.doi.org/10.5061/dryad.4b58d.

35. Salpeter SJ, Klein AM, Huangfu D, Grimsby J, Dor Y (2010) Glucose and aging control the quiescence period that follows pancreatic beta cell replication. Development 137: 3205–3213. doi: 10.1242/dev.054304 PMID: 20823063

36. Itzkovitz S, Blat IC, Jacks T, Clevers H, van Oudenaarden A (2012) Optimality in the development of intestinal crypts. Cell 148: 608–619. doi: 10.1016/j.cell.2011.12.025 PMID: 22304925

37. Imayoshi I, Isomura A, Harima Y, Kawaguchi K, Kori H, et al. (2013) Oscillatory control of factors determining multipotency and fate in mouse neural progenitors. Science 342: 1203–1208. doi: 10.1126/science.1242366 PMID: 24179156

38. Lange C, Huttner WB, Calegari F (2009) Cdk4/cyclinD1 overexpression in neural stem cells shortens G1, delays neurogenesis, and promotes the generation and expansion of basal progenitors. Cell Stem Cell 5: 320–331. doi: 10.1016/j.stem.2009.05.026 PMID: 19733543

39. Lim S, Kaldis P (2012) Loss of Cdk2 and Cdk4 induces a switch from proliferation to differentiation in neural stem cells. Stem Cells 30: 1509–1520. doi: 10.1002/stem.1114 PMID: 22532528

40. Tsunekawa Y, Britto JM, Takahashi M, Polleux F, Tan SS, et al. (2012) Cyclin D2 in the basal process of neural progenitors is linked to non-equivalent cell fates. EMBO J 31: 1879–1892. doi: 10.1038/emboj.2012.43 PMID: 22395070

41. Afelik S, Jensen J (2013) Notch signaling in the pancreas: patterning and cell fate specification. Wiley Interdiscip Rev Dev Biol 2: 531–544. doi: 10.1002/wdev.99 PMID: 24014421

42. Holland AM, Hale MA, Kagami H, Hammer RE, MacDonald RJ (2002) Experimental control of pancreatic development and maintenance. Proc Natl Acad Sci U S A 99: 12236–12241. PMID: 12221286

43. Tumbar T, Guasch G, Greco V, Blanpain C, Lowry WE, et al. (2004) Defining the epithelial stem cell niche in skin. Science 303: 359–363. PMID: 14671312

44. Muzumdar MD, Tasic B, Miyamichi K, Li L, Luo L (2007) A global double-fluorescent Cre reporter mouse. Genesis 45: 593–605. PMID: 17868096

Supporting Information

Text S1. Supplemental methods

Text S1.1. Cell cycle analysis

Pooled pancreata from 1 or 2 litters of E14.5 embryos with different genotypes from *Pdx1$^{tTA/+}$;Neurog3-RFP x tetO-H2B-GFP* breeding were dissociated mechanically using 0.05% Trypsin containing DNase I (200 U/ml), and fixed in 4% PFA. After washing with PBS, the dissociated cells were nuclear-stained by DAPI (1 μg/ml). Then cell cycle analysis was performed by sorting GFP$^+$ and RFP$^+$ single cells by LSRFortessa cell analyzer (BD Bioscences). Cell cycle curve fitting and calculation were done using FCS express software (De Novo Software).

Text S1.2. Time-lapse imaging with Neurog3-EYFP;Neurog3-RFP pancreata

Pancreatic explant culture and live imaging were performed as described in the Materials and Methods, with imaging modifications of 10 minute intervals for up to 65 hours using a 20X glycerol-immersion objective.

Text S1.3. Quantitative characterization of transient Neurog3-RFP response in differentiating cells

To study the dynamics of cells during fate specification we performed live tracking of single cells using a novel Neurog3-RFP reporter. As a first step, we quantitatively characterized the response of the fluorescent reporter upon cell differentiation. We extracted fluorescence time traces of individual cells at a high temporal resolution (10 frames/hour) and used the average signal intensity over a spherical region of interest of radius (5 μm) approximately located around the center of cell nuclei. We selected those cells for which we could completely track the response of the signal. Figure S5A shows the RFP fluorescence traces for those cells (n=6). All cells displayed a transient rise in fluorescence followed by a rapid descent. Despite the maximum signal amplitude varied from cell to cell, the shape of the transient response was fairly conserved amongst cells. To confirm this pattern we aligned signals in time and normalized their maximum amplitude to one. With this transformation fluorescence signals from all cells collapsed into one stereotypical response curve (Figure S5B), a pulse consisting a rapid increase in fluorescence followed by an exponential decay. According to this shape, the total persistence of the fluorescence after the onset is of about 20-30 hours. Fitting an exponential to the decay we estimated an effective half-life of 5-6 hours for the RFP (Figure S5C). Such fast turnover indicates that the perdurance of the RFP signal might be due to constant transcription.
Another important aspect of the dynamics of the RFP signal in reporting the cell differentiation state is the delay between the priming event and the reporter onset. Analysis of cells bearing both EYFP and RFP reporters indicates that the latter is delayed by about 2.8 to 6.3 hours with respect to the former (Figure S4D-E). Because the onset of the EYFP reporter might also be delayed with respect to the priming event, we consider the estimated range to be a lower boundary of the true delay between the differentiation priming and the onset of the RFP reporter.

Text S1.4. Analysis of tissue level coordination of cell differentiation

Live imaging of the RFP reported onset allowed us to detect individual cells undergoing NEUROG3 differentiation within the expanding tissue. An initial analysis of the RFP onset events pointed towards discrete waves of differentiation. This is best illustrated by the undulated profiles of the cell differentiation probability. These profiles were obtained by gaussian kernel density estimation (bandwidth: 10 minutes) and depicted in Figure 4A (reproduced in Figure S6B). However, because the results of kernel density estimation depend on the selected bandwidth, we decided to further analyze the statistics of the time intervals between consecutive differentiating cells. To do so, we compared our data to a homogeneous Poisson process. In such process each event (i.e., the RFP onset of one cell) is independent of the others, the rate of events is constant over time and the time between consecutive events has an exponential distribution. This means that the

average time between consecutive events is equal to its standard deviation and hence the coefficient of variation (standard deviation normalized to the mean, CV) is equal to one. Using the data of four explant locations during the initial 35 hours of time-lapse movies (right panels in Figure S6B), we estimated the CV of the time between consecutive RFP onset events to be close to one (1.16±0.08). We also computed the CVs using a sliding window of width 10 hours and found that this is maintained around one most of the time (Figure S6B, left panels). Hence, with these results we cannot completely rule out the possibility that the observed patterns of differentiation are mere instances of a homogeneous process.

Text S1.5. Estimation of the probability of differentiation and association between cell cycle and differentiation priming

In tissues with only two cellular types, namely a proliferating and a differentiated fate, each cell division can be classified into either symmetric proliferating (SP) if the two newly formed cells are proliferative (*P* cells); symmetric differentiating (SD) if the two daughters differentiate (*N* cells), or asymmetric (AD) divisions if there is one daughter of each kind.

This classification provides a straightforward way to indirectly estimate the probability of cell differentiation, *q*, given the probabilities (frequencies) of division types:

$$q = \Pr[SD] + \tfrac{1}{2} \Pr[AD].$$

That is to say, the probability of differentiation can be regarded as the contribution of all cells stemming from SD divisions plus half of the cells from asymmetric divisions.

It is important to note, however, that the relation between the probability of differentiation *q* and the frequency of each division type is not unambiguous, i.e., there are infinitely many combinations of Pr[*SP*], Pr[*SD*] and Pr[*AD*] that lead to the same probability of differentiation *q*. Thus, given only *q* we cannot infer the frequencies of each division type.

However, with the proportions of each division type we can test whether the fate adopted by pairs of sibling cells is statistically independent or tied. In the case where sibling cells decide to differentiate independently of each other, the frequencies of the cell division modes follow a binomial relation as in the case of allele frequencies of a population in Hardy-Weinberg equilibrium:

$$\Pr[SD] = q^2, \quad \Pr[AD] = 2q(1-q), \quad \text{and} \quad \Pr[SP] = (1-q)^2$$

Lack of independence (or linkage disequilibrium) can be statistically assessed by means of contingency table tests such as Pearson's χ^2 or Fisher's exact test.

In the case developing pancreatic progenitors, we estimated the proportions of SP (P/P), AD (P/N) and SD (N/N) division from the *in vivo* clonal analysis (Figure 2H). These are 69.9%, 18.6% and 11.5%, respectively. From these we estimate the probability of cell differentiation to be q=0.208. That is to say, around 20.8% of the newly born cells will eventually differentiate. This probability of differentiation implies a net exponential growth of the tissue ($q<0.5$). If these differentiation events were independent in sibling cells, the proportions of each division type would be 62.7% for *SP divisions*, 33% for AD and only 4.3% for SD divisions. These proportions are far from the observed ones thus suggesting that fates of sibling cells are statistically linked. This is further confirmed with statistical tests on the absolute numbers of divisions recorded ($p<10^{-7}$ for both Pearson's χ^2 or Fisher's exact tests). Note that even though the above proportions have not been directly computed from the recorded raw numbers of divisions of each type (SP: 146, SD: 34, SD: 21), the raw relative amounts of each division mode do not differ from the above estimates (146/201=72.6% vs 69.9%, 33/201=17% vs 18.6% and 21/201=10.4% vs 11.5%) and nor does *q (3.6%* vs *4.3%).*

Text S1.6. Mathematical modeling

In order to gain conceptual and quantitative insight into the cell proliferation and differentiation dynamics during pancreas development, we conceived a simple model of cell cycle-dependent stochastic priming of

progenitors to endocrine fate. The model considers three different cell types: pancreatic progenitors (P), post-mitotic Neurog3 cells (N), and cells primed for differentiation that will complete the division cycle (L cells). Each newly formed cell from a dividing P cell will adopt one of the three fates above with certain probabilities: a cell might differentiate with probability q or remain as a P cell with probability $1 - q$. Furthermore, a differentiating cell might either adopt N or L fate with probabilities θ and $1- \theta$, respectively (Figure 6D). All L cells eventually divide generating two N cells. Note that the cellular state L is transient and thus from an experimental point of view L cells might not be distinguishable from P cells. These rules lead to seven different division events that can be classified into the three modes generally considered:

- **SP divisions:** $P \rightarrow P + P$, $P \rightarrow L + L$ and $P \rightarrow P + L$,
- **AD divisions:** $P \rightarrow L + N$ and $P \rightarrow P + N$, and
- **SD divisions:** $P \rightarrow N + N$ and $L \rightarrow N + N$.

We have formally stated and analyzed these events in terms of a model of discrete-time dynamic equations - mathematical details can be found elsewhere(Rué et al., 2014). Here we briefly summarize the model results.

- Given the parameters q and θ, the frequencies of each division mode are: $\Pr[SP] = (1-q)(1-q\theta)$, $\Pr[SD] = q(1-\theta(1-q))$, and $\Pr[AD] = (1-q)2q\theta$.
- Conversely, the parameters q and θ can be inferred from the experimentally observed frequencies of each division mode: $q = \Pr[SD] + \frac{1}{2}\Pr[AD]$ and $\theta = \frac{1}{2}\Pr[AD]/(q(1-q))$. Therefore, from the *in vivo* data we estimate $q=0.208$ and $\theta=0.565$.
- The long-term composition of the tissue can also be predicted from the model. The fractions of each cell type are given by the following equations $\pi_P=(1-2q)(1-q)/(1- q\theta)$, $\pi_L=(1-2q)(q-q\theta)/(1- q\theta)$ and $\pi_N=2q$. For the experimentally estimated values the model predicts that 52.5% of the cells are progenitors, 41.5% are post-mitotic cells, and only 6% of the cells are of the type L (i.e., they are committed to differentiation but will divide once).
- The model also discriminates between those SD divisions that are due to an L cell from those that occur in P cells when the two daughter cells independently adopt the N fate. The fraction of divisions of the former type is given by:
  $\Pr[\text{mother cell is } L \mid SD] = (q\theta-q^2\theta^2)/(1 – \theta + q\theta - q\theta^2)$, and
  $\Pr[\text{mother cell is } P \mid SD] = (1 - \theta)/(1 – \theta + q\theta - q\theta^2)$.
  With our data we estimate these proportions to be 90.2% vs 9.8%. That is to say, the vast majority of SD divisions are due to cells that are already primed for differentiation before division.

In addition to these predictions, the model can also prognosticate the dynamics of cell differentiation. For that to occur we need to interpret the model in a specific manner by linking the probability θ to the cell cycle phase. In particular, we need to assume that progenitor cells are susceptible to be primed for differentiation within a window of the cell cycle (which could correspond to the whole cycle or to a specific phase). In addition, this priming event might have different outcomes depending on whether it occurs at the beginning or the end of this time window. If this time window has a length of one, then θ might represent the time when the cell commits to cell cycle completion. Any priming event before θ implies the exit from cell cycle and terminal differentiation (N state adoption), and any event after θ involves a cell that will divide into two differentiated cells (L state adoption). Therefore, if the probability of being primed is approximately uniform throughout the time window, then the model presented above precisely describes this system. This interpretation in terms of priming time implies further testable predictions. Hereafter we assume $\langle T \rangle$ to be the average cell cycle and the susceptibility window to span the whole cell cycle duration:

- Obviously, sibling cells stemming from L cells will be perfectly synchronized, as there is only one priming event common to both cells (it occurs in the mother L cell). Hence, according to the model, a perfect synchronization is expected in at least 93.8% of all SD divisions (see above).
- On average, the time between birth and priming in differentiated cells stemming from a P cell is $\langle \Delta t_P \rangle = \frac{1}{2}\theta\langle T \rangle$. On the other hand, in differentiated cells stemming from a L cell this time becomes $\langle \Delta t_L \rangle = -\frac{1}{2}(1-\theta)\langle T \rangle$ (i.e., the priming event occurs before division). Therefore, on average, N cells stemming from L cells will anticipate their differentiation programme by about $\langle \Delta t_P \rangle - \langle \Delta t_L \rangle = \frac{1}{2}\langle T \rangle$ (i.e., half a cell cycle) the cells from stemming from P cells.
- On average, lag time between birth and priming in differentiated cells stemming from asymmetric divisions is $\langle \Delta t_{AD} \rangle = \langle \Delta t_P \rangle$ (all cells stem from a P cell). In cells stemming from SD divisions, this

time becomes $\langle \Delta t_{SD} \rangle = \langle \Delta t_P \rangle$ Pr[mother cell is $P \mid SD$] + $\langle \Delta t_L \rangle$ Pr[mother cell is $L \mid SD$] $\approx \langle \Delta t_L \rangle$, and therefore cells from SD divisions anticipate those from AD divisions in differentiation by approximately $\frac{1}{2}\langle T \rangle$.

Despite the simplicity of the model, the generated predictions are approximately fulfilled by the experimental data (see Figure 6), thus suggesting that the model might be capturing the dynamics of cell fate adoption during pancreas development.

We decided to include more details in the model in order to generate more quantitatively accurate predictions and compare them to the experimental data. We proceeded by performing Monte Carlo simulations of the model including the observed variability in the cell cycle length and the delay in the onset of the reporter. In the simulations each newly born cell n is randomly assigned a cell cycle length T_n from a Gamma shifted distribution (shift 17, shape 4, scale 1). This distribution (Figure S9A) has a mean time of 21 hours and standard deviation of 2 hours, which closely resemble those measured experimentally (Figure 4D). These cells become randomly primed with probability q. Once a cell is primed for differentiation, it is assigned a delay δ_{rep} for the onset of the reporter. In the first set of simulations we consider this delay to be fixed to 8 hours, which we consider to be a reasonable delay for the RFP (see previous section for an estimate of the lower boundary of this delay). For each cell primed for differentiation, a random number r between 0 and 1 is drawn, and the priming event is considered to occur at time $T_n r$ after cell birth. If $r<\vartheta$ then the cell differentiates into an N cell (i.e., becomes post mitotic). Conversely, if $r \geq \vartheta$ the cell commits to cell cycle completion and divides at time T_n, giving rise to two N cells. It can be shown that the average behaviour of this computational model corresponds to the analytic model described above.

Individual clones starting from an individual progenitor cell are simulated for a period of 150 hours. Figure S11 shows a graphical representation of 5 simulated clones. The results from the simulation of 10,000 clones are displayed in Figure S9. Panel B in this figure shows the distribution of times from division (of the mother cell) to the priming event for cells stemming from P and L cells. As expected, the former cells display positive times, as the decision is made after the last division; and the latter show negative times, as the decision is made in the mother (L) cell. Now, if cells are classified according to the division type they stem from, the results are slightly different (Figure S9C). In this case, the distribution of times for AD divisions is basically the same as for P mother cells (cf. panels B and C) but the distribution for SD divisions includes a small tail upwards. This tail corresponds to the residual fraction of SD divisions that stem from a P cell rather than from an L cell. For a constant delay of the fluorescent reporter, the distributions of lag times between cell division and the reporter onset are basically the same but shifted (cf. panels D, C in Figure S9). Now, if we classify differentiated cells into those stemming from AD vs SD divisions, then the results are slightly different (Figure S9C). Interestingly, even when the delay considered for the reporter is as long as 8 hours, the model predicts a very small fraction of cells from SD divisions that will turn on the reporter before dividing. We have observed this phenomenon in a few cells (Figure 5 and Table S6). The model simulations also anticipate a high degree of synchronization in the lag time of reporter onset between sibling cells (Figure S9E and 6G).

We have also considered the effect of introducing variability in the delay of the RFP onset. We assumed that the delay in the RFP onset is normally distributed around 8 hours with a standard deviation of 0.25 (i.e, that 99.99% of cells turn on the RFP between 7 and 9 hours after being primed, see Figure S9F). This level of variability had little impact in the distribution of lag times in ACD and SCD originated cells (Figure S9G) and also in the synchronization of sibling cells

(Figure S9H). As we increased the variability in the delay, we observed that synchronization progressively deteriorated.
Finally, we included the 11.6% false negative rate in the reporter (Figure S4C) of the model. We did that by relabeling 11.6% of the SCD originated cells as being originated by ACD. This re-assignation of cells introduced a tail in the lower range of the distribution of lag times in ACD cells (Figure S10) but overall the results were not significantly affected.

Supplementary Figure and Supplementary Figure Legends

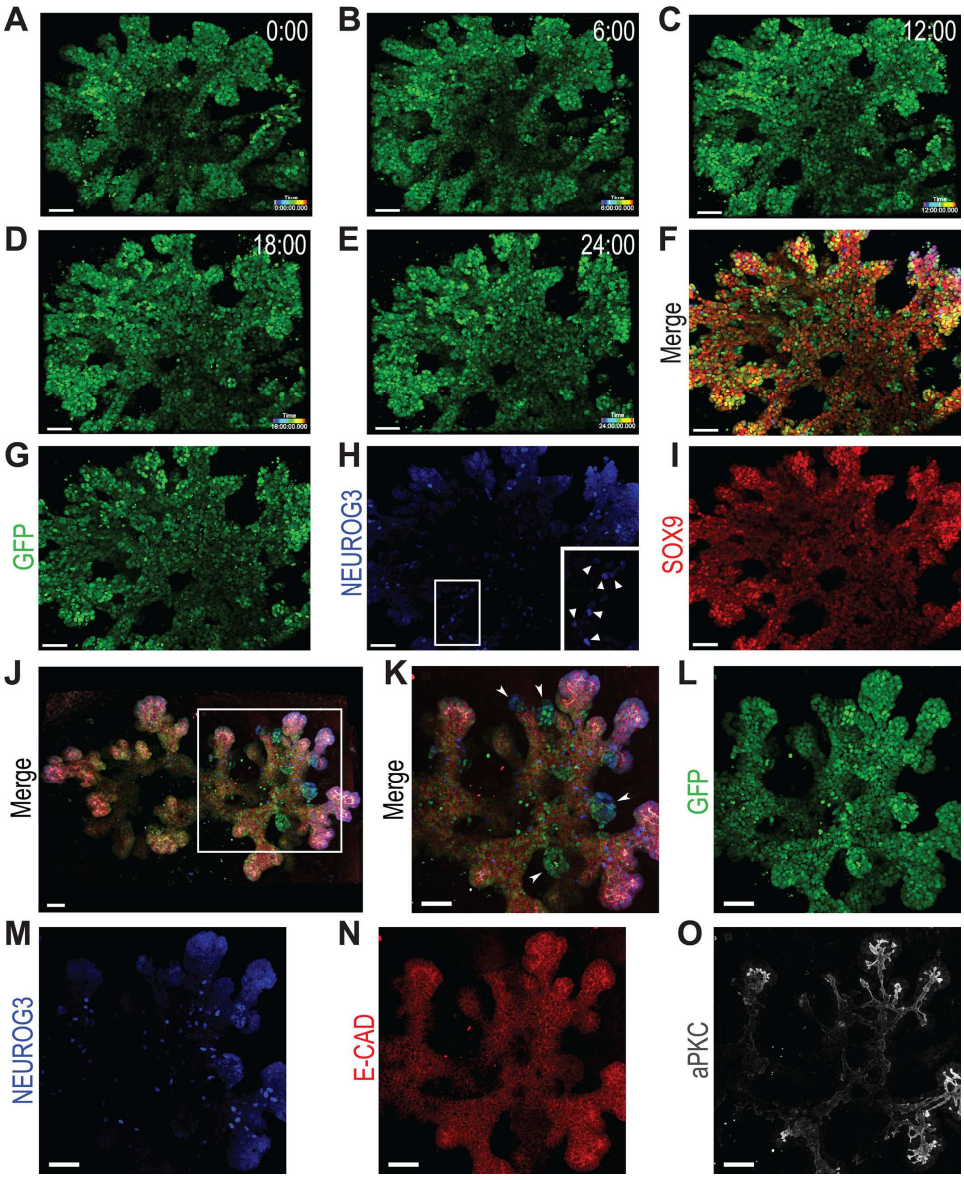

Figure S1. 3-D live imaging of dividing cells in pancreatic explants.
(A-E) Still images of 24-hour live imaging in 3-D maximum intensity projection from Movie 1, showing an overall growth of explant and cell divisions. Numbering denotes elapsed time in hr:min. (F-I) Images in 3-D projection of fixed explant with native GFP (G) and immunostained for NEUROG3 (H) and SOX9 (I). Insert shows NEUROG3^{+} cells (H, nuclear signal; arrowheads) in high magnification. Channels in (H) and (I) are masked by native GFP channel (G) to exclude non-specific background in mesenchymal regions. (J-O) Images in 3-D maximum intensity projection of immunostained control explant without imaging and laser exposure. The overall morphology after 48 hours of culture, equivalent to 24-hour live imaging, reveals that the epithelium branches (J). The white square is an area zoomed in (K-O). Cells in the trunk region are differentiating into NEUROG3^{+} endocrine progenitors (M, nuclear signal). The epithelium is intact as shown by E-CADHERIN staining (M), and branching ducts and acini are apically polarized as revealed by aPKC staining (O). Arrowheads in (K) indicate endocrine cell clusters. The blue channel (M) is masked by the native GFP channel (L) to exclude non-specific background in mesenchymal regions. A Z-stack is shown in Movie 2 (J-O). Scale bars, 50 µm.

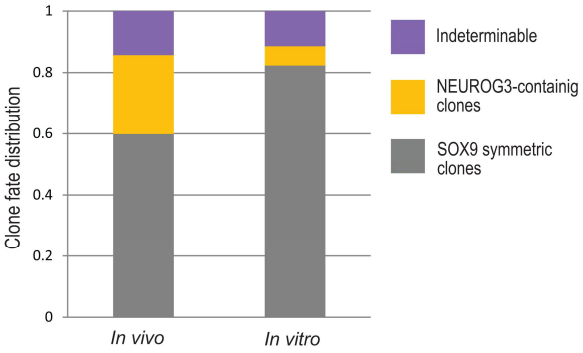

Figure S2. NEUROG3^{+} endocrine progenitor generation is more efficient *in vivo* than *in vitro*.
Comparison of 2-cell clone frequency distribution from *in vivo* clonal analysis (left column, *n* = 244), and *in vitro* clonal analysis (right column, *n* = 96) using E13.5 *Hnf1bCreER;mTmG* explants cultured on filters.

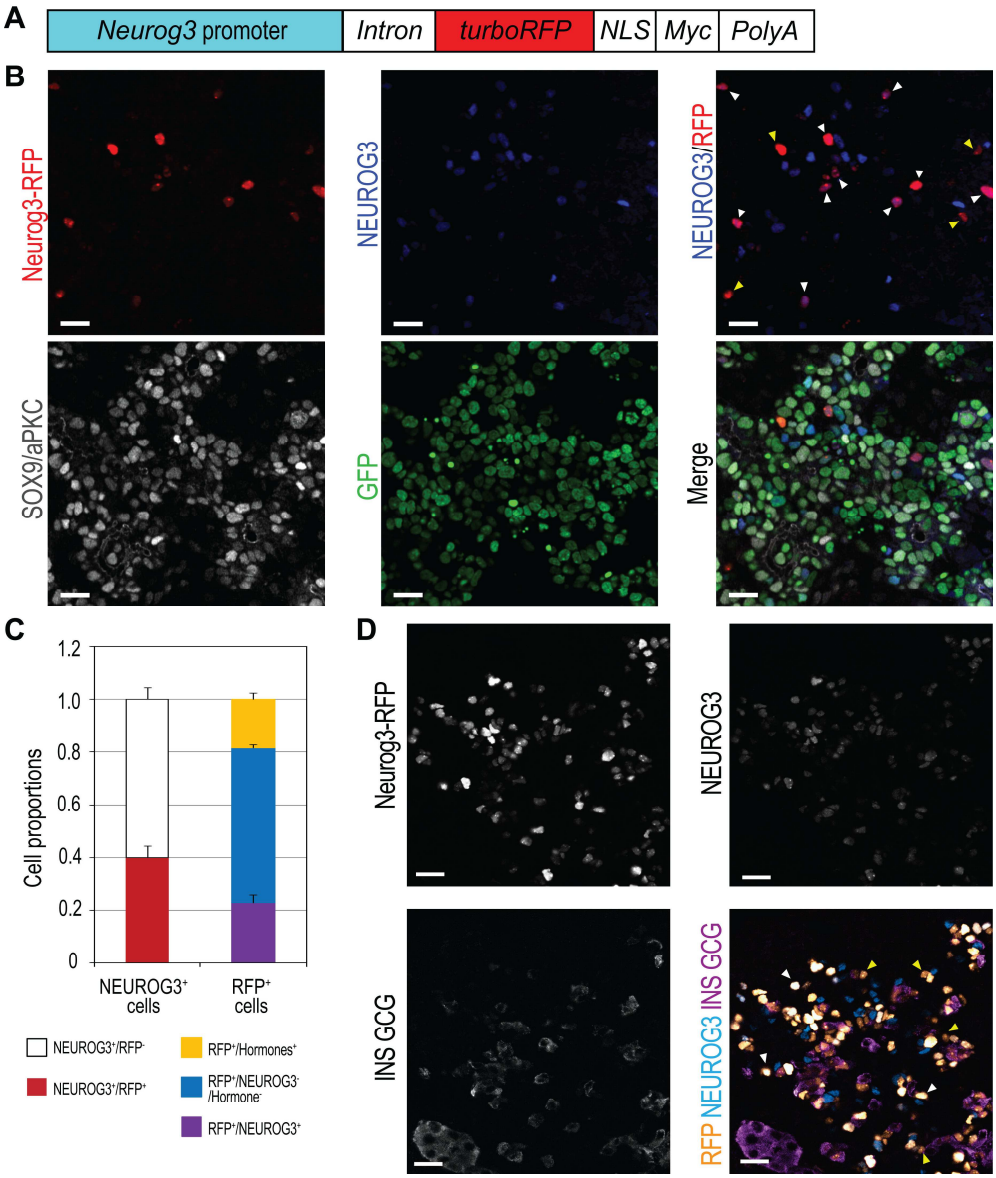

Figure S3. *Neurog3-RFP* transgenic line.
(A) Construct. A 7.6 kb *Neurog3* promoter region is linked to an intron, open reading frame of turboRFP, which contains a nuclear localization signal (NLS) and a Myc-tagC (Myc), and a bGH-PolyA signal (PolyA). The transgenic construct injection resulted in 2 transgenic mouse lines. (B) Optical section of a pancreatic explant from a *Pdx1*^{tTA}*;tetO-H2B-GFP;Neurog3-RFP* embryo, immunostained for NEUROG3 (blue), SOX9 (white) and aPKC (white). The RFP (red) and GFP (green) channels are native signals from each fluorescent protein. (C) Characterization of Neurog3-RFP in the E14.5 pancreas: Proportion of RFP^{+} (immunostained for Myc) (red) and RFP^{-} (white) in NEUROG3^{+} cells, and proportion of NEUROG3^{+}, Hormones^{+} (identified by INSULIN (INS) and GLUCAGON(GCG)) and NEUROG3^{-}/Hormones^{-} in RFP^{+} cells. (D) Optical section of E14.5 *Neurog3-RFP* pancreas, immunostained for NEUROG3 (cyan), RFP (Orange; immnostained for Myc), and INS and GCG (Magenta). White arrowheads indicate RFP^{+}/NEUROG3^{+} cells, and yellow arrowheads indicate RFP^{+}/NEUROG3^{-} cells. Scale bars, 20 μm. Histograms and error bars represent the mean and standard deviation (n = 4).

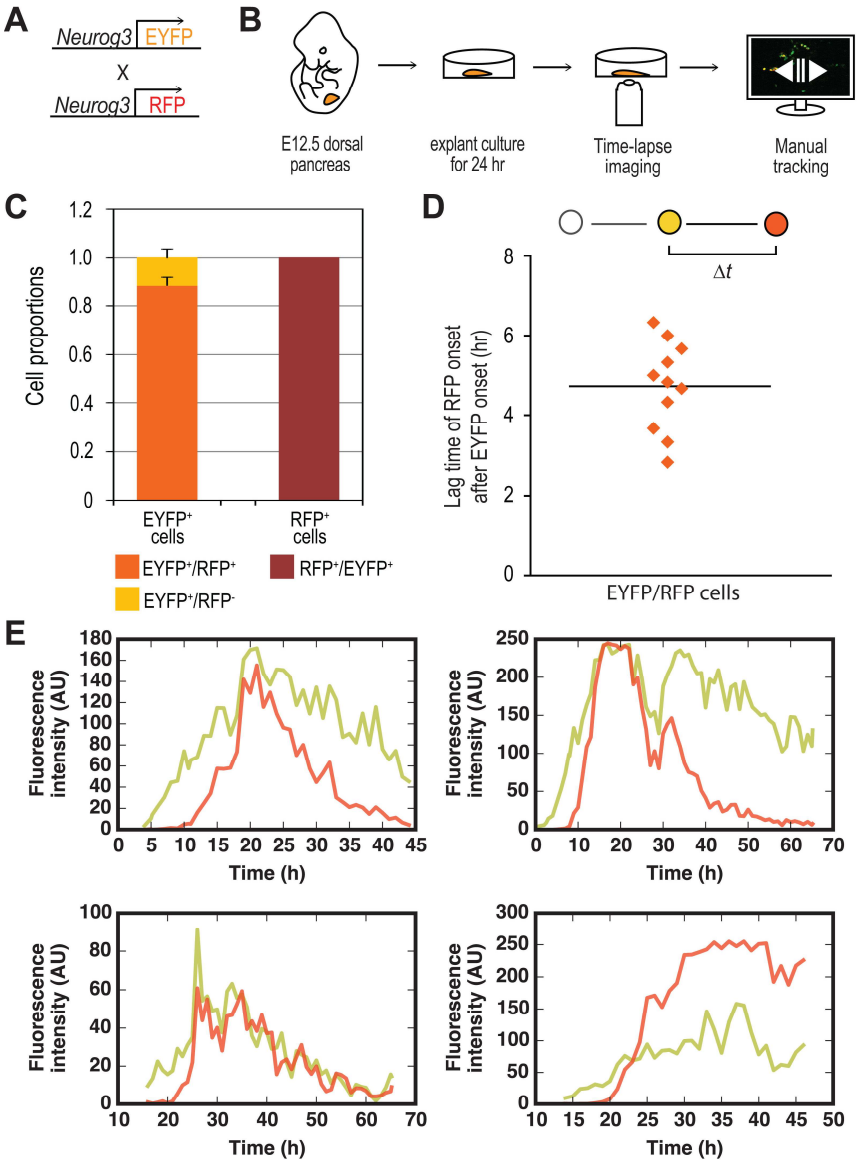

Figure S4. Comparison of *Neurog3-RFP* transgenic line to *Neurog3-EYFP* knock-add-on line.
(A) Scheme summarizing the genetic strategy to evaluate *Neurog3-RFP* fidelity compared to *Neurog3-EYFP*. (B) Scheme of imaging and analysis. Pancreatic explants from E12.5 *Neurog3-EYFP*; *Neurog3-RFP* embryos are cultured, and 3-D time-lapse imaging is done for over 48 hours. Then, EYFP- and RFP-expressing cells are tracked. (C) Quantification of EYFP and RFP cells at time 0 of time-lapse movies. Note that $EYFP^+/RFP^+$ bar (orange) includes cells that are initially RFP^- but acquire RFP over time, whereas $EYFP^+/RFP^-$ bar indicates cells express EYFP only throughout the movie. All RFP^+ cells are $EYFP^+$ (brown bar). Histograms and error bars represent the mean and standard deviation (n = 3). (D) Lag time of RFP onset after EYFP onset. RFP expression is delayed by 4.7 (±1.1) hours in $EYFP^+$ cells. (E) Fluorescence intensity of EYFP and RFP in 4 cells in time-lapse movies. The green and red lines indicate EYFP and RFP signals, respectively. Note RFP signal is delayed by several hours, and both EYFP and RFP signals have similar trend of increase and decrease over time. See Table S5 for further data.

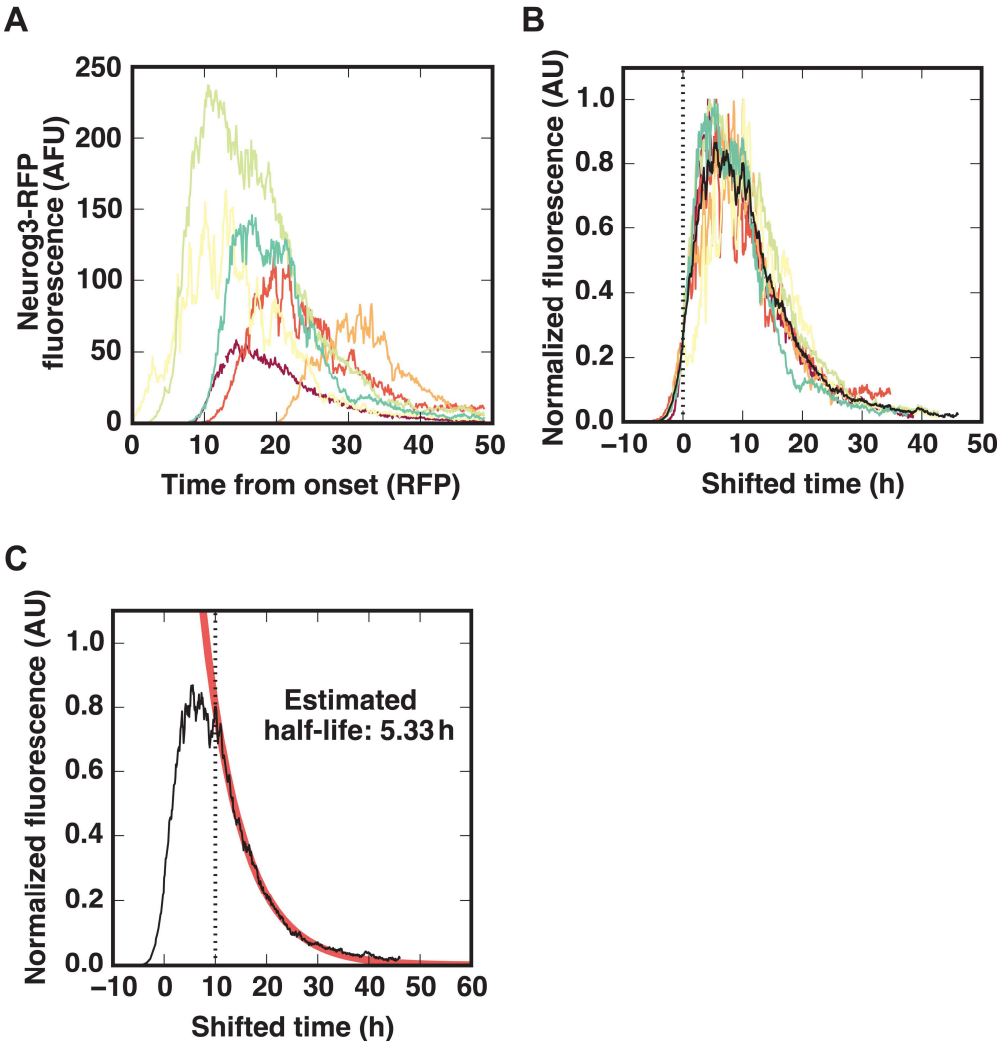

Figure S5. Dynamics of *Neurog3-RFP* during 48-hour time-lapse.
(A) Fluorescence intensity of individual Neurog3-RFP cells over time. Different colored lines indicate individual RFP cells. (B) Normalized fluorescence of all the RFP signals from (A) and aligned by 25% intensity to time 0. Black line indicates average intensity of all RFP signals. (C) Estimation of RFP half-life. Red line indicates the trend of exponential decay. RFP half-life is estimated as 5.3 hours.

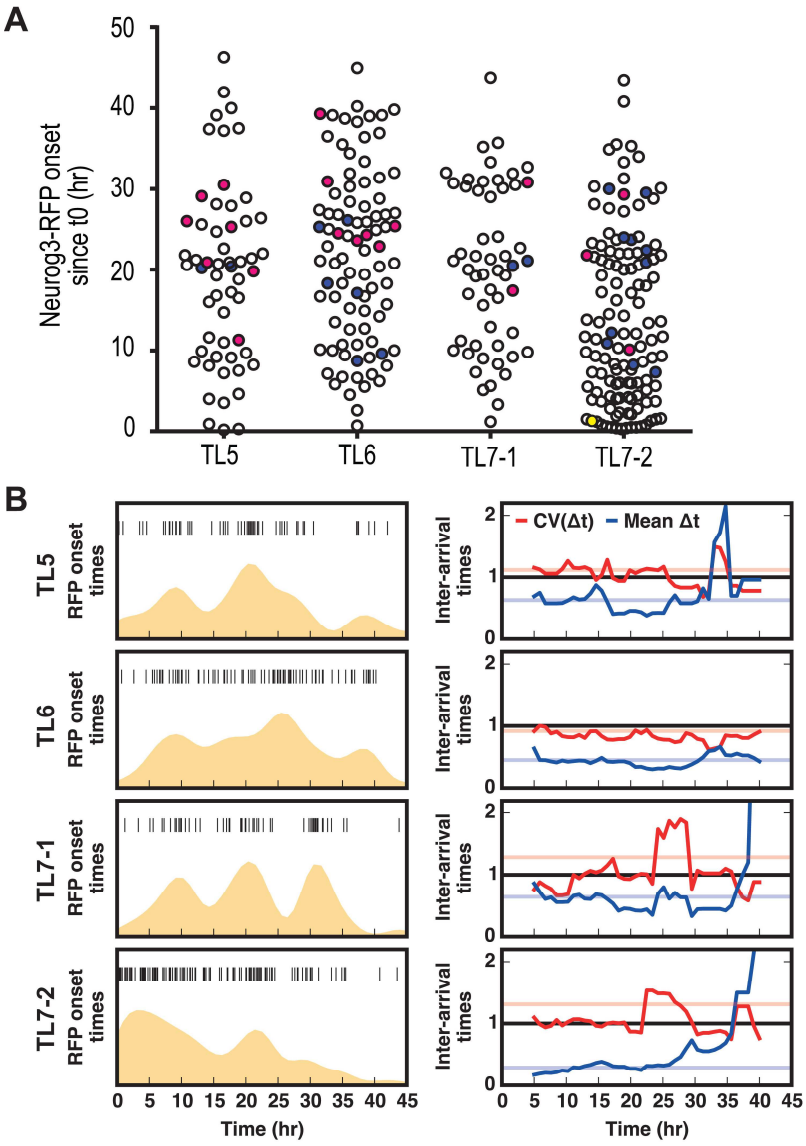

Figure S6. Analysis of Neurog3-RFP onset from time-lapse movies.
(A) RFP onset time distribution from 4 time-lapse movie positions (*n* = 56, 89, 54 and 125). Each circle indicates onset time of RFP cell. Red, blue, and yellow circles indicate RFP cells arising from asymmetric, symmetric, and RFP divisions, respectively. (B) Analyses of RFP onset Coefficient of Variance and sliding window for oscillatory patterns. The Coefficient of Variance of each time-lapse onset distribution is equivalent to a homogeneous process, which is equal to 1.

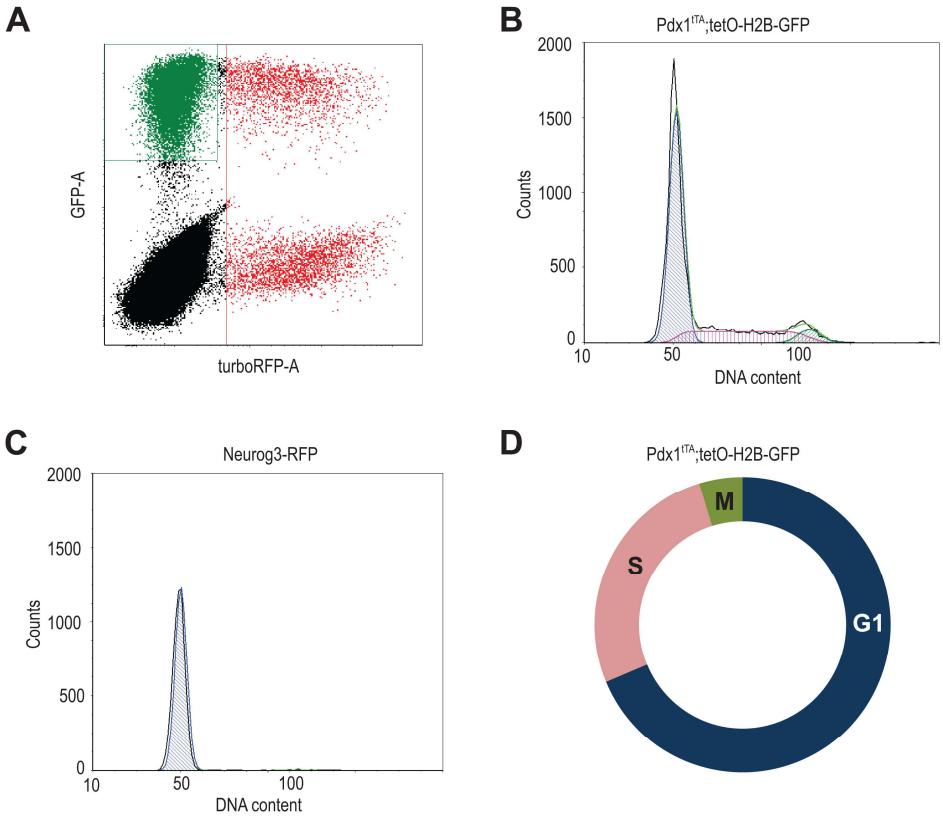

Figure S7. Cell cycle analysis of e14.5 *Pdx1$^{tTA/+}$;tetO-H2B-GFP;Neurog3-RFP* pancreata.
(A) Flow cytometry of dissociated pancreatic cells from pooled pancreata from a litter (10 embryos: 2 GFP$^+$/RFP$^+$, 1 GFP$^+$, 1 RFP$^+$, and 6 negative pancreata) for DNA content by DAPI staining. (B) Cell cycle analysis of pancreatic progenitors (Pdx1$^{tTA/+}$;tetO-H2B-GFP) by DAPI-stained DNA content. This panel shows 66.3% of cells in G1/G0 phase, 29.2% in S phase, and 4.5% in G2/M phase. (C) Cell cycle analysis of endocrine progenitors (Neurog3-RFP) by DAPI-stained DNA content. Note 97.2% of cells in G1/G0 phase, 1.6% in S phase and 1.2 in G2/M phase, as endocrine progenitors are mostly post-mitotic. (D) Average cell cycle of pancreatic progenitors (n = 3). 68.7 (± 2.1)% of cells are in G0/G1, 26.6 (± 2.4)% in S phase, and 4.7 (± 1.2)% in G2/M phase.

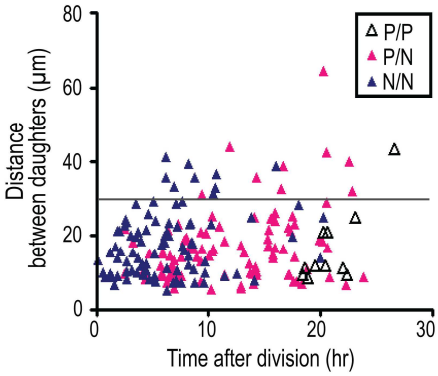

Figure S8. Distance between two daughters relative to time after division.
The X axis represents the time between division and NEUROG3 end-point immunostaining. White triangles show the distance between 2 progenitor daughters originating from symmetric divisions (P/P), pink triangles, distance between 1 progenitor and 1 NEUROG3 cell from asymmetric divisions (P/N), and blue triangles, distance between 2 NEUROG3 cells from symmetric divisions (N/N). Distance from P/P divisions was measured one frame prior to daughter divisions, which time indicates doubling time between mother and daughter divisions. There is therefore no data point before 18 hours. Regardless of the cell division mode, the distance between daughters increased, as time after division increased (Pearson's r, 0.81 (P/P), 0.33 (P/N), and 0.27 (N/N)). All 3 different modes of division showed statistically significant correlations between daughter distance and time: P/P division, p=0.0025, P/N division, p=0.0012, and N/N division, p=0.016. The gray line indicates 30 μm threshold used for *in vivo* clonal analysis for 2-cell clone boundaries. 90.2% of all data are under this threshold.

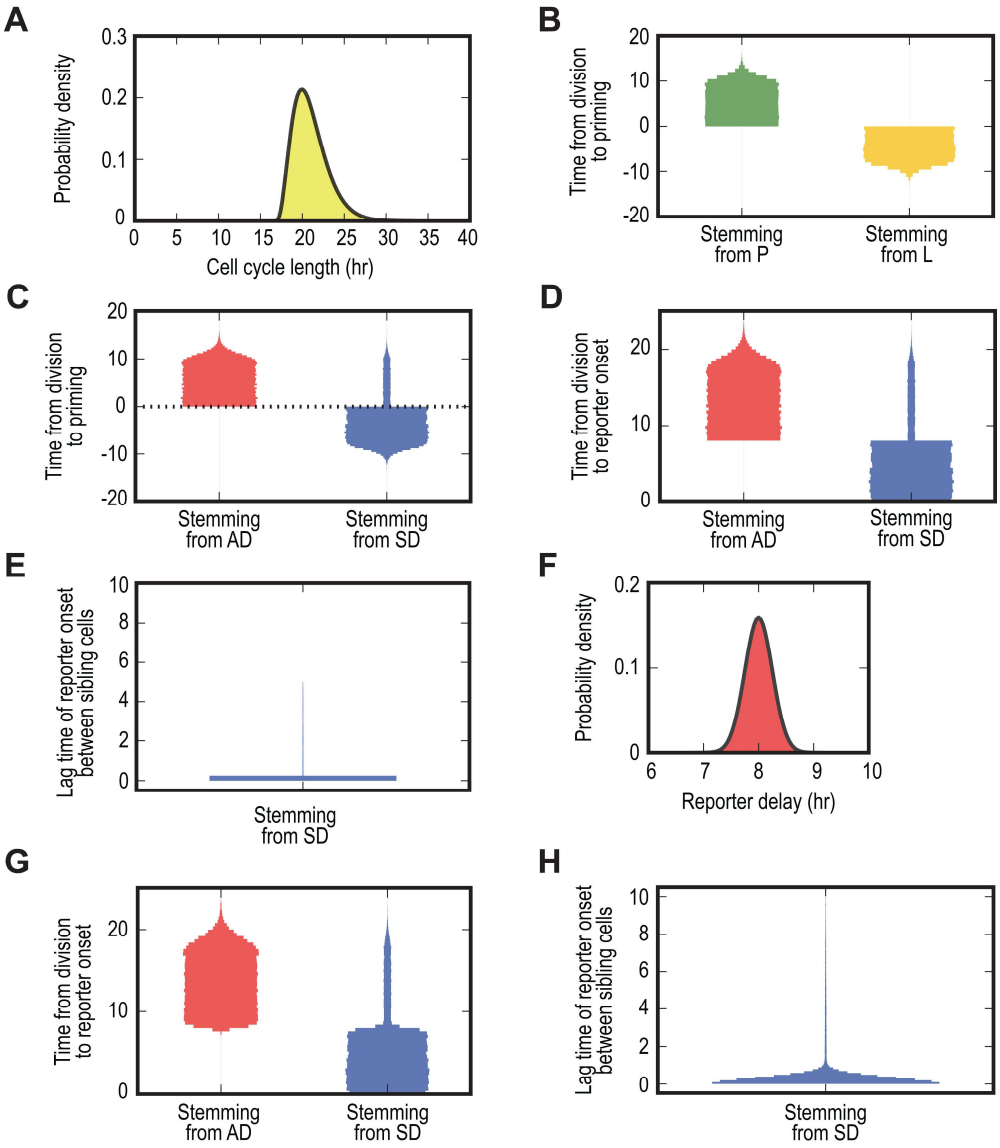

Figure S9. A model of cell cycle-dependent stochastic priming of progenitors to endocrine fate accounts for the observed RFP onset dynamics.

Monte Carlo simulations of clone expansion according to the model. Each newly born cell is randomly assigned a cell cycle length from a Gamma shifted (A) with mean and variance matching the experimentally measured. (B) Distribution of times from division to the priming event for cells stemming from P and L cells. Note that in the latter the priming event occurs prior to division. (C) Distribution of times from division to the priming event for cells stemming from AD and SD divisions. (D) Distribution of set times for a reporter with constant delay. (E) Lag time between the reporter onset in sibling cells. The simulations anticipate a high degree of synchronization. (F-H) Effect of heterogeneity in the reporter delay. (F) The distribution of delays of the reporter onset is assumed Gaussian. Variability in the reporter delay has little impact in the distribution of lag times in ACD and SCD originated cells (G) and in the synchronization of sibling cells (H)

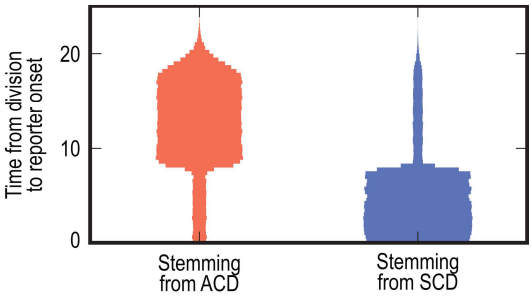

Figure S10. Model results including cell misclassification.
In order to account for the effect of possible misclassification biases in the distribution of lag times we performed an in silico misclassification experiment. We randomly sampled 11.6% of simulated cells stemming from SCD and classified them as stemming from ACD. The resulting distribution of reporter onset lag times for this latter group features a tail at low times that might partly account for the observed (cf. Figure 4C). This tail in the distribution, however, does not substantially affect the average lag time.

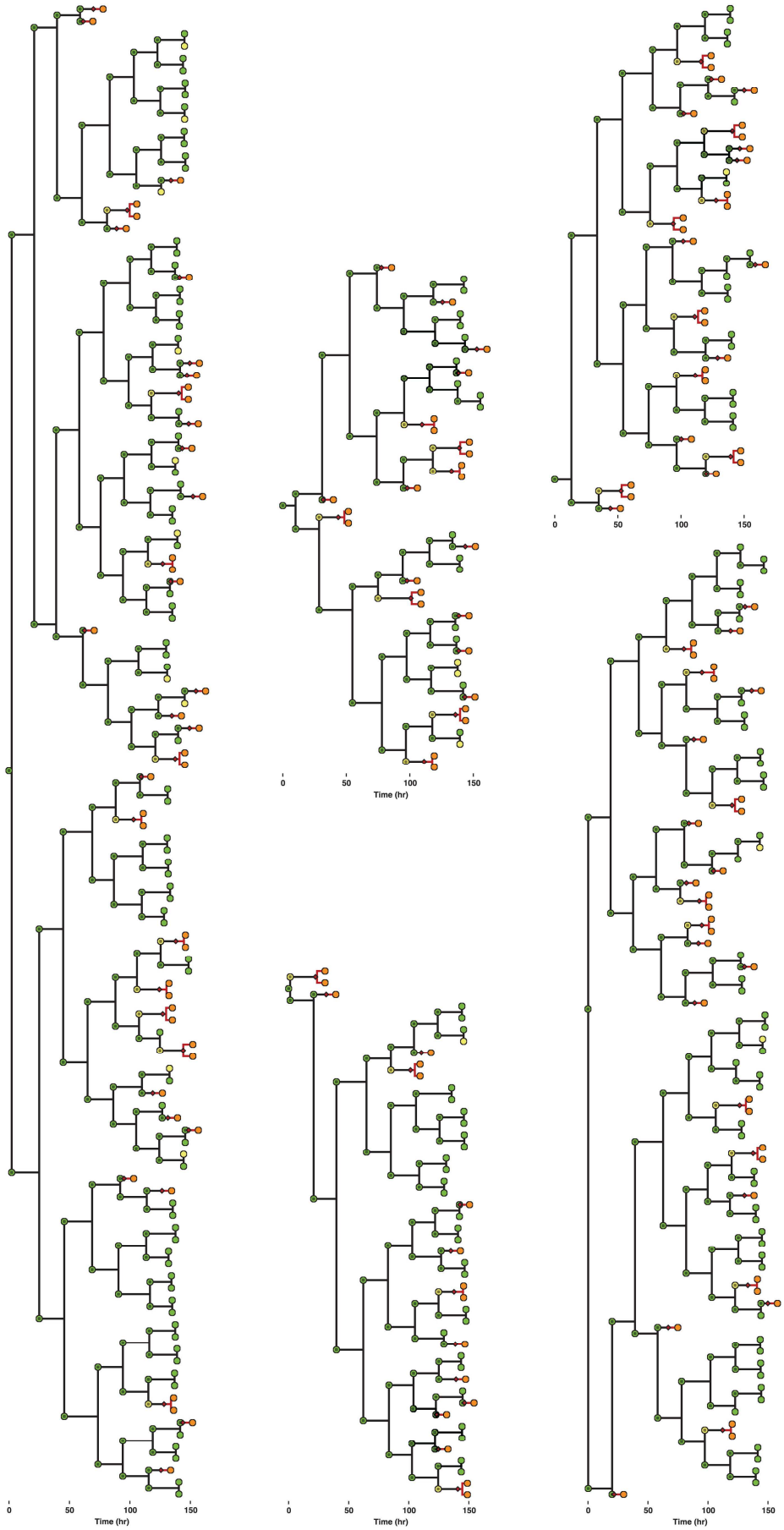
0
50
100
150
Time (hr)

Figure S11. Representative *in silico* clone lineages generated.
Temporal evolution of the expansion of five representative clones obtained with Monte-Carlo simulations of the model (*q=0.2, θ=0.55)*. X axis indicates experimental time. All simulations start at time zero with one progenitor cell (P, green circle) whose cell cycle phase is set uniformly at random and run for 150 hours. Progenitor cells continuously divide according to the distribution of cell cycles in Figure S9A. Stochastic priming events are indicated by red diamonds. Events occurring early following cell division lead to cells exiting the cell cycle and differentiating (N cells, orange circles). Events taking place later on lead to primed cells that are already committed to complete the cell cycle (L cells, yellow circles) and that will give rise to two differentiated post-mitotic cells (N cells).

Supplementary Tables

Table S1. Fraction of NEUROG3 over *Pdx1*$^{tTA/+}$;tetO-H2B-GFP cells from immunostaining images after time-lapse imaging.

	TL1	TL2	TL3	TL4	Mean	SD	Control*	E14.5 WT**
Ngn3 #	228	333	298	243			154	
H2B-GFP #	7069	7090	5608	6644			6145	
Ngn3/GFP	0.032	0.047	0.053	0.037	0.042	0.0095	0.025	0.089±0.009

*Explant control without imaging.

**Ngn3/PDX1 measurements (Mean ± standard deviation) from E14.5 pancreata (n=4).

Table S2. Data from NEUROG3^{+} cell tracking in time-lapse movies (*Pdx1*$^{tTA/+}$*;tetO-H2B-GFP*).

	TL1		TL2		TL3		TL4		Total	
Imaging duration (hr:mm)	18:36		18:48		24:00		24:06			
total div*	221		546		250		611		1628	
Ngn3-prod. div*	19		38		15		30		102	
Back-traced	Division	Ngn3 #	Division	Ngn3 #	Division	Ngn3 #	Division	Ngn3 #	Division	Ngn3 #
Asym div (P/N)	24	24	24	24	21	21	36	36	105	105
Sym div (N/N)	17	34	30	60	7	14	40	80	94	188
sister lost	11	11	1	1	7	7	5	5	24	24
sister dead	9	9	4	4	6	6	6	6	25	25
No div		55		52		28		36		171
lost		42		18		10		12		82
Total	61	175	59	159	41	86	87	175	248	595

* Number of division counted in a cropped position.

Table S3. Data from *in vivo* clonal analysis (*Hnf1bCreER;mT/mG*).

Sample ID	1	2	3	4	5	6	7	8	9	10	11	12	13	14	15	16	17	18	19	20	21	22	total
No. Of Recombined cells*	18	65	18	61	45	95	60	40	57	40	39	60	38	65	48	61	19	31	118	63	108	16	1165
No. of 2-cell clones	4	18	5	16	10	20	12	10	14	10	10	11	8	13	10	15	2	4	18	12	20	2	244
$SOX9^+/SOX9^+$	1	13	3	8	6	14	7	5	6	5	5	6	4	8	6	9	1	4	10	10	14	1	146
$SOX9^+/NEUROG3^+$	0	0	0	1	4	0	3	2	4	3	2	1	1	2	1	5	0	0	1	1	3	0	34
$NEUROG3^+/NEUROG3^+$	0	2	0	2	0	1	0	1	2	0	1	1	1	1	2	1	0	0	6	0	0	0	21
$NEUROG3^+/NEUROG3^-SOX9^-$	0	0	0	1	0	2	0	1	2	1	0	0	0	1	0	0	0	0	0	0	0	0	8
$SOX9^+/SOX9^-NEUROG3^-$	2	1	0	3	0	0	1	0	0	1	1	2	2	1	1	0	0	0	1	0	1	0	17
$SOX9^-NEUROG3^-/SOX9^-NEUROG3^-$	1	2	2	1	0	3	1	1	0	0	1	1	0	0	0	0	1	0	0	1	2	1	18

*mostly 1-cell clones except 14 3-cell clones and 2 4-cell clones out of 1165 recombined cells.

Table S4. Data from *in vitro* clonal analysis (*Hnf1bCreER;mT/mG*).

Sample ID	1	2	3	4	5	6	7	8	9	10	11	Total	Frequency
2-cell clones	11	13	0	9	10	7	9	9	9	8	11	96	-
SOX9 SCD	11	10	0	6	7	6	7	8	9	8	7	79	0.8229167
NEUROG3/SOX9 ACD	0	2	0	0	0	0	1	1	0	0	1	5	0.0520833
NEUROG3 SCD	0	0	0	0	0	0	0	0	0	0	1	1	0.0104167
SOX9+/SOX9-	0	1	0	2	2	1	1	0	0	0	1	8	0.0833333
SOX9-/SOX9-	0	0	0	1	1	0	0	0	0	0	1	3	0.03125

Table S5. Data from Neurog3-EYFP;Neurog3-RFP explant time-lapse.

	exp1	exp2	exp3	Total	avg	stdev
YFP+ # @t0	178	134	165	477		
RFP+ # @t0	153	110	141	404		
RFP+ # after t0	6	3	10	19		
potent. double (+)*#	159	113	151	423		
YFP+RFP- # @t0	19	21	14	54		
RFP+/YFP+ ratio @t0	0.86	0.82	0.85		0.84	0.02
YFP+/RFP+ ratio @t0	1	1	1		1	
double (+)*/YFP+ ratio	0.89	0.84	0.92		0.88	0.04
RFP-/YFP+ ratio	0.11	0.16	0.08		0.12	0.04

*Potentially double positive cells that acquire RFP expression at later time points from time-lapse movies, although the cells were initially YFP^+/RFP^- at time 0.

Table S6. Data from RFP$^+$ cell tracking in time-lapse movies (*Pdx1$^{tTA/+}$;tetO-H2B-GFP;Neurog3-RFP*).

	TL5		TL6		TL7		Total	
Imaging duration (hr:mm)	48:30		47:54		48:42			
Back-traced	Division	RFP #	Division	RFP #	Division	RFP #	Division	RFP #
Asym div (P/N)	11	11	9	9	7	7	27	27
Sym div (N/N)	6	12	4	8	8	16	18	36
sister lost*	3	3	5	5	3	3	11	11
sister dead	3	3	1	1	2	2	6	6
No division		49		17		20		86
Lost**		146		160		103		409
RFP+ cell division	2	4	0	0	1	2	3	6
Total	25	228	19	200	21	153	65	581

*Mostly due to low GFP signal.

**Mostly due to moving out of Z position during backtracking. i.e. During the acquisition of images, the explants flatten, therefore, the majority of lost RFP cells appear during the flattening process over time.

Table S7. Primary antibodies used for immunostainings.

Epitope	Species generated	Dilution factor	Provider	Catalog number
NEUROG3	goat	1:1,000	BCBC*	AB2774
SOX9	rabbit	1:2,000	Millipore	AB5535
aPKC	rabbit	1:1,000	Santa Cruz	sc-216
E-CAD	mouse	1:200	BD Trasduction Lab	C20820
MYC	mouse	1:200	Invitrogen	13-2500
GFP	chicken	1:1,000	Abcam	AB13970
INSULIN	guinea pig	1:50	Dako	A0564
GLUCAGON	guinea pig	1:800	Linco	4031-01F

*BCBC, Beta Cell Biology Consortium, funded by NIDDK U01DK072473.

11 REFERENCES

11.1 Articles

Afelik, S., Pool, B., Schmerr, M., Perron, C. and Jensen, J. (2015). Wnt7b is required for epithelial progenitor growth and operates during epithelial-to-mesenchymal signaling in pancreatic development. *Developmental Biology* **pii: S0012-1606**, 00672-00671.

Agrons, G. A., Corse, W. R., Markowitz, R. I., Suarez, E. S. and Perry, D. R. (1996). Gastrointestinal manifestations of cystic fibrosis: radiologic-pathologic correlation. *Radiographics : a review publication of the Radiological Society of North America, Inc* **16**, 871-893.

Ahlgren, U., Jonsson, J. and Edlund, H. (1996). The morphogenesis of the pancreatic mesenchyme is uncoupled from that of the pancreatic epithelium in IPF1/PDX1-deficient mice. *Development (Cambridge, England)* **122**, 1409-1416.

Ahlgren, U., Pfaff, S. L., Jessell, T. M., Edlund, T. and Edlund, H. (1997). Independent requirement for ISL1 in formation of pancreatic mesenchyme and islet cells. *Nature* **385**, 257-260.

Ahlgren, U., Jonsson, J., Jonsson, L., Simu, K. and Edlund, H. (1998). beta-cell-specific inactivation of the mouse Ipf1/Pdx1 gene results in loss of the beta-cell phenotype and maturity onset diabetes. *Genes & development* **12**, 1763-1768.

Ahnfelt-Rønne, J., Ravassard, P., Pardanaud-Glavieux, C., Scharfmann, R. and Serup, P. (2010). Mesenchymal Bone Morphogenetic Protein Signaling Is Required for Normal Pancreas Development. *Diabetes* **59**, 1948-1956.

Ahnfelt-Rønne, J., Jørgensen, M. C., Klinck, R., Jensen, J. N., Füchtbauer, E.-M. M., Deering, T., MacDonald, R. J., Wright, C. V., Madsen, O. D. and Serup, P. (2012). Ptf1a-mediated control of Dll1 reveals an alternative to the lateral inhibition mechanism. *Development (Cambridge, England)* **139**, 33-45.

Albaqumi, M., Srivastava, S., Li, Z., Zhdnova, O., Wulff, H., Itani, O., Wallace, D. P. and Skolnik, E. Y. (2008). KCa3.1 potassium channels are critical for cAMP-dependent chloride secretion and cyst growth in autosomal-dominant polycystic kidney disease. *Kidney international* **74**, 740-749.

Anders, S. and Huber, W. (2010). Differential expression analysis for sequence count data. *Genome Biol* **11**, R106.

Ang, S. L. and Rossant, J. (1994). HNF-3β is essential for node and notochord formation in mouse development. *Cell* **78**, 561-574.

Ang, S. L., Wierda, A., Wong, D., Stevens, K. A., Cascio, S., Rossant, J. and Zaret, K. S. (1993). The formation and maintenance of the definitive endoderm lineage in the mouse: involvement of HNF3/forkhead proteins. *Development (Cambridge, England)* **119**, 1301-1315.

Apelqvist, A., Ahlgren, U. and Edlund, H. (1997). Sonic hedgehog directs specialised mesoderm differentiation in the intestine and pancreas. *Current biology : CB* **7**, 801-804.

Apelqvist, A., Li, H., Sommer, L., Beatus, P., Anderson, D., Honjo, T., Hrabe de Angelis, M., Lendahl, U. and Edlund, H. (1999). Notch signalling controls pancreatic cell differentiation. *Nature* **400**, 877-881.

Apte, M. V., Haber, P. S., Applegate, T. L., Norton, I. D., McCaughan, G. W., Korsten, M. A., Pirola, R. C. and Wilson, J. S. (1998). Periacinar stellate shaped cells in rat pancreas: identification, isolation, and culture. *Gut* **43**, 128-133.

Apte, M. V., Haber, P. S., Darby, S. J., Rodgers, S. C., McCaughan, G. W., Korsten, M. A., Pirola, R. C. and Wilson, J. S. (1999). Pancreatic stellate cells are activated by proinflammatory cytokines: implications for pancreatic fibrogenesis. *Gut* **44**, 534-541.

Arda, H. E., Benitez, C. M. and Kim, S. K. (2013). Gene regulatory networks governing pancreas development. *Dev. Cell* **25**, 5-13.

Ashcroft, F. M. and Rorsman, P. (2012). Diabetes mellitus and the β cell: the last ten years. *Cell* **148**, 1160-1171.

Babenko, A. P., Polak, M., Cavé, H., Busiah, K., Czernichow, P., Scharfmann, R., Bryan, J., Aguilar-Bryan, L., Vaxillaire, M. and Froguel, P. (2006). Activating mutations in the ABCC8 gene in neonatal diabetes mellitus. *The New England journal of medicine* **355**, 456-466.

Balci, S., Bostanoglu, S., Altınok, G. and Özaltin, F. (1999). Sibs diagnosed prenatally with situs inversus totalis, renal and pancreatic dysplasia, and cysts: A new syndrome? *Am. J. Med. Genet.* **82**, 166-169.

Banaei-Bouchareb, L., Gouon-Evans, V., Samara-Boustani, D., Castellotti, M. c., Czernichow, P., Pollard, J. W. and Polak, M. (2004). Insulin cell mass is altered in Csf1op/Csf1op macrophage-deficient mice. *Journal of Leukocyte Biology* **76**, 359-367.

Barbacci, E., Reber, M., Ott, M. O., Breillat, C., Huetz, F. and Cereghini, S. (1999). Variant hepatocyte nuclear factor 1 is required for visceral endoderm specification. *Development (Cambridge, England)* **126**, 4795-4805.

Baumgartner, B. K., Cash, G., Hansen, H., Ostler, S. and Murtaugh, L. C. (2014). Distinct requirements for beta-catenin in pancreatic epithelial growth and patterning. *Developmental biology* **391**, 89-98.

Belibi, F. A., Reif, G., Wallace, D. P., Yamaguchi, T., Olsen, L., Li, H., Helmkamp, G. M. and Grantham, J. J. (2004). Cyclic AMP promotes growth and secretion in human polycystic kidney epithelial cells. *Kidney international* **66**, 964-973.

Bellanné-Chantelot, C., Clauin, S., Chauveau, D., Collin, P., Daumont, M., Douillard, C., Dubois-Laforgue, D., Dusselier, L., Gautier, J.-F., Jadoul, M. et al. (2005). Large genomic rearrangements in the hepatocyte nuclear factor-1beta (TCF2) gene are the most frequent cause of maturity-onset diabetes of the young type 5. *Diabetes* **54**, 3126-3132.

Belo, J. A., Bachiller, D., Agius, E., Kemp, C., Borges, A. C., Marques, S., Piccolo, S. and De Robertis, E. M. (2000). Cerberus-like is a secreted BMP and nodal antagonist not essential for mouse development. *genesis* **26**, 265-270.

Beres, T. M., Masui, T., Swift, G. H., Shi, L., Henke, R. M. and MacDonald, R. J. (2006). PTF1 is an organ-specific and Notch-independent basic helix-loop-helix complex containing the mammalian Suppressor of Hairless (RBP-J) or its paralogue, RBP-L. *Molecular and cellular biology* **26**, 117-130.

Bergmann, C., Fliegauf, M., Brüchle, N. O., Frank, V., Olbrich, H., Kirschner, J., Schermer, B., Schmedding, I., Kispert, A., Kränzlin, B. et al. (2008). Loss of nephrocystin-3 function can cause embryonic lethality, Meckel-Gruber-like syndrome, situs inversus, and renal-hepatic-pancreatic dysplasia. *American journal of human genetics* **82**, 959-970.

Berrocal, T., Pajares, M. P. and Zubillaga, A. F. (2005). Pancreatic cystosis in children and young adults with cystic fibrosis: sonographic, CT, and MRI findings. *AJR. American journal of roentgenology* **184**, 1305-1309.

Besnard, V., Wert, S. E., Hull, W. M. and Whitsett, J. A. (2004). Immunohistochemical localization of Foxa1 and Foxa2 in mouse embryos and adult tissues. *Gene Expression Patterns* **5**, 193-208.

Beucher, A., Martín, M., Spenle, C., Poulet, M., Collin, C. and Gradwohl, G. (2012). Competence of failed endocrine progenitors to give rise to acinar but not ductal cells is restricted to early pancreas development. *Developmental biology* **361**, 277-285.

Bhushan, A., Itoh, N., Kato, S. and Thiery, J. P. (2001). Fgf10 is essential for maintaining the proliferative capacity of epithelial progenitor cells during early pancreatic organogenesis. *Development* **128**, 5109-5117.

Boczonadi, V. and Määttä, A. (2012). Annexin A9 is a periplakin interacting partner in membrane-targeted cytoskeletal linker protein complexes. *FEBS Lett.* **586**, 3090-3096.

Bodmer, B. and Siboo, R. (1977). Isolation of mouse C-reactive protein from liver and serum. *Journal of immunology (Baltimore, Md. : 1950)* **118**, 1086-1089.

Bonnefond, A., Vaillant, E., Philippe, J. and Skrobek, B. (2013). Transcription factor gene< i> MNX1</i> is a novel cause of permanent neonatal diabetes in a consanguineous family. *Diabetes Metab.* **39**, 276-280.

Bonnefond, A., Lomberk, G., Buttar, N., Busiah, K., Vaillant, E., Lobbens, S., Yengo, L., Dechaume, A., Mignot, B., Simon, A. et al. (2011). Disruption of a Novel Krüppel-like Transcription Factor p300-regulated Pathway for Insulin Biosynthesis Revealed by Studies of the c.-331 INS Mutation Found in Neonatal Diabetes Mellitus*. *The Journal of biological chemistry* **286**, 28414-28424.

Boquist, L. (1968). Cilia in normal and regenerating islet tissue. *Zeitschrift f**r Zellforschung und Mikroskopische Anatomie* **89**, 519-532.

Boulter, C., Mulroy, S., Webb, S., Fleming, S., Brindle, K. and Sandford, R. (2001). Cardiovascular, skeletal, and renal defects in mice with a targeted disruption of the Pkd1 gene. *Proceedings of the National Academy of Sciences* **98**, 12174-12179.
Bouvrette, D. J., Price, S. J. and Bryda, E. C. (2008). K Homology Domains of the Mouse Polycystic Kidney Disease-Related Protein, Bicaudal-C (Bicc1), Mediate RNA Binding in vitro. *Nephron Experimental Nephrology* **108**, e27-34.
Bouvrette, D. J., Sittaramane, V., Heidel, J. R., Chandrasekhar, A. and Bryda, E. C. (2010). Knockdown of bicaudal C in zebrafish (Danio rerio) causes cystic kidneys: a nonmammalian model of polycystic kidney disease. *Comparative medicine* **60**, 96-106.
Bowman, P., Flanagan, S. E., Edghill, E. L., Damhuis, A., Shepherd, M. H., Paisey, R., Hattersley, A. T. and Ellard, S. (2011). Heterozygous ABCC8 mutations are a cause of MODY. *Diabetologia* **55**, 123-127.
Brissova, M., Shostak, A., Shiota, M. and Wiebe, P. O. (2006). Pancreatic islet production of vascular endothelial growth factor-a is essential for islet vascularization, revascularization, and function. *Diabetes* **55**, 2974-2985.
Burlison, J. S., Long, Q., Fujitani, Y., Wright, C. V. E. and Magnuson, M. A. (2008). Pdx-1 and Ptf1a concurrently determine fate specification of pancreatic multipotent progenitor cells. *Developmental biology* **316**, 74-86.
Böttinger, E. P., Jakubczak, J. L., Roberts, I. S., Mumy, M., Hemmati, P., Bagnall, K., Merlino, G. and Wakefield, L. M. (1997). Expression of a dominant-negative mutant TGF-beta type II receptor in transgenic mice reveals essential roles for TGF-beta in regulation of growth and differentiation in the exocrine pancreas. *The EMBO journal* **16**, 2621-2633.
Cai, Y., Maeda, Y., Cedzich, A., Torres, V. E., Wu, G., Hayashi, T., Mochizuki, T., Park, J. H., Witzgall, R. and Somlo, S. (1999). Identification and characterization of polycystin-2, the PKD2 gene product. *The Journal of biological chemistry* **274**, 28557-28565.
Cano, D. A., Sekine, S. and Hebrok, M. (2006). Primary cilia deletion in pancreatic epithelial cells results in cyst formation and pancreatitis. *Gastroenterology* **131**, 1856-1869.
Cano, D. A., Murcia, N. S., Pazour, G. J. and Hebrok, M. (2004). Orpk mouse model of polycystic kidney disease reveals essential role of primary cilia in pancreatic tissue organization. *Development* **131**, 3457-3467.
Carthew, R. W. and Sontheimer, E. J. (2009). Origins and Mechanisms of miRNAs and siRNAs. *Cell* **136**.
Castagnetti, S. and Ephrussi, A. (2003). Orb and a long poly (A) tail are required for efficient oskar translation at the posterior pole of the Drosophila oocyte. *Development* **130**, 835-843.
Cervantes, S., Lau, J., Cano, D. A., Borromeo-Austin, C. and Hebrok, M. (2010). Primary cilia regulate Gli/Hedgehog activation in pancreas. *Proceedings of the National Academy of Sciences of the United States of America* **107**, 10109-10114.
Chabardès, D., Imbert-Teboul, M. and Elalouf, J. M. (1999). Functional properties of Ca2+-inhibitable type 5 and type 6 adenylyl cyclases and role of Ca2+ increase in the inhibition of intracellular cAMP content. *Cell. Signal.* **11**, 651-663.
Chang, M. Y., Parker, E., Ibrahim, S., Shortland, J. R., Nahas, M. E., Haylor, J. L. and Ong, A. C. (2006). Haploinsufficiency of Pkd2 is associated with increased tubular cell proliferation and interstitial fibrosis in two murine Pkd2 models. *Nephrology, dialysis, transplantation : official publication of the European Dialysis and Transplant Association - European Renal Association* **21**, 2078-2084.
Chao-Nan, Q., Jared, K., Peter, I., Fangming, L., Uko, Z., Bin Tean, T. and Bart, O. W. (2005). Cystic Renal Neoplasia Following Conditional Inactivation of Apc in Mouse Renal Tubular Epithelium. *J. Biol. Chem.* **280**, 3938-3945.
Chen, W. S., Manova, K., Weinstein, D. C., Duncan, S. A., Plump, A. S., Prezioso, V. R., Bachvarova, R. F. and Darnell, J. E. (1994). Disruption of the HNF-4 gene, expressed in visceral endoderm, leads to cell death in embryonic ectoderm and impaired gastrulation of mouse embryos. *Genes & development* **8**, 2466-2477.
Chen, Z., Herman, A. E., Matos, M., Mathis, D. and Benoist, C. (2005). Where CD4+CD25+ T reg cells impinge on autoimmune diabetes. *The Journal of experimental medicine* **202**, 1387-1397.

Chicoine, J., Benoit, P., Gamberi, C., Paliouras, M., Simonelig, M. and Lasko, P. (2007). Bicaudal-C recruits CCR4-NOT deadenylase to target mRNAs and regulates oogenesis, cytoskeletal organization, and its own expression. *Dev. Cell* **13**, 691-704.
Choi, E., Kraus, M. R., Lemaire, L. A., Yoshimoto, M., Vemula, S., Potter, L. A., Manduchi, E., Stoeckert, C. J., Grapin-Botton, A. and Magnuson, M. A. (2012). Dual lineage-specific expression of Sox17 during mouse embryogenesis. *Stem cells (Dayton, Ohio)* **30**, 2297-2308.
Clotman, F., Jacquemin, P., Plumb-Rudewiez, N., Pierreux, C. E., Van der Smissen, P., Dietz, H. C., Courtoy, P. J., Rousseau, G. G. and Lemaigre, F. P. (2005). Control of liver cell fate decision by a gradient of TGFβ signaling modulated by Onecut transcription factors. *Genes & development* **19**, 1849-1854.
Coffinier, C., Barra, J., Badinet, C. and Yaniv, M. (1999a). Expression of the vHNF1/HNF1β homeoprotein gene during mouse organogenesis. *Mech. Dev.* **89**, 211-213.
Coffinier, C., Thépot, D., Babinet, C., Yaniv, M. and Barra, J. (1999b). Essential role for the homeoprotein vHNF1/HNF1beta in visceral endoderm differentiation. *Development (Cambridge, England)* **126**, 4785-4794.
Coffinier, C., Gresh, L., Fiette, L., Tronche, F., Schütz, G., Babinet, C., Pontoglio, M., Yaniv, M. and Barra, J. (2002). Bile system morphogenesis defects and liver dysfunction upon targeted deletion of HNF1beta. *Development (Cambridge, England)* **129**, 1829-1838.
Cogswell, C., Price, S. J., Hou, X., Guay-Woodford, L. M., Flaherty, L. and Bryda, E. C. (2003). Positional cloning of jcpk/bpk locus of the mouse. *Mammalian genome : official journal of the International Mammalian Genome Society* **14**, 242-249.
Cole, B. R., Kaufman, R. L., McAlister, W. H. and Kissane, J. M. (1976). Bilateral renal dysplasia in three siblings: report of a survivor. *Clin. Nephrol.* **5**, 83-87.
Collin, G. B., Cyr, E., Bronson, R., Marshall, J. D., Gifford, E. J., Hicks, W., Murray, S. A., Zheng, Q. Y., S., S. R., Nishina, P. M. et al. (2005). Alms1-disrupted mice recapitulate human Alström syndrome. *Human Molecular Genetics* **14**, 2323-2333.
Collin, G. B., Marshall, J. D., Ikeda, A., So, W. V., Russell-Eggitt, I., Maffei, P., Beck, S., Boerkoel, C. F., Sicolo, N., Martin, M. et al. (2002). Mutations in ALMS1 cause obesity, type 2 diabetes and neurosensory degeneration in Alström syndrome. *Nature genetics* **31**, 74-78.
Collombat, P., Mansouri, A., Hecksher-Sørensen, J., Serup, P., Krull, J., Gradwohl, G. and Gruss, P. (2003). Opposing actions of Arx and Pax4 in endocrine pancreas development. *Gene Dev* **17**, 2591-2603.
Collombat, P., Hecksher-Sørensen, J., Krull, J., Berger, J., Riedel, D., Herrera, P. L., Serup, P. and Mansouri, A. (2007). Embryonic endocrine pancreas and mature β cells acquire α and PP cell phenotypes upon Arx misexpression. *J. Clin. Invest.* **117**, 961-970.
Collombat, P., Hecksher-Sørensen, J., Broccoli, V., Krull, J., Ponte, I., Mundiger, T., Smith, J., Gruss, P., Serup, P. and Mansouri, A. (2005). The simultaneous loss of Arx and Pax4 genes promotes a somatostatin-producing cell fate specification at the expense of the α-and β-cell lineages in the mouse …. *Development* **132**, 2969-2980.
Collombat, P., Xu, X., Ravassard, P., Sosa-Pineda, B., Dussaud, S., Billestrup, N., Madsen, O. D., Serup, P., Heimberg, H. and Mansouri, A. (2009). The Ectopic Expression of Pax4 in the Mouse Pancreas Converts Progenitor Cells into α and Subsequently β Cells. *Cell* **138**, 449-462.
Copp, D. H. and Cheney, B. (1962). Calcitonin - a Hormone from the Parathyroid which Lowers the Calcium-level of the Blood. *Nature* **193**, 381-382.
Cortijo, C., Gouzi, M., Tissir, F. and Grapin-Botton, A. (2012). Planar cell polarity controls pancreatic beta cell differentiation and glucose homeostasis. *Cell Rep.* **2**, 1593-1606.
Davenport, J. R., Watts, A. J., Roper, V. C., Croyle, M. J., van Groen, T., Wyss, J. M., Nagy, T. R., Kesterson, R. A. and Yoder, B. K. (2007). Disruption of intraflagellar transport in adult mice leads to obesity and slow-onset cystic kidney disease. *Current biology : CB* **17**, 1586-1594.
Davis, R. L., Weintraub, H. and Lassar, A. B. (1987). Expression of a single transfected cDNA converts fibroblasts to myoblasts. *Cell* **51**, 987-1000.
De Vas, M. G., Kopp, J. L., Sander, M., Cereghini, S. and Haumaitre, C. (2015). Hnf1b controls pancreas morphogenesis and generation of Ngn3+ endocrine progenitors. *Development* **142**, 871-882.

Delépine, M., Nicolino, M., Barrett, T., Golamaully, M., Lathrop, M. G. and Julier, C. (2000). EIF2AK3, encoding translation initiation factor 2-α kinase 3, is mutated in patients with Wolcott-Rallison syndrome. *Nature Genetics* **25**, 406-409.
Deltour, L., Leduque, P., Paldi, M. A., Ripoche, P., Dubois, P. and Jami, J. (1991). Polyclonal origin of pancreatic islets in aggregation mouse chimaeras. *Development (Cambridge, England)* **112**, 1115-1121.
Demos, T. C., Posniak, H. V., Harmath, C., Olson, M. C. and Aranha, G. (2002). Cystic lesions of the pancreas. *AJR. American journal of roentgenology* **179**, 1375-1388.
Desgraz, R. and Herrera, P. (2009). Pancreatic neurogenin 3-expressing cells are unipotent islet precursors. *Development* **136**, 3567-3574.
Dessimoz, J., Bonnard, C., Huelsken, J. and Grapin-Botton, A. (2005). Pancreas-specific deletion of beta-catenin reveals Wnt-dependent and Wnt-independent functions during development. *Curr. Biol.* **15**, 1677-1683.
Dichmann, D. S., Miller, C. P., Jensen, J., Scott Heller, R. and Serup, P. (2003). Expression and misexpression of members of the FGF and TGFbeta families of growth factors in the developing mouse pancreas. *Dev Dyn* **226**, 663-674.
Dorey, K. and Hill, C. S. (2006). A novel Cripto-related protein reveals an essential role for EGF-CFCs in Nodal signalling in Xenopus embryos. *Developmental biology* **292**, 303-316.
Dorey, K. and Amaya, E. (2010). FGF signalling: diverse roles during early vertebrate embryogenesis. *Development* **137**, 3731-3742.
Du, A., Hunter, C. S., Murray, J., Noble, D., Cai, C.-L. L., Evans, S. M., Stein, R. and May, C. L. (2009). Islet-1 is required for the maturation, proliferation, and survival of the endocrine pancreas. *Diabetes* **58**, 2059-2069.
Dubois, C. L., Shih, H. P., Seymour, P. A., Patel, N. A., Behrmann, J. M., Ngo, V. and Sander, M. (2011). Sox9-haploinsufficiency causes glucose intolerance in mice. *PloS one* **6**, e23131.
Duvillie, B., Cordonnier, N., Deltour, L., Dandoy-Dron, F., Itier, J. M., Monthioux, E., Jami, J., Joshi, R. L. and Bucchini, D. (1997). Phenotypic alterations in insulin-deficient mutant mice. *Proceedings of the National Academy of Sciences* **94**, 5137-5140.
Duvillié, B., Currie, C., Chrones, T., Bicchini, D., Jami, J., Joshi, R. L. and Hill, D. J. (2002). Increased islet cell proliferation, decreased apoptosis, and greater vascularization leading to beta-cell hyperplasia in mutant mice lacking insulin. *Endocrinology* **143**, 1530-1537.
Eckmann, C. R., Kraemer, B., Wickens, M. and Kimble, J. (2002). GLD-3, a bicaudal-C homolog that inhibits FBF to control germline sex determination in C. elegans. *Dev. Cell* **3**, 697-710.
Eckmann, C. R., Crittenden, S. L., Suh, N. and Kimble, J. (2004). GLD-3 and Control of the Mitosis/Meiosis Decision in the Germline of Caenorhabditis elegans. *Genetics* **168**, 147-160.
Edghill, E. L., Flanagan, S. E., Patch, A. M., Boustred, C., Parrish, A., Shields, B., Shepherd, M. H., Hussain, K., Kapoor, R. R., Malecki, M. et al. (2007). Insulin Mutation Screening in 1,044 Patients With Diabetes: Mutations in the INS Gene Are a Common Cause of Neonatal Diabetes but a Rare Cause of Diabetes Diagnosed in Childhood or Adulthood. *Diabetes* **57**, 10341042.
Edsbagge, J., Johansson, J., K., Esni, F., Luo, Y., Radice, G. L. and Semb, H. (2005). Vascular function and sphingosine-1-phosphate regulate development of the dorsal pancreatic mesenchyme. *Development* **132**, 1085-1092.
Ejarque, M., Cervantes, S., Pujadas, G., Tutusaus, A., Sanchez, L. and Gasa, R. (2013). Neurogenin3 cooperates with Foxa2 to autoactivate its own expression. *The Journal of biological chemistry* **288**, 11705-11717.
Ellard, S., Flanagan, S. E., Girard, C. A., Patch, A. M., Harries, L. W., Parrish, A., Edghill, E. L., Mackay, D. J. G., Proks, P., Shimomura, K. et al. (2007). Permanent neonatal diabetes caused by dominant, recessive, or compound heterozygous SUR1 mutations with opposite functional effects. *Am. J. Hum. Genet.* **81**, 375-382.
Fangming, L., Thomas, H., Kimberly, C., Angus, M. S., Lawrence, S. B. G., Stefan, S. and Peter, I. (2003). Kidney-specific inactivation of the KIF3A subunit of kinesin-II inhibits renal ciliogenesis and produces polycystic kidney disease. *Proceedings of the National Academy of Sciences* **100**, 5286-5291.
Federation, I. D. (2014). 2014 update. In *IDF Diabetes Atlas*. Online.

Fernandez-del Castillo, C., Targarona, J., Thayer, S. P., Rattner, D. W., Brugge, W. R. and Warshaw, A. L. (2003). Incidental Pancreatic Cysts: Clinicopathologic Characteristics and Comparison With Symptomatic Patients. *Arch. Surg.* **138**, 427-434.
Finegood, D. T., Scaglia, L. and Bonner-Weir, S. (1995). Dynamics of beta-cell mass in the growing rat pancreas. Estimation with a simple mathematical model. *Diabetes* **44**, 249-256.
Fischer, E., Legue, E., Doyen, A., Nato, J.-F., Torres, V., Yaniv, M. and Pontoglio, M. (2006). Defective planar cell polarity in polycystic kidney disease. *Nature Genetics* **38**, 21-23.
Fiskerstrand, T., Houge, G., Sund, S., Scheie, D., Leh, S., Boman, H. and Knappskog, P. (2010). Identification of a gene for renal-hepatic-pancreatic dysplasia by microarray-based homozygosity mapping. *J. Mol. Diagn.* **12**, 125-131.
Flaherty, L., Bryda, E. C., Collins, D., Rudofsky, U. and Montogomery, J. C. (1995). New mouse model for polycystic kidney disease with both recessive and dominant gene effects. *Kidney international* **47**, 552-558.
Flanagan, S. E., Patch, A.-M. M., Mackay, D. J., Edghill, E. L., Gloyn, A. L., Robinson, D., Shield, J. P., Temple, K., Ellard, S. and Hattersley, A. T. (2007). Mutations in ATP-sensitive K+ channel genes cause transient neonatal diabetes and permanent diabetes in childhood or adulthood. *Diabetes* **56**, 1930-1937.
Flanagan, S. E., De Franco, E., Lango Allen, H., Zerah, M., Abdul-Rasoul, M. M., Edge, J. A., Stewart, H., Alamiri, E., Hussain, K., Wallis, S. et al. (2014). Analysis of transcription factors key for mouse pancreatic development establishes NKX2-2 and MNX1 mutations as causes of neonatal diabetes in man. *Cell Metab.* **19**, 146-154.
Flasse, L. C., Pirson, J. L., Stern, D. G., Von Berg, V., Manfroid, I., Peers, B. and Voz, M. L. (2013). Ascl1b and Neurod1, instead of Neurog3, control pancreatic endocrine cell fate in zebrafish. *BMC biology* **11**, 78.
Foggensteiner, L., Bevan, A. P., Thomas, R., Coleman, N., Boulter, C., Bradley, J., Ibraghimov-Beskrovnaya, O., Klinger, K. and Sandford, R. (2000). Cellular and subcellular distribution of polycystin-2, the protein product of the PKD2 gene. *J. Am. Soc. Nephrol.* **11**, 814-827.
Frank, V., Habbig, S., Bartram, M. P., Eisenberger, T., Veenstra-Knol, H. E., Decker, C., Boorsma, R. A. C., Göbel, H., Nürnberg, G., Griessmann, A. et al. (2013). Mutations in NEK8 link multiple organ dysplasia with altered Hippo signalling and increased c-MYC expression. *Human Molecular Genetics* **22**, 2177-2185.
Fujikura, J., Hosoda, K., Iwakura, H., Tomita, T., Noguchi, M., Masuzaki, H., Tanigaki, K., Yabe, D., Honjo, T. and Nakao, K. (2006). Notch/Rbp-j signaling prevents premature endocrine and ductal cell differentiation in the pancreas. *Cell Metab.* **3**, 59-65.
Fujikura, J., Hosoda, K., Kawaguchi, Y., Noguchi, M., Iwakura, H., Odori, S., Mori, E., Tomita, T., Hirata, M., Ebihara, K. et al. (2007). Rbp-j regulates expansion of pancreatic epithelial cells and their differentiation into exocrine cells during mouse development. *Dev Dyn* **236**, 2779-2791.
Fujitani, Y., Fujitani, S., Boyer, D. F., Gannon, M., Kawaguchi, Y., Ray, M., Shiota, M., W. Stein, R., Magnuson, M. A. and Wright, C. V. E. (2006). Targeted deletion of a cis-regulatory region reveals differential gene dosage requirements for Pdx1 in foregut organ differentiation and pancreas formation. *Genes & development* **20**, 253-266.
Gallagher, A.-R. R., Esquivel, E. L., Briere, T. S., Tian, X., Mitobe, M., Menezes, L. F., Markowitz, G. S., Jain, D., Onuchic, L. F. and Somlo, S. (2008). Biliary and pancreatic dysgenesis in mice harboring a mutation in Pkhd1. *The American journal of pathology* **172**, 417-429.
Gamberi, C. and Lasko, P. (2012). The bic-C family of developmental translational regulators. *Comparative and functional genomics* **2012**, 141386.
Gao, N., LeLay, J., Vatamaniuk, M. Z., Rieck, S., Friedman, J. R. and Kaestner, K. H. (2008). Dynamic regulation of Pdx1 enhancers by Foxa1 and Foxa2 is essential for pancreas development. *Genes & development* **22**, 3435-3448.
Garin, I., Edghill, E. L., Akerman, I., Rubio-Cabezas, O., Rica, I., Locke, J. M., Maestro, M. A., Alshaikh, A., Bundak, R., del Castillo, G. et al. (2010). Recessive mutations in the INS gene result in neonatal diabetes through reduced insulin biosynthesis. *Proceedings of the National Academy of Sciences of the United States of America* **107**, 3105-3110.

Gattone, V. H., MacNaughton, K. A. and Kraybill, A. L. (1996). Murine autosomal recessive polycystic kidney disease with multiorgan involvement induced by the cpk gene. *The Anatomical record* **245**, 488-499.
Gattone, V. H., Sinders, R. M., Hornberger, T. A. and Robling, A. G. (2009). Late progression of renal pathology and cyst enlargement is reduced by rapamycin in a mouse model of nephronophthisis. *Kidney international* **76**, 178-182.
Georgia, S. and Bhushan, A. (2004). β cell replication is the primary mechanism for maintaining postnatal β cell mass. *J. Clin. Invest.* **114**, 963968.
Georgia, S., Soliz, R., Li, M., Zhang, P. and Bhushan, A. (2006). p57 and Hes1 coordinate cell cycle exit with self-renewal of pancreatic progenitors. *Developmental biology* **298**, 22-31.
Gerdes, J. M., Davis, E. E. and Katsanis, N. (2009). The Vertebrate Primary Cilium in Development, Homeostasis, and Disease. *Cell* **137**, 32-45.
Geutskens, S. B., Otonkoski, T., Pulkkinen, M.-A., Drexhage, H. A. and Leenen, P. J. M. (2005). Macrophages in the murine pancreas and their involvement in fetal endocrine development in vitro. *J Leuko Biol* **78**, 845-852.
Gierl, M. S., Karoulias, N., Wende, H., Strehle, M. and Birchmeier, C. (2006). The zinc-finger factor Insm1 (IA-1) is essential for the development of pancreatic beta cells and intestinal endocrine cells. *Genes & development* **20**, 2465-2478.
Gloyn, A. L., Pearson, E. R., Antcliff, J. F., Proks, P., Bruining, G. J., Slingerland, A. S., Howard, N., Molnes, J., Edghill, E. L., Frayling, T. M. et al. (2004). Activating mutations in the gene encoding the ATP-sensitive potassium-channel subunit Kir6. 2 and permanent neonatal diabetes. *N. Engl. J. Med.* **350**, 1838-1849.
Golosow, N. and Grobstein, C. (1962). Epitheliomesenchymal interaction in pancreatic morphogenesis. *Developmental biology* **4**, 242-255.
Golson, M. L., Le Lay, J., Gao, N., Brämswig, N., Loomes, K. M., Oakey, R., May, C. L., White, P. and Kaestner, K. H. (2009). Jagged1 is a competitive inhibitor of Notch signaling in the embryonic pancreas. *Mech. Dev.* **126**, 687-699.
González-Perrett, S., Kim, K., Ibarra, C., Damiano, A. E., Zotta, E., Batelli, M., Harris, P. C., Reisin, I. L., Arnaout, M. A. and Cantiello, H. F. (2001). Polycystin-2, the protein mutated in autosomal dominant polycystic kidney disease (ADPKD), is a Ca2+-permeable nonselective cation channel. *Proceedings of the National Academy of Sciences of the United States of America* **98**, 1182-1187.
Gouzi, M., Kim, Y. H., Katsumoto, K., Johansson, K. and Grapin-Botton, A. (2011). Neurogenin3 initiates stepwise delamination of differentiating endocrine cells during pancreas development. *Dev Dyn* **240**, 589-604.
Gradwohl, G., Dierich, A., LeMeur, M. and Guillemot, F. (2000). neurogenin3 is required for the development of the four endocrine cell lineages of the pancreas. *Proc Natl Acad Sci U S A* **97**, 1607-1611.
Greggio, C., De Franceschi, F., Figueiredo-Larsen, M., Gobaa, S., Ranga, A., Semb, H., Lutolf, M. and Grapin-Botton, A. (2013). Artificial three-dimensional niches deconstruct pancreas development in vitro. *Development (Cambridge, England)* **140**, 4452-4462.
Gresh, L., Fischer, E., Reimann, A., Tanguy, M., Garbay, S., Shao, X., Hiesberger, T., Fiette, L., Igarashi, P., Yaniv, M. et al. (2004). A transcriptional network in polycystic kidney disease. *The EMBO journal* **23**, 1657-1668.
Grimm, D. H., Cai, Y., Chauvet, V. and Rajendran, V. (2003). Polycystin-1 distribution is modulated by polycystin-2 expression in mammalian cells. *Journal of Biological …* **278**, 36786-36793.
Gu, C., Stein, G. H., Pan, N., Goebbels, S., Hörnberg, H., Nave, K.-A. A., Herrera, P., White, P., Kaestner, K. H., Sussel, L. et al. (2010). Pancreatic beta cells require NeuroD to achieve and maintain functional maturity. *Cell Metab.* **11**, 298-310.
Gu, G., Brown, J. R. and Melton, D. A. (2003). Direct lineage tracing reveals the ontogeny of pancreatic cell fates during mouse embryogenesis. *Mech. Dev.* **120**, 35-43.
Guillam, M. T., Hümmler, E., Scharer, E., Wu, J.-Y., Birnbaum, M. J., Beermann, F., Schmidt, A., Dériaz, N. and Thorens, B. (1997). Early diabetes and abnormal postnatal pancreatic islet development in mice lacking Glut-2. *Nature Genetics* **17**, 327-330.

Gupta, R. K., Vatamaniuk, M. Z., Lee, C. S., Flaschen, R. C., Fulmer, J. T., Duncan, S. A. and Kaestner, K. H. (2005). The MODY1 gene HNF-4α regulates selected genes involved in insulin secretion. *J. Clin. Invest.* **115**, 10061015.

Guz, Y., Montminy, M. R., Stein, R. and Leonard, J. (1995). Expression of murine STF-1, a putative insulin gene transcription factor, in beta cells of pancreas, duodenal epithelium and pancreatic exocrine and endocrine …. *Development* **121**, 11-18.

Haber, P. S., Keogh, G. W., Apte, M. V., Moran, C. S., Stewart, N. L., Crawford, D. H., Pirola, R. C., McCaughan, G. W., Ramm, G. A. and Wilson, J. S. (1999). Activation of pancreatic stellate cells in human and experimental pancreatic fibrosis. *Am. J. Pathol.* **155**, 1087-1095.

Hald, J., Hjorth, J. P., German, M. S., Madsen, O. D., Serup, P. and Jensen, J. (2003). Activated Notch1 prevents differentiation of pancreatic acinar cells and attenuate endocrine development. *Developmental biology* **260**, 426-437.

Hald, J., Sprinkel, A. E., Ray, M., Serup, P., Wright, C. V. and Madsen, O. (2008). Generation and characterization of Ptf1a antiserum and localization of Ptf1a in relation to Nkx6. 1 and Pdx1 during the earliest stages of mouse pancreas development. … *of Histochemistry &* … **56**, 587-595.

Hale, M. A., Kagami, H., Shi, L., Holland, A. M., Elsässer, H.-P. P., Hammer, R. E. and MacDonald, R. J. (2005). The homeodomain protein PDX1 is required at mid-pancreatic development for the formation of the exocrine pancreas. *Developmental biology* **286**, 225-237.

Halestrap, A. P. (2013). The SLC16 gene family - structure, role and regulation in health and disease. *Mol. Aspects Med.* **34**, 337-349.

Hanaoka, K. and Guggino, W. B. (2000). cAMP regulates cell proliferation and cyst formation in autosomal polycystic kidney disease cells. *J. Am. Soc. Nephrol.* **11**, 1179-1187.

Hanaoka, K., Qian, F., Boletta, A., Bhunia, A. K., Piontek, K., Tsiokas, L., Sukhatme, V. P., Guggino, W. B. and Germino, G. G. (2000). Co-assembly of polycystin-1 and -2 produces unique cation-permeable currents. *Nature* **408**, 990-994.

Happé, H., van der Wal, A. M., Salvatori, D. C., Leonhard, W. N., Breuning, M. H., de Heer, E. and Peters, D. J. (2013). Cyst expansion and regression in a mouse model of polycystic kidney disease. *Kidney international* **83**, 1099-1108.

Harding, H. P., Zeng, H., Zhang, Y., Jungries, R., Chung, P., Plesken, H., Sabatini, D. D. and Ron, D. (2001). Diabetes Mellitus and Exocrine Pancreatic Dysfunction in< i> Perk-/-</i> Mice Reveals a Role for Translational Control in Secretory Cell Survival. *Mol. Cell* **7**, 1153-1163.

Harmon, E. B., Apelqvist, A. A., Smart, N. G., Gu, X., Osborne, D. H. and Kim, S. K. (2004). GDF11 modulates NGN3+ islet progenitor cell number and promotes beta-cell differentiation in pancreas development. *Development (Cambridge, England)* **131**, 6163-6174.

Harrison, K. A., Thaler, J., Pfaff, S. L., Gu, H. and Kehrl, J. H. (1999). Pancreas dorsal lobe agenesis and abnormal islets of Langerhans in Hlxb9-deficient mice. *Nature Genetics* **23**, 71-75.

Hart, A., Papadopoulou, S. and Edlund, H. (2003). Fgf10 maintains notch activation, stimulates proliferation, and blocks differentiation of pancreatic epithelial cells. *Dev Dyn* **228**, 185-193.

Hassane, S., Leonhard, W. N., van der Wal, A., Hawinkels, L. J. A. C., Lantinga-van Leeuwen, I. S., ten Dijke, P., Breuning, M. H., de Heer, E. and Peters, D. J. M. (2010). Elevated TGFβ-Smad signalling in experimental Pkd1 models and human patients with polycystic kidney disease. *The Journal of Pathology* **222**, 21-31.

Haumaitre, C., Barbacci, E., Jenny, M., Ott, M. O., Gradwohl, G. and Cereghini, S. (2005). Lack of TCF2/vHNF1 in mice leads to pancreas agenesis. *Proceedings of the National Academy of Sciences of the United States of America* **102**, 1490-1495.

Haumaitre, C., Fabre, M., Cormier, S., Baumann, C., Delezoide, A.-L. L. and Cereghini, S. (2006). Severe pancreas hypoplasia and multicystic renal dysplasia in two human fetuses carrying novel HNF1beta/MODY5 mutations. *Hum. Mol. Genet.* **15**, 2363-2375.

Hearn, T., Renforth, G. L., Spalluto, C., Hanley, N. A., Piper, K., Brickwood, S., White, C., Connolly, V., Taylor, J. F., Russell-Eggitt, I. et al. (2002). Mutation of ALMS1, a large gene with a tandem repeat encoding 47 amino acids, causes Alström syndrome. *Nature genetics* **31**, 79-83.

Hebrok, M., Kim, S. K., Jacques, B., McMahon, A. P. and Melton, D. A. (2000). Regulation of pancreas development by hedgehog signaling. *Development* **127**, 4905-4913.

Heiser, P. W., Lau, J., Taketo, M. M., Herrera, P. L. and Hebrok, M. (2006). Stabilization of beta-catenin impacts pancreas growth. *Development (Cambridge, England)* **133**, 2023-2032.
Heller, S. R., Dichmann, D. S., Jensen, J., Miller, C., Wong, G., Madsen, O. D. and Serup, P. (2002). Expression patterns of Wnts, Frizzleds, sFRPs, and misexpression in transgenic mice suggesting a role for Wnts in pancreas and foregut pattern formation. *Dev. Dyn.* **225**, 260-270.
Henseleit, K. D., Nelson, S. B., Kuhlbrodt, K., Hennings, J. C., Ericson, J. and Sander, M. (2005). NKX6 transcription factor activity is required for - and -cell development in the pancreas. *Development* **132**, 3139-3149.
Herrera, P. L., Huarte, J., Sanvito, F., Meda, P., Orci, L. and Vassalli, J. D. (1991). Embryogenesis of the murine endocrine pancreas; early expression of pancreatic polypeptide gene. *Development (Cambridge, England)* **113**, 1257-1265.
Hopp, K., Ward, C. J., Hommerding, C. J., Nasr, S. H., Tuan, H.-F. F., Gainullin, V. G., Rossetti, S., Torres, V. E. and Harris, P. C. (2012). Functional polycystin-1 dosage governs autosomal dominant polycystic kidney disease severity. *The Journal of clinical investigation* **122**, 4257-4273.
Hori, K., Sen, A., Kirchhausen, T. and Artavanis-Tsakonas, S. (2012). Regulation of ligand-independent Notch signal through intracellular trafficking. *Communicative & Integrative Biology* **5**, 374.
Horikawa, Y., Iwasaki, N., Hara, M., Furuta, H., Hinokio, Y., Cockburn, B. N., Lindner, T., Yamagata, K., Ogata, M., Tomonaga, O. et al. (1997). Mutation in hepatocyte nuclear factor-1 beta gene (TCF2) associated with MODY. *Nature genetics* **17**, 384-385.
Horn, S., Kobberup, S., Jørgensen, M. C., Kalisz, M., Klein, T., Kageyama, R., Gegg, M., Lickert, H., Lindner, J., Magnuson, M. A. et al. (2012). Mind bomb 1 is required for pancreatic β-cell formation. *Proceedings of the National Academy of Sciences of the United States of America* **109**, 7356-7361.
Hou, X., Mrug, M., Yoder, B. K., Lefkowitz, E. J., Kremmidiotis, G., D'Eustachio, P., Beier, D. R. and Guay-Woodford, L. M. (2002). Cystin, a novel cilia-associated protein, is disrupted in the cpk mouse model of polycystic kidney disease. *The Journal of clinical investigation* **109**, 533-540.
Huang, H. P., Liu, M., El-Hodiri, H. M. and Chu, K. (2000). Regulation of the Pancreatic Islet-Specific GeneBETA2 (neuroD) by Neurogenin 3. … *and cellular biology* **20**, 3292-3307.
Hughes, J., Ward, C. J., Peral, B., Aspinwall, R., Clark, K., San Millán, J. L., Gamble, V. and Harris, P. C. (1995). The polycystic kidney disease 1 (PKD1) gene encodes a novel protein with multiple cell recognition domains. *Nature genetics* **10**, 151-160.
Huotari, M.-A., Miettinen, P. J., Palgi, J., Koivisto, T., Ustinov, J., Harari, D., Yarden, Y. and Otonkoski, T. (2002). ErbB Signaling Regulates Lineage Determination of Developing Pancreatic Islet Cells in Embryonic Organ Culture. *Endocrinology* **143**, 4437-4446.
Inoue, H., Tanizawa, Y., Wasson, J., Behn, P., Kalidas, K., Bernal-Mizrachi, E., Mueckler, M., Marshall, H., Donis-Keller, H., Crock, P. et al. (1998). A gene encoding a transmembrane protein is mutated in patients with diabetes mellitus and optic atrophy (Wolfram syndrome). *Nature genetics* **20**, 143-148.
Inzucchi, S. E., Bergensta, l. M., Buse, J. B., Diamant, M., Ferrannini, E., Nauck, M., Peters, A. L., Tsapas, A., Wender, R. and Matthews, D. R. (2015). Management of Hyperglycemia in Type 2 Diabetes, 2015: A Patient-Centered Approach: Update to a Position Statement of the American Diabetes Association and the European Association for the Study of Diabetes. *Diabetes care* **38**, 140-149.
Ishihara, H., Takeda, S., Tamura, A., Takahashi, R., Yamaguchi, S., Takei, D., Yamada, T., Inoue, H., Soga, H., Katagiri, H. et al. (2004). Disruption of the WFS1 gene in mice causes progressive β-cell loss and impaired stimulus–secretion coupling in insulin secretion. *Human Molecular Genetics* **13**, 1159-1170.
Ivemark, B. I., Oldfelt, V. and Zetterstrom, R. (1959). Familial dysplasia of kidneys, liver and pancreas: a probably genetically determined syndrome. *Acta paediatrica* **48**, 1-11.
Jacquemin, P., Lemaigre, F. P. and Rousseau, G. G. (2003a). The Onecut transcription factor HNF-6 (OC-1) is required for timely specification of the pancreas and acts upstream of Pdx-1 in the specification cascade. *Developmental biology* **258**, 105-116.
Jacquemin, P., Pierreux, C. E., Fierens, S., van Eyll, J. M., Lemaigre, F. P. and Rousseau, G. G. (2003b). Cloning and embryonic expression pattern of the mouse Onecut transcription factor OC-2. *Gene Expression Patterns* **3**, 639644.

Jacquemin, P., Yoshitomi, H., Kashima, Y., Rousseau, G. G., Lemaigre, F. P. and Zaret, K. S. (2006). An endothelial-mesenchymal relay pathway regulates early phases of pancreas development. *Developmental biology* **290**, 189-199.

Jacquemin, P., Durviaux, S., Jensen, J., Godfraind, C., Gradwohl, G., Guillemot, F., Madsen, O., Carmeliet, P., Dewerchin, M., Collen, D. et al. (2000). Transcription factor hepatocyte nuclear factor 6 regulates pancreatic endocrine cell differentiation and controls expression of the proendocrine gene ngn3. *Mol. Cell. Biol.* **20**, 4445-4454.

Jensen, J., Heller, R. S., Funder-Nielsen, T., Pedersen, E., Lindsell, C., Weinnmaster, G., Madsen, O. and Serup, P. (2000a). Independent development of pancreatic alpha-and beta-cells from neurogenin3-expressing precursors: a role for the notch pathway in repression of premature …. *Diabetes* **49**, 163-176.

Jensen, J., Pedersen, E. E., Galante, P., Hald, J., Heller, R. S., Ishibashi, M., Kageyama, R., Guillemot, F., Serup, P. and Madsen, O. D. (2000b). Control of endodermal endocrine development by Hes-1. *Nature genetics* **24**, 36-44.

Jhappan, C., Stahle, C., Harkins, R. N., Fausto, N., Smith, G. H. and Merlino, G. (1990). TGFα overexpression in transgenic mice induces liver neoplasia and abnormal development of the mammary gland and pancreas. *Cell* **61**, 11371146.

Jiang, S.-T. T., Chiou, Y.-Y. Y., Wang, E., Lin, H.-K. K., Lin, Y.-T. T., Chi, Y.-C. C., Wang, C.-K. L. K., Tang, M.-J. J. and Li, H. (2006). Defining a link with autosomal-dominant polycystic kidney disease in mice with congenitally low expression of Pkd1. *The American journal of pathology* **168**, 205-220.

Johansson, K. A., Dursun, U., Jordan, N., Gu, G., Beermann, F., Gradwohl, G. and Grapin-Botton, A. (2007). Temporal control of neurogenin3 activity in pancreas progenitors reveals competence windows for the generation of different endocrine cell types. *Dev. Cell* **12**, 457-465.

Jones, M. R., Rose, A. M. and Baillie, D. L. (2012). Oligoarray Comparative Genomic Hybridization-Mediated Mapping of Suppressor Mutations Generated in a Deletion-Biased Mutagenesis Screen. *G3: Genes|Genomes|Genetics* **2**, 657-663.

Jonsson, J., Carlsson, L., Edlund, T. and Edlund, H. (1994). Insulin-promoter-factor 1 is required for pancreas development in mice. *Nature* **371**, 606-609.

Kaestner, K. H., Katz, J., Liu, Y. and Drucker, D. J. (1999). Inactivation of the winged helix transcription factor HNF3α affects glucose homeostasis and islet glucagon gene expression in vivo. *Genes & Dev* **13**, 495-504.

Kakiuchi, S., Yamazaki, R., Teshima, Y. and Uenishi, K. (1973). Regulation of Nucleoside Cyclic 3′:5′-Monophosphate Phosphodiesterase Activity from Rat Brain by a Modulator and Ca2+. *Proceedings of the National Academy of Sciences* **70**, 3526-3530.

Kakkar, R., Raju, R. V. S. and Sharma, R. K. (1999). Calmodulin-dependent cyclic nucleotide phosphodiesterase (PDE1). *Cell. Mol. Life Sci.* **55**, 1164-1186.

Kandachar, V. and Roegiers, F. (2012). Endocytosis and control of Notch signaling. *Curr. Opin. Cell Biol.* **24**, 534-540.

Kang, H. S., Beak, J. Y., Kim, Y.-S. S., Herbert, R. and Jetten, A. M. (2009a). Glis3 is associated with primary cilia and Wwtr1/TAZ and implicated in polycystic kidney disease. *Molecular and cellular biology* **29**, 2556-2569.

Kang, H. S., Kim, Y.-S. S., ZeRuth, G., Beak, J. Y., Gerrish, K., Kilic, G., Sosa-Pineda, B., Jensen, J., Pierreux, C. E., Lemaigre, F. P. et al. (2009b). Transcription factor Glis3, a novel critical player in the regulation of pancreatic beta-cell development and insulin gene expression. *Molecular and cellular biology* **29**, 6366-6379.

Karihaloo, A., Koraishy, F., Huen, S., Lee, Y., Merrick, D., Caplan, M., Somlo, S. and Cantley, L. (2011). Macrophages promote cyst growth in polycystic kidney disease. *J. Am. Soc. Nephrol.* **22**, 1809-1814.

Karner, C. M., Chirumamilla, R., Aoki, S., Igarashi, P., Wallingford, J. B. and Carroll, T. J. (2009). Wnt9b signaling regulates planar cell polarity and kidney tubule morphogenesis. *Nature genetics* **41**, 793-799.

Kawaguchi, Y., Cooper, B., Gannon, M., Ray, M., MacDonald, R. J. and Wright, C. V. (2002). The role of the transcriptional regulator Ptf1a in converting intestinal to pancreatic progenitors. *Nature genetics* **32**, 128-134.

Kerkhoff, C., Voss, A., Scholzen, T. E., Averill, M. M., Zänker, K. S. and Bornfeldt, K. E. (2012). Novel insights into the role of S100A8/A9 in skin biology. *Exp. Dermatol.* **21**, 822-826.
Kesavan, G., Sand, F. W., Greiner, T. U., Johansson, J. K., Kobberup, S., Wu, X., Brakebusch, C. and Semb, H. (2009). Cdc42-mediated tubulogenesis controls cell specification. *Cell* **139**, 791-801.
Kim, H. J., Schleiffarth, J. R., Jessurum, J., Sumanas, S., Petryk, A., Lin, S. and Ekker, S. C. (2005). Wnt5 signaling in vertebrate pancreas development. *BMC Biology* **3**, 23.
Kim, I., Ding, T., Fu, Y., Li, C., Cui, L., Li, A., Lian, P., Liang, D., Wang, D. W., Guo, C. et al. (2009). Conditional mutation of Pkd2 causes cystogenesis and upregulates beta-catenin. *J. Am. Soc. Nephrol.* **20**, 2556-2569.
Kim, Y.-S. S., Nakanishi, G., Lewandoski, M. and Jetten, A. M. (2003). GLIS3, a novel member of the GLIS subfamily of Krüppel-like zinc finger proteins with repressor and activation functions. *Nucleic Acids Res.* **31**, 5513-5525.
Kim, Y.-S. S., Kang, H. S., Takeda, Y., Hom, L., Song, H.-Y. Y., Jensen, J. and Jetten, A. M. (2012). Glis3 regulates neurogenin 3 expression in pancreatic β-cells and interacts with its activator, Hnf6. *Mol. Cells* **34**, 193-200.
Kim, Y. H., Larsen, H. L., Rué, P., Lemaire, L. A., Ferrer, J. and Grapin-Botton, A. (2015). Cell cycle-dependent differentiation dynamics balances growth and endocrine differentiation in the pancreas. *Plos Biol* **13**, e1002111.
Klussmann, E., Tamma, G., Lorenz, D., Wiesner, B., Maric, K., Hofmann, F., Aktories, K., Valenti, G. and Rosenthal, W. (2001). An inhibitory role of Rho in the vasopressin-mediated translocation of aquaporin-2 into cell membranes of renal principal cells. *The Journal of biological chemistry* **276**, 20451-20457.
Kobberup, S., Schmerr, M., Dang, M.-L. L., Nyeng, P., Jensen, J. N., MacDonald, R. J. and Jensen, J. (2010). Conditional control of the differentiation competence of pancreatic endocrine and ductal cells by Fgf10. *Mech. Dev.* **127**, 220-234.
Komuro, I. and Izumo, S. (1993). Csx: a murine homeobox-containing gene specifically expressed in the developing heart. *Proceedings of the National Academy of Sciences of the United States of America* **90**, 8145-8149.
Kopinke, D., Brailsford, M., Shea, J. E. and Leavitt, R. (2011). Lineage tracing reveals the dynamic contribution of Hes1+ cells to the developing and adult pancreas. … **138**, 431-441.
Kordowich, S., Collombat, P., Mansouri, A. and Serup, P. (2011). Arx and Nkx2.2 compound deficiency redirects pancreatic alpha- and beta-cell differentiation to a somatostatin/ghrelin co-expressing cell lineage. *BMC Developmental Biology* **31**, 52.
Kortenoeven, M. L. A., Trimpert, C., van den Brand, M., Li, Y., Wetzels, J. F. M. and Deen, P. M. T. (2012). In mpkCCD cells, long-term regulation of aquaporin-2 by vasopressin occurs independent of protein kinase A and CREB but may involve Epac. *American journal of physiology. Renal physiology* **302**, 401.
Koster, J. C., Marshall, B. A., Ensor, N., Corbett, J. A. and Nichols, C. G. (2000). Targeted overactivity of beta cell K(ATP) channels induces profound neonatal diabetes. *Cell* **100**, 645-654.
Koulen, P., Cai, Y., Geng, L., Maeda, Y., Nishimura, S., Witzgall, R., Ehrlich, B. E. and Somlo, S. (2002). Polycystin-2 is an intracellular calcium release channel. *Nat. Cell Biol.* **4**, 191-197.
Krapp, A., Knöfler, M., Frutiger, S., Hughes, G. J., Hagenbüchle, O. and Wellauer, P. K. (1996). The p48 DNA-binding subunit of transcription factor PTF1 is a new exocrine pancreas-specific basic helix-loop-helix protein. *The EMBO journal* **15**, 4317-4329.
Krapp, A., Knöfler, M., Ledermann, B., Bürki, K., Berney, C., Zoerkler, N., Hagenbüchle, O. and Wellauer, P. K. (1998). The bHLH protein PTF1-p48 is essential for the formation of the exocrine and the correct spatial organization of the endocrine pancreas. *Genes & development* **12**, 3752-3763.
Kraus, M., Clauin, S., Pfister, Y., Di Maïo, M., Ulinski, T., Constam, D., Bellanné-Chantelot, C. and Grapin-Botton, A. (2012). Two mutations in human BICC1 resulting in Wnt pathway hyperactivity associated with cystic renal dysplasia. *Hum. Mutat.* **33**, 86-90.
Kugler, J.-M. M., Chicoine, J. and Lasko, P. (2009). Bicaudal-C associates with a Trailer Hitch/Me31B complex and is required for efficient Gurken secretion. *Developmental biology* **328**, 160-172.

Laffan, T., A. , Horton, K., M. , Klein, A., P. , Berlanstein, B., Siegelman, S., S. , Kawamoto, S., Johnson, P., T. , Fishman, E., K. and Hruban, R., H. . (2008). Prevalence of Unsuspected Pancreatic Cysts on MDCT. *American Journal of Roentgenology* **191**, 802-807.
Lamiell, J. M., Salazar, F. G. and Hsia, Y. E. (1989). von Hippel-Lindau disease affecting 43 members of a single kindred. *Medicine* **68**, 1-29.
Lammert, E., Brown, J. and Melton, D. A. (2000). Notch gene expression during pancreatic organogenesis. *Mech. Dev.* **94**, 199-203.
Lammert, E., Cleaver, O. and Melton, D. (2001). Induction of pancreatic differentiation by signals from blood vessels. *Science (New York, N.Y.)* **294**, 564-567.
Landsman, L., Nijagal, A., Whitchurch, T. J., Vanderlaan, R. L., Zimmer, W. E., Mackenzie, T. C. and Hebrok, M. (2011). Pancreatic mesenchyme regulates epithelial organogenesis throughout development. *PLoS biology* **9**, e1001143.
Langmead, B., Trapnell, C., Pop, M. and Salzberg, S. L. (2009). Ultrafast and memory-efficient alignment of short DNA sequences to the human genome. *Genome Biol* **10**, R25.
Lango Allen, H., Flanagan, S. E., Shaw-Smith, C., De Franco, E., Akerman, I., Caswell, R., Consortium, t. I. P. A., Ferrer, J., Hattersley, A. T. and Ellard, S. (2011). GATA6 haploinsufficiency causes pancreatic agenesis in humans. *Nature Genetics* **44**, 20-22.
Lantinga-van Leeuwen, I. S., Dauwerse, J., G., Baelde, H. J., Leonhard, W., N., van de Wal, A., Ward, C., J., Verbeek, S., DeRuiter, M. C., Breuning, M. H., de Heer, E. et al. (2004). Lowering of Pkd1 expression is sufficient to cause polycystic kidney disease. *Human Molecular Genetics* **13**, 3069-3077.
Lantz, K. A., Vatamaniuk, M. Z., Brestelli, J. E., Friedman, J. R., Matschinsky, F. M. and Kaestner, K. H. (2004). Foxa2 regulates multiple pathways of insulin secretion. *J. Clin. Invest.* **114**, 512.
Lassar, A. B., Buskin, J. N., Lockshon, D., Davis, R. L., Apone, S., Hauschka, S. D. and Weintraub, H. (1989). MyoD is a sequence-specific DNA binding protein requiring a region of myc homology to bind to the muscle creatine kinase enhancer. *Cell* **58**, 823-831.
Lee, C. S., Sund, N. J., Behr, R., Herrera, P. L. and Kaestner, K. H. (2005). Foxa2 is required for the differentiation of pancreatic α-cells. *Developmental Biology* **278**.
Lee, C. S., Sund, N. J., Vatamaniuk, M. Z., Matschinsky, F. M., Stoffers, D. A. and Kaestner, K. H. (2002). Foxa2 controls Pdx1 gene expression in pancreatic beta-cells in vivo. *Diabetes* **51**, 2546-2551.
Lee, J., Smith, S., Watada, H., Lin, J., Scheel, D., Wang, J., Mirmira, R. and German, M. (2001). Regulation of the pancreatic pro-endocrine gene neurogenin3. *Diabetes* **50**, 928-936.
Lee, K. S., Sekhar, A., Rofsky, N. M. and Pedrosa, I. (2010). Prevalence of incidental pancreatic cysts in the adult population on MR imaging. *The American journal of gastroenterology* **105**, 2079-2084.
Lee, M. S., Gu, D., Feng, L., Curriden, S., Arnush, M., Krahl, T., Gurushanthaiah, D., Wilson, C., Loskutoff, D. L. and Fox, H. (1995). Accumulation of extracellular matrix and developmental dysregulation in the pancreas by transgenic production of transforming growth factor-beta 1. *The American journal of pathology* **147**, 42-52.
Lemaigre, F. P., Durviaux, S. M. and Truong, O. (1996). Hepatocyte nuclear factor 6, a transcription factor that contains a novel type of homeodomain and a single cut domain. *Proceedings of the …* **192**, 247-257.
Lemaire, L. A., Goulley, J., Kim, Y. H., Carat, S., Jacquemin, P., Rougemont, J., Constam, D. B. and Grapin-Botton, A. (*in press*). Bicaudal C1 promotes pancreatic NEUROG3+ endocrine progenitor differentiation and ductal morphogenesis. *Development.*
Lian, P., Li, A., Li, Y., Liu, H., Liang, D., Hu, B., Lin, D., Jiang, T., Moeckel, G., Qin, D. et al. (2014). Loss of polycystin-1 inhibits Bicc1 expression during mouse development. *PloS one* **9**, e88816.
Lindner, T. H., Njølstad, P. R., Horikawa, Y., Bostad, L., Bell, G. I. and Søvik, O. (1999). A Novel Syndrome of Diabetes Mellitus, Renal Dysfunction and Genital Malformation Associated with a Partial Deletion of the Pseudo-POU Domain of Hepatocyte Nuclear Factor-1β. *Human Molecular Genetics* **8**, 2001-2008.
Lu, W., Peissel, B., Babakhanlou, H., Pavlova, A., Geng, L., Fan, X., Larson, C., Brent, G. and Zhou, J. (1997). Perinatal lethality with kidney and pancreas defects in mice with a targetted Pkd1 mutation. *Nature genetics* **17**, 179-181.

Lu, W., Fan, X., Basora, N., Babakhanlou, H., Law, T., Rifai, N., Harris, P. C., Perez-Atayde, A. R., Rennke, H. G. and Zhou, J. (1999). Late onset of renal and hepatic cysts in Pkd1-targeted heterozygotes. *Nature genetics* **21**, 160-161.

Lu, W., Shen, X., Pavlova, A., Lakkis, M., Ward, C. J., Pritchard, L., Harris, P. C., Genest, D. R., Perez-Atayde, A. R. and Zhou, J. (2001). Comparison of Pkd1-targeted mutants reveals that loss of polycystin-1 causes cystogenesis and bone defects. *Human molecular genetics* **10**, 2385-2396.

Lundin, P. M. and Olow, I. (1961). Polycystic Kidneys in Newborns, Infants and Children A Clinical and Pathological Study. *Acta Paediatrica* **50**, 185-200.

Lustig, B., Jerchow, B., Sachs, M., Weiler, S., Pietsch, T., Karsten, U., van de Wetering, M., Clevers, H., Schlag, P. M., Birchmeier, W. et al. (2002). Negative feedback loop of Wnt signaling through upregulation of conductin/axin2 in colorectal and liver tumors. *Mol. Cell. Biol.* **22**, 1184-1193.

Lynn, F., Smith, S., Wilson, M., Yang, K., Nekrep, N. and German, M. (2007). Sox9 coordinates a transcriptional network in pancreatic progenitor cells. *Proc Natl Acad Sci U S A* **104**, 10500-10505.

Lyons, I., Parsons, L. M., Hartley, L., Li, R., Andrews, J. E., Robb, L. and Harvey, R. P. (1995). Myogenic and morphogenetic defects in the heart tubes of murine embryos lacking the homeo box gene Nkx2-5. *Genes & development* **9**, 1654-1666.

Lyons, K. M., Hogan, B. L. and Robertson, E. J. (1995). Colocalization of BMP 7 and BMP 2 RNAs suggests that these factors cooperatively mediate tissue interactions during murine development. *Mech. Dev.* **50**, 71-83.

Ma, D., Shield, J. P., Dean, W., Leclerc, I., Knauf, C., Burcelin R, R., Rutter, G. A. and Kelsey, G. (2004). Impaired glucose homeostasis in transgenic mice expressing the human transient neonatal diabetes mellitus locus, TNDM. *The Journal of clinical investigation* **114**, 339-348.

Maciej, B., Chong, W. L., Ryan, T., Watip, B., Jiang, H., Wojciech, M. M., Ilham El, K., Sung-Hoon, K., Lorella, M., Stephen, S. R. et al. (2009). Mutations at the BLK locus linked to maturity onset diabetes of the young and β-cell dysfunction. *Proceedings of the National Academy of Sciences* **106**, 14460-14465.

MacRae Dell, K., Raghad, N., Sweeney, W. E. J. and Avner, E. D. (2004). EGF-related growth factors in the pathogenesis of murine ARPKD1. *Kidney International* **65**, 2018-2029.

Maestro, M., Boj, S., Luco, R., Pierreux, C., Cabedo, J., Servitja, J., German, M., Rousseau, G., Lemaigre, F. and Ferrer, J. (2003). Hnf6 and Tcf2 (MODY5) are linked in a gene network operating in a precursor cell domain of the embryonic pancreas. *Hum. Mol. Genet.* **12**, 3307-3314.

Magenheim, J., Klein, A., Stanger, B., Ashery-Padan, R., Sosa-Pineda, B., Gu, G. and Dor, Y. (2011a). Ngn3(+) endocrine progenitor cells control the fate and morphogenesis of pancreatic ductal epithelium. *Dev. Biol.* **359**, 26-36.

Magenheim, J., Ilovich, O., Lazarus, A., Klochendler, A., Ziv, O., Werman, R., Hija, A., Cleaver, O., Mishani, E., Keshet, E. et al. (2011b). Blood vessels restrain pancreas branching, differentiation and growth. *Development (Cambridge, England)* **138**, 4743-4752.

Mahone, M., Saffman, E. E. and Lasko, P. F. (1995). Localized Bicaudal-C RNA encodes a protein containing a KH domain, the RNA binding motif of FMR1. *The EMBO journal* **14**, 2043-2055.

Maisonneuve, C., Guilleret, I., Vick, P., Weber, T., Andre, P., Beyer, T., Blum, M. and Constam, D. (2009). Bicaudal C, a novel regulator of Dvl signaling abutting RNA-processing bodies, controls cilia orientation and leftward flow. *Development* **136**, 3019-3030.

Malecki, M. T., Jhala, U. S., Antonellis, A., Fields, L., Doria, A., Orban, T., Saad, M., Warram, J. H., Montminy, M. and Krolewski, A. S. (1999). Mutations in NEUROD1 are associated with the development of type 2 diabetes mellitus. *Nature genetics* **23**, 323-328.

Mangoo-Karim, R., Uchic, M. E., Grant, M., Shumate, W. A., Calvet, J. P., Park, C. H. and Grantham, J. J. (1989). Renal epithelial fluid secretion and cyst growth: the role of cyclic AMP. *FASEB J.* **3**, 2629-2632.

Masamune, A. and Shimosegawa, T. (2013). Pancreatic stellate cells--multi-functional cells in the pancreas. *Pancreatology* **13**, 102-105.

Masamune, A., Watanabe, T., Kikuta, K. and Shimosegawa, T. (2009). Roles of pancreatic stellate cells in pancreatic inflammation and fibrosis. *Clin Gastroenterol Hepatol* **7**, S48-54.

Mastracci, T. L., Wilcox, C. L., Arnes, L., Panea, C., Golden, J. A., May, C. L. and Sussel, L. (2011). Nkx2.2 and Arx genetically interact to regulate pancreatic endocrine cell development and endocrine hormone expression. *Developmental biology* **359**, 1-11.
Masui, T., Long, Q., Beres, T. M., Magnuson, M. A. and MacDonald, R. J. (2007). Early pancreatic development requires the vertebrate Suppressor of Hairless (RBPJ) in the PTF1 bHLH complex. *Genes & development* **21**, 2629-2643.
May, C. L. and Kaestner, K. H. (2010). Gut endocrine cell development. *Mol. Cell. Endocrinol.* **323**, 70-75.
Mellitzer, G., Martín, M., Sidhoum-Jenny, M., Orvain, C., Barths, J., Seymour, P. A., Sander, M. and Gradwohl, G. (2004). Pancreatic islet progenitor cells in neurogenin 3-yellow fluorescent protein knock-add-on mice. *Molecular endocrinology (Baltimore, Md.)* **18**, 2765-2776.
Menezes, L. F., Zhou, F., Patterson, A. D., Piontek, K. B., Krausz, K. W., Gonzalez, F. J. and Germino, G. G. (2012). Network analysis of a Pkd1-mouse model of autosomal dominant polycystic kidney disease identifies HNF4α as a disease modifier. *PLoS genetics* **8**, e1003053.
Mesner, L. D., Ray, B., Hsu, Y.-H. H., Manichaikul, A., Lum, E., Bryda, E. C., Rich, S. S., Rosen, C. J., Criqui, M. H., Allison, M. et al. (2014). Bicc1 is a genetic determinant of osteoblastogenesis and bone mineral density. *The Journal of clinical investigation* **124**, 2736-2749.
Miettinen, P. J., Huotari, M.-A., Koivisto, T., Ustinov, J., Palgi, J., Rasilainen, S., Lehtonen, E., Keski-Oja, J. and Otonkoski, T. (2000). Impaired migration and delayed differentiation of pancreatic islet cells in mice lacking EGF-receptors. *Development (Cambridge, England)* **127**, 2617-2627.
Mitoma, C. (1956). Studies on partially purified phenylalanine hydroxylase. *Arch. Biochem. Biophys.* **60**, 476-484.
Miyatsuka, T., Kosaka, Y., Kim, H. and German, M. S. (2011). Neurogenin3 inhibits proliferation in endocrine progenitors by inducing Cdkn1a. *Proceedings of the National Academy of Sciences of the United States of America* **108**, 185-190.
Mochizuki, T., Wu, G., Hayashi, T., Xenophontos, S., Veldhuisen, B., Saris, J., Reynolds, D., Cai, Y., Gabow, P., Pierides, A. et al. (1996). PKD2, a gene for polycystic kidney disease that encodes an integral membrane protein. *Science (New York, N.Y.)* **272**, 1339-1342.
Mohler, J. and Wieschaus, E. F. (1986). Dominant maternal-effect mutations of Drosophila melanogaster causing the production of double-abdomen embryos. *Genetics* **112**, 803-822.
Montesano, R., Ghzili, H., Carrozzino, F., Rossier, B. C. and Féraille, E. (2009). cAMP-dependent chloride secretion mediates tubule enlargement and cyst formation by cultured mammalian collecting duct cells. *American journal of physiology. Renal physiology* **296**, 446-457.
Morales, M. M., Carroll, T. P., Morita, T., Schwiebert, E. M., Devuyst, O., Wilson, P. D., Lopes, A. G., Stanton, B. A., Dietz, H. C., Cutting, G. R. et al. (1996). Both the wild type and a functional isoform of CFTR are expressed in kidney. *The American journal of physiology* **270**, 1038-1048.
Mori, T. and Haga, A. (1960). Histological and histochemical observations on the developing pancreas of fetal mouse. *The Tohoku journal of experimental medicine* **72**, 42-58.
Moscinski, L. C. and Hill, B. (1995). Molecular cloning of a novel myeloid granule protein. *J. Cell. Biochem.* **59**, 431-442.
Moser, M., Matthiesen, S., Kirfel, J., Schorle, H., Bergmann, C., Senderek, J., Rudnik-Schöneborn, S., Zerres, K. and Buettner, R. (2005). A mouse model for cystic biliary dysgenesis in autosomal recessive polycystic kidney disease (ARPKD). *Hepatology (Baltimore, Md.)* **41**, 1113-1121.
Moyer, J. H., Lee-Tischler, M. J., Kwon, H. Y., Schrick, J. J., Avner, E. D., Sweeney, W. E., Godfrey, V. L., Cacheiro, N. L., Wilkinson, J. E. and Woychik, R. P. (1994). Candidate gene associated with a mutation causing recessive polycystic kidney disease in mice. *Science (New York, N.Y.)* **264**, 1329-1333.
Munger, B. L. (1958). A light and electron microscopic study of cellular differentiation in the pancreatic islets of the mouse. *American Journal of Anatomy* **103**, 275-311.
Murtaugh, L. C., Stanger, B. Z., Kwan, K. M. and Melton, D. A. (2003). Notch signaling controls multiple steps of pancreatic differentiation. *Proceedings of the National Academy of Sciences of the United States of America* **100**, 14920-14925.
Murtaugh, L. C., Law, A. C., Dor, Y. and Melton, D. A. (2005). Beta-catenin is essential for pancreatic acinar but not islet development. *Development (Cambridge, England)* **132**, 4663-4674.

Nakanishi, K., Sweeney, W. E., Macrae Dell, K., Cotton, C. U. and Avner, E. D. (2001). Role of CFTR in autosomal recessive polycystic kidney disease. *J. Am. Soc. Nephrol.* **12**, 719-725.
Nakashima, M., Toyono, T., Akamine, A. and Joyner, A. (1999). Expression of growth/differentiation factor 11, a new member of the BMP/TGFbeta superfamily during mouse embryogenesis. *Mech. Dev.* **80**, 185-189.
Nakel, K., Hartung, S. A., Bonneau, F., Eckmann, C. R. and Conti, E. (2010). Four KH domains of the C. elegans Bicaudal-C ortholog GLD-3 form a globular structural platform. *RNA (New York, N.Y.)* **16**, 2058-2067.
Nauli, S. M., Alenghat, F. J., Luo, Y., Williams, E., Vassilev, P., Li, X., Elia, A. E., Lu, W., Brown, E. M., Quinn, S. J. et al. (2003). Polycystins 1 and 2 mediate mechanosensation in the primary cilium of kidney cells. *Nature genetics* **33**, 129-137.
Nauta, J., Ozawa, Y., Sweeney, W. E., Rutledge, J. C. and Avner, E. D. (1993). Renal and biliary abnormalities in a new murine model of autosomal recessive polycystic kidney disease. *Pediatric nephrology (Berlin, Germany)* **7**, 163-172.
Naya, F. J., Huang, H. P., Qiu, Y., Mutoh, H., DeMayo, F. J., Leiter, A. B. and Tsai, M. J. (1997). Diabetes, defective pancreatic morphogenesis, and abnormal enteroendocrine differentiation in BETA2/neuroD-deficient mice. *Genes & development* **11**, 2323-2334.
Nekrep, N., Wang, J., Miyatsuka, T. and German, M. S. (2008). Signals from the neural crest regulate beta-cell mass in the pancreas. *Development (Cambridge, England)* **135**, 2151-2160.
Nelson, S. B., Schaffer, A. E. and Sander, M. (2007). The transcription factors Nkx6.1 and Nkx6.2 possess equivalent activities in promoting beta-cell fate specification in Pdx1+ pancreatic progenitor cells. *Development* **134**, 2491-2500.
Neve, B., Fernandez-Zapico, M. E., Ashkenazi-Katalan, V., Dina, C., H. Hamid, Y., Joly, E., Vaillant, E., Benmezroua, Y., Durand, E., Bakaher, N. et al. (2005). Role of transcription factor KLF11 and its diabetes-associated gene variants in pancreatic beta cell function. *Proceedings of the National Academy of Sciences of the United States of America* **102**, 4807-4812.
Nicolau, C., Torra, R., Bianchi, L., Vilana, R., Gilabert, R., Darnell, A. and Brú, C. (2000). Abdominal sonographic study of autosomal dominant polycystic kidney disease. *Journal of clinical ultrasound : JCU* **28**, 277-282.
Nicolino, M., Claiborn, K. C., Senée, V., Boland, A., Stoffers, D. A. and Julier, C. (2010). A Novel Hypomorphic PDX1 Mutation Responsible for Permanent Neonatal Diabetes With Subclinical Exocrine Deficiency. *Diabetes* **59**, 733-740.
Niehrs, C. (2012). The complex world of WNT receptor signalling. *Nature reviews. Molecular cell biology* **13**, 767-779.
Nikolova, G., Jabs, N., Konstantinova, I., Domogatskaya, A., Tryggvason, K., Sorokin, L., Fässler, R., Gu, G., Gerber, H.-P. and Ferrara, N. (2006). The vascular basement membrane: a niche for insulin gene expression and cell proliferation. *Dev. Cell* **10**, 397-405.
Njølstad, P. R., Søvik, O., Cuesta-Muñoz, A., Bjørkhaug, L. B., Massa, O., Barbetti, F., Undlien, D. E., Shiota, C., Magnuson, M. A., Molven, A. et al. (2001). Neonatal diabetes mellitus due to complete glucokinase deficiency. *N. Engl. J. Med.* **344**, 1588-1592.
Norgaard, G. A., Jensen, J. N. and Jensen, J. (2003). FGF10 signaling maintains the pancreatic progenitor cell state revealing a novel role of Notch in organ development. *Developmental Biology* **264**, 323-338.
Norris, D. O. and Carr, J. A. (2013a). Endocrinology of Mammalian reproduction. In *Vertebrate Endocrinology* (ed. Elsevier), pp. 329-367. Oxford, UK: Acadmic Press.
Norris, D. O. and Carr, J. A. (2013b). Chemical Regulation of Feeding, Digestion and Metabolism. In *Vertebrate Endocrinology* (ed. Elsevier), pp. 456-494. Oxford, UK: Acadmic Press.
O'Sullivan, D. A., Torres, V. E., Gabow, P. A., Thibodeau, S. N., King, B. F. and Bergstralh, E. J. (1998). Cystic fibrosis and the phenotypic expression of autosomal dominant polycystic kidney disease. *American journal of kidney diseases : the official journal of the National Kidney Foundation* **32**, 976-983.
Ockenden, B. G. and Blyth, H. H. (1971). Polycystic disease of the liver and kidneys in childhood. *Journal of Medical Genetics* **8**, 257–284.

Offield, M. F., Jetton, T. L., Labosky, P. A., Ray, M., Stein, R. W., Magnuson, M. A., Hogan, B. L. and Wright, C. V. (1996). PDX-1 is required for pancreatic outgrowth and differentiation of the rostral duodenum. *Development (Cambridge, England)* **122**, 983-995.
Ohlsson, H., Karlsson, K. and Edlund, T. (1993). IPF1, a homeodomain-containing transactivator of the insulin gene. *The EMBO journal* **12**, 4251-4259.
Ohtsu, H., Tanaka, S., Terui, T., Hori, Y., Makabe-Kobayashi, Y., Pejler, G., Tchougounova, E., Hellman, L., Gertsenstein, M., Hirasawa, N. et al. (2001). Mice lacking histidine decarboxylase exhibit abnormal mast cells. *FEBS Lett.* **502**, 53-56.
Oishi, K., Hofmann, S., Diaz, G. A., Brown, T., Manwani, D., Ng, L., Young, R., Vlassara, H., Ioannou, Y. A., Forrest, D. et al. (2002). Targeted disruption of Slc19a2, the gene encoding the high-affinity thiamin transporter Thtr-1, causes diabetes mellitus, sensorineural deafness and megaloblastosis in mice. *Human Molecular Genetics* **11**, 2951-2960.
Okada, H., Ban, S., Nagao, S., Takahashi, H., Suzuki, H. and Neilson, E. G. (2000). Progressive renal fibrosis in murine polycystic kidney disease: An immunohistochemical observation. *Kidney International* **58**, 587-597.
Olbrich, H., Fliegauf, M., Hoefele, J., Kispert, A., Otto, E., Volz, A., Wolf, M. T., Sasmaz, G., Trauer, U., Reinhart, R. et al. (2003). Mutations in a novel gene, NPHP3, cause adolescent nephronophthisis, tapeto-retinal degeneration and hepatic fibrosis. *Nature Genetics* **34**, 455-459.
Oliver-Krasinski, J. M., Kasner, M. T., Yang, J., Crutchlow, M. F., Rustgi, A. K., Kaestner, K. H. and Stoffers, D. A. (2009). The diabetes gene Pdx1 regulates the transcriptional network of pancreatic endocrine progenitor cells in mice. *The Journal of clinical investigation* **119**, 1888-1898.
Oliver, G., Wehr, R., Jenkins, N. A., Copeland, N. G., Cheyette, B. N., Hartenstein, V., Zipursky, S. L. and Gruss, P. (1995). Homeobox genes and connective tissue patterning. *Development (Cambridge, England)* **121**, 693-705.
Olsen, B. S., Hahnemann, J., Schwartz, M. and Østergaard, E. (2007). Thiamine-responsive megaloblastic anaemia: a cause of syndromic diabetes in childhood. *Pediatric Diabetes* **8**, 239-341.
Osipovich, A. B., Long, Q., Manduchi, E., Gangula, R., Hipkens, S. B., Schneider, J., Okubo, T., Stoeckert, C. J., Takada, S. and Magnuson, M. A. (2014). Insm1 promotes endocrine cell differentiation by modulating the expression of a network of genes that includes Neurog3 and Ripply3. *Development* **141**, 2939-2949.
Otto, E. A., Schermer, B., Obara, T., O'Toole, J. F., Hiller, K. S., Mueller, A. M., Ruf, R. G., Hoefele, J., Beekmann, F., Landau, D. et al. (2003). Mutations in INVS encoding inversin cause nephronophthisis type 2, linking renal cystic disease to the function of primary cilia and left-right axis determination. *Nature genetics* **34**, 413-420.
Pan, F. C., Bankaitis, E. D., Boyer, D., Xu, X., Van de Casteele, M., Magnuson, M. A., Heimberg, H. and Wright, C. V. (2013). Spatiotemporal patterns of multipotentiality in Ptf1a-expressing cells during pancreas organogenesis and injury-induced facultative restoration. *Development (Cambridge, England)* **140**, 751-764.
Papadopoulou, S. and Edlund, H. (2005). Attenuated Wnt signaling perturbs pancreatic growth but not pancreatic function. *Diabetes* **54**, 2844-2851.
Park, E. Y., Sung, Y. H., Yang, M. H., Noh, J. Y., Park, S. Y., Lee, T. Y., Yook, Y. J., Yoo, K. H., Roh, K. J., Kim, I. et al. (2009). Cyst formation in kidney via B-Raf signaling in the PKD2 transgenic mice. *The Journal of biological chemistry* **284**, 7214-7222.
Patel, V., Williams, D., Hajarnis, S., Hunter, R., Pontoglio, M., Somlo, S. and Igarashi, P. (2013). miR-17~92 miRNA cluster promotes kidney cyst growth in polycystic kidney disease. *Proceedings of the National Academy of Sciences of the United States of America* **110**, 10765-10770.
Pazour, G. J., Dickert, B. L., Vucica, Y., Seeley, E. S., Rosenbaum, J. L., Witman, G. B. and Cole, D. G. (2000). Chlamydomonas IFT88 and its mouse homologue, polycystic kidney disease gene tg737, are required for assembly of cilia and flagella. *The Journal of cell biology* **151**, 709-718.
Pedersen, J. K., Nelson, S. B., Jorgensen, M. C., Henseleit, K. D., Fujitani, Y., Wright, C. V., Sander, M., Serup, P. and Consortium, B. C. B. (2005). Endodermal expression of Nkx6 genes depends differentially on Pdx1. *Developmental Biology* **288**, 487-501.

Piazzon, N., Maisonneuve, C., Guilleret, I., Rotman, S. and Constam, D. B. (2012). Bicc1 links the regulation of cAMP signaling in polycystic kidneys to microRNA-induced gene silencing. *Journal of molecular cell biology* **4**, 398-408.
Pictet, R. L., Clark, W. R., Williams, R. H. and Rutter, W. J. (1972). An ultrastructural analysis of the developing embryonic pancreas. *Developmental biology* **29**, 436-467.
Pierreux, C. E., Vanhorenbeeck, V., Jacquemin, P., Lemaigre, F. P. and Rousseau, G. G. (2004). The transcription factor hepatocyte nuclear factor-6/Onecut-1 controls the expression of its paralog Onecut-3 in developing mouse endoderm. *J. Biol. Chem.* **279**, 51298-51304.
Pierreux, C. E., Cordi, S., Hick, A.-C. C., Achouri, Y., Ruiz de Almodovar, C., Prévot, P.-P. P., Courtoy, P. J., Carmeliet, P. and Lemaigre, F. P. (2010). Epithelial: Endothelial cross-talk regulates exocrine differentiation in developing pancreas. *Developmental biology* **347**, 216-227.
Pierreux, C. E., Poll, A. V., Kemp, C. R., Clotman, F., Maestro, M. A., Cordi, S., Ferrer, J., Leyns, L., Rousseau, G. G. and Lemaigre, F. P. (2006). The transcription factor hepatocyte nuclear factor-6 controls the development of pancreatic ducts in the mouse. *Gastroenterology* **130**, 532-541.
Piontek, K., Menezes, L. F., Garcia-Gonzalez, M. A., Huso, D. L. and Germino, G. G. (2007). A critical developmental switch defines the kinetics of kidney cyst formation after loss of Pkd1. *Nat. Med.* **13**, 1490-1495.
Plank, J. L., Mundell, N. A., Frist, A. Y., LeGrone, A. W., Kim, T., Musser, M. A., Walter, T. J. and Labosky, P. A. (2011). Influence and timing of arrival of murine neural crest on pancreatic beta cell development and maturation. *Developmental Biology* **15**, 321-330.
Plengvidhya, N., Kooptiwut, S., Songtawee, N., Doi, A., Furuta, H., Nishi, M., Nanjo, K., Tantibhedhyangkul, W., Boonyasrisawat, W., Yenchitsomanus, P.-t. et al. (2007). PAX4 Mutations in Thais with Maturity Onset Diabetes of the Young. *Journal of Clinical Endocrinology & Metabolism* **92**, 2821-2826.
Polak, M. and Shield, J. (2004). Neonatal and very-early-onset diabetes mellitus. *Seminars in Neonatology* **9**, 59-65.
Poll, A. V., Pierreux, C. E., Lokmane, L., Haumaitre, C., Achouri, Y., Jacquemin, P., Rousseau, G. G., Cereghini, S. and Lemaigre, F. P. (2006). A vHNF1/TCF2-HNF6 cascade regulates the transcription factor network that controls generation of pancreatic precursor cells. *Diabetes* **55**, 61-69.
Pontoglio, M., Barra, J., Hadchouel, M., Doyen, A., Kress, C., Bach, J. P., Babinet, C. and Yaniv, M. (1996). Hepatocyte nuclear factor 1 inactivation results in hepatic dysfunction, phenylketonuria, and renal Fanconi syndrome. *Cell* **84**, 575-585.
Pontoglio, M., Sreenan, S., Roe, M., Pugh, W., Ostrega, D., Doyen, A., Pick, A. J., Baldwin, A., Velho, G., Froguel, P. et al. (1998). Defective insulin secretion in hepatocyte nuclear factor 1alpha-deficient mice. *The Journal of clinical investigation* **101**, 2215-2222.
Proks, P., Arnold, A. L., Bruining, J., Girard, C., Flanagan, S. E., Larkin, B., Colclough, K., Hattersley, A. T., Ashcroft, F. M. and Ellard, S. (2006). A heterozygous activating mutation in the sulphonylurea receptor SUR1 (ABCC8) causes neonatal diabetes. *Human Molecular Genetics* **15**, 1793-1800.
Pulkinnen, M.-A., Spencer-Dene, B., Dickson, C. and Otonkoski, T. (2003). The IIIb isoform of fibroblast growth factor receptor 2 is required for proper growth and branching of pancreatic ductal epithelium but not for differentiation of exocrine or endocrine cells. *Mech. Dev.* **120**, 167-175.
Qian, F., Watnick, T. J., Onuchic, L. F. and Germino, G. G. (1996). The Molecular Basis of Focal Cyst Formation in Human Autosomal Dominant Polycystic Kidney Disease Type I. *Cell* **87**, 979-987.
Rall, L. B., Pictet, R. L., Williams, R. H. and Rutter, W. J. (1973). Early Differentiation of Glucagon-Producing Cells in Embryonic Pancreas: A Possible Developmental Role for Glucagon. *Proceedings of the National Academy of Sciences* **70**, 3478-3482.
Reeders, S. T. (1992). Multilocus polycystic disease. *Nature Genetics* **1**, 235-237.
Rees, S., Kittikulsuth, W., Roos, K., Strait, K. A., Van Hoek, A. and Kohan, D. E. (2014). Adenylyl cyclase 6 deficiency ameliorates polycystic kidney disease. *J. Am. Soc. Nephrol.* **25**, 232-237.
Reynolds, D. S., Stevens, R. L. and Lane, W. S. (1990). Different mouse mast cell populations express various combinations of at least six distinct mast cell serine proteases. *Proceedings of the …* **87**, 3230-3234.

Riella, C., Czarnecki, P. G. and Steinman, T. I. (2015). Therapeutic Advances in the Treatment of Polycystic Kidney Disease. *Nephron Clinical Practice* **128**, 297-302.
Robb, L., Hilton, D. J., Brook-Carter, P. and Begley, C. G. (1997). Identification of a Second Murine Interleukin-11 Receptor α-Chain Gene (IL11Ra2) with a Restricted Pattern of Expression. *Genomics* **40**, 387394.
Rosenbauer, F., Wagner, K., Zhang, P., Knobeloch, K.-P. P., Iwama, A. and Tenen, D. G. (2004). pDP4, a novel glycoprotein secreted by mature granulocytes, is regulated by transcription factor PU.1. *Blood* **103**, 4294-4301.
Rossetti, S., Kubly, V. J., Consugar, M. B., Hopp, K., Roy, S., Horsley, S. W., Chauveau, D., Rees, L., Barratt, T. M., van't Hoff, W. G. et al. (2009). Incompletely penetrant PKD1 alleles suggest a role for gene dosage in cyst initiation in polycystic kidney disease. *Kidney international* **75**, 848-855.
Roux, E., Strubin, M., Hagenbüchle, O. and Wellauer, P. K. (1989). The cell-specific transcription factor PTF1 contains two different subunits that interact with the DNA. *Genes & development* **3**, 1613-1624.
Rowe, I., Chiaravalli, M., Mannella, V., Ulisse, V., Quilici, G., Pema, M., Song, X. W., Xu, H., Mari, S., Qian, F. et al. (2013). Defective glucose metabolism in polycystic kidney disease identifies a new therapeutic strategy. *Nat. Med.* **19**, 488-493.
Rubio-Cabezas, O., Minton, J. A. L., Kantor, I., Williams, D., Ellard, S. and Hattersley, A. T. (2010). Homozygous Mutations in NEUROD1 Are Responsible for a Novel Syndrome of Permanent Neonatal Diabetes and Neurological Abnormalities. *Diabetes* **59**, 2326-2331.
Rubio-Cabezas, O., Codner, E., Flanagan, S. E., Gómez, J. L., Ellard, S. and Hattersley, A. T. (2014). Neurogenin 3 is important but not essential for pancreatic islet development in humans. *Diabetologia* **57**, 2421-2424.
Rubio-Cabezas, O., Jensen, J. N., Hodgson, M. I., Codner, E., Ellard, S., Serup, P. and Hattersley, A. T. (2011). Permanent Neonatal Diabetes and Enteric Anendocrinosis Associated With Biallelic Mutations in NEUROG3. *Diabetes* **60**, 1349-1353.
Rué, P., Kim, Y. H., Larsen, H. L., Grapin-Botton, A. and Martinez Arias, A. (2014). A framework for the analysis of symmetric and asymmetric divisions in developmental processes. *bioRxiv*.
Rutter, W. J., Kemp, J. D., Bradshaw, W. S., Clark, W. R., Ronzio, R. A. and Sanders, T. G. (1968). Regulation of specific protein synthesis in cytodifferentiation. *J. Cell. Physiol.* **72**, 1-18.
Ryan, S., Verghese, S., Cianciola, N. L., Cotton, C. U. and Carlin, C. R. (2010). Autosomal recessive polycystic kidney disease epithelial cell model reveals multiple basolateral epidermal growth factor receptor sorting pathways. *Mol. Biol. Cell* **21**, 2732-2745.
Ræder, H., Johansson, S., Holm, P. I., Haldorsen, I. S., Mas, E., Sbarra, V., Nermoen, I., Eide, S. Å., Grevle, L., Bjørkhaug, L. et al. (2005). Mutations in the CEL VNTR cause a syndrome of diabetes and pancreatic exocrine dysfunction. *Nature Genetics* **38**, 54-62.
Saffman, E. E., Styhler, S., Rother, K., Li, W., Richard, S. and Lasko, P. (1998). Premature translation of oskar in oocytes lacking the RNA-binding protein bicaudal-C. *Molecular and cellular biology* **18**, 4855-4862.
Sammels, E., DEvogelaere, B., Mekahli, D., Bultynck, G., Ludwig, M., Parys, J. B., Cai, Y., Somlo, S. and De Smedt, H. (2010). Polycystin-2 Activation by Inositol 1,4,5-Trisphosphate-induced Ca2+ Release Requires Its Direct Association with the Inositol 1,4,5-Trisphosphate Receptor in a Signaling Microdomain. *J. Biol. Chem.* **285**, 18794-18805.
Sand, F. W., Hörnblad, A., Johansson, J. K., Lorén, C., Edsbagge, J., Ståhlberg, A., Magenheim, J., Ilovich, O., Mishani, E., Dor, Y. et al. (2011). Growth-limiting role of endothelial cells in endoderm development. *Developmental biology* **352**, 267-277.
Sander, M., Neubüser, A. and Kalamaras, J. (1997). Genetic analysis reveals that PAX6 is required for normal transcription of pancreatic hormone genes and islet development. *Genes & Dev* **11**, 1662-1673.
Sander, M., Sussel, L., Conners, J., Scheel, D., Kalamaras, J., Dela Cruz, F., Schwitzgebel, V., Hayes-Jordan, A. and German, M. (2000). Homeobox gene Nkx6.1 lies downstream of Nkx2.2 in the major pathway of beta-cell formation in the pancreas. *Development (Cambridge, England)* **127**, 5533-5540.
Sandgren, E. P., Luetteke, N. C., Palmiter, R. D., Brinster, R. L. and Lee, D. C. (1990). Overexpression of TGF alpha in transgenic mice: induction of epithelial hyperplasia, pancreatic metaplasia, and carcinoma of the breast. *Cell* **61**, 1121-1135.

Schaffer, A. E., Freude, K. K., Nelson, S. B. and Sander, M. (2010). Nkx6 transcription factors and Ptf1a function as antagonistic lineage determinants in multipotent pancreatic progenitors. *Dev. Cell* **18**, 1022-1029.
Schaffer, A. E., Taylor, B. L., Benthuysen, J. R., Liu, J., Thorel, F., Yuan, W., Jiao, Y., Kaestner, K. H., Herrera, P. L., Magnuson, M. A. et al. (2013). Nkx6.1 controls a gene regulatory network required for establishing and maintaining pancreatic Beta cell identity. *PLoS genetics* **9**, e1003274.
Schindelin, J., Arganda-Carreras, I., Frise, E., Kaynig, V., Longair, M., Pietzsch, T., Preibisch, S., Rueden, C., Saalfeld, S., Schmid, B. et al. (2012). Fiji: an open-source platform for biological-image analysis. *Nature methods* **9**, 676-682.
Schmid-Kotsas, A., Gross, H. J., Menke, A., Weidenbach, H., Adler, G., Siech, M., Beger, H., Grünert, A. and Bachem, M. G. (1999). Lipopolysaccharide-activated macrophages stimulate the synthesis of collagen type I and C-fibronectin in cultured pancreatic stellate cells. *Am. J. Pathol.* **155**, 1749-1758.
Schonhoff, S., Giel-Moloney, M. and Leiter, A. (2004). Neurogenin 3-expressing progenitor cells in the gastrointestinal tract differentiate into both endocrine and non-endocrine cell types. *Developmental biology* **270**, 443-454.
Schonhoff, S. E., Giel-Moloney, M. and Leiter, A. B. (2004). Neurogenin 3-expressing progenitor cells in the gastrointestinal tract differentiate into both endocrine and non-endocrine cell types. *Developmental biology* **270**, 443-454.
Schwitzgebel, V. M., Scheel, D. W., Conners, J. R., Kalamaras, J., Lee, J. E., Anderson, D. J., Sussel, L., Johnson, J. D. and German, M. S. (2000). Expression of neurogenin3 reveals an islet cell precursor population in the pancreas. *Development (Cambridge, England)* **127**, 3533-3542.
Schüpbach, T. and Wieschaus, E. (1991). Female sterile mutations on the second chromosome of Drosophila melanogaster. II. Mutations blocking oogenesis or altering egg morphology. *Genetics* **129**, 1119-1136.
Scobie, I. N. and Samaras, K. (2014a). Type 1 diabetes mellitus. In *Fast Facts: Diabetes Mellitus*, pp. 18-26: HEALTH PRESS LIMITED.
Scobie, I. N. and Samaras, K. (2014b). Type 2 diabetes mellitus. In *Fast Facts: Diabetes Mellitus*, pp. 27-34: HEALTH PRESS LIMITED.
Seghers, V., Nakazaki, M., DeMayo, F., Aguilar-Bryan, L. and Bryan, J. (2000). Sur1 knockout mice. A model for K(ATP) channel-independent regulation of insulin secretion. *The Journal of biological chemistry* **275**, 9270-9277.
Seifert, J. R. and Mlodzik, M. (2007). Frizzled/PCP signalling: a conserved mechanism regulating cell polarity and directed motility. *Nat. Rev. Genet.* **8**, 126-138.
Self, M., Lagutin, O. V., Bowling, B., Hendrix, J., Cai, Y., Dressler, G. R. and Oliver, G. (2006). Six2 is required for suppression of nephrogenesis and progenitor renewal in the developing kidney. *The EMBO journal* **25**, 5214-5228.
Sellick, G. S., Barker, K. T., Irene, S.-D., Fleischmann, C., Coleman, R. J., Garrett, C., Gloyn, A. L., L., E. E., Hattersley, A., Wellauer, P. K. et al. (2004). Mutations in PTF1A cause pancreatic and cerebellar agenesis. *Nature Genetics* **36**, 1301-1305.
Senée, V., Chelala, C., Duchatelet, S., Feng, D., Blanc, H., Cossec, J.-C. C., Charon, C., Nicolino, M., Boileau, P., Cavener, D. R. et al. (2006). Mutations in GLIS3 are responsible for a rare syndrome with neonatal diabetes mellitus and congenital hypothyroidism. *Nature genetics* **38**, 682-687.
Seymour, P. A., Freude, K. K., Dubois, C. L., Shih, H.-P. P., Patel, N. A. and Sander, M. (2008). A dosage-dependent requirement for Sox9 in pancreatic endocrine cell formation. *Developmental biology* **323**, 19-30.
Seymour, P. A., Shih, H. P., Patel, N. A., Freude, K. K., Xie, R., Lim, C. J. and Sander, M. (2012). A Sox9/Fgf feed-forward loop maintains pancreatic organ identity. *Development (Cambridge, England)* **139**, 3363-3372.
Seymour, P. A., Freude, K. K., Tran, M. N., Mayes, E. E., Jensen, J., Kist, R., Scherer, G. and Sander, M. (2007). SOX9 is required for maintenance of the pancreatic progenitor cell pool. *Proceedings of the National Academy of Sciences* **104**, 1865-1870.
Sharma, N., Malarkey, E. B., Berbari, N. F., O'Connor, A. K., Vanden Heuvel, G. B., Mrug, M. and Yoder, B. K. (2013). Proximal tubule proliferation is insufficient to induce rapid cyst formation after cilia disruption. *J. Am. Soc. Nephrol.* **24**, 456-464.

Sharov, A. A., Dudekula, D. B. and Minoru, S. H. K. (2005). A web-based tool for principal component and significance analysis of microarray data. *Bioinformatics* **21**, 2548-2549.
Shaw-Smith, C., De Franco, E., Lango Allen, H., Batlle, M., Flanagan, S. E., Borowiec, M., Taplin, C. E., van Alfen-van der Velden, J., Cruz-Rojo, J., Perez de Nanclares, G. et al. (2014). GATA4 Mutations Are a Cause of Neonatal and Childhood-Onset Diabetes. *Diabetes* **63**, 2888-2894.
Shi, C., Washington, M., Chaturvedi, R., Drosos, Y., Revetta, F., Weaver, C., Buzhardt, E., Yull, F., Blackwell, T., Sosa-Pineda, B. et al. (2014). Fibrogenesis in pancreatic cancer is a dynamic process regulated by macrophage-stellate cell interaction. *Lab. Invest.* **94**, 409-421.
Shield, J. P. H., Gardner, R. J., Wadsworth, E. J. K., Whiteford, M. L., James, R. S., Robinson, D. O., Baum, J. D. and K, T. I. (1997). Aetiopathology and genetic basis of neonatal diabetes. *Archives of Disease in Childhood - Fetal and Neonatal Edition* **76**, F39-42.
Shih, H. P., Wang, A. and Sander, M. (2013). Pancreas organogenesis: from lineage determination to morphogenesis. *Ann. Rev. Cell Dev. Biol.* **29**, 81-105.
Shih, H. P., Kopp, J. L., Sandhu, M., Dubois, C. L., Seymour, P. A., Grapin-Botton, A. and Sander, M. (2012). A Notch-dependent molecular circuitry initiates pancreatic endocrine and ductal cell differentiation. *Development (Cambridge, England)* **139**, 2488-2499.
Shillingford, J. M., Murcia, N. S., Larson, C. H., Low, S. H., Hedgepeth, R., Brown, N., Flask, C. A., Novick, A. C., Goldfarb, D. A., Kramer-Zucker, A. et al. (2006). The mTOR pathway is regulated by polycystin-1, and its inhibition reverses renal cystogenesis in polycystic kidney disease. *Proceedings of the National Academy of Sciences of the United States of America* **103**, 5466-5471.
Simons, M., Gloy, J., Ganner, A., Bullerkotte, A., Bashkurov, M., Krönig, C., Schermer, B., Benzing, T., Cabello, O. A., Jenny, A. et al. (2005). Inversin, the gene product mutated in nephronophthisis type II, functions as a molecular switch between Wnt signaling pathways. *Nature genetics* **37**, 537-543.
Smith, S., B. , Qu, H.-Q., Taleb, N., Kishimoto, N. Y., Scheel, D. W., Lu, Y., Patch, A.-M., Grabs, R., Wang, J., Lynn, F. C. et al. (2010). Rfx6 directs islet formation and insulin production in mice and humans. *Nature* **463**, 775-780.
Smith, S. B., Gasa, R., Watada, H., Wang, J., Griffen, S. C. and German, M. S. (2003). Neurogenin3 and hepatic nuclear factor 1 cooperate in activating pancreatic expression of Pax4. *The Journal of biological chemistry* **278**, 38254-38259.
Snee, M. J. and Macdonald, P. M. (2009). Bicaudal C and trailer hitch have similar roles in gurken mRNA localization and cytoskeletal organization. *Developmental biology* **328**, 434-444.
Solomon, B. D., Pineda-Alvarez, D. E., Balog, J. Z., Hadley, D., Gropman, A., Nandagopal, R., Han, J. C., Hahn, J. S., Blain, D., Brooks, B. et al. (2009). Compound heterozygosity for mutations in PAX6 in a patient with complex brain anomaly, neonatal diabetes mellitus, and microophthalmia. *American Journal of Medical Genetics Part A* **149A**, 2543-2546.
Sommer, L., Ma, D. and Anderson, D. J. (1996). neurogenins,a Novel Family ofatonal-Related bHLH Transcription Factors, Are Putative Mammalian Neuronal Determination Genes That Reveal Progenitor Cell Heterogeneity in the Developing CNS and PNS. *Molecular and Cellular Neuroscience* **8**, 221-241.
Soriano, P. (1999). Generalized lacZ expression with the ROSA26 Cre reporter strain. *Nature genetics* **21**, 70-71.
Sosa-Pineda, B., Chowdhury, K., Torres, M., Oliver, G. and Gruss, P. (1997). The Pax4 gene is essential for differentiation of insulin-producing beta cells in the mammalian pancreas. *Nature* **386**, 399-402.
Spooner, B. S., Walther, B. T. and Rutter, W. J. (1970). The development of the dorsal and ventral mammalian pancreas in viva and in vitro. *The Journal of Cell Biology* **47**, 235-246.
Srinivas, S., Watanabe, T., Lin, C., William, C., Tanabe, Y., Jessell, T. and Costantini, F. (2001). Cre reporter strains produced by targeted insertion of EYFP and ECFP into the ROSA26 locus. *BMC Dev Biol* **1**, 4.
St-Onge, L., Sosa-Pineda, B., Chowdhury, K., Mansouri, A. and Gruss, P. (1997). Pax6 is required for differentiation of glucagon-producing alpha-cells in mouse pancreas. *Nature* **387**, 406-409.
Star, R. A., Nonoguchi, H., Balaban, R. and Knepper, M. A. (1988). Calcium and cyclic adenosine monophosphate as second messengers for vasopressin in the rat inner medullary collecting duct. *The Journal of clinical investigation* **81**, 1879-1888.

Starremans, P. G., Li, X., Finnerty, P. E., Guo, L., Takakura, A., Neilson, E. G. and Zhou, J. (2008). A mouse model for polycystic kidney disease through a somatic in-frame deletion in the 5' end of Pkd1. *Kidney international* **73**, 1394-1405.
Stoffers, D. A., Ferrer, J., Clarke, W. L. and Habener, J. F. (1997a). Early-onset type-II diabetes mellitus (MODY4) linked to IPF1. *Nature genetics* **17**, 138-139.
Stoffers, D. A., Zinkin, N. T., Stanojevic, V., Clarke, W. L. and Habener, J. F. (1997b). Pancreatic agenesis attributable to a single nucleotide deletion in the human IPF1 gene coding sequence. *Nature Genetics* **15**, 106-110.
Støy, J., Edghill, E. L., Flanagan, S. E., Ye, H., Paz, V. P., Pluzhnikov, A., Below, J. E., Hayes, M. G., Cox, N. J., Lipkind, G. M. et al. (2007). Insulin gene mutations as a cause of permanent neonatal diabetes. *Proceedings of the National Academy of Sciences of the United States of America* **104**, 15040-15044.
Sullivan, L. P., Wallace, D. P. and Grantham, J. J. (1998). Chloride and fluid secretion in polycystic kidney disease. *J. Am. Soc. Nephrol.* **9**, 903-916.
Sun, H., Li, Q.-W. W., Lv, X.-Y. Y., Ai, J.-Z. Z., Yang, Q.-T. T., Duan, J.-J. J., Bian, G.-H. H., Xiao, Y., Wang, Y.-D. D., Zhang, Z. et al. (2010). MicroRNA-17 post-transcriptionally regulates polycystic kidney disease-2 gene and promotes cell proliferation. *Mol. Biol. Rep.* **37**, 2951-2958.
Sund, N. J., Vatamaniuk, M. Z. and Casey, M. (2001). Tissue-specific deletion of Foxa2 in pancreatic β cells results in hyperinsulinemic hypoglycemia. *Genes & Dev* **15**, 1706-1715.
Sussel, L., Kalamaras, J., Hartigan-O'Connor, D. J., Meneses, J. J., Pedersen, R. A., Rubenstein, J. L. and German, M. S. (1998). Mice lacking the homeodomain transcription factor Nkx2.2 have diabetes due to arrested differentiation of pancreatic beta cells. *Development (Cambridge, England)* **125**, 2213-2221.
Sweeney, W. E. and Avner, E. D. (1998). Functional activity of epidermal growth factor receptors in autosomal recessive polycystic kidney disease. *The American journal of physiology* **275**, 94.
Swenson-Fields, K. I., Vivian, C. J., Salah, S. M., Peda, J. D., Davis, B. M., van Rooijen, N., Wallace, D. P. and Fields, T. A. (2013). Macrophages promote polycystic kidney disease progression. *Kidney Int.* **83**, 855-864.
Saadi-Kheddouci, S., Berrebi, D., Romagnolo, B., Cluzeaud, F., Peuchmaur, M., Kahn, A., Vandewalle, A. and Perret, C. (2001). Early development of polycystic kidney disease in transgenic mice expressing an activated mutant of the beta-catenin gene. *Oncogene* **20**, 5972-5981.
Ta, M., Harris, D. and Rangan, G. (2013). Role of interstitial inflammation in the pathogenesis of polycystic kidney disease. *Nephrology (Carlton)* **18**, 317-330.
Takahashi, H., Calvet, J. P., Dittemore-Hoover, D., Yoshida, K., Grantham, J. J. and Gattone, V. H. (1991). A hereditary model of slowly progressive polycystic kidney disease in the mouse. *J. Am. Soc. Nephrol.* **1**, 980-989.
Tamma, G., Klussmann, E., Procino, G., Svelto, M., Rosenthal, W. and Valenti, G. (2003). cAMP-induced AQP2 translocation is associated with RhoA inhibition through RhoA phosphorylation and interaction with RhoGDI. *J. Cell Sci.* **116**, 1519-1525.
Tazawa, S., Yamato, T., Fujikura, H., Hiratochi, M., Itoh, F., Tomae, M., Takemura, Y., Maruyama, H., Sugiyama, T., Wakamatsu, A. et al. (2005). SLC5A9/SGLT4, a new Na+-dependent glucose transporter, is an essential transporter for mannose, 1,5-anhydro-D-glucitol, and fructose. *Life Sci.* **76**, 1039-1050.
Temple, I. K., James, R., S., Crolla, J. A., Sitch, F. L., Jacobs, P. A., Howell, W. M., Betts, P., Baum, J. D. and Shield, J. P. H. (1995). An imprinted gene(s) for diabetes? *Nature Genetics* **9**, 110-112.
Temple, I. K., Gardner, R. J., Robinson, D. O., Kibirige, M. S., Ferguson, A. W., Baum, J. D., Barber, J. C. K., James, R. S. and Shield, J. P. H. (1996). Further Evidence for an Imprinted Gene for Neonatal Diabetes Localised to Chromosome 6q22–q23. *Human Molecular Genetics* **5**, 1117-1121.
Terauchi, Y., Sakura, H., Yasuda, K., Iwamoto, K., Takahashi, N., Ito, K., Kasai, H., Suzuki, H., Ueda, O. and Kamada, N. (1995). Pancreatic beta-cell-specific targeted disruption of glucokinase gene. Diabetes mellitus due to defective insulin secretion to glucose. *The Journal of biological chemistry* **270**, 30253-30256.
Texido, G., Su, I. h., Mecklenbräuker, I., Saijo, K., Malek, S. N., Desiderio, S., Rajewsky, K. and Tarakhovsky, A. (2000). The B-cell-specific Src-family kinase Blk is dispensable for B-cell development and activation. *Molecular and cellular biology* **20**, 1227-1233.

Thivierge, C., Kurbegovic, A., Couillard, M., Guillaume, R., Coté, O. and Trudel, M. (2006). Overexpression of PKD1 causes polycystic kidney disease. *Molecular and cellular biology* **26**, 1538-1548.
Thompson, N., Gésina, E., Scheinert, P., Bucher, P. and Grapin-Botton, A. (2012). RNA profiling and chromatin immunoprecipitation-sequencing reveal that PTF1a stabilizes pancreas progenitor identity via the control of MNX1/HLXB9 and a network of other transcription factors. *Molecular and cellular biology* **32**, 1189-1199.
Torra, R., Badenas, C., San Millán, J. L., Pérez-Oller, L., Estivill, X. and Darnell, A. (1999). A loss-of-function model for cystogenesis in human autosomal dominant polycystic kidney disease type 2. *American journal of human genetics* **65**, 345-352.
Tran, U., Pickney, L. M., Ozpolat, B. D. and Wessely, O. (2007). Xenopus Bicaudal-C is required for the differentiation of the amphibian pronephros. *Developmental biology* **307**, 152-164.
Tran, U., Zakin, L., Schweickert, A., Agrawal, R., Döger, R., Blum, M., De Robertis, E. and Wessely, O. (2010). The RNA-binding protein bicaudal C regulates polycystin 2 in the kidney by antagonizing miR-17 activity. *Development* **137**, 1107-1116.
Tulachan, S. S., Tei, E., Hembree, M., Crisera, C., Prasadan, K., Koizumi, M., Shah, S., Guo, P., Bottinger, E. and Gittes, G. K. (2007). TGF-beta isoform signaling regulates secondary transition and mesenchymal-induced endocrine development in the embryonic mouse pancreas. *Developmental biology* **305**, 508-521.
Umenishi, F., Narikiyo, T., Vandewalle, A. and Schrier, R. W. (2006). cAMP regulates vasopressin-induced AQP2 expression via protein kinase A-independent pathway. *Biochimica et Biophysica Acta (BBA) - Biomembranes* **1758**, 1100-1105.
Vanhorenbeeck, V., Jenny, M., Cornut, J.-F., Gradwohl, G., Lemaigre, F., Rousseau, G. and Jacquemin, P. (2007). Role of the Onecut transcription factors in pancreas morphogenesis and in pancreatic and enteric endocrine differentiation. *Dev. Biol.* **305**, 685-694.
Vankalakunti, M., Gupta, K., Kakkar, N. and Das, A. (2007). Renal-hepatic-pancreatic dysplasia syndrome (Ivemark's syndrome). *Diagn Pathol* **2**, 24.
Vassilev, P. M., Guo, L., Xing-Zhen, C., Segal, Y., Peng, J.-B., Basora, N., Babakhanlou, H., Cruger, G., Kanazirska, M., Ye, C.-p. et al. (2001). Polycystin-2 Is a Novel Cation Channel Implicated in Defective Intracellular Ca2+ Homeostasis in Polycystic Kidney Disease. *Biochem. Biophys. Res. Commun.* **282**, 341-350.
Verdeguer, F., Le Corre, S., Fischer, E., Callens, C., Garbay, S., Doyen, A., Igarashi, P., Terzi, F. and Pontoglio, M. (2010). A mitotic transcriptional switch in polycystic kidney disease. *Nat. Med.* **16**, 106-110.
Vesterhus, M., Ræder, H., Kurpad, A. J., Kawamori, D., Molven, A., Kulkarni, R. N., Kahn, C. R. and Njølstad, P. R. (2010). Pancreatic Function in Carboxyl-Ester Lipase Knockout Mice. *Pancreatology* **10**, 467-476.
Villasenor, A., Chong, D. C. and Cleaver, O. (2008). Biphasic Ngn3 expression in the developing pancreas. *Dev Dyn* **237**, 3270-3279.
Villasenor, A., Chong, D. C., Henkemeyer, M. and Cleaver, O. (2010). Epithelial dynamics of pancreatic branching morphogenesis. *Development (Cambridge, England)* **137**, 4295-4305.
Vionnet, N., Stoffel, M., Takeda, J., Yasuda, K., Bell, G. I., Zouali, H., Lesage, S., Velho, G., Iris, F., Passa, P. et al. (1992). Nonsense mutation in the glucokinase gene causes early-onset non-insulin-dependent diabetes mellitus. *Nature* **356**, 721-722.
Vujic, M., Heyer, C. M., Ars, E., Hopp, K., Markoff, A., Orndal, C., Rudenhed, B., Nasr, S. H., Torres, V. E., Torra, R. et al. (2010). Incompletely penetrant PKD1 alleles mimic the renal manifestations of ARPKD. *J. Am. Soc. Nephrol.* **21**, 1097-1102.
Wallace, D. P., Rome, L. A., Sullivan, L. P. and Grantham, J. J. (2001). cAMP-dependent fluid secretion in rat inner medullary collecting ducts. *American journal of physiology. Renal physiology* **280**, 29.
Wallace, D. P., White, C., Savinkova, L., Nivens, E., Reif, G. A., Pinto, C. S., Raman, A., Parnell, S. C., Conway, S. J. and Fields, T. A. (2014). Periostin promotes renal cyst growth and interstitial fibrosis in polycystic kidney disease. *Kidney international* **85**, 845-854.
Wang, J., Elghazi, L., Parker, S. E., Kizilocak, H., Asano, M., Sussel, L. and Sosa-Pineda, B. (2004). The concerted activities of Pax4 and Nkx2.2 are essential to initiate pancreatic β-cell differentiation. *Developmental Biology* **266**, 178-189.

Wang, L., Eckmann, C. R., Kadyk, L. C., Wickens, M. and Kimble, J. (2002). A regulatory cytoplasmic poly(A) polymerase in Caenorhabditis elegans. *Nature* **419**, 312-316.
Wang, Q., Elghazi, L., Martin, S., Martins, I., Srinivasan, R. S., Geng, X., Sleeman, M., Collombat, P., Houghton, J. and Sosa-Pineda, B. (2008). ghrelin is a novel target of Pax4 in endocrine progenitors of the pancreas and duodenum. *Dev. Dyn.* **237**, 51-61.
Wang, S., Zhang, J., Zhao, A., Hipkens, S., Magnuson, M. A. and Gu, G. (2007). Loss of Myt1 function partially compromises endocrine islet cell differentiation and pancreatic physiological function in the mouse. *Mech. Dev.* **124**, 898-910.
Wang, S., Hecksher-Sorensen, J., Xu, Y., Zhao, A., Dor, Y., Rosenberg, L., Serup, P. and Gu, G. (2008). Myt1 and Ngn3 form a feed-forward expression loop to promote endocrine islet cell differentiation. *Developmental biology* **317**, 531-540.
Wang, S., Yan, J., Anderson, D., Xu, Y., Kanal, M., Cao, Z., Wright, C. and Gu, G. (2010). Neurog3 gene dosage regulates allocation of endocrine and exocrine cell fates in the developing mouse pancreas. *Developmental biology* **339**, 26-37.
Wang, S., Jensen, J. N., Seymour, P. A., Hsu, W., Dor, Y., Sander, M., Magnuson, M. A., Serup, P. and Gu, G. (2009). Sustained Neurog3 expression in hormone-expressing islet cells is required for endocrine maturation and function. *Proceedings of the National Academy of Sciences of the United States of America* **106**, 9715-9720.
Wang, X., Ward, C. J., Harris, P. C. and Torres, V. E. (2009). Cyclic nucleotide signaling in polycystic kidney disease. *Kidney International* **77**, 129-140.
Watanabe, D., Saijoh, Y., Nonaka, S., Sasaki, G., Ikawa, Y., Yokoyama, T. and Hamada, H. (2003). The left-right determinant Inversin is a component of node monocilia and other 9+0 cilia. *Development* **130**, 1725-1734.
Watanabe, T., Masamune, A., Kikuta, K., Hirota, M., Kume, K., Satoh, K. and Shimosegawa, T. (2009). Bone marrow contributes to the population of pancreatic stellate cells in mice. *American journal of physiology. Gastrointestinal and liver physiology* **297**, 46.
Watari, N., Hotta, Y. and Mabuchi, Y. (1982). Morphological studies on a vitamin A-storing cell and its complex with macrophage observed in mouse pancreatic tissues following excess vitamin A administration. *Okajimas Folia Anat. Jpn.* **58**, 837-858.
Watt, A. J., Zhao, R., Li, J. and Duncan, S. A. (2007). Development of the mammalian liver and ventral pancreas is dependent on GATA4. *BMC developmental biology* **7**, 37.
Weinstein, D. C., Ruiz i Altaba, A., Chen, W. S., Hoodless, P., Prezioso, V. R., Jessell, T. M. and Darnell, J. E. J. (1994). The winged-helix transcription factor HNF-3β is required for notochord development in the mouse embryo. *Cell* **78**, 575588.
Wells, J. M., Esni, F., Boivin, G. P., Aronow, B. J., Stuart, W., Combs, C., Sklenka, A., Leach, S. D. and Lowy, A. M. (2007). Wnt/beta-catenin signaling is required for development of the exocrine pancreas. *BMC developmental biology* **7**, 4.
Werle, E. (1936). The formation of histamine from histidine in animal tissue. *Biochem Z* **288**, 292-293.
Wescott, M. P., Rovira, M., Reichert, M., von Burstin, J., Means, A., Leach, S. D. and Rustgi, A. K. (2009). Pancreatic ductal morphogenesis and the Pdx1 homeodomain transcription factor. *Mol. Biol. Cell* **20**, 4838-4844.
Wessells, N. K. and Cohen, J. H. (1967). Early pancreas organogenesis: Morphogenesis, tissue interactions, and mass effects. *Developmental Biology* **15**, 237270.
Wessely, O. and De Robertis, E. M. (2000). The Xenopus homologue of Bicaudal-C is a localized maternal mRNA that can induce endoderm formation. *Development (Cambridge, England)* **127**, 2053-2062.
Wessely, O., Tran, U., Zakin, L. and De Robertis, E. M. (2001). Identification and expression of the mammalian homologue of Bicaudal-C. *Mech. Dev.* **101**, 267-270.
Wiebe, P. O., Kormish, J. D., Roper, V. T., Fujitani, Y., Alston, N. I., Zaret, K. S., Wright, C. V. E., Stein, R. W. and Gannon, M. (2007). Ptf1a Binds to and Activates Area III, a Highly Conserved Region of the Pdx1 Promoter That Mediates Early Pancreas-Wide Pdx1 Expression. *Molecular and Cellular Biology* **27**, 4093-4104.

Wildin, R. S., Ramsdell, F., Peake, J., Faravelli, F., Casanova, J. L., Buist, N., Levy-Lahad, E., Mazzella, M., Goulet, O., Perroni, L. et al. (2001). X-linked neonatal diabetes mellitus, enteropathy and endocrinopathy syndrome is the human equivalent of mouse scurfy. *Nature genetics* **27**, 18-20.
Wilhelm, J. E., Buszczak, M. and Sayles, S. (2005). Efficient Protein Trafficking Requires Trailer Hitch, a Component of a Ribonucleoprotein Complex Localized to the ER in< i> Drosophila</i>. *Dev. Cell* **9**, 675-685.
Williams, S. S., Cobo-Stark, P., James, L. R., Somlo, S. and Igarashi, P. (2008). Kidney cysts, pancreatic cysts, and biliary disease in a mouse model of autosomal recessive polycystic kidney disease. *Pediatric nephrology (Berlin, Germany)* **23**, 733-741.
Wilson, P. D. and Goilav, B. (2007). Cystic Disease of the Kidney. *Pathology: Mechanisms of Disease* **2**, 341-368.
Wu, G., D'Agati, V., Cai, Y., Markowitz, G., Park, J. H., Reynolds, D. M., Maeda, Y., Le, T. C., Hou, H., Kucherlapati, R. et al. (1998). Somatic inactivation of Pkd2 results in polycystic kidney disease. *Cell* **93**, 177-188.
Wu, G., Tian, X., Nishimura, S., Markowitz, G. S., D'Agati, V., Park, J. H., Yao, L., Li, L., Geng, L., Zhao, H. et al. (2002). Trans-heterozygous Pkd1 and Pkd2 mutations modify expression of polycystic kidney disease. *Human Molecular Genetics* **11**, 1845-1854.
Wu, G., Markowitz, G. S., Li, L., D'Agati, V. D., Factor, S. M., Geng, L., Tibara, S., Tuchman, J., Cai, Y., Park, J. H. et al. (2000). Cardiac defects and renal failure in mice with targeted mutations in Pkd2. *Nat. Genet.* **24**, 75-78.
Wu, K.-L., Gannon, M., Peshavaria, M., Offield, M. F., Henderson, E., Ray, M., Marks, A., Gamer, L. W., Wright, C. V. and Stein, R. (1997). Hepatocyte nuclear factor 3beta is involved in pancreatic beta-cell-specific transcription of the pdx-1 gene. *Molecular and Cellular Biology* **17**, 6002.
Xu, M. G., González-Perrett, S., Essafi, M., Timpanaro, G. A., Montalbetti, N., Arnaout, M. A. and Cantiello, H. F. (2003). Polycystin-1 Activates and Stabilizes the Polycystin-2 Channel. *J. Biol. Chem.* **278**, 1457-1462.
Yabe, S.-I., Tanegashima, K., Haramoto, Y., Takahashi, S., Fujii, T., Kozuma, S., Taketani, Y. and Asashima, M. (2003). FRL-1, a member of the EGF-CFC family, is essential for neural differentiation in Xenopus early development. *Development* **130**, 2071-2081.
Yamada, S., Nishigori, H., Onda, H., Utsugi, T., Yanagawa, T., Maruyama, T., Onigata, K., Nagashima, K., Nagai, R., Morikawa, A. et al. (1997). Identification of mutations in the hepatocyte nuclear factor (HNF)-1 alpha gene in Japanese subjects with IDDM. *Diabetes* **46**, 1643-1647.
Yamagata, K., Furuta, H., Oda, N., Kaisaki, P. J., Menzel, S., Cox, N. J., Fajans, S. S., Signorini, S., Stoffel, M. and Bell, G. I. (1996). Mutations in the hepatocyte nuclear factor-4alpha gene in maturity-onset diabetes of the young (MODY1). *Nature* **384**, 458-460.
Yamaguchi, T., Wallace, D., P. , Magenheimer, B., S. , Hempson, S., J. , Grantham, J., J. and Calvet, J., P. . (2004). Calcium Restriction Allows cAMP Activation of the B-Raf/ERK Pathway, Switching Cells to a cAMP-dependent Growth-stimulated Phenotype. *J. Biol. Chem.* **279**, 40419-40430.
Yamaguchi, T., Nagao, S., Wallace, D. P., Belibi, F. A., Cowley, B. D., Pelling, J. C. and Grantham, J. J. (2003). Cyclic AMP activates B-Raf and ERK in cyst epithelial cells from autosomal-dominant polycystic kidneys. *Kidney international* **63**, 1983-1994.
Yamaguchi, T., Pelling, J. C., Ramaswamy, N. T., Eppler, J. W., Wallace, D. P., Nagao, S., Rome, L. A., Sullivan, L. P. and Grantham, J. J. (2000). cAMP stimulates the in vitro proliferation of renal cyst epithelial cells by activating the extracellular signal-regulated kinase pathway. *Kidney international* **57**, 1460-1471.
Yamin, M., Gorn, A. H., Flannery, M. E., Jenkins, N. A., Gilbert, D. J., Copeland, N. G., Tapp, D. R., Krane, S. M. and Goldring, S. R. (1994). Cloning and characterization of a mouse brain calcitonin receptor complementary deoxyribonucleic acid and mapping of the calcitonin receptor gene. *Endocrinology* **135**, 2635-2643.
Yang, Y., Chang, B. H., Yechoor, V., Chen, W., Li, L., Tsai, M. J. J. and Chan, L. (2011). The Krüppel-like zinc finger protein GLIS3 transactivates neurogenin 3 for proper fetal pancreatic islet differentiation in mice. *Diabetologia* **54**, 2595-2605.

Yoder, B. K., Hou, X. and Guay-Woodford, L. M. (2002). The polycystic kidney disease proteins, polycystin-1, polycystin-2, polaris, and cystin, are co-localized in renal cilia. *J. Am. Soc. Nephrol.* **13**, 2508-2516.
Yoo, H.-W., Shin, Y.-L., Seo, E.-J. and Kim, G.-H. (2002). Identification of a novel mutation in the GLUT2 gene in a patient with Fanconi-Bickel syndrome presenting with neonatal diabetes mellitus and galactosaemia. *Eur. J. Pediatr.* **161**, 351-353.
Yoshioka, M., Kayo, T., Ikeda, T. and Koizumi, A. (1997). A novel locus, Mody4, distal to D7Mit189 on chromosome 7 determines early-onset NIDDM in nonobese C57BL/6 (Akita) mutant mice. *Diabetes* **46**, 887-894.
Yoshitomi, H. and Zaret, K. S. (2004). Endothelial cell interactions initiate dorsal pancreas development by selectively inducing the transcription factor Ptf1a. *Development*.
Yu, H.-M. I. M., Jerchow, B., Sheu, T.-J. J., Liu, B., Costantini, F., Puzas, J. E., Birchmeier, W. and Hsu, W. (2005). The role of Axin2 in calvarial morphogenesis and craniosynostosis. *Development (Cambridge, England)* **132**, 1995-2005.
ZeRuth, g. T., Takeda, Y. and Jetten, A. M. (2013). The Krüppel-like protein Gli-similar 3 (Glis3) functions as a key regulator of insulin transcription. *Molecular endocrinology (Baltimore, Md.)* **27**, 1692-1705.
Zhang, H., Ables, E. T., Pope, C. F., Washington, M. K., Hipkens, S., Means, A. L., Path, G., Seufert, J., Costa, R. H., Leiter, A. B. et al. (2009). Multiple, temporal-specific roles for HNF6 in pancreatic endocrine and ductal differentiation. *Mech. Dev.* **126**, 958-973.
Zhang, Y., Park, S., Blaser, S. and Sheets, M. D. (2014). Determinants of RNA binding and translational repression by the Bicaudal-C regulatory protein. *The Journal of biological chemistry* **289**, 7497-7504.
Zhang, Y., Cooke, A., Park, S., Dewey, C. N., Wickens, M. and Sheets, M. D. (2013). Bicaudal-C spatially controls translation of vertebrate maternal mRNAs. *RNA (New York, N.Y.)* **19**, 1575-1582.
Zhou, Q., Law, A. C., Rajagopal, J., Anderson, W. J., Gray, P. A. and Melton, D. A. (2007). A multipotent progenitor domain guides pancreatic organogenesis. *Dev. Cell* **13**, 103-114.

11.2Websites

http://www.ncbi.nlm.nih.gov/pubmedhealth

http://www.ncbi.nlm.nih.gov/mesh

http://pkdb.mayo.edu

http://www.ncbi.nlm.nih.gov/omim/

http://www.ensembl.org

http://smart.embl-heidelberg.de

12 ACKNOWLEDGEMENTS - *REMERCIEMENTS*

First of all, I am deeply grateful to my thesis supervisor, Pr. Anne Grapin-Botton, for giving me the opportunity to carry out my PhD in her lab. Her great guidance helped me to accomplish my thesis, while her patience and her humanity encourage me to give the best of myself. I also thank her for the possibility to keep in touch with human diseases, one of the most stimulating parts of my project. I would like also to acknowledge my present thesis director at EPFL, Pr. Daniel Constam, for his pertinent and highly valuable comments.

I thank the former Grapin lab members at EPFL: Corinne, Chiara, Marianne, David, Filippo, Marine, Cédric, Nancy, Mathieu, and Yvan. Their presence, along with Keiichi and Yung Hae, made a lively lab with laughter never very far … they were also extremely helpful for all technical or scientific problems. For these reasons, the EPFL lab was quite hard to leave knowing that they could not come join us.

Special thanks to Chhavi, I did not manage to teach her French, due to my poor abilities to teach languages. But we had really great moments that I often miss. I wish her good luck for the rest of her PhD, all the best for her future life and reminder her that she will always be welcome wherever I live. Of course, many thanks to my EPFL friends too numerous to be cited here; thanks to them, I discovered so many cultures… It was very nice to see them when I was coming back from time to time to EPFL.

Des remerciements tout particuliers pour Philippe, Claire, Pierre-Olivier, Corinne et les filles, grâce à eux mon séjour helvétique ne fut jamais un dépaysement et, un de mes grands regrets en partant fut de savoir que je ne les verrais plus aussi souvent.

Moving had both sad and happy sides. I lost mountains, and do not see so much of my “Swiss” friends, but Copenhagen is a great city even without any hills. I found people and make new friends. The move has also been smoothed by the presence of Yung Hae and Keiichi. Thanks you for having brought the lab back on track, and again for your continuous scientific advice and your friendship.

I also thank the other Grapin lab members in Copenhagen: Hjalte, Manuel, Svend, Carla, Laura, Lydie, Benedikte, Dror, and Maja. You presence make for a very lively and friendly lab, where it is nice to speak about science or anything else.

Many thanks to all DanStem people, friends and colleagues, for making DanStem a great place to work. I would like to particularly thank Jurriaan mainly for its help on image analysis that saved me so much time. To Billy and Hanna for so many technical help or tips and generally for all the good discussions. I thank Katie, Fabian and, again, Billy for their great proofreading work on this thesis.

Je remercie mes parents, Philippe et Anne-Marie, mes frères, Etienne et Cédric, et ma sœur, Cécile, pour leur soutien indéfectible. Je n'arrive toujours pas à comprendre comment ils font pour me supporter depuis tant d'années…

Pour finir, comme nous n'avons jamais été très forts en long discours, Jean-Benoît, un tout grand merci!

CURRICULUM VITAE

First and last names : Laurence Lemaire

Birth date and place : The 9th of October, 1987 in Liège (Belgium)

E-mail address : laurence.lemaire@sund.ku.dk

Address : Stockholmsgade, 11 st tv
2100 Copenhagen
Denmark

Cell Phone : +45 71572288

Education

2010 - present:	PhD, École Polytechnique Fédérale de Lausanne (EPFL). Switzerland Role of Bicaudal C1 in pancreas development
2008 - 2010:	Master in Biomedical Sciences, University of Liège (ULg), Belgium Research focus, oncology and immunology Grade: Plus grande distinction (Maxima Cum Laude)
2005 - 2008:	Bachelor in Biomedical Sciences, ULg, Belgium Grade: Plus grande distinction (Maxima Cum Laude)
2005:	High school graduation at Dames de l'Instruction Chrétienne, Liège, Belgium

Laboratory experience

2012 - present:	PhD student (degree expected from EPFL) Laboratory of Pr. Anne Grapin-Botton, DanStem, University of Copenhagen "Role of Bicaudal C1 in pancreas organogenesis"
2010 - 2012:	PhD student Laboratory of Pr. Anne Grapin-Botton, ISREC, EPFL "Role of Bicaudal C1 in pancreas organogenesis"
2010 (7months):	Master student Laboratory of Dr. Keisuke Kaji, ISCR, University of Edinburgh "Characterization of drug inducible iPS cell lines and introduction of an Oct4 reporter gene"
2008-2009:	Student researcher Laboratory of Tumor and Development Biology, ULg "Protective effect of curcumin in metastasis dissemination"

2007:	International Summer Research Program 2007 in Life science and Technology Laboratory of Pr. Anne Grapin-Botton, ISREC, EPFL "Characterization of novel genes involved in endocrine progenitor cell delamination"

Teaching experience

2014:	Master student supervision "Role of BMP signalling in dorso-ventral patterning of the gut" University of Copenhagen
2011:	Teaching assistant Physiology (Practice course) and Biology (Exercises) SV faculty, EPFL
2006 - 2008:	Teaching assistant Biology (Practice course) Medicine faculty, ULg

Language Skills

French : mother tongue **English :** fluent **Dutch :** basic

Publications

Kim Y. H., Larsen H. L., Rué P., Lemaire L. A., Ferrer J, Grapin-Botton A (2015). **Cell cycle-dependent differentiation dynamics balances growth and endocrine differentiation in the pancreas**. PloS Biology, 13, e1002111.

Lemaire L. A., Goulley J., Kim Y. H., Carat S., Jacquemin P., Rougemont J., Constam D. B., Grapin-Botton A. (2015) **Bicaudal C1 promotes pancreatic NEUROG3+ endocrine progenitor differentiation and ductal morphogenesis.** Development, 142, 858-870.

Choi, E., Kraus, M. R., Lemaire, L. A., Yoshimoto, M., Vemula, S., Potter, L. A., Manduchi, E., Stoeckert, C. J., Jr., Grapin-Botton, A. and Magnuson, M. A. (2012). **Dual lineage-specific expression of Sox17 during mouse embryogenesis**. Stem Cells 30, 2297-2308.

Meeting attendance

British Society for Developmental Biology, Spring meeting 2015, Warwick, UK
Bicaudal C1 promotes pancreatic NEUROG3^{+} endocrine progenitor differentiation and ductal morphogenesis (*Poster presentation – Selected for oral presentation in the student symposium*).

18th International Conference of the International Society of Differentiation in conjunction with the British Society for Developmental Biology, 2014, London, UK

Bicaudal C1 promotes pancreatic NEUROG3^{+} endocrine progenitor differentiation and ductal morphogenesis *(Poster presentation)*. The poster won a poster award.

Mouse Molecular Genetics 2014, Pacific Groove, USA
Bicaudal C1 promotes pancreatic NEUROG3^{+} endocrine progenitor differentiation and ductal morphogenesis *(Selected for oral presentation)*.

British Society for Developmental Biology, Spring meeting 2013, Warwick, UK
Regulation of pancreas endocrine differentiation and morphogenesis by Bicaudal C1 *(Poster presentation)*.

Stem Cell Niche 2012, Copenhagen, Denmark
Regulation of pancreas endocrine differentiation and morphogenesis by Bicaudal C1 *(Poster presentation)*.

British Society for Developmental Biology, Spring meeting, 2012, Warwick, UK
Regulation of pancreas endocrine differentiation and morphogenesis by Bicaudal C1 *(Poster presentation)*.